Dynamics of Planar Polarity in the Vertebrate Nervous System

Andrew Walter Mathewson

A dissertation

submitted in partial fulfillment of the

requirements for the degree of

Doctor of Philosophy

University of Washington

2017

Reading Committee:

Cecilia Moens, Chair

Dave Raible

Timothy Cox

Program Authorized to Offer Degree:

Molecular and Cellular Biology

University of Washington

Abstract

Dynamics of Planar Polarity in the Vertebrate Nervous System

Andrew Walter Mathewson

Chair of the Supervisory Committee:
Principal Investigator, Cecilia B. Moens
Division of Basic Sciences, Fred Hutchinson Cancer Research Center

The asymmetric localization of planar cell polarity (PCP) proteins is essential for the establishment of many planar polarized cellular processes, but the mechanisms that maintain these asymmetric distributions remain poorly understood. A body of evidence has tied oriented subapical microtubules (MTs) to the establishment of PCP protein polarity, yet recent studies have suggested that the MT cytoskeleton is later dispensable for the maintenance of this asymmetry. As MTs underlie the vesicular trafficking of membrane-bound proteins within cells, the requirement for MTs in the maintenance of PCP merited further investigation. I sought to investigate the complex interactions between PCP proteins and the MT cytoskeleton in the polarized context of the floorplate of the zebrafish neural tube. We demonstrated that the progressive posterior polarization of the primary cilia of floorplate cells requires not only Vangl2 but also Fzd3a. I determined that GFP-Vangl2 asymmetrically localizes to anterior

membranes whereas Fzd3a-GFP is equally distributed on anterior and posterior membranes but maintains a cytosolic enrichment at the base of the primary cilium. Vesicular Fzd3a-GFP is rapidly trafficked along MTs primarily toward the apical membrane during a period of PCP maintenance, whereas GFP-Vangl2 appears to be less dynamic, maintaining asymmetry at the membrane. Nocodazole-induced loss of MT polymerization disrupts basal body positioning as well as GFP-Vangl2 localization and reduces cytosolic Fzd3a-GFP movements. Removal of nocodazole after MT disruption restores MT polymerization but does not restore basal body polarity. Interestingly, GFP-Vangl2 repolarizes to anterior membranes and Fzd3a-GFP largely re-establishes normal dynamics after multiple hours of recovery, even in the context of unpolarized basal bodies. Together my findings challenge previous work by revealing an ongoing role for MT-dependent transport of PCP proteins in maintaining both cellular and PCP protein asymmetry during development.

PCP signaling has been implicated in the directional migration of single cells during development, especially within the developing nervous system. One such migration is the tangential migration of facial branchiomotor neurons (FBMNs) in the highly polarized context of the vertebrate hindbrain. It is well-established that many core PCP and PCP-related signaling components are required for FBMN migration, yet how PCP signaling is used to enable this migration is not well understood. By systematically disrupting PCP signaling in a rhombomere-restricted manner we show that PCP signaling is required both within FBMNs and the hindbrain rhombomere 4 environment at the time when they initiate their migration. Correspondingly, we demonstrate planar polarized localization of PCP core components Vangl2 and Fzd3a in the

hindbrain neuroepithelium, and transient localization of Vangl2 at the tips of retracting FBMN filopodia. Using high-resolution timelapse imaging of FBMNs in genetic chimeras we uncover opposing cell-autonomous and non-cell-autonomous functions for Fzd3a and Vangl2 in regulating FBMN protrusive activity. Within FBMNs, Fzd3a is required to stabilize filopodia while Vangl2 has an antagonistic, destabilizing role. However, in the migratory environment Fzd3a acts to destabilize FBMN filopodia while Vangl2 has a stabilizing role. Together, our findings suggest a model in which PCP signaling between the planar polarized neuroepithelial environment and FBMNs directs migration by the selective stabilization of FBMN filopodia.

Table of Contents

List of Tables and Figures

This thesis is for my dad.

Adam Warren Mathewson

March 29, 1961---March 24, 2016

Acknowledgements

I would like to thank the expansive community of people who have helped me get this far. First, I would like to thank Cecilia for taking a chance on me. I appreciate her meticulous hands-on approach to my training in zebrafish and developmental biology, as well as her insightful scientific guidance over these many years. Mostly, I want to thank her for the many unique educational opportunities she has provided to me throughout my graduate education, as well as her continual patience with me as I found my own way.

The Moens lab has been a remarkable place to learn and grow and I would like to thank all the members of the lab that have contributed to my graduate experience. I collaborated with Crystal for several years and would like to thank her for her exceptional contributions to the work presented in Chapter 3. Dan started the work presented in Chapter 2, and I am grateful that I could build on his foundation. I would like to thank Greg, who got me started, Adam, who pushed me to think outside the box, and Minna, for her thoughtful and empathetic mentorship, which helped me navigate through many scientific and life challenges. None of our work would be possible without Rachel keeping our fish happy, and I want to thank her for her skilled husbandry and smiling contributions to the lab.

I would like to thank my thesis committee for their support and guidance throughout my graduate career. I would especially like to thank Dave Raible, who managed the Developmental Biology Training Grant which funded much of my graduate work and was instrumental in my personal development as a scientist. I also want to thank the other members of my reading committee, Cecilia Moens and Timothy Cox, for their careful review of this dissertation.

I would like to thank the developmental biology and zebrafish research communities for their open and curious cultures. My time in the Embryology course at the Marine Biological Laboratories in Woods Hole will be fondly remembered as one of the most exciting and playful periods of my scientific career. Many skilled scientists have contributed ideas and reagents that aided my work over the years, but I especially want to thank Mary Halloran, whose insightful suggestion helped me finish my story.

Most importantly, I want to thank my loving friends and family who have believed in me from the start. My mom, dad, and other assorted parental units have always encouraged my educational pursuits, and I would not have made it here without their loving support. My wife Lisa has kept me alive and (mostly) sane throughout my time in graduate school, and I will never be able to thank her enough for her enduring love and emotional support. I also want to thank my cats, Element and Zucchini, for tolerating my distracted presence and for not judging me after many failed experiments. Finally, I want to thank all my weird and wonderful friends, who continue to enrich the human experience of being.

Chapter 1: Introduction

What is PCP?

Cellular polarization is a fundamental aspect of development that enables cells to organize intracellularly and perform specialized behaviors in response to their cellular context. Coordination of this organization across cell boundaries is essential for cohesive tissue generation and organogenesis. Planar cell polarity (PCP) describes one aspect of cellular polarization and it is best understood in tissues composed of sheets of epithelial cells. Epithelia exhibit two types of cellular polarity: apicobasal polarity, which defines the axis between the apical and basal membranes, and PCP, which is cell polarization on the plane orthogonal to the apicobasal axis. Coordinated planar polarization in epithelia is essential for development of a wide variety of animal tissues, as it allows cells to synchronize their growth and behavior to form functional and specialized organs. The PCP signaling pathway was originally discovered in *Drosophila* mutants that displayed misoriented and supernumerary actin-based hairs and bristles on the adult wing and legs (Gubb and García-Bellido, 1982). PCP is a highly conserved signaling pathway and has been implicated in a growing number of developmental processes including but not limited to the orientation and angle of mammalian skin hair follicles (Devenport and Fuchs, 2008), the oriented cell division in developing kidney tubules(Babayeva et al., 2011; Brzoska et al., 2016), inner ear sensory hair orientation(Etheridge et al., 2008; Montcouquiol et al., 2003), directed migration of neuronal cells (Calisto et al., 2005; Davey et al., 2016; Jessen et al., 2002) and collective movements of multiple cell types during gastrulation(Heisenberg et al., 2000; Tada and Smith, 2000; Wallingford and Harland, 2001) and

neural tube closure(Curtin et al., 2003; Wallingford and Harland, 2001; Wang et al., 2006), as well as cilia positioning and directional ciliary beating in trachea(Vladar et al., 2012), oviducts(Shi et al., 2014, 2016), and the central nervous system(Borovina et al., 2010; Boutin et al., 2014). Additionally, mutations that disrupt PCP signaling have been linked to a growing number of human developmental diseases(Kibar et al., 2007; Wallingford et al., 2013) and cancers(Anastas et al., 2012; Luga et al., 2012; MacMillan et al., 2014). The PCP pathway functions at the protein level to polarize subcellular information intracellularly and propagate this information through direct cell-cell interactions, which result in locally coordinated tissue polarity (Tree et al., 2002). A "core" set of PCP proteins that maintain a basic set of molecular behaviors and relationships are highly conserved across multicellular life. However, the mechanistic details of how cells engage with this pathway vary depending on specific cellular context and function. Due to its simplicity and historical legacy, most PCP research has been conducted in the fly wing, and as such the most detailed and mechanistic studies of PCP come from this work. Therefore, much of my writing, unless otherwise stated, will refer to PCP signaling as it is understood in the *Drosophila* wing.

The Core Pathway

The classic "core" PCP pathway of the fly wing is composed of two membrane-localized protein complexes, the distally-localized Frizzled (Fz or Fzd in vertebrates), Dishevelled (Dsh or Dvl in vertebrates), Diego (Dg, or Diversin in vertebrates) complex and the proximally localized Van Gogh/Strabismus (Vang/Stbm, or Vangl in vertebrates), Prickle (Pk) complex (for review see

(Goodrich and Strutt, 2011)). Flamingo (Fmi or Celsr in vertebrates), localizes to both proximal and distal membranes and is essential for mediating the extracellular interactions between PCP signaling complexes. Importantly, PCP proteins need to be positioned along the apicobasal axis in order to interact with one another and this localization is accomplished through a Scribble-(Scrib) dependent mechanism(Courbard et al., 2009; Montcouquiol et al., 2003; Murdoch et al., 2003; Wada et al., 2005). In the fly wing, these PCP protein complexes sort into complementary and mutually exclusive distributions along the cell cortex, with Fmi-Fz-Dsh-Dgo localizing to distal membranes and Fmi-Vang-Pk on proximal membranes (Strutt and Strutt, 2007; Strutt et al., 2002). The asymmetry of these complexes establishes subcellular polarity information that acts on the cytoskeleton and cellular adhesions to generate distally-localized extracellular actin-based hairs known as trichomes. The complex relationships between PCP proteins were largely worked out through experiments examining directional non-autonomy, a behavior first described in the fly wing where *fz* mutant clones disrupt polarity in WT neighbor cells (Vinson and Adler, 1987). Groups of cells that lack Fz induce WT neighbor cells to point hairs towards mutants, whereas loss of Vang/Stbm causes WT neighbor cells to point hairs away(Gubb and García-Bellido, 1982; Taylor et al., 1998; Vinson and Adler, 1987). These types of analyses, along with rapid advances in cell imaging and genetic manipulation, especially in vertebrate models, have revealed a complex and expanding web of protein interactions that broadly define the conserved PCP signaling pathway shared across multicellular life.

PCP Downstream Effectors

Actin regulation is a major outcome of PCP signaling across many systems, and in the fly wing PCP signaling regulates actin to distally localize the generation and orientation of trichomes(Collier and Gubb, 1997; Collier et al., 2005; Gubb and García-Bellido, 1982; Lee and Adler, 2002; Park et al., 1996). Here the PCP pathway acts on a dedicated set of downstream signaling proteins known as PCP effectors, which include Fuzzy (Fy), Inturned (In) and Fritz (Frtz). These effectors colocalize with Fmi, Vang/Stbm and Pk on proximal edges along the apical surfaces of cells and regulate the subcellular distribution of the non-canonical formin-family protein multiple wing hairs (Mwh) (Adler et al., 2004; Strutt and Warrington, 2008; Yan et al., 2008). *mwh* mutants display multiple trichomes across apical cell membranes as Mwh normally functions to fuse actin bundles while antagonizing the formation of nascent actin polymers (Lu et al., 2015). Meanwhile, the small Rho GTPases Cdc42 and RhoA are recruited via a Dsh-dependent process to nucleate actin polymerization in distal cell domains with Rac1 restricting actin activity to these regions, which contributes to polarized hair growth on distal apical membranes(Eaton et al., 1995, 1996; Gray et al., 2009; Strutt et al., 1997). *cdc42* or *rhoA* mutant wing cells have stunted wing hairs or none at all, whereas overexpression of Rac1DN produces a multiple cell hair phenotype, just like *mwh*, *fy*, *in,* or *frtz* mutants(Eaton et al., 1995, 1996; Lee and Adler, 2002; Lu et al., 2010; Yun et al., 1999). The roles of Fy, In, and Frtz in vertebrate systems are generally less clear. For example, the loss of *Xenopus* orthologs of Fy and In exhibit very weak convergent extension (CE) (discussed below) defects but dramatically altered ciliogenesis as In influences docking of the basal body (BB)(see below) to apical

membranes, and Fy governs vesicular trafficking to the BB and along ciliary axonemes (Gray et al., 2009; Park et al., 2006, 2008). Furthermore, loss of Frtz in *Xenopus* only disrupts cell elongation but not cellular polarity (Kim et al., 2010). Though the downstream consequences of PCP signaling are diverse and not well understood across systems, the essential mechanics of core PCP protein function are generally highly conserved.

Vertebrate Outcomes of PCP

Orthologs of the all the core PCP genes are conserved in vertebrate genomes and largely preserve the interdependent relationships that establish their cellular asymmetry(Butler and Wallingford, 2015; Hale and Strutt, 2015). PCP signaling has essential roles in the planar polarization of diverse vertebrate epithelial contexts, including within the central nervous system, skin, trachea, and oviduct(Borovina et al., 2010; Devenport and Fuchs, 2008; Shi et al., 2014; Vladar et al., 2012). Important to my work, PCP signaling enables zebrafish neuroepithelial cells to become highly polarized along the planar (anterior-posterior) axis during development (Borovina et al., 2010; Ciruna et al., 2006; Walsh et al., 2011). The conserved pattern of asymmetrically localized core PCP protein complexes underlies most planar polarized epithelial tissues, and can be visualized by immunostaining or through imaging of ectopically-expressed fluorescently-fused PCP proteins(Davey and Moens, 2017). In addition to polarizing static epithelia, PCP signaling is used in coordinated movements of vertebrate cells undergoing collective migration, including the migration of neural crest placodes (Calisto et al., 2005; Carmona-Fontaine et al., 2008), the movements of sheets of mesodermal and epithelial

cells during gastrulation and neural tube closure(Ciruna et al., 2006; Jessen et al., 2002; Wallingford and Harland, 2001; Wang et al., 2006), cell migration during wound healing(Ossipova et al., 2014; Sawyer et al., 2010), as well as non-collective cell movements like the migration of facial branchiomotor neurons (FBMNs) in the vertebrate hindbrain (Davey et al., 2016; Jessen et al., 2002; Wada et al., 2006). As an example, during vertebrate gastrulation sheets of mesodermal cells polarize, move medially, and intercalate with one another, which causes cells to become distributed along the antero-posterior (AP) axis, extending the AP axis (Heisenberg et al., 2000). These collective cell movements in multiple contexts are described by the term "convergent extension" (CE), as cell converge on one axis to extend another. All core PCP signaling components are essential for CE movements during fish, frog, and mouse gastrulation and neural tube closure, and mutants display a short wide body axis and open neural tube(Ciruna et al., 2006; Curtin et al., 2003; Wallingford et al., 2000; Wang et al., 2006; Ybot-Gonzalez et al., 2007). PCP is also used by cells undergoing non-collective movements, such as during the migration of FBMNs as will be discussed at the end of this section, as well as in **Chapter 3.**

PCP and Cilia Positioning

Primary Cilia and PCP

Whereas the primary outcome of PCP signaling in the fly wing is asymmetric localization of actin-based trichomes, one common product of PCP signaling in many vertebrate epithelia is the asymmetric localization of the microtubule-based primary cilium (Borovina et al., 2010;

Hashimoto et al., 2010; Nonaka et al., 2005; Okada et al., 2005). Primary cilia of many epithelial systems undergo a PCP signaling dependent "translational" migration toward the cell periphery, which is important for cellular signaling and tissue specific functions. For example, PCP signaling has been implicated in regulating the translational positioning of primary cilia in the mouse node, an important signaling structure during development, where cilia position, orientation, and rotational dynamics determine embryonic left-right patterning (Antic et al., 2010; Hashimoto et al., 2010; Song et al., 2010), in sensory hair cells of the mouse cochlea where cilia positioning is crucial for auditory function (Ezan et al., 2013; Jones et al., 2008), in zebrafish neuroepithelial cells where motile primary cilia direct ventricular fluid flow (Borovina et al., 2010), and in lens cells in the eyes of mice (Sugiyama et al., 2010). In the mouse node, PCP signaling controls the uniform positioning and tilting of motile primary cilia towards cell posteriors, which is essential for the leftward fluid flow that determines left-right patterning of the entire body axis (Antic et al., 2010; Borovina et al., 2010; Essner et al., 2002; Hashimoto et al., 2010; Nonaka et al., 2005; Okada et al., 2005; Song et al., 2010). Similar to the fly wing where Fmi-Fz-Dsh complexes localize to distal membranes prior to the assembly of distally localized trichomes, in the node the asymmetric localization of Dvl to posterior membranes precedes primary cilia assembly at cell posteriors, whereas Vangl2 and Pk localize to anterior membranes (Antic et al., 2010; Borovina et al., 2010; Hashimoto et al., 2010). Important to my work, the floorplate of the zebrafish neural tube closely resembles the node in that the motile primary cilia of floorplate cells polarize toward cell posteriors by two days post fertilization (dpf), and Vangl2 controls this behavior cell-autonomously(Borovina et al., 2010). Separate

from this work, in mouse cochlear cells, the axoneme of the kinocilium (a specialized primary cilia) extends from the BB once it reaches the apical membrane at the cell center and then undergoes a PCP-dependent migration to the lateral edge of the cell apex where it coordinates the positioning of a V-shaped bundle of sensory microvilli (Ezan et al., 2013; Jones et al., 2008). This was demonstrated through *Vangl2, Celsr1,* and *Fzd3/Fzd6* double mutants, which display randomized BB/kinocilium orientation on apical membranes (Curtin et al., 2003; Montcouquiol et al., 2006; Wang et al., 2006). In sum, PCP signaling has been implicated in the proper positioning of primary cilia in diverse cell types, yet the mechanisms by which this is accomplished remains an open area of study.

PCP and Multiciliated Cells

PCP signaling is also essential for positioning cilia in many vertebrate multiciliated cell (MCC) contexts, including the positioning and orientation of cilia in frog epidermal MCCs (Mitchell et al., 2009; Park et al., 2006, 2008), ependymal cells in mice (Guirao et al., 2010), and epithelial cells in the mouse oviduct (Shi et al., 2014, 2016). BBs of motile cilia in MCCs are generated post-mitotically through a poorly understood "de-novo" biogenesis that relies on a structure known as the nucleosome (for review see (Brooks and Wallingford, 2014)), and then apically dock through an actin-dependent mechanism (Boisvieux-Ulrich et al., 1985; Dawe et al., 2007). Importantly, MCC BBs are linked subapically through a cortical network of actin and MTs which link the orientation of the basal feet and rootlets, structures associated with MCC BBs that direct the tilting of cilia but also synchronize the motile ciliary beating in these tissues

(Boutin et al., 2014; Mitchell et al., 2007; Wallingford, 2012). This subapical cytoskeletal network of linked BBs functions as a microtubule organizing center (MTOC) for cells in some contexts where it is used to position organelles and initiate apico-basal polarity (for review see(Sanchez and Feldman, 2016).

MCCs use PCP signaling to establish multiple levels of planar polarity. First, "rotational" polarity refers to the parallel alignment of all motile ciliary BBs within each MCC, which reflects the PCP-dependent organization and assembly of the subapical cytoskeletal network that links ciliary BBs (for review, see(Brooks and Wallingford, 2014)). Second, as in other systems, PCP coordinates "tissue-level" planar polarity information across cell boundaries so that BBs, motile cilia, and ciliary beating are oriented across entire tissues (Mitchell et al., 2009). Coordinated orientation and movements of motile cilia are essential for MCC function, which includes the removal of dust and mucus from the apical lumen of the trachea (Vladar et al., 2012), moving cerebral spinal fluid in the brain ventricles (Boutin et al., 2014; Ohata and Álvarez-Buylla, 2016), delivery of oocytes to the uterus through the oviduct (Shi et al., 2014, 2016), and the movement of protective mucus across *Xenopus* epidermis (Park et al., 2008). Whereas motile cilia distribute across the entire apical membranes of MCCs of the airway, oviduct, and *Xenopus* skin, mouse ependymal cells display a third type of polarity by restricting motile cilia to distinct apical clusters (Mirzadeh et al., 2010). These clusters arise at the center of each cell and then undergo a PCP-dependent "translational" migration toward posterior apical membranes, much like the translational migration of primary cilia in other contexts (Guirao et al., 2010). Interestingly, fluid flow generated by asymmetric ciliary beating can reinforce translational and

tissue level polarity by causing tension on motile cilia (the link between tension and PCP is discussed below) (Mirzadeh et al., 2010). This process of "entrainment" of polarity by fluid flow also occurs in *Xenopus* MCCs, and exposure to exogenous fluid flow can reorient the axis of polarity (Mitchell et al., 2007). Dvl normally localizes to the base of motile cilia in *Xenopus* MCCs, and knockdown of Dvl1, Dvl2, or Dvl3, either singly or combined, or expressing DN-Dvl, causes defects in BB apical docking, rotational polarity of BBs, disorganized beating of cilia, and impairment of fluid flow (Park et al., 2006, 2008). Additionally, *dvl1, dvl2, dvl3* triple knockout mice display hydrocephalus due to abnormal cilia patch positioning within ependymal cells, indicating that PCP signaling is essential for fluid flow coordination (Ohata et al., 2014). Furthermore, in mouse ependymal cells, Celsr1, Celsr2, Celsr3, Fzd3, and Vangl2 are required for translational polarity of cilia, and also affect rotational polarity of individual BBs (Boutin et al., 2014; Tissir et al., 2010). Though PCP signaling has been established as essential for the positioning of cilia, the requirement for asymmetric cilia positioning in the propagation and maintenance and of PCP signaling is an active area of study.

PCP and Centriole Positioning

Ciliogenesis requires a specialized subapical centriolar structure known as the basal body (BB), and positioning of BBs is an actively maintained process that depends on actin and MT dynamics, MT motors like myosins, kinesins, and dyneins, as well as PCP signaling, even in systems that lack primary cilia (Carvajal-Gonzalez et al., 2016a; Zhu et al., 2010). BBs are specialized centrosomes, which themselves are formed by association of the mother and

daughter centrioles. Centrioles are conserved cellular organelles whose main structure consists of short beta and gamma tubulin polymers and the protein centrin, which assemble into a barrel shape with a central cavity (Azimzadeh and Marshall, 2010; Beisson and Wright, 2003; Bornens, 2012; Carvalho-Santos et al., 2011). Centriole positioning can be dynamic, such as during cell division when mother and daughter centrioles migrate to opposite poles at the plasma membrane, where they project MTs to establish the mitotic spindle, or during the cell movements of wound closure when centrioles move towards the leading edge (Blitzer et al., 2011; Yadav et al., 2009). Many proteins associate with centrioles to perform roles in centrosome assembly, function, as well as subcellular positioning, and the subcellular cloud of dynamic proteins associated with the centrosome is known as the pericentriolar matrix (PCM). Centrosomes have many cellular functions including major roles in cell division, cell motility, as well as cellular sensing and polarity (Bettencourt-Dias and Glover, 2007; Nigg and Raff, 2009). Importantly, within apicobasally polarized epithelial cells the centrosome moves toward the apical membrane to become the BB of the primary cilium, where it nucleates ciliogenesis and determines cilia positioning (Avasthi and Marshall, 2012; Buendia, 1990; Reiter et al., 2012; Rodriguez-Boulan and Macara, 2014; Rodríguez-Fraticelli et al., 2012).

One of the main roles that centrosomes perform within proliferating cells is that of the primary MTOC. MTOCs nucleate and organize the MT cytoskeleton, position the Golgi complex, primary cilium, and proteasome, and MTOC position can polarize many cellular functions (Badano et al., 2005). The formation of new MT filaments at the centrosome requires a process known as MT nucleation, which is dependent on γ-tubulin ring complexes (γ-TuRCs) within the

PCM (Moritz and Agard, 2001). Importantly, many cell types reorganize MTs into non-centrosomal arrays after they exit the cell cycle and differentiate, and thus reassign at least partial MTOC function to other cellular structures (for review see (Muroyama and Lechler, 2017; Sanchez and Feldman, 2016)). Additionally, in fly interphase, MTs do not depend on centrioles and mutant flies that lack centrioles have remarkably normal phenotypes (Basto et al., 2006; Gogendeau and Basto, 2010; Rogers et al., 2008). MTOC reassignment is coincident with γ-tubulin delocalization at the centrosome, which suggests that PCM dissociation inactivates the centrosome as the primary MTOC (Brodu et al., 2010). Non-centrosomal MTOCs are poorly characterized, but include membrane associated proteins like calmodulin-regulated spectrin associated protein 3 (CAMSAP3), which can nucleate MTs in mammalian cell culture (Tanaka et al., 2012). Despite the ability of differentiated cells to reassign MTOC function to non-centrosomal structures, centrosomes often retain the ability to nucleate and organize radial arrays of MTs in many cell types including mammalian epidermal cells (Lechler and Fuchs, 2007) and neurons (Yu et al., 1993). It remains to be determined how differentiated cells maintain complex patterns of MT organization during the process of MTOC reassignment.

How does PCP Control Basal Body Polarity?

Current models suggest that PCP signaling directs BB positioning primarily through the regulation of actin. Actin filament polymerization is needed for proper positioning of ciliary BBs in polarized epithelial cells, as cytochalasin D, an actin polymerization inhibitor interferes with BB migration and ciliogenesis (Boisvieux-Ulrich et al., 1990). Rac1, a regulator of actin dynamics,

is important for the positioning of BBs as NSC23766, a Rac1 inhibitor, causes cilia in the mouse node to remain centrally localized and disrupts the position of the BB in auditory hair cells (Hashimoto et al., 2010). Additionally, PAK, a cytoskeletal regulator downstream of Rac and CDC42 (Bokoch, 2003) is inhibited by the small molecule inhibitor IPA-3, which impairs ciliary positioning in inner ear hair cells (Sipe and Lu, 2011). DN RhoA (RhoA-N19) disrupts actin polymerization and causes BB misalignment in *Xenopus* epithelial MCCs, likely through disrupting the directed apical actin polymerization that is involved in docking BBs to the apical membrane (Park et al., 2008). In mouse ependymal cells Celsr2 and 3 are needed for the regulation of actin to organize BB rotational polarity and organization of BB patches (Boutin et al., 2014). Dvl and In are normally localized near the BB of cilia in *Xenopus* epithelial MCCs and work to regulate Rho activation and localization (Park et al., 2006, 2008). The loss of Dvl or Fy or In decreases apical actin assembly in these cells, which affects BB positioning and cilia orientation (Park et al., 2006, 2008; Werner et al., 2014). Thus, PCP signaling regulates actin dynamics to position BBs and cilia in many cellular contexts.

Reciprocal Relationships Between PCP and Cilia

Ciliogenesis and cilia positioning is generally considered downstream of PCP signaling due to the above examples, as well as the fact that *ift88* and *kif3a* mouse mutants, both of which lack primary cilia, display disrupted BB planar polarization yet retain normally localized PCP proteins (Jones et al., 2008). However, it should be mentioned that in addition to PCP influencing cilia positioning, there is also evidence that cilia themselves have reciprocal

influence on PCP signaling. This idea partially comes from studies on Bardet Biedl Syndrome (BBS) proteins, which are involved in intraflagellar transport (IFT) and are required for ciliogenesis (for review, see(Blacque and Leroux, 2006)). It has been hypothesized that BBS proteins could have roles in trafficking of PCP proteins, as multiple core PCP components localize the BB, including Dvl2 in *Xenopus* epithelial cells, as well as Vangl2 in mouse kidney epithelial cells (Park et al., 2008; Ross et al., 2005). Importantly, PCP and BBS proteins are thought to genetically interact as BBS and PCP mutations cause related phenotypes that are exacerbated when combined. For example, mice with mutations in Vangl2, Scrb1, or Celsr1, exhibit midbrain exencephaly resulting from a failure in neural tube closure, which also occurs in *Bbs4* mutant mice (Curtin et al., 2003; Montcouquiol et al., 2003; Ross et al., 2005). Additionally, these PCP mutant mice display defects in cochlear stereociliary bundle orientation, which occurs at a lower frequency in *Bbs1, Bbs4*, and *Bbs6* mutants (Ross et al., 2005). Heterozygous combination of *Bbs1* and *Vangl2* (Looptail) mutations results in significant embryo lethality as well as increased frequency of stereociliary defects. Furthermore, *vangl2* mutant zebrafish display convergent extension defects that result in a shortened and widened body axis, which is enhanced by Bbs4 or Bbs8 knockdown (May-Simera et al., 2010; Ross et al., 2005). Furthermore, deletion of *Bbs8* disrupts the asymmetric accumulation of Vangl2 in the mouse cochlea and co-immunoprecipitation assays revealed direct interactions between these proteins (May-Simera et al., 2015). However, (Carvajal-Gonzalez et al., 2016b) points out that whereas PCP loss of function randomizes cochlear kinocilia position but does not affect the positioning and organization of stereocilia relative to the kinocilia, BBS mutants display distinct

circular and flat distributions of stereocilia that more closely resemble phenotypes caused by the loss of G-protein signaling components $G\alpha_{i3}$ and mPins (Ezan et al., 2013). Additionally, the asymmetric localization of Vangl2 is retained in $G\alpha_{i3}$ and mPins mutants, which suggests that PCP functions upstream of these factors and BBS proteins. Aside from this observation, the links between PCP signaling, ciliogenesis and cilia positioning remain controversial as they are not understood at a mechanistic level.

Models of Global Planar Polarity Establishment and Coordination

Interactive properties of core PCP proteins when coupled with the dynamics of endocytic flux (both are discussed below) are sufficient to establish and propagate PCP in local regions of animal cells, but the mechanism by which cells across entire tissues coordinate their initial asymmetry has remained controversial. The stochastic breaking of cellular symmetry during development can cause locally aligned patches of asymmetry, but to form fully functional organs this asymmetry needs to be coordinated across entire tissues (Aw et al., 2016; Strutt and Strutt, 2007; Vladar et al., 2012). Though no single conserved mechanism for coordinating PCP establishment is known to date, there are multiple interrelated models that are thought to act in specific cellular contexts.

Fat/Daschous/Four-jointed Signaling

The most well-understood process for coordinated PCP establishment is dependent on the Fat/Daschous/Four-jointed (Ft/Ds/Fj) signaling pathway in *Drosophila* (Harumoto et al., 2010; Olofsson et al., 2014; Shimada et al., 2006; Simon, 2004; Yang et al., 2002; Zeidler et al.,

1999). Ft and Ds are atypical cadherins that preferentially bind to one another in heterophilic interactions at the cell surface (Ma et al., 2003; Matakatsu and Blair, 2004; Strutt and Strutt, 2002). Ds forms a gradient across the fly wing in a proximal to distal direction, whereas Ft is uniformly expressed, and the Golgi-associated protein Fj is expressed in a gradient in the distal to proximal direction (Strutt et al., 2004; Zeidler et al., 1999). Fj regulates the interactions between Ft and Ds through phosphorylation of Ft, which leads to asymmetric localization of these proteins within individual cells (Ma et al., 2003; Strutt and Strutt, 2002). Ft and Ds also display an asymmetry of binding activity across cell membranes which is affected by the phosphorylation of the cytosolic tail of Ft induced by Ds binding (Feng and Irvine, 2009; Sopko et al., 2009). Asymmetry of Ft and Ds activity can polarize subcellular Dachs, an atypical myosin that helps orient cell division along the proximal-distal axis in fly wing (Baena-López et al., 2005; Mao et al., 2011). This in turn contributes to wing extension and likely causes tissue strain that can contribute to orienting PCP (Baena-López et al., 2005). However, the main mechanism by which the Ft/Ds/Fj pathway has been identified as a global regulator of PCP is through its ability to control the orientation of a polarized subapical non-centrosomal array of MTs within epidermal cells in the *Drosophila* wing and abdomen (Eaton et al., 1996; Harumoto et al., 2010; Turner and Adler, 1998).

Microtubules

MTs are used throughout development to break symmetry, and arrays of planar polarized MTs have been identified in many PCP-polarized tissues (Eaton et al., 1996; Hannus et

al., 2002; Vladar et al., 2012). In the case of the fly wing, plus ends of MTs within subapical arrays are slightly biased toward distal cell membranes before the onset of PCP protein asymmetry (Matis et al., 2014; Olofsson et al., 2014; Shimada et al., 2006). This bias was detected through an extensive analysis of the dynamics EB1-GFP comets, which track MT plus ends during polymerization (Harumoto et al., 2010; Stepanova et al., 2003). This slight bias in MT orientation biases the kinesin-based trafficking of vesicles containing Fmi, Fz, and Dsh distally, creating a slight excess of these proteins at distal membranes (Harumoto et al., 2010; Olofsson et al., 2014; Shimada et al., 2006). Importantly, in the fly the response that MTs and PCP proteins themselves have to gradients of Ft/Ds/Fj activity is determined through an unknown mechanism that responds to differential *Pk* isoform expression (Olofsson et al., 2014). For example, in the fly wing where Pk is dominantly expressed over the alternative splice form Pk-Sple, Vang and Pk localize to the proximal membrane, where Ft is localized. Unsurprisingly, *pk* mutant wings have severely disrupted wing hair patterning, whereas *pk-sple* mutant wings are normally polarized, indicating that Pk is normally the active isoform in the wing (Gubb et al., 1999). Overexpression of Pk in a *pk* mutant wing restores normal wing polarity whereas overexpression of Pk-Sple reverses the bias in the direction of EB1-GFP comets toward the proximal membrane, reverses Fz and Vang polarity, and ultimately disrupts trichome orientation (Olofsson et al., 2014). In the fly abdomen, where Pk-Sple is the dominant isoform, the above relationships are reversed. Thus, Ft/Ds/Fj expression and activity affects the orientation of subapical MT arrays as interpreted via an unknown mechanism that is dependent on Pk isoform expression. The biased orientation of MT plus ends towards distal membranes

enables the biased kinesin-based trafficking of Fmi/Fz/Dsh containing vesicles towards distal membranes. This initial asymmetry of PCP protein localization towards distal membranes is sufficient to enable the activities of core PCP proteins (discussed below) to amplify and stabilize the asymmetric distribution of membrane-associated PCP signaling complexes and establish a coordinated PCP axis across entire tissues. This PCP polarization in turn influences actin dynamics which work to asymmetrically localize trichome biogenesis to distal apical cell surfaces. Importantly, some aspects of this MT-dependent mode of PCP establishment appear to be conserved in vertebrates (Boutin et al., 2014; Sepich et al., 2011; Shi et al., 2016; Vladar et al., 2012). For example, injecting mouse embryonic brain ventricles with the MT-depolymerizing drug nocodazole at the onset of PCP protein asymmetry in ependymal cells disrupts the coordination of Celsr1 and Vangl2 polarization between cells (Boutin et al., 2014). Additionally, in mouse tracheal epithelial cells (MTECs), a MT network connects the neighboring BBs of motile cilia along apical membranes and helps organize and coordinate synchronized ciliary beating (Vladar et al., 2012; Werner et al., 2011). However, even in cases where MTs are essential for PCP establishment, PCP proteins themselves are needed for the polarization of MTs, so the link between PCP and MTs is not unidirectional (Chien et al., 2015; Olofsson et al., 2014; Vladar et al., 2012). Additionally, in the *Ciona* notochord, the PCP-dependent posterior positioning of nuclei and establishment of asymmetric Pk localization is not disrupted by treatment with nocodazole, suggesting that MTs are not needed for PCP establishment in some contexts (Newman-Smith et al., 2015). In this system, disruption of actin or myosin by cytochalasin or blebbistatin upsets nuclear polarization as well as asymmetric distribution of Pk

and Stbm, suggesting that alternative cytoskeletal components may be used to establish PCP in some contexts (Kourakis et al., 2014; Newman-Smith et al., 2015). Hence, though it is well-established that MTs function to enable the initial establishment of PCP protein asymmetry in *Drosophilia*, the mechanistic links between MTs and PCP signaling proteins are complex and may not be universally conserved.

Tissue Strain

Physical tissue strain during morphogenesis is one process that has been shown to orient PCP axes in multiple contexts (Aw et al., 2016; Mitchell et al., 2009). For example, in the *Xenopus* epidermis the PCP axis is initially defined by gastrulation forces, with core PCP protein complexes becoming most stable near cell junctions experiencing high strain (Mitchell et al., 2009). This polarization can reorient in response to exogenous strain, as *Xenopus* ectodermal explants localize Fzd3-GFP to cellular junctions aligned with applied tension (Chien et al., 2015). Additionally, forces generated through tissue deformation caused by cell division and rearrangements are able to reorient the polarity axis of Celsr1 localization within mammalian skin (Aw et al., 2016). Furthermore, in the fly wing, the axis of planar polarization reorients along the proximal-distal axis in response to tissue strain during wing hinge contraction and cellular elongation (Aigouy et al., 2010). The mechanism by which PCP orients in relation to tissue strain requires MTs, as *Xenopus* epidermal explants treated with nocodazole do not accumulate Fzd3-GFP at cellular junctions when exogenous strain is applied (Chien et al., 2015). Actin also appears to be involved as the actin regulators WDR1 and Cofilin1 are needed to

maintain cortical tension, and the loss of either prevents robust polarization of Vangl2 and Celsr1 in the mouse embryonic node (Mahaffey et al., 2013). Tissue strain may influence PCP dynamics through localizing endocytic recycling machinery. Rab11 is important for trafficking and recycling PCP components to apicolateral junctions (Strutt et al., 2011), and Rab11 planar polarizes towards the strain generated by the central fold of the neural plate during mouse neural tube closure (Mahaffey et al., 2013). Importantly, Rab11 does not localize towards sources of strain in the absence of PCP signaling, and DN-Rab11 disrupts actomyosin-based cell shape changes involved in wound healing (Ossipova et al., 2014). As mentioned above, in multiciliated cells of the *Xenopus* epidermis or mouse ependyma, extracellular forces generated by fluid flow can orient and strengthen planar polarity (Guirao et al., 2010; Mitchell et al., 2007, 2009). Regulation of polarity by tissue strain appears to be an effective way for animal tissues to coordinate certain cell movements regardless of developmental context and may be a conserved mechanism to establish planar polarity in some cases, but it seems unlikely to be the sole mechanism for coordinating global PCP patterning across entire tissues.

Wnts

An attractive yet elusive model for global PCP patterning is that gradients of Wnt ligands provide a polarizing cue for core PCP machinery, as Fz is itself a Wg receptor and Wnt gradients are often aligned to PCP axes (Adler et al., 1997; Lawrence et al., 2002; Sokol, 2015). Indeed, Fz and Dvl perform major roles in canonical Wnt signaling (for review see(Clevers and Nusse, 2012), which is why PCP signaling is sometimes referred to as the “non-canonical Wnt signaling

pathway". Non-canonical Wnt ligands that are primarily associated with PCP signaling include Wnt5- and Wnt11-like proteins in multiple systems (Chu and Sokol, 2016; Heisenberg et al., 2000; Ossipova et al., 2015; Qian et al., 2007). Aside from functioning as ligands for Fzd receptors, these Wnt proteins can regulate the post-translational modifications or stability of PCP proteins (Gao et al., 2011; Narimatsu et al., 2009). For example, Wnt5a promotes the association of Vangl2 with the tyrosine-protein kinase receptor Ror2 complex in the mouse limb, which promotes Vangl2 phosphorylation (Gao et al., 2011). Also in mouse, Wnt5a stimulates the phosphorylation of Dvl2, which causes it to colocalize with the apical polarity protein Par6 and ubiquitin ligase Smurf2 (Narimatsu et al., 2009). This complex in turn regulates Pk1 through promoting its ubiquitylation, which increases its degradation. These studies have demonstrated that Wnt proteins are involved in PCP-dependent processes, but whether Wnts play a permissive or instructive role in PCP remains controversial (Gao et al., 2011; Heisenberg et al., 2000; Ossipova et al., 2015; Qian et al., 2007; Wu et al., 2013). For example, in early fly wing development Fmi-Fz-Dsh complexes orient towards the source of Wg and Wnt4 at the wing margin, and clones expressing Wg or Wnt4 produce gradients that can establish PCP over many cell lengths (Wu et al., 2013). Similarly, in the *Xenopus* ectoderm Pk and Vangl orient away from ectopic Wnt5a, Wnt11, and Wnt11b, but not Wnt3a. (Chu and Sokol, 2016). Additionally, *wnt5a* mutant mice display cochlear sensory hair orientation defects (Qian et al., 2007), and *wnt11* mutant zebrafish display disrupted convergent extension during gastrulation (Heisenberg et al., 2000). However, ubiquitously expressed Wnt11 can largely restores WT phenotypes to *wnt11* mutant zebrafish, suggesting that Wnt11 performs a permissive rather

than instructive role. As Wnt signaling leads to different outcomes depending on cellular context, a clear mechanism through which Wnts may direct global PCP patterning remains to be resolved.

Mechanics of PCP Establishment and Maintenance

Transmembrane Core PCP Proteins

Once asymmetrically localized, the mutually attractive and repulsive behaviors of core PCP proteins are sufficient to amplify and maintain PCP intracellularly, as well as to coordinate this asymmetry between cells to generate cohesive tissues (Chen et al., 2008; Strutt and Strutt, 2008; Wu and Mlodzik, 2008). In *Drosophila,* the extracellular domains of Fz and Vang interact extracellularly through an association with the Fmi to propagate polarity information across cell boundaries (Chen et al., 2008; Lawrence et al., 2004; Strutt and Strutt, 2008; Usui et al., 1999). In pupal fly wings before the onset of planar polarity, both Fz and Dsh move from the cytoplasm to the cell cortex to form a symmetric apical ring of localization along cell boundaries (Axelrod, 2001; Strutt, 2001). Fmi, a non-classical cadherin localizes to these same plasma membranes, and at the onset of PCP, the cadherin repeat domains of Fmi interact extracellularly to promote the formation of Fmi homodimers at apical cell-cell junctions (Chen et al., 2008; Strutt and Strutt, 2008; Wu and Mlodzik, 2008). Formation of homodimers across cell membranes increases the stability of Fmi at cell junctions, where it is able to recruit and bind Fz and Vangl (Bastock et al., 2003; Strutt, 2001; Usui et al., 1999). Importantly, the association of Fmi with Vang and Fz is essential for the establishment of the stable polarity of each protein as Fmi is

diffuse in *fz, vang* double mutants and Vang and Fz are diffuse in *fmi* mutants (Bastock et al., 2003; Strutt, 2001; Strutt and Strutt, 2008; Usui et al., 1999). Fmi preferentially binds Fz over Vang, and Fmi-Fz complexes will bind either unbound Fmi or Fmi-Vang but not Fmi-Fz across cell membranes (Chen et al., 2008; Lawrence et al., 2004; Struhl et al., 2012; Strutt and Strutt, 2008). Thus, in the fly wing Fmi propagates intracellular PCP protein asymmetry across cell membranes by preferentially recruiting Fmi bound to the opposite core protein in neighboring cells. Once Fmi-Fz and Fmi-Vang become localized, they are progressively assembled into distinct signaling complexes through this positive feedback loop, strengthening the polarity of these proteins along the proximal to distal axis.

Cytosolic Core PCP Proteins

Though these positive intercellular interactions are enough to establish asymmetric localization of Fz and Vang across neighboring cells, this asymmetry must be amplified through positive and negative interactions between core cytosolic PCP proteins to be robustly stable throughout development. For example, Fmi recruits Fz to apicolateral regions of the cell, and the cytoplasmic tail of Fz binds the DEP domain of Dsh, which recruits Dsh to the membrane as well (Axelrod, 2001; Axelrod et al., 1998; Strutt, 2001). Fz and Fmi levels at junctional membranes decrease in *dsh* mutants, indicating that the association of Dsh with Fmi-Fz complexes increases complex stability at the membrane (Bastock et al., 2003; Strutt, 2001; Strutt and Strutt, 2008; Usui et al., 1999). The ankrin repeat region of Dgo in turn is able to bind to the PDZ domain of Dsh, and the association of all these proteins promotes local clustering of

Fmi-Fz-Dsh-Dgo complexes, which greatly stabilizes the localization of each protein on the membrane (Jenny et al., 2005). The second core membrane-localized PCP protein complex is composed of the proteins Vang and Pk. The c-terminal regions of these two proteins interact and this interaction increases binding between Vang and Pk but also homotypic binding of each protein to itself, thus increasing local clustering and stability at junctional membranes (Butler and Wallingford, 2015; Jenny et al., 2003). The c-terminal regions of Pk and Vang also associate with the PDZ domain of Dsh and the ankrin repeats of Dgo (Das et al., 2004; Jenny et al., 2005). As the c-terminus is what links Vang and Pk, it has been proposed that a negative feedback mechanism works by Pk inhibiting the association of Dsh with Fmi-Vang by competing for the same binding region on Vang, while Dgo competes with Pk to bind to Dsh (Das et al., 2004; Jenny et al., 2003, 2005). Additionally, Fz promotes the removal of Fmi-Vang-Pk complexes from the membrane where Fz has already accumulated (Cho et al., 2015). This negative feedback enables Fmi-Fz-Dsh-Dgo and Fmi-Vang-Pk complexes to exclude complementary sets of proteins from localizing to the same membrane, reinforcing the characteristic PCP pattern of alternating membrane-associated protein localizations along planar axes (Bastock et al., 2003; Tree et al., 2002).

Endocytic Flux of PCP Proteins

The localization of core PCP proteins is influenced and partially maintained by a process known as "endocytic flux," where membrane-bound proteins are continuously endocytosed, trafficked along MTs, and then either recycled to the membrane or degraded in lysosomes

(Butler and Wallingford, 2017). Endocytosis is a normal cellular behavior that removes unstable proteins from the membrane, and Rab5, clathrin, and dynamin have been shown to be involved in endocytosis of core PCP proteins (Classen et al., 2005; Mottola et al., 2010, Strutt and Strutt, 2008). The relationship between endocytosis and PCP is most clearly demonstrated when endocytosis is inhibited (through Rab5 dominant negative (DN) expression), which causes an overaccumulation of Fmi at the membrane, indicating that is an essential process for maintaining proper levels of PCP protein at the membrane (Strutt and Strutt, 2008; Strutt et al., 2011). Furthermore, Fmi is endocytosed more rapidly in *fz* and *vang* single and double mutants, as the loss of these proteins removes the stabilizing intercellular interactions and clustering properties that normally prevent Fmi internalization (Strutt and Strutt, 2008). Regulation of endocytic behavior is one mechanism by which PCP protein complexes establish their characteristic mutually-exclusive membrane localization patterning. For example, Pk stabilizes Fmi/Vang/Pk complexes at cell junctions by promoting clustering, but it can also facilitate the removal of unstable Vang from the membrane when it is ubiquitinylated by the Cullin1 SkpA and Slimb ubiquitin ligase complex, which causes endocytosis of Fmi-Vang-Pk complexes (Cho et al., 2015). This internalization is reduced in Fz mutants, as Fz can promote the removal of Fmi-Vang-Pk complexes from membrane regions where Fz is abundant (Cho et al., 2015; Strutt and Strutt, 2008; Strutt et al., 2011). Furthermore, disrupting the interaction between Dvl2 and the clathrin associated adaptor protein AP2 decreases Fzd4 internalization, which causes gastrulation defects in *Xenopus* (Simons et al., 2009; Wong et al., 2003; Yu et al., 2007). In mouse axon growth cones Vangl2 promotes the dephosphorylation and internalization of Fzd3,

and loss of Dvl1 disrupts Fzd3 phosphorylation and localization (Shafer et al., 2011). Furthermore, regulated endocytosis of PCP proteins is essential for maintaining PCP during cell rearrangements and divisions in multiple systems (Classen et al., 2005; Devenport et al., 2011). For example, during mitosis in the mouse epidermis the internalization of Celsr1 is regulated by Polo-like Kinase 1 (PLK1), which phosphorylates a dileucine motif on the cytoplasmic tail of Celsr1, promoting its endocytosis (Devenport et al., 2011; Shrestha et al., 2015). Vangl2 and Fzd6 are recruited to endosomes by Celsr1, which themselves are equally distributed to daughter cells and then returned to membranes, where they engage with neighboring polarized cells to reestablish PCP.

Once PCP proteins are endocytosed they can be recycled back to the membrane, sometimes after relocation across the cell through vesicular-based directed trafficking along MTs, or they can be degraded. For example, the clathrin adaptor protein AP1 as well as the GTPase ARF1 are involved in the trafficking of vesicles from the Golgi and endosomes, respectively, to the membrane, and each is required for normal PCP patterning (Carvajal-Gonzalez et al., 2015). Internalized Fmi colocalizes with Rabs 4, 5, 7, and 11, and both Rab 4 and 11 are involved in the recycling of Fmi back to the membrane whereas Rab 7 is required for its degradation (Classen et al., 2005; Strutt and Strutt, 2008; Strutt et al., 2011). Also, the deubiquitylating enzyme Fat Facet (Faf) helps maintain proper Fmi localization at junctional membranes by preventing Fmi accumulation in Rab5 positive endosomes and by promoting Fmi recycling to the membrane (Strutt et al., 2013). The degradation of damaged or excess PCP proteins contained in endocytic vesicles is the final stage of endocytic flux that can impact PCP.

For example, inhibiting lysosomal maturation leads to intracellular accumulation of Fmi, suggesting that it is subject to a level of constant degradation (Strutt and Strutt, 2008; Strutt et al., 2011). Vang modulates the degradation of Pk in *Drosophila* through a ubiquitylation mechanism involving Cullin1, and as such loss of Vang leads to an increase of cellular Pk protein levels (Cho et al., 2015; Strutt et al., 2013). This function is conserved in *Xenopus* epidermal cells as *pk* overexpression leads to an increase of Vang at cell junctions, but *vang* overexpression decreases Pk at these same junctions (Bastock et al., 2003; Butler and Wallingford, 2015). In sum, the endocytosis, recycling, as well as the regulated degradation of PCP proteins are all essential processes in the establishment and maintenance of PCP signaling in living tissues.

Are MTs required for PCP maintenance?

The asymmetric localization of PCP proteins is essential for the establishment of many planar polarized cellular processes, but the mechanism of maintaining these asymmetric PCP protein distributions after cells produce polarized structures and behaviors remains understudied. As discussed above, a body of evidence has tied oriented subapical MTs to the establishment of PCP protein polarity in the fly (Harumoto et al., 2010; Olofsson et al., 2014; Shimada et al., 2006). However, the asymmetric distribution of these PCP proteins is transient and rapidly dissipates after the formation of distal trichomes, limiting the study of MT function during PCP maintenance within this system. In vertebrate epithelia, the initial asymmetric patterning of PCP proteins at the membrane is often maintained beyond its establishment to

coordinate cellular structure or dynamic behavior (for review see (Butler and Wallingford, 2017; Davey and Moens, 2017)). Importantly, multiple recent studies suggest that the role of subapical MT networks in the establishment of PCP protein asymmetry is largely conserved in vertebrates, yet this work also suggests that the MT cytoskeleton is later dispensable for the maintenance of PCP protein asymmetry (Boutin et al., 2014; Sepich et al., 2011; Shi et al., 2016; Vladar et al., 2012). This is surprising, as endocytic flux of membrane-associated proteins is a ubiquitous and ongoing process within living cells, and trafficking of protein-containing vesicles along MTs is expected to be an integral part of this process (Butler and Wallingford, 2017). Importantly, none of these studies have made the requirement of MTs in PCP maintenance the focus of their investigation and leave many questions unanswered. Treatment of MTECs with the MT depolymerizing drug nocodazole at the onset of PCP protein asymmetry disrupts Vangl1 and Pk2 membrane polarity, whereas treatment after PCP is established appears to have no effect on Pk2 polarization (Vladar et al., 2012). Importantly, the differences between each condition were subtle and not quantitated, making interpretation of these results difficult. Additionally, epidermal and mesodermal cells undergoing convergent extension during zebrafish gastrulation have been shown to asymmetrically localize ectopically expressed *Drosophila* GFP-Pk to anterior membranes (Sepich et al., 2011). In this study, the localization of GFP-Pk was disrupted by 1hr nocodazole treatment early in gastrulation but was largely unaffected by treatments at later stages, after Pk has become asymmetrically localized to anterior membranes. Though this suggests that the maintenance of Pk is not dependent on polymerized MTs, it is unclear if Pk asymmetry would decrease with longer nocodazole

treatments. Finally, in the mouse oviduct epithelium, Vangl2-EGFP moves in cytosolic vesicles and enriches to ovarian side cell junctions (Shi et al., 2016). An apical network of stable MTs as well as a more dynamic subapical MT population has been observed in these cells and are thought to have conserved roles in PCP protein trafficking (Shi et al., 2014, 2016). Surprisingly, after a 24hr nocodazole treatment that disrupts dynamic MTs, Vangl2-EGFP remains asymmetrically enriched to ovarian side cell junctions, leading the authors to conclude that MTs are not needed for PCP maintenance. However, the authors do note that the stable apical MT network within these cells was still present after 24hrs of treatment, suggesting they did not actually fully disrupt cellular MTs, which calls their conclusion into question. In sum, though MTs have a well-established role in setting up initial PCP protein asymmetry in many systems, the requirement for MTs in maintaining this asymmetry has not been adequately investigated in any context.

The Zebrafish Floorplate as a Model for PCP

Does the maintenance of PCP protein asymmetry depend on the MT-based trafficking of vesicles during endocytic flux? Do PCP proteins only traffic on subapical MT arrays, or do they also use centrosomal MTs throughout the cytosol? What roles do stable versus dynamic MT populations play in PCP establishment and maintenance? How does the positioning of primary cilia with its associated BB/MTOC influence maintenance of PCP protein asymmetry? My work described in **Chapter 2** sought to address these questions in the planar polarized cellular context of the floorplate of the zebrafish neural tube.

The vertebrate floorplate is a small group of cells along the ventral midline of the neural tube that has major functions in the specification and patterning of neuronal cells (for review see (Placzek and Briscoe, 2005)). Early in neural tube development floorplate cells are stimulated by the notochord to secrete the glycoprotein sonic hedgehog (Shh), which forms a localization gradient along the dorsal-ventral axis of the neural tube that specifies neuronal and glial identities (Patten and Placzek, 2000). The floorplate also directs axonal trajectories through the secretion of Shh and netrin1 (Charron et al., 2003). Importantly, the floorplate uses PCP signaling to become highly planar polarized along the anterior-posterior axis, which can be determined by visualizing the posterior positioning of floorplate primary cilia and their associated BBs, as well as asymmetric localization of core PCP components within individual floorplate cells (Borovina et al., 2010; Davey et al., 2016; Walsh et al., 2011).

Our ability to visualize the *in vivo* dynamics of PCP proteins in the context of the polarized primary cilium makes the zebrafish floorplate an ideal model for the study of the complex interactions between PCP proteins, the MT cytoskeleton, and positioning of the primary cilium. Thus, I first characterized the progressive posterior polarization of floorplate cell primary cilia/BBs and found that this process requires not only Vangl2 but also Fzd3a. I next determined the subcellular distributions of GFP-Vangl2 and Fzd3a-GFP and found that GFP-Vangl2 asymmetrically localizes to anterior membranes whereas Fzd3a-GFP is equally distributed on anterior and posterior membranes but maintains a cytosolic enrichment at the base of the primary cilium. I discovered that vesicular Fzd3a-GFP is rapidly trafficked along MTs primarily toward the apical membrane during the period of PCP maintenance, whereas GFP-

Vangl2 is overall less dynamic, maintaining asymmetry at the membrane. Nocodazole-induced loss of MT polymerization disrupts BB positioning as well as GFP-Vangl2 localization and reduces cytosolic Fzd3a-GFP movements. Removal of nocodazole after MT disruption restores MT polymerization but does not restore BB polarity. Interestingly, GFP-Vangl2 repolarizes to anterior membranes and Fzd3a-GFP largely re-establishes normal dynamics after multiple hours of recovery, even in the context of mislocalized BBs. Together my findings challenge previous work by revealing an ongoing role for MT-dependent transport of PCP proteins in maintaining both cellular and PCP protein asymmetry during development.

Outcomes of a Planar Polarized Neuroepithelium

As discussed above, PCP signaling has a wide variety of roles in static epithelial contexts as well as during collective cell migration. Additionally, PCP signaling has been implicated in the directional migration of single cells during development, especially within the developing nervous system. Many neuronal types in the developing brain undergo some type of migration event, either radially along glial cells, or tangentially, within the plane of the epithelium in which they are present. One such migration is the tangential migration of facial branchiomotor neurons (FBMNs) in the vertebrate hindbrain. FBMNs are a group of cranial branchiomotor neurons that are born in rhombomere (r)4 and undergo a highly stereotyped posterior migration into r6 and r7, where they turn and migrate dorso-laterally to form the facial motor nucleus while extending axons out of r4 to innervate muscles derived from the second branchial arch (Chandrasekhar, 2004; Wanner and Prince, 2013). Work from our lab

demonstrated that FBMNs migrate through the plane of the neuroepithelium adjacent to the floorplate in while maintaining contact with neuroepithelial progenitors as well as with other migrating neurons (Grant and Moens, 2010). Importantly, neuroepithelial cells, including those within the floorplate, are highly polarized along the apico-basal and planar (anterior-posterior) axes (Borovina et al., 2010; Ciruna et al., 2006; Walsh et al., 2011).

It is well-established that many core PCP and PCP-related signaling components are required for the tangential migration of FBMNs. For example, in zebrafish, FBMNs fail to migrate in embryos with zygotic loss-of-function of Vangl2, Pk1b, Fzd3a, and Celsr2 (Bingham et al., 2002; Carreira-Barbosa et al., 2003; Jessen et al., 2002; Mapp et al., 2011; Rohrschneider et al., 2007; Wada et al., 2006). Additionally, Vangl2, Fzd3, Pk1, and Celsr have conserved roles in FBMN migration within the mouse hindbrain (Qu et al., 2010; Vivancos et al., 2009; Yang et al., 2014). Other PCP-related signaling components are required for FBMN migration, including the apical-basal polarity protein Scribble (Scrib), as well as the FBMN-specific PCP effector Nance-Horan syndrome-like 1b (Nhsl1b) (Wada et al., 2005; Walsh et al., 2011). However, how PCP signaling is used within FBMNs (cell-autonomously) and throughout their neuroepithelial environment (non-autonomously) is not well understood.

It stands to reason that PCP signaling could be used in several interdependent processes to enable FBMN migration. First, as one of the most established roles for PCP signaling is to orient actin-based cellular dynamics, FBMNs could use PCP to orient cellular protrusions and migration machinery to sense their cellular environment and physically transpose their cell

bodies. Indeed, Pk1b and Nhsl1b are expressed within FBMNs but not in their migratory environment, and chimeric analysis revealed cell-autonomous roles for each as well as for Vangl2 and Scrib in FBMN migration (Mapp et al., 2010; Walsh et al., 2011). Second, PCP signaling could be used to coordinate the polarity of the FBMN neuroepithelial migratory environment to provide polarized guidance cues during FBMN migration. Indeed, the neuroepithelium is highly planar polarized and non-cell autonomous roles for Vangl2, Fzd3a, Celsr2 have been identified for FBMN migration (Bingham et al., 2002; Carreira-Barbosa et al., 2003; Mapp et al., 2011; Qu et al., 2010). It is likely that either of these roles would require an active maintenance of PCP protein as well as downstream signaling factor asymmetry within one or both cellular contexts during migration. Though PCP signaling has roles in directing FBMN migration, the mechanisms through which PCP signaling is used during this dynamic process are not well-understood. Thus, the goal of my work presented in **Chapter 3** sought to better understand how PCP signaling is used within both migrating FBMNs and their polarized neuroepithelial environment to orient and enable their tangential migration. Together, our findings led us to propose the model in which FBMN migration uses the canonical transmembrane interactions of Vangl2 and Fzd3a between migrating FBMNs and their polarized neuroepithelial environment to regulate FBMN filapodial dynamics and thus enable signaling and/or adhesion for directional migration.

Chapter 2: Microtubules are required for the maintenance of planar cell polarity in monociliated floorplate cells.

Andrew W. Mathewson[1], Daniel Berman, Cecilia B. Moens*

Division of Basic Science, Fred Hutchinson Cancer Research Center, Seattle, Washington, United States of America

[1] Molecular and Cellular Biology Graduate Program, University of Washington, Seattle, Washington, United States of America

*Corresponding author

E-mail: cmoens@fhcrc.org

Abstract

The asymmetric localization of planar cell polarity (PCP) proteins is essential for many cellular processes, but the mechanisms that maintain these asymmetric distributions remain poorly understood. A body of evidence has tied oriented subapical microtubules (MTs) to the establishment of PCP protein polarity, yet recent studies have suggested that the MT cytoskeleton is later dispensable for the maintenance of this asymmetry. As MTs underlie the vesicular trafficking of membrane-bound proteins within cells, the requirement for MTs in the maintenance of PCP merited further investigation. We investigated the complex interactions between PCP proteins and the MT cytoskeleton in the context of the zebrafish neural tube floorplate whose planar polarization is conspicuous in the posterior localization of the primary cilium and its basal body, which also serves as the MT organizing center of the cell. We demonstrated that the progressive posterior polarization of the primary cilia of floorplate cells requires not only Vangl2 but also Fzd3a. We determined that GFP-Vangl2 asymmetrically localizes to anterior cell membranes whereas Fzd3a-GFP is not detectably asymmetric at the cell membrane but maintains a cytosolic enrichment in vesicles that cluster at the base of the primary cilium. Vesicular Fzd3a-GFP is rapidly trafficked along MTs primarily toward the apical membrane during a period of PCP maintenance, whereas vesicular GFP-Vangl2 is less frequently observed. Nocodazole-induced loss of MT polymerization disrupts basal body positioning as well as GFP-Vangl2 localization and reduces cytosolic Fzd3a-GFP movements. After removal of Nocodazole, GFP-Vangl2 planar polarization and Fzd3a-GFP vesicular dynamics recover but basal bodies remain unpolarized. Together our findings challenge previous work by revealing an

ongoing role for MT-dependent transport of PCP proteins in maintaining both cellular and PCP protein asymmetry during development.

Introduction

Cellular polarization is a fundamental aspect of development that enables cells to organize intracellularly and perform specialized behaviors in response to their cellular context. Planar cell polarity (PCP) describes one aspect of cellular polarization and it is best understood in epithelial tissues. Epithelia exhibit two types of cellular polarity: apicobasal polarity, which defines polarity across the epithelium, and PCP, which is cell polarization in the plane of the epithelium and is orthogonal to the apicobasal axis. Coordinated planar polarization in epithelia is essential for development of a wide variety of animal tissues, as it allows cells to synchronize their growth and behavior to form functional and specialized organs. The components of the PCP signaling pathway were originally discovered in *Drosophila* mutants that displayed misoriented and supernumerary actin-based hairs and bristles on the adult wing and legs (Gubb and García-Bellido, 1982). A highly conserved signaling pathway, PCP has been implicated in a growing number of developmental processes including but not limited to the orientation and angle of mammalian skin hair follicles (Devenport and Fuchs, 2008), inner ear sensory hair orientation (Etheridge et al., 2008; Montcouquiol et al., 2003), directed migration of neuronal cells (Calisto et al., 2005; Davey et al., 2016; Jessen et al., 2002) and collective movements of multiple cell types during gastrulation (Heisenberg et al., 2000; Tada and Smith, 2000; Wallingford and Harland, 2001) and neural tube closure (Curtin et al., 2003; Wallingford and

Harland, 2001; Wang et al., 2006), as well as cilia positioning and directional ciliary beating in trachea (Vladar et al., 2012), oviducts (Shi et al., 2014, 2016), and the central nervous system (Borovina et al., 2010; Boutin et al., 2014).

The PCP signaling pathway functions at the protein level to polarize subcellular information intracellularly and propagate this information through direct cell-cell interactions, which result in locally coordinated tissue polarity (Tree et al., 2002). The classic "core" PCP pathway of the fly wing is composed of two membrane-localized protein complexes, the distally-localized Frizzled (Fz or Fzd in vertebrates), Dishevelled (Dsh or Dvl in vertebrates), Diego (Dg, or Diversin in vertebrates) complex and the proximally localized Van Gogh/Strabismus (Vang/Stbm, or Vangl in vertebrates), Prickle (Pk) complex (for review see (Goodrich and Strutt, 2011)). Flamingo (Fmi or Celsr in vertebrates), localizes to both proximal and distal membranes and is essential for mediating the extracellular interactions between PCP signaling complexes. These PCP protein complexes sort into complementary and mutually exclusive distributions along the cell cortex, with Fmi-Fz-Dsh-Dgo localizing to distal membranes and Fmi-Vang-Pk on proximal membranes (Strutt and Strutt, 2007; Strutt et al., 2002). This conserved pattern of asymmetrically localized core PCP protein complexes underlies most planar polarized epithelial tissues, and can be visualized by immunostaining or through imaging of ectopically-expressed fluorescently-fused PCP proteins (Butler and Wallingford, 2017; Davey and Moens, 2017). The intracellular organization of core PCP proteins is dependent on "endocytic flux," where membrane-bound proteins are continuously endocytosed, trafficked along MTs, and then either recycled to the membrane or degraded in lysosomes ((Classen et al.,

2005; Mottola et al., 2010, Strutt and Strutt, 2008) for review see Butler and Wallingford, (2017)). Precise control and maintenance of PCP protein distribution may be essential for ongoing planar polarized cellular processes including neuronal migration (Davey et al., 2016), but the mechanisms by which any cell type maintains PCP asymmetry remain understudied.

MTs are used throughout development to break symmetry, and arrays of planar polarized MTs have been identified in many PCP-polarized tissues (Eaton et al., 1996; Hannus et al., 2002; Vladar et al., 2012). In the case of the fly wing, plus ends of subapical MTs bias slightly toward distal cell membranes before the onset of PCP protein asymmetry (Matis et al., 2014; Olofsson et al., 2014; Shimada et al., 2006). This slight bias in MT orientation biases the kinesin-based trafficking of vesicles containing Fmi, Fz, and Dsh distally, creating a slight excess of these proteins at distal membranes (Harumoto et al., 2010; Olofsson et al., 2014; Shimada et al., 2006). This initial asymmetric bias is sufficient to enable the mutually attractive and repulsive behaviors of core PCP proteins to amplify and maintain PCP protein organization intracellularly, as well as to coordinate this asymmetry between cells to generate cohesive tissues (Chen et al., 2008; Strutt and Strutt, 2008; Wu and Mlodzik, 2008).

Multiple recent studies suggest that the role of subapical MT networks in the establishment of PCP protein asymmetry is conserved in vertebrates, yet this work also suggests that the MT cytoskeleton is later dispensable for the maintenance of PCP protein asymmetry (Boutin et al., 2014; Sepich et al., 2011; Shi et al., 2016; Vladar et al., 2012). This is surprising, as endocytic flux of membrane-associated proteins is a ubiquitous and ongoing

process within living cells, and trafficking of protein-containing vesicles along MTs is expected to be an integral part of this process (Butler and Wallingford, 2017). Our ability to visualize the *in vivo* dynamics of PCP and MT fluorescent fusion proteins after cellular PCP has been established makes the zebrafish floorplate an ideal model for the study of the complex interactions between PCP proteins, the MT cytoskeleton, and control of cellular architecture.

In this work, we characterize the progressive posterior polarization and subsequent maintenance of floorplate polarity and find that this process requires not only Vangl2 but also Fzd3a. Using live imaging in the zebrafish floorplate we describe the MT-dependent localization and trafficking of Vangl2 and Fzd3a during the period of PCP maintenance. Nocodazole-induced loss of MT polymerization disrupts primary cilia basal body (BB) positioning as well as PCP protein localization and dynamics, demonstrating for the first time an ongoing requirement for MTs in the maintenance of PCP protein localization. Consistent with this, after removal of nocodazole PCP protein asymmetry and dynamics are recovered. Interestingly, however, cellular asymmetry (detectable in the localization of the basal body) never recovers, indicating that although PCP proteins traffic on MTs, a polarized MTOC is non-essential for the re-establishment of molecular asymmetry (detectable at the level of PCP protein localization). Together our findings challenge previous work by revealing an ongoing role for MT-dependent transport of PCP proteins in maintaining both cellular and PCP protein asymmetry during development.

Methods

Ethics statement

The Fred Hutchinson Cancer Research Center Institutional Animal Care and Use Committee (IACUC) follow the guidelines of the Office of Laboratory Animal Welfare and set its policies according to The Guide for the Care and Use of Laboratory Animals. Fred Hutchinson Cancer Research Center maintains full accreditation from the Association for Assessment and Accreditation of Laboratory Animal Care (AAALAC) and has letters of assurance on file with OLAW. The IACUC routinely evaluates the Fred Hutchinson animal facilities and programs to assure compliance with federal, state, local, and institution laws, regulations, and policies. The OLAW Assurance number is D16-00142.

Zebrafish Lines and maintenance

Zebrafish (*Danio rerio*) were raised at the Fred Hutchinson Cancer Research Center, and animal care and experiments were approved by the Institutional Animal Care and Use Committee. All animals were maintained according to standard procedures (Westerfield, 2000) and staged as previously described (Kimmel et al., 1995). All mutant lines used were previously described and are registered at The Zebrafish International Resource Center (ZIRC): *fzd3a*^{rw689} (*olt*^{rw689}) (Wada et al., 2006), and *vangl2*^{m209} (*tri*^{m209}) (Jessen et al., 2002).

Cloning and transgenic line generation

The following transgenic lines were generated for this study: *Tg(shh:Gal4VP16)fh445* (Davey et al., 2016), *Tg(uas:GFP-Vangl2)fh453, Tg(uas:mkate2-Vangl2)fh496, Tg(uas:Fzd3a-GFP)fh497, Tg(uas:Fzd3a-mEOS)fh499, Tg(uas:EB3-mkate2)fh500, Tg(uas:p50p2a-eGFPCAAX)fh501*. Transgenic elements were cloned using the Gateway (Life Technologies) system using the gene specific primer sequences listed in

Supp. Table 1. Final DNA constructs were assembled in the pDESTpBHR4R3 plasmid (gift from the Brockerhoff Lab). Transgenic embryos were generated by Tol2 transposase RNA co-injection with each plasmid at the single cell stage (Kawakami et al., 2000).

Drug treatments

Nocodazole treatments were done using a modified protocol from McFarland et al., (2017). Briefly, nocodazole (Sigma) solutions were prepared fresh in DMSO and diluted in embryo media (Westerfield, 2000), with final concentrations of 5ng/mL and placed on ice. Embryos were anesthetized and placed in 60mm polystyrene petri dishes (Fisher Scientific) on ice. Embryo media was removed from embryos and replaced with 3mL ice cold nocodazole or DMSO solution for the duration of drug treatment. Embryos were removed from ice after treatment and were either fixed immediately or washed at least 4x in room-temperature embryo media. Embryo recovery periods occurred in embryo media in a 28°C incubator. Importantly, within minutes of removal from ice, treated embryos fully recover from multiple hours on ice (data not shown).

Whole-mount immunohistochemistry

Anesthetized zebrafish embryos were fixed in 2% trichloroacetic (TCA) acid for 3 hours or 4% paraformaldehyde (PFA)/4% sucrose in PBS for 1 hour at room temperature. Fixed tissue was washed in PBS + 0.5% TritonX100, brain tissue was dissected and then blocked by standard antibody incubations. Following staining, tissue was cleared step-wise in a 25%, 50%, 75% glycerol series and mounted for confocal imaging. The following antibodies were used: chicken anti-GFP (1:500, Abcam Cat# ab13970); rabbit anti-ZO-1 (1:500, Zymed Cat# 61–7300); mouse anti-Cc2d2a (1:100, (Bachmann-Gagescu et al., 2011)); rabbit anti-RFP (1:1000, Abcam Cat# ab62341) (cross reacts with mkate2); mouse anti-acetylated

tubulin (1:2000, Sigma Aldrich Cat# T6793) and rabbit anti-alpha tyrosinated tubulin (1:500, Millipore Cat# ABT171).

Imaging and data analysis

Imaging was performed using a Zeiss 700 confocal microscope with a 40x C-Apochromat 1,2 W-Korr UV-Vis-IR water immersion objective with the Zen 2010 software package. BB Polarity indices were determined by dividing the distance between the anterior cell membrane and the position of the BB by the distance between the anterior and posterior membranes at the level of the BB. For time-lapse imaging, short Z-stack images at 0.50 µm steps were captured every 5 seconds until photobleaching of fluorescent proteins hindered image acquisition. Live lateral imaging was limited to floorplate cells in the posterior halves of animals as the increased body thickness of the anterior halves of embryos obscures imaging of the medially located floorplate. Imaging of fluorescent fusion proteins was performed in isolated expressing cells in mosaically expressing embryos generated via plasmid injection or in stable transgenic lines that exhibited UAS silencing (Goll et al., 2009). Z-stacks of whole cell fluorescence were obtained and analyzed for polarized GFP-Vangl2 or Fzd3a-GFP localization. Anterior versus posterior asymmetry of GFP-Vangl2 and Fzd3a-GFP localization was measured by drawing ROIs on cell anterior and posterior halves and recording average pixel intensity with the plot profile tool in ImageJ (schematic, **Fig 2c**) (Schneider et al., 2012). Anterior versus posterior membrane enrichment of GFP-Vangl2 and Fzd3a-GFP was determined by measuring fluorescence intensities of maximum intensity projections using a 1µm wide trace along anterior and posterior membranes in ImageJ (schematic, **Fig 2d**). To visualize Fzd3a localization in the context of p50-p2a-eGFPCAAX we photoconverted Fzd3a-mEOS to red fluorescence. As p2a sequences are cleaved during translation (Kim et al., 2011) we used eGFPCAAX localization to determine the position of the primary cilia along the apical membranes of

floorplate cells co-expressing both transgenes. Fzd3a-GFP puncta dynamics were tracked and recorded using the MTrackJ plugin in ImageJ (Meijering et al., 2012). Movies were corrected for bleaching and levels were adjusted in ImageJ. All movies were exported as AVIs at 7 frames/sec. Graphs were generated and statistics were computed using GraphPad Prism software. All statistical analyses were performed using a 95% confidence interval. Figure images and diagrams were created using Zeiss Zen software, ImageJ, Adobe Photoshop CC, and Adobe Illustrator CC.

Kymographs

Kymographs of Fzd3a-GFP vesicular trafficking along MT tracks were generated in ImageJ from time-lapse movies by tracing 1µm wide segmented user-drawn lines along MTs that were then superimposed on the corresponding fluorescently labeled PCP protein channel, straightened, and then timepoints were combined into montages. Kymograph traces were generated using the multi-kymograph overlay ImageJ plugin.

Rose-plots

Overall vesicle displacement directionality was determined by measuring the angle between the first and last positions of tracked Fzd3a-GFP vesicles. Rose plots were generated using the polarhistogram function in MatLab (https://www.mathworks.com/help/matlab/ref/polarhistogram.html). Outer plot numbers reflect relative angle of displacement while internal numbers indicate number of vesicles counted that were displaced at those relative angles, grouped into 15 degree bins. Apical movement defined as displacement between 45 and 135 degrees, anterior defined as 135 to 225 degrees, basal defined as 225 to 315 degrees, and posterior defined as 315 to 45 degrees.

Results

The floorplate is progressively planar polarized in a Vangl2 and Fzd3a-dependent manner

Previous studies establish that the apically docked BB of the primary cilium is asymmetrically localized toward the posterior side of floorplate cells in zebrafish by two days post-fertilization (dpf), and that this polarity requires planar cell polarity (PCP) signaling (Borovina et al., 2010; Davey et al., 2016; Walsh et al., 2011)**(Fig 1a-d)**. The position of the primary cilium can be visualized *in vivo* through live imaging of floorplate cells expressing membrane-localized fluorescent proteins **(Fig 1c, Supp Movie 1)**, and the position of the BB can be determined in fixed tissue using a Cc2d2a antibody that localizes to the transition zone of the primary cilium, adjacent to the BB (Bachmann-Gagescu et al., 2011)**(Fig 1d)**. To understand the timing during which the BB becomes posteriorly localized, we assessed BB localization in fixed embryos at various stages of development. As early as the 10-somite stage (ss, equivalent to 14 hours post fertilization, hpf), the initial timepoint at which we can identify and image floorplate cells in the developing embryo, BBs within floorplate cells have docked at apical membranes and are localized towards cell posteriors (polarity index: 0.72, n=125 cells, 12 embryos, see methods; **Fig. 1e**). The BB becomes progressively more posteriorly localized from the 10ss until 30 hpf, at which point BBs display a polarity index of 0.84 (n=206 cells, 12 embryos). After this time the position of the BB is maintained through the end of our analysis at 72hpf ($p>0.9999$, n=100 cells, 10 embryos) **(Fig 1e).** We thus define the period between 30 and 72 hpf as the maintenance phase of floorplate planar polarity.

Floorplate planar polarization is critically dependent on the core PCP transmembrane protein Vangl2 as has been shown previously (Borovina et al., 2010; Davey et al., 2016), and we quantified this requirement using our polarity index measurement (Vangl2 polarity index: 0.47, $p<0.0001$, n=100 cells, 10 embryos) **(Fig 1g)**. We also found that the opposing transmembrane core component, Fzd3a, is required for floorplate planar polarization, although less dramatically, suggesting a possible redundancy with other Fzd proteins in the floorplate (polarity index: 0.67, $p=0.0018$, n=198 cells, 19 embryos) **(Fig 1f-g)**. Taken together, we find that the zebrafish floorplate becomes progressively polarized through a Fzd3a and Vangl2-dependent mechanism that positions BBs near the posterior apical membrane by 30hpf, and that this polarity is maintained at least until 72hpf.

Vangl2 and Fzd3a localization in the floorplate

One of the characteristics of the PCP pathway is that cellular asymmetry, which in the floorplate is reflected in the position of the BB, is underlain by molecular asymmetry of the PCP core components themselves. To understand how floorplate cellular asymmetry is established and maintained, we examined the dynamics of Vangl2 and Fzd3a localization in live zebrafish embryos using fluorescent fusion proteins. Use of mosaic expression of fusion proteins to visualize PCP protein distributions in vertebrate epithelia enables anterior and posterior membranes of irregularly shaped cells to be distinguished from the membranes of adjacent non-expressing cells (Davey et al., 2016; Roszko et al., 2009). We previously reported that within the floorplate, GFP-Vangl2 (corroborated by Vangl2 immunostaining) and Fzd3a-GFP are

planar polarized to the anterior and posterior apical sides of floorplate cells, respectively (Davey et al., 2016). In order to quantify the dynamics of this polarization we used *Tg(shh:Gal4VP16)* embryos, which express Gal4 in the floorplate under control of the Ar-B sonic hedgehog (shh) enhancer element (Davey et al., 2016; Ertzer et al., 2007)**(Fig 1a)**. We generated *Tg(shh:GAL4VP16); Tg(uas:GFP-Vangl2); Tg(uas:mAppleCAAX);* and *Tg(shh:GAL4VP16); Tg(uas:Fzd3a-GFP); Tg(uas:mAppleCAAX)* embryos that co-express either GFP-Vangl2 or Fzd3a-GFP along with the membrane marker mAppleCAAX in floorplate cells to visualize PCP protein localization (green) relative to the membrane (red) in isolated expressing cells. We found that at 48 hpf GFP-Vangl2 is significantly polarized to the anterior half of the cell (p=0.0035, n=54 cells, 12 embryos) whereas Fzd3a-GFP localizes to the posterior half (p=0.0266, n=59 cells, 25 embryos), when compared to the non-polarized localization of mAppleCAAX (n=39 cells, 20 embryos) **(Fig 2a-c).** This asymmetry is even more dramatic for GFP-Vangl2 when we considered 1 µm wide areas encompassing the anterior and posterior membranes themselves (mean anterior/posterior (A/P) expression ratio of 1.8 (p=0.0154, n=18 cells, 10 embryos compared to mAppleCAAX: average ratio of 1.1 (n=29 cells, 13 embryos), **Fig 2d**, see methods). However, we were unable to detect Fzd3a-GFP asymmetry at the posterior membrane. Therefore, the Fzd3a-GFP asymmetry we observed when measuring the posterior half of the cell (**Fig 2c** and (Davey et al., 2016)) represents an asymmetrically localized *cytosolic* pool of the protein.

To examine the localization of this cytosolic pool of Fzd3a-GFP and to correlate it with cellular planar polarity as detected by mAppleCAAX in the motile primary cilium **(Fig 1c, Supp Movie 1)**, we imaged the floorplate in live 48hpf *Tg(shh:GAL4VP16); Tg(uas:Fzd3a-GFP);*

Tg(uas:mAppleCAAX) embryos **(Fig 2e)**. Measuring pixel intensity in a 3 µm wide band along the apical surface of the cell **(Fig 2f,** see methods), we found that peak apical Fzd3a-GFP localization is highly correlated with the position of the primary cilium at 48hpf (r^2=0.79, n=96 cells, 16 embryos) **(Fig. 2f, Supp Movie 2)**. Previous studies have identified interactions between the BB and core PCP components that localize near the BB (Butler and Wallingford, 2015; Hashimoto et al., 2010; Park et al., 2008; Vladar et al., 2012; Werner and Mitchell, 2012), suggesting that BB could be influencing Fzd3a dynamics within floorplate cells.

Planar polarized Fzd3a and Vangl2 exhibit different dynamics in the floorplate

Live imaging also showed that cytosolic Fzd3a-GFP localizes to highly dynamic puncta (each puncta defined as a point of local signal intensity ranging from 0.4—0.7um in diameter that can be traced across multiple timepoints) that concentrate around the base of the primary cilium **(Supp Movies 2 & 3)**. We hypothesized that these puncta were Fzd3a-GFP-containing vesicles undergoing MT-based transport during the endocytosis, recycling, and degradation processes of ongoing endocytic flux (Strutt et al., 2011). Therefore, we generated *Tg(shh:GAL4VP16); Tg(uas:mApple-Rab5c); Tg(uas:Fzd3a-GFP)* and *Tg(shh:GAL4VP16); Tg(uas:mAppleRab7); Tg(uas:Fzd3a-GFP)* embryos and found that Fzd3a-GFP puncta colocalize with both Rab5c- and Rab7-bound vesicles **(Supp Movies 4 & 5)**. As Rab5 is a marker of early endosomes and Rab7 is associated with late endosomes destined for lysosomal degradation, and both have been found to colocalize with PCP proteins in other contexts, these data are

consistent with the model that maintenance of core PCP protein asymmetry requires ongoing endocytic flux (Mottola et al., 2010; Strutt and Strutt, 2008; Strutt et al., 2011).

Given the role of the BB as a cellular microtubule organizing center (Badano et al., 2005), and given the role that MTs play in the establishment of PCP via directional trafficking of PCP proteins including Fzd (Harumoto et al., 2010; Matis et al., 2014; Olofsson et al., 2014; Shimada et al., 2006), we examined the organization of MTs in floorplate cells to discover their role in floorplate planar polarization. MTs are composed of αβ-tubulin heterodimers that are modified post-translationally to influence MT stability and function (Westermann and Weber, 2003). The subunits of nascent and dynamic MTs are typically tyrosinated, whereas stable MTs become de-tyrosinated and acetylated over time (Bulinski and Gundersen, 1991; Westermann and Weber, 2003). To identify which MT populations are present within the floorplate at 30 hpf we used established antibody protocols ((McFarland et al., 2017), see methods) to visualize acetylated and tyrosinated tubulin localization. Confocal imaging confirmed the acetylation of primary cilia and revealed a dense cloud of tyrosinated tubulin originating at the base of the primary cilium and extending throughout the cytoplasm of floorplate cells **(Supp Fig 1a-b)**. These findings are consistent with the BB functioning as the microtubule organizing center (MTOC) at this stage of floorplate development, as tyrosinated tubulin is a marker of dynamic tubulin populations associated with MT nucleation.

Visualizing floorplate MTs by immunohistochemistry does not capture their dynamics or the dynamics of vesicle trafficking along them. Thus, we expressed EB3-mkate2, which marks

MT plus-ends (Stepanova et al., 2003) in the floorplate in *Tg(shh:GAL4VP16); Tg(uas:EB3-mkate2)* embryos at 30 hpf **(Supp Fig 1b, Supp Movie 6**) and 48hpf **(Supp Movie 7)** and observed dynamic EB3 comets spreading throughout the cytoplasm from the posterior apical region of most cells. This region corresponds to the location where the BB is most frequently observed in floorplate cells, again consistent with the BB acting as the primary MTOC at this stage. EB3-mkate2 comets are slowly occluded by the accumulation of EB3-mkate2 along non-centrosomal bundles of MTs at later time points, enabling clear visualization of MT organization *in vivo* **(Supp Fig 1b, Supp Movie 8)**. GFP-Tubulin also localizes to MTs when expressed in floorplate cells but also maintains a diffuse cytosolic population of free GFP-tubulin subunits, making it less ideal for visualizing distinct MT networks **(Supp Fig 1b)**.

We next considered whether the dynamic Fzd3a-GFP-containing vesicles we detected in floorplate cells are undergoing MT-based trafficking. By live imaging of Fzd3a-GFP puncta and EB3-mkate2 MTs in *Tg(shh:GAL4VP16); Tg(uas:EB3-mkate2); Tg(uas:Fzd3a-GFP)* embryos we determined that dynamic Fzd3a-GFP vesicles are indeed strongly associated with MTs by 48 hpf (n=240 vesicles, 89 cells, 9 embryos). Fzd3a-GFP vesicles move bidirectionally along MT tracks with frequent periods of stalling and switching between MT tracks at junctions **(Supp Movie 9; Fig. 3a-b)**. We sought to characterize the dynamics of the overall vesicular population of Fzd3a-GFP by tracking individual puncta throughout time lapse movies to determine average Fzd3a-GFP vesicle velocities, displacement, and directionality. Overall Fzd3a-GFP vesicle movements measured at 30, 48, and 60 hpf are biased towards the apical membrane of floorplate cells, with 48% of all vesicles tracked (n=240 vesicles, 89 cells, 9 embryos) moving in the apical

quadrant between first and last timepoints measured **(Fig 3c)** (see methods). Normalized vesicle displacement was quantified as a measure of perdurance of vesicular motion by dividing the distance between the first and last tracked positions of each vesicle by the total time the vesicle was tracked. Between 30, 48, and 60hpf, average vesicular displacement does not significantly change (p=0.1094, 30hpf compared to 60hpf), with an overall average displacement in a one-minute time interval of 2.4µm **(Fig 3d)**. Average vesicle velocity varies across timepoints with vesicles moving significantly faster at 30hpf with an average velocity of 0.09µm/sec (n=66 vesicles, 27 cells, 4 embryos) compared to 0.07µm/sec at 48hpf (p=0.0023, n=69 vesicles, 29 cells, 2 embryos) and at 60hpf (p<0.0001, n=102 vesicles, 33 cells, 3 embryos) **(Fig 3e)**.

Whereas much of Fzd3a-GFP localizes in dynamic MT-associated vesicles, GFP-Vangl2 is predominantly localized to the anterior apical membrane between 30 and 72hpf**.** However, in rare instances we were able to detect individual dynamic vesicular GFP-Vangl2 in Tg(*shh:Gal4VP16); Tg(uas-GFP-Vangl2)* embryos, suggesting intracellular trafficking of vesicular Vangl2, like that of Fzd3a, is ongoing during PCP maintenance within the floorplate **(Fig 3h; Supp Movie 11)**. However, the rarity of these vesicles and their susceptibility to photobleaching limited our ability to further investigate the dynamics of vesicular GFP-Vangl2 or to correlate their localization with MTs.

Microtubules are required to maintain floorplate PCP

The role of MTs in maintaining PCP protein asymmetric localization after its establishment, or in re-establishing PCP protein asymmetry after it has been disrupted, is controversial (Newman-Smith et al., 2015; Sepich et al., 2011; Shi et al., 2016; Vladar et al., 2012). The defined maintenance phase of floorplate planar polarity from 30-72 hpf gave us the opportunity to assess the role of MTs in polarity maintenance in a monociliated cell in vivo. We used a modified nocodazole treatment protocol, in which embryos are exposed to 5ng/ml ice cold nocodazole for one hour to inducibly disrupt MTs in live embryos (McFarland et al., 2017). This treatment fully disrupts MTs as visualized live in *Tg(shh:GAL4VP16); Tg(uas:GFP-Tubulin)* and *Tg(shh:GAL4VP16); Tg(uas:EB3-mkate2)* embryos: GFP-Tubulin becomes diffusely cytoplasmic **(Supp Fig 2a)** and EB3-mkate2 contracts to subapical puncta which correspond to the position of the remnant BB/MTOC **(Fig 4a)**. In contrast, treating embryos with nocodazole at room temperature for 1 hour, even at increased concentrations of 20ng/ml, only partially disrupts MTs, while treating embryos on ice for 1hr in the absence of the drug has no effect on MTs **(Supp Fig 2b)**. After 1hr cold nocodazole treatment, floorplate BBs become significantly unpolarized compared to DMSO treated controls, with an average polarity index of 0.64 ($p=0.0011$, n=100 cells, 10 embryos) **(Fig 4b-c)**. Failure to maintain BB polarization could be because of loss of PCP protein localization and consequent loss of cellular planar polarization, or it may be due to a more direct role for MTs in anchoring the BB to the posterior membrane as has been proposed (Vladar et al., 2012). To investigate the role of MTs in the maintenance of PCP protein asymmetry, we treated 30hpf *Tg(shh:GAL4VP16); Tg(uas:GFP-Vangl2*) and *Tg(shh:GAL4VP16); Tg(uas:Fzd3a-GFP)* embryos with cold nocodazole at 30 hpf and examined

GFP-Vangl2 and Fzd3a-GFP localization. Fzd3a-GFP vesicles exhibit reduced motility but remain associated with the BB after nocodazole treatment, even though the BB itself becomes unpolarized within the cell (**Fig. 4d,f-h; Supp Fig 4; Supp Movie 12).** Importantly, after 1hr of treatment, GFP-Vangl2 becomes significantly less polarized to anterior membranes with an A/P membrane ratio of 1.2 (p=0.0013, n=166 cells, 21 embryos) compared to an A/P membrane ratio of 1.4 in DMSO controls at this stage (n=202 cells, 24 embryos) **(Fig 4e, i-j).** Thus contrary to previous reports (Shi et al., 2016; Vladar et al., 2012), Vangl2 polarization is actively maintained in a MT-dependent manner. Notably, a cytosolic population of GFP-Vangl2 that is faintly detectable around the BB in control embryos becomes progressively concentrated there during nocodazole treatment concurrent with the retraction of MTs (**Fig. 4e, k**), consistent with a MT-dependent Vangl2 trafficking mechanism. Together our results suggest that asymmetric distribution of Vangl2 is actively maintained in a MT-dependent manner.

As nocodazole treatment disrupts MTs throughout the entire embryo, the changes we observe in floorplate PCP could be influenced by loss of MTs in other tissues. Therefore, we sought a method to disrupt MT-based vesicular trafficking specifically in the floorplate. P50, or dynamitin, is a subunit of the motor protein dynein that when overexpressed functions as a dominant-negative (DN) for dynein-based minus end-directed trafficking of cargo along MTs (Burkhardt et al., 1997; Tsujikawa et al., 2007). We hypothesized that disrupting directed trafficking of vesicles along MTs would affect floorplate PCP, since we found that Fzd3a-GFP is actively trafficked along MTs (**Fig 3a-c**). p50 expression significantly disrupts BB localization when expressed in the floorplate in *Tg(shh:GAL4VP16); Tg(uas:p50p2a-eGFPCAAX)* embryos

with an average BB polarity index of 0.55 ($p<0.0001$, n=116 cells, 10 embryos) at 48hpf, compared to a BB polarity index of 0.77 in non-expressing cells (n=114 cells, 10 embryos) **(Supp Fig 3a-b)**. Importantly, Vangl2 polarization is significantly diminished in the floorplate in *Tg(shh:GAL4VP16); Tg(uas:p50p2a-eGFPCAAX); Tg(uas:mkate2-Vangl2)* expressing cells (A-P ratio of 1.4; $p=0.0225$, n=17 cells, 10 embryos) compared to non-expressing cells (A-P ratio of 1.6; n=21 cells, 10 embryos) **(Supp Fig 3c-d)**. As with nocodazole treatment, Fzd3a puncta remain concentrated near the base of the mislocalized primary cilium in p50-expressing cells in *Tg(shh:GAL4VP16); Tg(uas:p50p2a-eGFPCAAX); Tg(uas:Fzd3a-mEOS^{red})* embryos, suggesting that this population is stably associated with the BB ($r^2=0.75$, n=38 cells, 7 embryos) **(Supp Fig 3e-f)**. In sum, disrupting directed trafficking in the floorplate disrupts BB polarity and GFP-Vangl2 asymmetry at the membrane, consistent with a role for MT-dependent transport in the maintenance of PCP in the floorplate. It should be noted that in *Tg(shh:GAL4VP16); Tg(uas:p50p2a-eGFPCAAX)* embryos p50 is expressed in floorplate cells before 30hpf, which is the start of what we have defined as the maintenance period of floorplate PCP. This early expression makes it difficult to rule out the possibility that the disruption of vesicular trafficking caused by p50 disrupts the initial establishment of PCP protein asymmetry, rather than its maintenance.

As disruption of MTs or directed trafficking along MTs disrupts GFP-Vangl2 asymmetry and primary cilia positioning, and Fzd3a-GFP traffics on centrosomal MTs, we next asked how MT loss affects Fzd3a dynamics. We examined the effect of nocodazole treatment on the dynamic movements of Fzd3a-GFP vesicles. As before, we treated 30hpf *Tg(shh:GAL4VP16);*

Tg(uas:Fzd3a-GFP); Tg(uas:EB3-mkate2) embryos with ice cold nocodazole for 1 hour and then immediately mounted and imaged time lapse movies of Fzd3a-GFP dynamics. Whereas Fzd3a-GFP vesicles are highly dynamic in control embryos at 30hpf **(Supp Fig 4a, e-f)**, Fzd3a-GFP vesicles in nocodazole treated embryos stay relatively stationary over time **(Supp Fig 4b, e-f, Supp Movie 12)**. To further characterize Fzd3a-GFP vesicular movements in the absence of MTs we tracked individual vesicles as before. Loss of MTs significantly disrupted Fzd3a-GFP vesicle dynamics, as Fzd3a-GFP vesicles in nocodazole treated embryos lose their apically biased directionality compared to controls **(Supp Fig 4c-d).** Furthermore, nocodazole treatment reduced total Fzd3a-GFP vesicle displacement over time from 1.8µm per minute in controls (n=66 vesicles, 27 cells, 4 embryos) to 0.6µm per minute (p=0.0001, n=79 vesicles, 16 cells, 3 embryos, **Supp Fig 4e)** and decreases average Fzd3a-GFP velocity from 0.09µm/sec to 0.07µm/sec (p=0.0043, **Supp Fig 4f**)**.** In sum, our results further support a model in which Fzd3a and Vangl2 actively traffic on MTs during a period of PCP maintenance in the developing floorplate, contrary to previous reports (Sepich et al., 2011; Shi et al., 2016; Vladar et al., 2012), and that this is essential for the maintenance of asymmetric PCP protein localization as visualized by the loss of anterior membrane localization of GFP-Vangl2.

Maintenance of PCP protein polarity does not depend on a polarized BB

The link between BB positioning and PCP signaling is controversial. From our work and the work of others, it is clear that PCP signaling plays an essential role in the polarization of the BB (Borovina et al., 2010; Carvajal-Gonzalez et al., 2016a; Hashimoto et al., 2010; Song et al.,

2010; Vladar et al., 2012). However, there are also reports that the BB may also feed back into PCP protein asymmetry and function (Boutin et al., 2014; Gerdes et al., 2007; May-Simera et al., 2010; Ross et al., 2005). To examine the relationship that exists between a polarized BB and the maintenance of PCP protein asymmetry we treated 30hpf *Tg(shh:GAL4VP16); Tg(uas-GFP-Vangl2)* embryos with cold nocodazole for 1hr to disrupt MTs, BB polarity and GFP-Vangl2 localization. We then removed the drug and allowed the embryos to recover overnight (O/N). After an O/N recovery from nocodazole treatment, EB3-labeled MTs repolymerize throughout floorplate cells **(Fig 5a).** As loss of MTs dramatically disrupts Fzd3a-GFP trafficking we wanted to know if Fzd-GFP vesicular dynamics can recover after nocodazole treatment. We treated 30hpf *Tg(shh:GAL4VP16); Tg(uas-Fzd3a-GFP)* embryos with cold nocodazole for 1hr and at 48hpf, after an O/N recovery, Fzd3a-GFP vesicles in nocodazole-treated embryos appear similarly dynamic overall when compared to controls (**Supp Movie 13)**. However, at 48hpf of recovery, when control embryos display a BB polarity index of 0.79 (n=200 cells, 21 embryos), BBs failed to repolarize in nocodazole-treated embryos with an average BB polarity index of 0.61 ($p<0.0001$, n=203 cells, 19 embryos), which is not significantly different from the polarity index immediately after nocodazole treatment (BB polarity index=0.60, $p<0.9999$, n=212 cells, 18 embryos, **Fig 5b-c)**. Thus the recovery of a MT network in floorplate cells is insufficient to re-establish BB polarization.

Given that the establishment of cellular planar polarity depends on the asymmetric localization of PCP complexes, we considered that the failure of BB repolarization after recovery from nocodazole might reflect a failure of floorplate cells to re-establish molecular planar

polarity as assessed by GFP-Vangl2 membrane localization. Embryos that were treated for 1hr with nocodazole and not given time to recover had an average GFP-Vangl2 A/P membrane ratio of 1.2 (n=156 cells, 20 embryos), whereas embryos that recovered for 3hrs post treatment repolarize GFP-Vangl2 to anterior membranes with an A/P ratio of 1.4 (p=0.0891, n=74 cells, 10 embryos), and embryos that recovered O/N had a mean A/P ratio of 1.5 (p=0.0004, n=169 cells, 20 embryos, compared to 1hr treated with no recovery) **(Fig 5d-e)**. Furthermore, the dense localization of GFP-Vangl2 near the BB that we detected immediately after nocodazole treatment is no longer present after this recovery period **(Fig 5d)**. Thus the failure of the BB to re-polarize is not due to a failure to re-establish PCP protein asymmetry. Furthermore, by dissociating molecular from cellular PCP in this experiment, we can also conclude that although under normal circumstances PCP proteins traffic towards an asymmetrically localized MTOC during the PCP maintenance phase of floorplate development, the polarized localization of the MTOC is not required for the maintenance of PCP protein localization.

Discussion

Our work sought to investigate the role of MTs in the maintenance of PCP protein asymmetry and cellular polarity in the floorplate of the developing zebrafish neural tube. Using *in vivo* time-lapse imaging of fluorescently-labeled core PCP proteins and MTs we demonstrated an ongoing role for MTs after the establishment of PCP in maintaining the molecular polarization of PCP proteins at the membrane, as well as for the maintenance of cellular polarity at the level of the primary cilium/BB/MTOC. We characterized the progressive

polarization of the BB within floorplate cells and identified two distinct phases of polarity, an establishment phase during which the BB is progressively localized toward cell posteriors, and a maintenance phase during which BB position is stably maintained. We confirmed that Vangl2 is required for BB polarization and further demonstrated that Fzd3a is involved in this process. We expressed fluorescently-fused Vangl2 and Fzd3a proteins and determined that GFP-Vangl2 asymmetrically localizes to anterior membranes whereas Fzd3a-GFP does not detectably localize asymmetrically to either anterior or posterior membranes but accumulates near the BB. We found that MT loss after PCP establishment disrupts the posterior positioning of the BB of the primary cilium as well as the anterior localization of GFP-Vangl2, demonstrating that MTs are actively required for the maintenance of these asymmetries**.** We directly visualized and characterized the directional trafficking of cytosolic Fzd3a-GFP along EB3-mkate2 labeled MTs within floorplate cells during a period of PCP maintenance and demonstrated that MT loss dramatically disrupts the average velocity, perdurance, and apically-oriented directionality of Fzd3a-GFP trafficking. We found that cytosolic Fzd3a-GFP maintains its colocalization with the BB even when the BB becomes unpolarized, whereas GFP-Vangl2 increases its accumulation near the BB in the absence of MTs, which suggests the BB may play an active intermediary role in vesicular trafficking of PCP proteins. Finally, as GFP-Vangl2 re-establishes its asymmetric localization to anterior membranes in the context of an unpolarized BB, we find that BB polarity does not reciprocally influence PCP protein asymmetry in the floor plate. Together our findings point to a model in which the maintenance of asymmetric PCP protein patterning depends on MT-based vesicular transport of PCP proteins, but does not require a polarized MTOC.

PCP Establishment and Maintenance

The standard for what defines the transition from PCP establishment to PCP maintenance has relied on the onset of observable subcellular PCP protein asymmetry or planar polarized cellular structures including cilia (Shi et al., 2016; Vladar et al., 2012). As the BB is stably polarized by 30hpf and GFP-Vangl2 is stably maintained at anterior cell membranes after this stage, we defined the 30-72hpf developmental period as a PCP maintenance phase. This distinction enabled us to investigate the cell biology of PCP maintenance processes while most other studies have solely examined mechanisms of PCP establishment. Although floorplate cells are highly planar polarized by 30hpf, the asymmetric localization of GFP-Vangl2 to anterior membranes continued to increase until at least 48hpf. This is not surprising, as asymmetric distributions of core PCP proteins are known to self-amplify over time in other contexts (see Goodrich and Strutt, (2011) for review), and this does not conflict with our model that cellular PCP is actively maintained after 30hpf. No matter how one distinguishes between establishment and maintenance, our findings indicate that PCP protein dynamics and localization is actively regulated multiple days after its initial onset. This maintenance implies that there are ongoing roles for PCP protein asymmetry during development, which may have disease consequences if disrupted later in life. Thus, the functional consequences of PCP disruption at later stages in development may merit further investigation.

PCP Protein Dynamics and Localization

Our work further characterized the asymmetric localizations of GFP-Vangl2 and Fzd3a-GFP within zebrafish floorplate cells originally described in (Davey et al., 2016), and measured the localization and movements of vesicular Fzd3a-GFP throughout the cytoplasm. Our findings are consistent with established PCP models in that subcellular asymmetric localization of core PCP components underlies most planar polarized systems to date, and Fzd proteins have long been known to traffic in vesicles in order to establish planar polarity in fly (Butler and Wallingford, 2015; Shimada et al., 2006). The fact that we were unable to detect Fzd3a-GFP asymmetry at the membrane is not unexpected, as PCP protein asymmetries, including Fzd proteins, can be quite subtle or undetectable in other contexts (Aw et al., 2016; Strutt and Strutt, 2007). Furthermore, the colocalization of Fzd3a-GFP with BBs has precedent as multiple PCP proteins have been described near BBs, including Vangl2 in mouse kidney epithelia (Ross et al., 2005) and Dvl2 as well as the PCP effectors like Fuz, In, and Wdpcp in *Xenopus* MCCs (Gray et al., 2009; Kim et al., 2010; Park et al., 2006; Zeng et al., 2010). Fzd3a could be performing multiple roles at the BB as PCP signaling has been implicated in numerous BB-related processes including the translational polarity of BBs, the Dvl-dependent apical docking of BBs (Park et al., 2008) and PCP-dependent coordinated tilting and motility of cilia in multiple systems (Butler and Wallingford, 2015; Hashimoto et al., 2010; Vladar et al., 2012; Werner and Mitchell, 2012).

However, it is possible that vesicular Fzd3a-GFP aggregates to local concentrations of MTs, as the BB is a major hub of MT nucleation. Importantly, we observed floorplate cells undergoing cell division up until 48hpf (data not shown), suggesting that at least some cells are not fully differentiated at earlier timepoints. Given that the BB is a nexus of many MTs within

these cells, it is possible that individual Fzd3a-GFP containing vesicles transiently accumulate near the BB before they are distributed to individual MTs for directional trafficking towards cell membranes. If this is the case one would predict that the BB has an active role in coordinating the polarized distribution of PCP components throughout the cell. Indeed, when MTs are disrupted we observe that GFP-Vangl2, which normally asymmetrically localizes to anterior membranes accumulates near the BB. This could indicate that vesicular Vangl2 normally traffics along centrosomal MTs and cannot reach anterior or posterior membranes in the absence of centrosomal MT tracks. Our observation that GFP-Vangl2 also becomes less asymmetrically distributed on membranes after nocodazole treatment supports the model in which maintenance of Vangl2 asymmetry is normally distributed to membranes via directional MT-based trafficking. Though we only rarely detected GFP-Vangl2 puncta within untreated floorplate cells during our analysis, vesicular Vangl2 is also rarely detected in other models (Shi et al., 2016), which could indicate that fewer individual Vangl2 proteins are packaged into distinct vesicles and endosomes than those that contain Fzd3a. We cannot rule out that these differences could be artefactual from the use fluorescently-fused PCP proteins to visualize protein dynamics, but our observations support a model in which both Fzd3a and Vangl2 proteins are actively trafficked along MTs during phases of cellular PCP maintenance.

Microtubules and Maintenance of PCP Protein Asymmetry

Our findings conflict with previous studies in multiple vertebrate models that suggested MTs are dispensable for maintenance of molecular asymmetry of PCP proteins once cells

establish planar polarity (Sepich et al., 2011; Shi et al., 2016; Vladar et al., 2012). However, there are important differences between our work and these previous investigations. For example, Vladar et al., 2012 examined mouse tracheal epithelia cells (MTECs) and Shi et al. 2016 studied mouse oviduct, both of which are multiciliated cell (MCC) types. MCCs display multiple apically localized motile cilia, the BBs of which are linked through a subapical cytoskeletal network composed of MTs and actin. Conversely, cells within the zebrafish floorplate are monociliated with single motile primary cilia projecting apically from a single BB, which also functions as a MTOC (Borovina et al., 2010)(and our findings). It is possible that vesicular PCP signaling proteins engage with the subapical arrays of MTs in MCC contexts differently than with MTs emanating from a single MTOC as these structures have unique organizations and perform distinct cellular functions. However, another study in the monociliated context of zebrafish epidermal and mesodermal cells undergoing CE movements also claimed that MTs are largely dispensable for maintenance of the asymmetric distribution of PCP proteins (Sepich et al., 2011). This analysis examined PCP protein localization in cells undergoing collective migration, a process which requires cells to undergo dynamic membrane, adhesion, and cytoskeletal remodeling (Davey and Moens, 2017). It is possible that cells undergoing dynamic movements have alternative modes of PCP protein distribution as MTs and centrosomes/MTOCs are actively repositioned during cell migration (Euteneur and Schliwa, 1992; Sepich and Solnica-Krezel, 2016; Sepich et al., 2011). It is also possible, however, that MTs were not fully disrupted in these three studies, and thus did not truly test the requirement for MTs in the maintenance of PCP protein asymmetry. For example, Shi et al. 2016 noted that

their nocodazole treatment failed to completely abolish the subapical lattice of MTs that link ciliary BBs, and Vladar et al., 2012 examined primarily unstable tyrosinated tubulin in nocodazole-treated MTECs and not more stabilized MT populations. This is important as other studies have determined that MCC ciliary BBs are often linked by subapical MT networks that stabilize over time (Muroyama and Lechler, 2017; Werner et al., 2011), and nocodazole primarily targets more dynamic MTs by binding free tubulin subunits (Baas et al., 2016). Indeed, our own early experiments with nocodazole failed to fully disrupt floorplate MTs or PCP protein asymmetry, even at elevated concentrations. However, combining nocodazole treatment with cold temperatures(McFarland et al., 2017), completely destabilized stable MTs as well as dynamic MT populations within the floorplate and disrupted planar polarity. In sum, our study challenges the model that MTs are dispensable after PCP protein asymmetry has been established by directly visualizing the *in vivo* consequences that MT destabilization has on maintenance of PCP protein distribution and dynamics.

The Basal Body and PCP

The links between PCP signaling and BB positioning are complex and not fully understood at a mechanistic level. Though it is well-established that PCP signaling is required for the actin-based translational positioning of the BB in many systems (Borovina et al., 2010; Carvajal-Gonzalez et al., 2016a; Hashimoto et al., 2010; Vladar et al., 2012), whether the asymmetric position of the BB can reciprocally influence the establishment and maintenance of PCP protein asymmetry has not been investigated. As nocodazole-induced loss of BB

asymmetry occurred simultaneously with a decrease of asymmetric GFP-Vangl2 at the membrane, we were curious if BB position could influence PCP protein distribution. Intriguingly, we discovered that restoration of MTs after their disruption does not rescue BB posterior positioning, but largely restores GFP-Vangl2 asymmetry at the membrane as well as vesicular Fzd3a-GFP dynamics. This decoupling of asymmetrically localized BBs from the polarized localization of GFP-Vangl2 is strong evidence that BB position does not significantly affect PCP protein asymmetry. This is surprising as the BB likely retains at least partial MTOC function and we directly observed Fzd3a-GFP localizing near the BB and trafficking along MTs under control conditions. The position of the MTOC likely affects the orientation of MTs that nucleate there, which could affect the careful balance of directional trafficking of PCP protein-containing vesicles to specific membranes. Alternatively, non-centrosomal MTs may be sufficient to enable directional trafficking and asymmetric localization of PCP proteins, as many differentiated cell types reassign primary MTOC function to non-centrosomal sites (Muroyama and Lechler, 2017) and MTs in the zebrafish floorplate appear to stabilize into non-centrosomal bundles at later time points. As the functional consequences MTOC reassignment and a changing MT organization are poorly characterized in any context, how floorplate cells regulate the maintenance of asymmetric MT-based directional trafficking of PCP protein-containing vesicles remains to be determined.

Acknowledgements

We would like to acknowledge the many people that have contributed to this work. We thank the members of the Moens lab for many helpful discussions, especially Minna Roh who provided comments

on the manuscript and Adam Isabella for his aid in generating rose plots. We also thank Lisa Voelker for assistance with analysis of vesicular dynamics, Jarema Malicki for providing the p50 plasmid, and Mary Halloran who offered a critical suggestion regarding MT stability. This work was supported by NIH Grant 5R01NS082567-05.

Figures

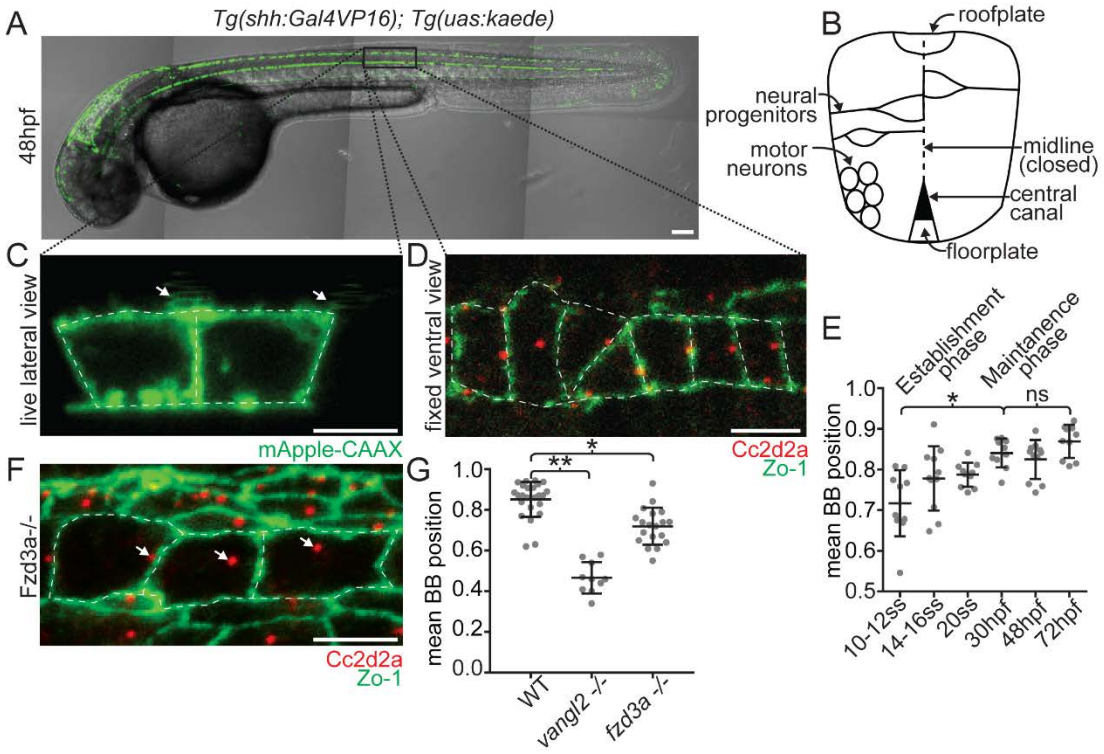

Figure 1. The Floorplate is progressively planar polarized in a Vangl2 and Fzd3a-dependent manner.

(A) Representative image of a 48hpf *Tg:(shh:Gal4VP16); Tg(uas:Kaede)* zebrafish embryo that expresses Kaede in the floorplate of the neural tube and to a lesser extent in the notochord and roofplate. (B) Schematic of a cross-section of the zebrafish neural tube at 48hpf (not to scale). (C) Single time point from a time lapse of a *Tg(shh:Gal4VP16); Tg(uas:mApple-CAAX)* embryos at 48hpf in which two adjacent floorplate cells are expressing membrane-localized mApple-CAAX (green). Posteriorly localized primary cilia (arrows) appear as squiggles due to their rapid motion. (D) Fixed ventral view of a 48hpf WT floorplate co-immunostained with ZO-1 to mark sub-apical tight junctions (green) and Cc2d2a to mark BBs (red). (E) Quantitation of per embryo polarity index from the 10-12ss through 72hpf. Each dot represents the average polarity index of at least 10 cells within a single embryo. Total N=62 embryos, 1130 cells. *p<0.0001; significance was determined with a Kruskal-Wallis test with Dunn's multiple comparison. (F) Fixed ventral view of a 48hpf *fzd3a-/-* floorplate stained as in D. White dotted line indicates position of cell boundaries, as determined by mApple-CAAX fluorescence (C) or ZO-1 staining (D,F), arrows indicate BB positions. (G) BB polarity indices of WT, *vangl2-/-* and *fzd3a-/-* embryos at 48hpf. Each dot

represents the average polarity index of at least 10 cells within a single embryo. Total N=54 embryos, 448 cells; **p<0.0001; *p=0.0018; significance was determined with a Kruskal-Wallis test with Dunn's multiple comparison. Anterior is to left in all images. Scale bars: 100µm (A) or 5µm (C,D,F).

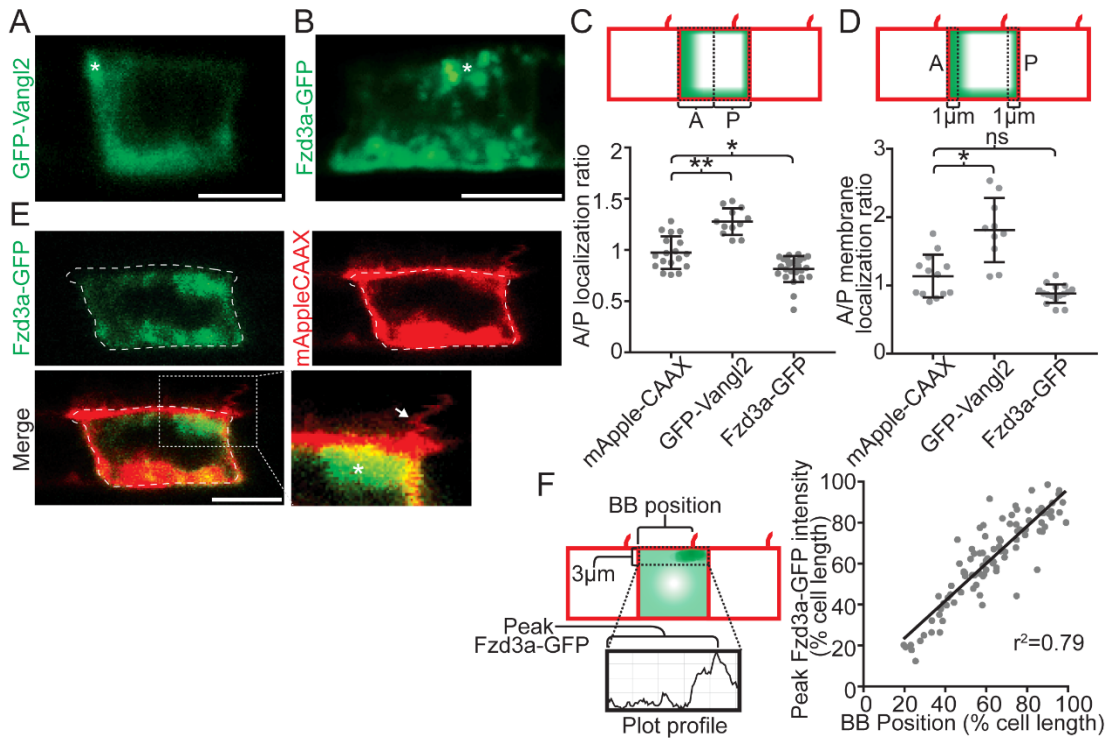

Figure 2. Vangl2 and Fzd3a localization in the floorplate.
(A-B) Live lateral views of 48hpf (A) *Tg(shh:Gal4VP16); Tg(uas:GFP-Vangl2)* and (B) *Tg(shh:Gal4VP16); Tg(uas:Fzd3a-GFP)* single expressing floorplate cells. Asterisks indicate positions of fusion protein (green) concentration along the apical membrane. (C) Schematic: diagram indicating how total fusion protein localization was measured on anterior vs. posterior cell halves. Graph: quantitation of anterior vs. posterior fusion protein localization in isolated expressing cells. Each dot represents the ratio of the mean fluorescence level within a single cell anterior half divided by the mean fluorescence level of its posterior half. N=57 embryos, 152 cells; **p=0.0035; *p=0.0266; significance was determined with a Kruskal-Wallis test with Dunn's multiple comparison. (D) Schematic: diagram indicating how fusion protein localization was measured on anterior vs. posterior membranes. Graph: quantitation of anterior vs. posterior fusion protein membrane localization in isolated expressing cells. Each dot represents the ratio of the mean fluorescence level along the anterior membrane a single cell divided by the mean fluorescence level along its posterior membrane. N=39 embryos, 106 cells; *p=0.0154; significance was determined with a Kruskal-Wallis test with Dunn's multiple comparison. (E) Live lateral views of a 48hpf *Tg(shh:Gal4VP16); Tg(uas:Fzd3a-GFP); Tg(uas:mAppleCAAX)* dual transgene expressing floorplate cell. Inset: magnified view of the posterior apical cellular membrane where Fzd3a-GFP (green, asterisk) is concentrated near the base of the primary cilia (red apical extension, arrow). Approximate cell boundaries, as determined by mAppleCAAX expression, indicated by white dotted lines. (F)

Schematic: diagram indicating how apically localized cytosolic Fzd3a-GFP levels were quantified (see methods) Graph: correspondence of Fzd3a-GFP peak localization with primary cilium position. Each point corresponds to measurements from a single cell. R2=0.79. Anterior to left in all images. Scale bars: 5µm.

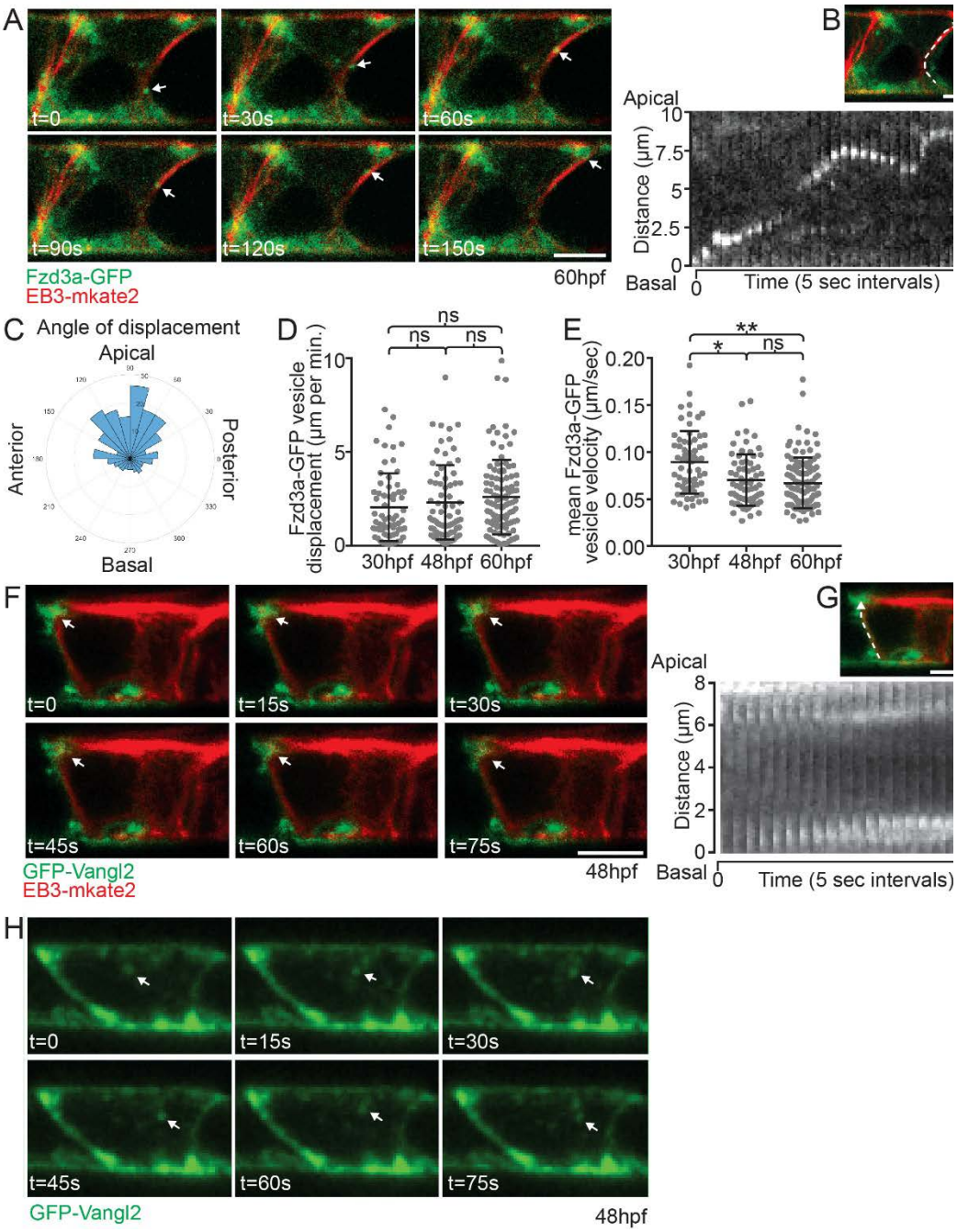

Figure 3. Fzd3a and Vangl2 trafficking in the floorplate.

(A) Single timepoints from a time lapse movie of a 60hpf *Tg(shh:Gal4VP16); Tg(uas:Fzd3a-GFP); Tg(uas:EB3-mkate2)* dual transgene expressing floorplate cell in lateral view showing EB3-mKate2-labeled MTs (red) and Fzd3a-GFP vesicles (green). Arrows track an individual Fzd3a-GFP vesicle as is moves in the apical and posterior direction along a MT. (B) inset image: overlays shows measurement path used to

generate kymograph. Kymograph: plot showing the apically directed movement of a single Fzd3a-GFP vesicle along a MT polymer. (C-E) Fzd3a-GFP vesicular movements were tracked during 5-second interval time lapse movies of laterally-viewed floorplate cells in *Tg(shh:Gal4VP16); Tg(uas:Fzd3a-GFP); Tg(uas:EB3-mkate2)* embryos at 30, 48, and 60hpf. N=240 vesicles, 89 cells, 9 embryos. (C) Rose plot of final relative displacement angles of individual Fzd3a-GFP containing vesicles between first and last measured positions. (D) Quantitation of individual Fzd3a-GFP vesicle displacement distances between first and last timepoint measured, divided but total tracking time. Significance was determined with a Kruskal-Wallis test with Dunn's multiple comparison. (E) Quantitation of average velocities of individual Fzd3a-GFP vesicles. **p<0.0001; *p=0.0023; significance was determined with a Kruskal-Wallis test with Dunn's multiple comparison. (F) Single timepoints from a time lapse movie of a 48hpf *Tg(shh:Gal4VP16); Tg(uas:GFP-Vangl2); Tg(uas:EB3-mkate2)* dual transgene expressing floorplate cell in lateral view. MTs are labeled by EB3-mkate2 (red) and GFP-Vangl2 is shown in green. Arrows indicate GFP-Vangl2 anterior apical localization, which does not change over time. (G) inset image: overlay showing measurement path used to generate kymograph. Kymograph showing the absence of GFP-Vangl2 trafficking along the MT polymer. (H) Single timepoints of a *Tg(shh:GAL4VP16); Tg(uas:GFP-Vangl2)* floorplate cell demonstrating a rare example of detectable GFP-Vangl2 cytosolic puncta. Anterior to left in all images. Approximate cell boundaries indicated by white dotted lines. Scale bars: 5µm.

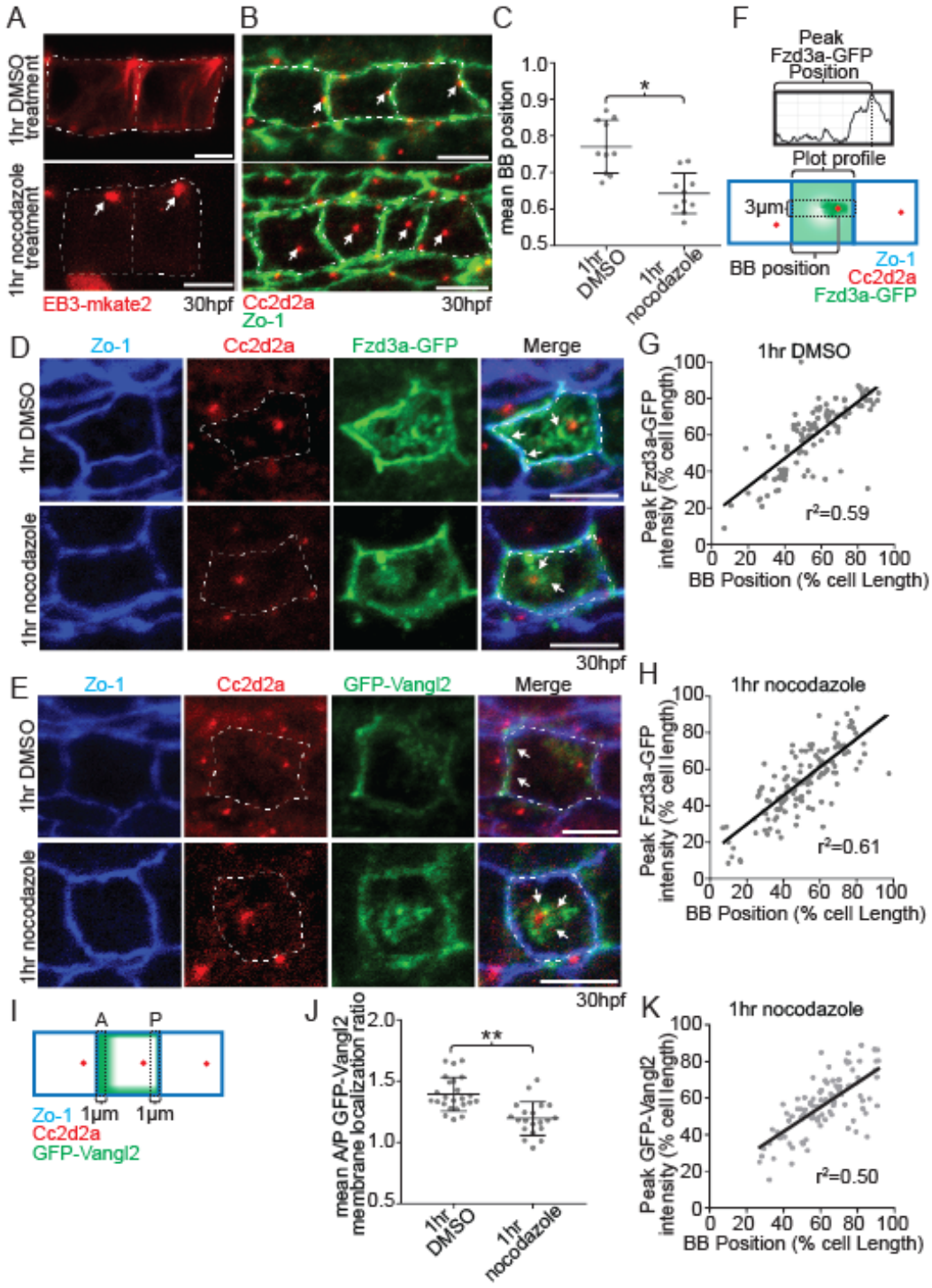

Figure 4. Microtubules are required to maintain floorplate PCP.

(A) Live lateral views of expressing floorplate cells in 30hpf untreated and 1hr nocodazole *Tg(shh:Gal4VP16); Tg(uas:EB3-mkate2*). Upon nocodazole treatment EB3-mkate2 labeled MTs collapse to subapical foci near the BB (see arrows). (B) Ventral images of fixed 30hpf WT floorplates coimmunostained for Cc2d2a (red) and Zo-1 (green) after 1hr of treatment with DMSO (control) or cold 5ng/µl nocodazole. Arrows indicate position of BBs as labeled by Cc2d2a. Note that BBs are more centrally localized in nocodazole treated floorplate cells. (B) Quantitation of per embryo average BB polarity index after 1hr DMSO treatment (control) or 1hr nocodazole treatment. N=200 cells, 20 embryos; *p=0.0003; significance was determined with Mann-Whitney test. (C) Ventral views of a 30hpf *Tg(shh:Gal4VP16); Tg(uas:Fzd3a-GFP)* floorplate cells expressing Fzd3a-GFP coimmunostained for Zo-1 (blue), Cc2d2a (red) and GFP (green) after 1hr DMSO treatment (control) or 1hr nocodazole treatment. Arrows indicate BB position. (D) Ventral views of GFP-Vangl2 expressing floorplate cells in 1hr DMSO and 1hr nocodazole treated 30hpf *Tg(shh:Gal4VP16); Tg(uas:GFP-Vangl2)* embryos. Arrows indicate GFP-Vangl2 localization. White dotted lines indicate cell boundaries based on Zo-1. (E) Ventral views of Fzd3a-GFP expressing floorplate cells in 1hr DMSO and 1hr nocodazole treated 30hpf *Tg(shh:Gal4VP16); Tg(uas:Fzd3a-GFP)* embryos. Arrows indicate Fzd3a-GFP localization. White dotted lines indicate cell boundaries based on Zo-1.(F) Diagram illustrating how peak Fzd3a-GFP localization and BB positions were measured. Briefly, in fixed ventral images of Fzd3a-GFP expressing floorplate cells in 30hpf *Tg(shh:Gal4VP16); Tg(uas:Fzd3a-GFP)* embryos post 1hr DMSO (G) or 1hr nocodazole treatment (H), BB distance from anterior membrane was measured compared to overall anterior-posterior cell length. A 3µm wide ROI centered on the position of the BB was drawn from anterior to posterior membranes. The "plot profile" tool in ImageJ was used to measure average GFP levels across the anterior to posterior cell axis. (G-H) the location of peak GFP localization at the level of the BB (y-axes) was recorded and plotted as percent total cell length from the anterior membrane and compared to the measured position of the BB (x-axes). Each data point represents the measurements from a single cell. (G) DMSO treatment N=100 cells, 10 embryos; r^2=0.59. (H) Nocodazole treatment N=100 cells, 10 embryos; r^2=0.61. (I) Diagram illustrating how anterior and posterior membrane levels of GFP-Vangl2 were measured in fixed ventral floorplate images. (J) Quantitation of per embryo average GFP-Vangl2 anterior vs. posterior membrane localization ratios in isolated floorplate cells expressing *Tg(shh:Gal4VP16); Tg(uas:GFP-Vangl2)*. N=416 cells, 66 embryos; **p<0.0001, *p=0.0013; significance was determined with a Kruskal-Wallis test with Dunn's multiple comparison. (K) GFP-Vangl2 association with the BB after nocodazole treatment was measured as in (F) and graphed as in (G-H). After 1hr nocodazole treatment peak GFP-Vangl2 intensity correlates with the position of the BB N=10 embryos, 100 cells, r^2=0.50. Scale bars: 5µm.

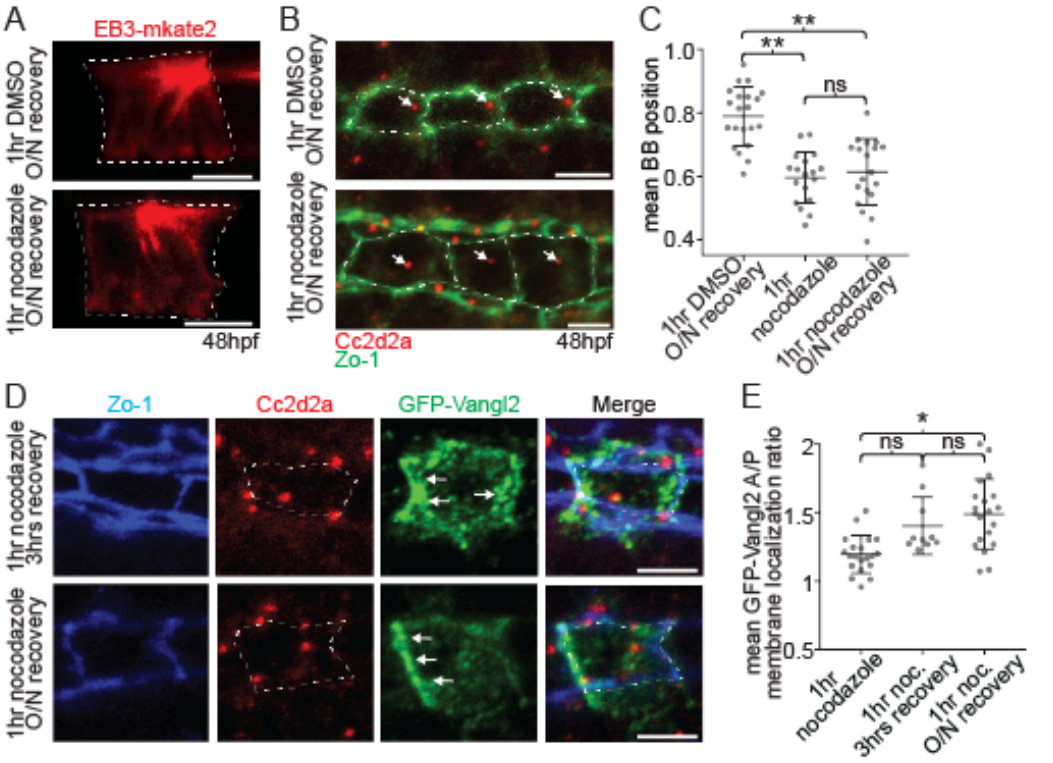

Figure 5. Maintenance of PCP protein polarity does not depend on a polarized BB. (A) EB3-mkate concentrates to the subapical posterior corners of expressing floorplate cells and radiates along cytoplasmic MTs in untreated 48hpf embryos. 1hr of cold nocodazole treatment followed by an O/N recovery causes EB3-mkate2 to concentrate subapically in cell centers, where it still radiates along centrosomal MTs. (B) Ventral images of fixed 48hpf WT floorplates coimmunostained for Cc2d2a (red) and Zo-1 (green). Embryos were treated with either DMSO (control) or cold 5ng/µl nocodazole for 1hr and then recovered overnight. Arrows indicate position of BBs as labeled by Cc2d2a. (C) Quantitation of per embryo average BB polarity index in WT embryos that were treated with either DMSO (control) or cold 5ng/µl nocodazole for 1hr and then either fixed immediately or allowed to recover O/N. N=615 cells, 58 embryos; **p<0.0001; significance was determined with a Kruskal-Wallis test with Dunn's multiple comparison. (D) Ventral images of fixed GFP-Vangl2 expressing floorplate cells in *Tg(shh:Gal4VP16); Tg(uas:GFP-Vangl2)* embryos that were treated with nocodazole for 1hr and then either given 3hrs or an O/N recovery period. Arrows indicate Fzd3a-GFP localization at membranes. (E) Quantitation of GFP-Vangl2 anterior vs. posterior membrane localization ratios after 1hr nocodazole treatment followed by different recovery periods. N=236 cells, 29 embryos; *p=0.0004; significance was determined with a Kruskal-Wallis test with Dunn's multiple comparison. White dotted lines mark approximate cell boundaries, based on ZO-1 staining of tight junctions. Scale bars: 5µm.

Supplemental Figures

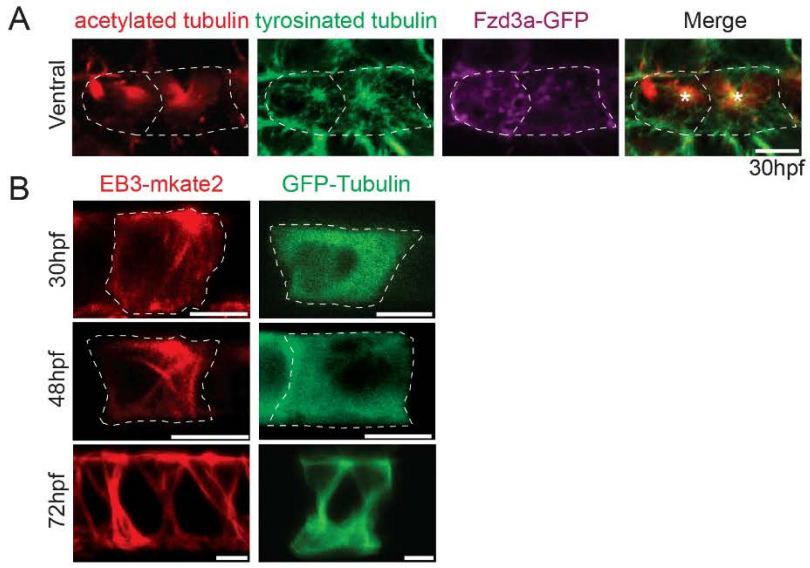

Supplemental Figure 1. The BB serves as the MTOC in floorplate cells
(A) Fixed ventral views of 30hpf *Tg(shh:Gal4VP16); Tg(uas:Fzd3a-GFP)* floorplate cells coimmunostained for GFP (to visualize floorplate cell boundaries), acetylated tubulin, and tyrosinated tubulin. Asterisks indicate the positions of primary cilia as determined by acetylated tubulin staining (out of image plane). (B) Live lateral views of expressing floorplate cells in 30, 48, and 72hpf *Tg(shh:Gal4VP16); Tg(uas:EB3-mkate2*) embryos and *Tg(shh:Gal4VP16*) embryos injected UAS:GFP-Tubulin. MTs emanate from posterior apical cell corners at 30 and 48hpf, whereas MTs appear to organize into non-centrosomal bundles by 72hpf. Anterior to left in all images. Approximate cell boundaries indicated by white dotted lines. Scale bars: 5µm.

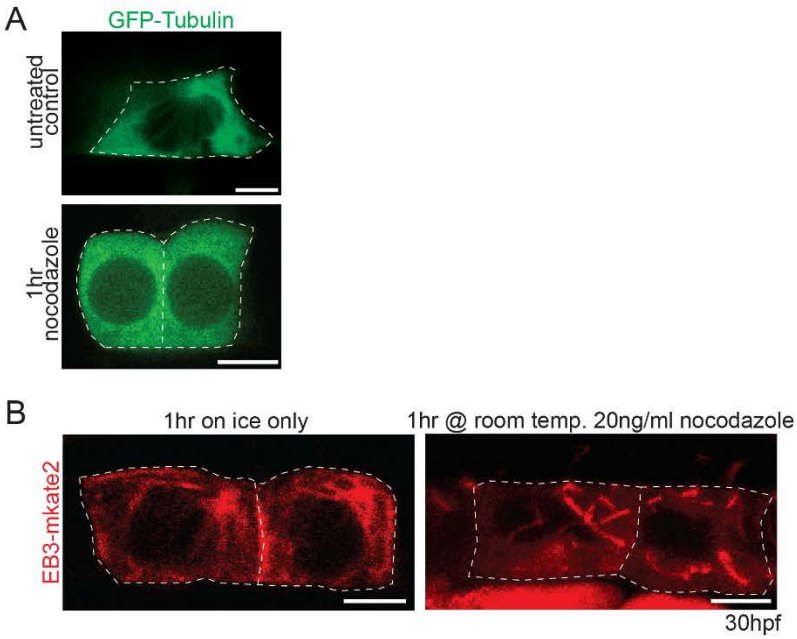

Supplemental Figure 2. Nocodazole disrupts MTs within the floorplate
(A) Live lateral views of expressing floorplate cells in 30hpf untreated and 1hr nocodazole treated *Tg(shh:Gal4VP16)* embryos injected with UAS-GFP-Tubulin. GFP-Tubulin becomes diffuse throughout the cytoplasm upon nocodazole treatment (B) Live lateral images of expressing floorplate cells in *Tg(shh:Gal4VP16); Tg(uas:EB3-mkate2)* embryos. 1hr of treatment on ice has little to no effect on EB3-mkate2 localization and dynamics whereas 1hr of room temperature 20µg/ml nocodazole treatment causes EB3-mkate2 to become more disorganized throughout the cell. Anterior to left in all images. Approximate cell boundaries indicated by white dotted lines. Scale bars: 5µm.

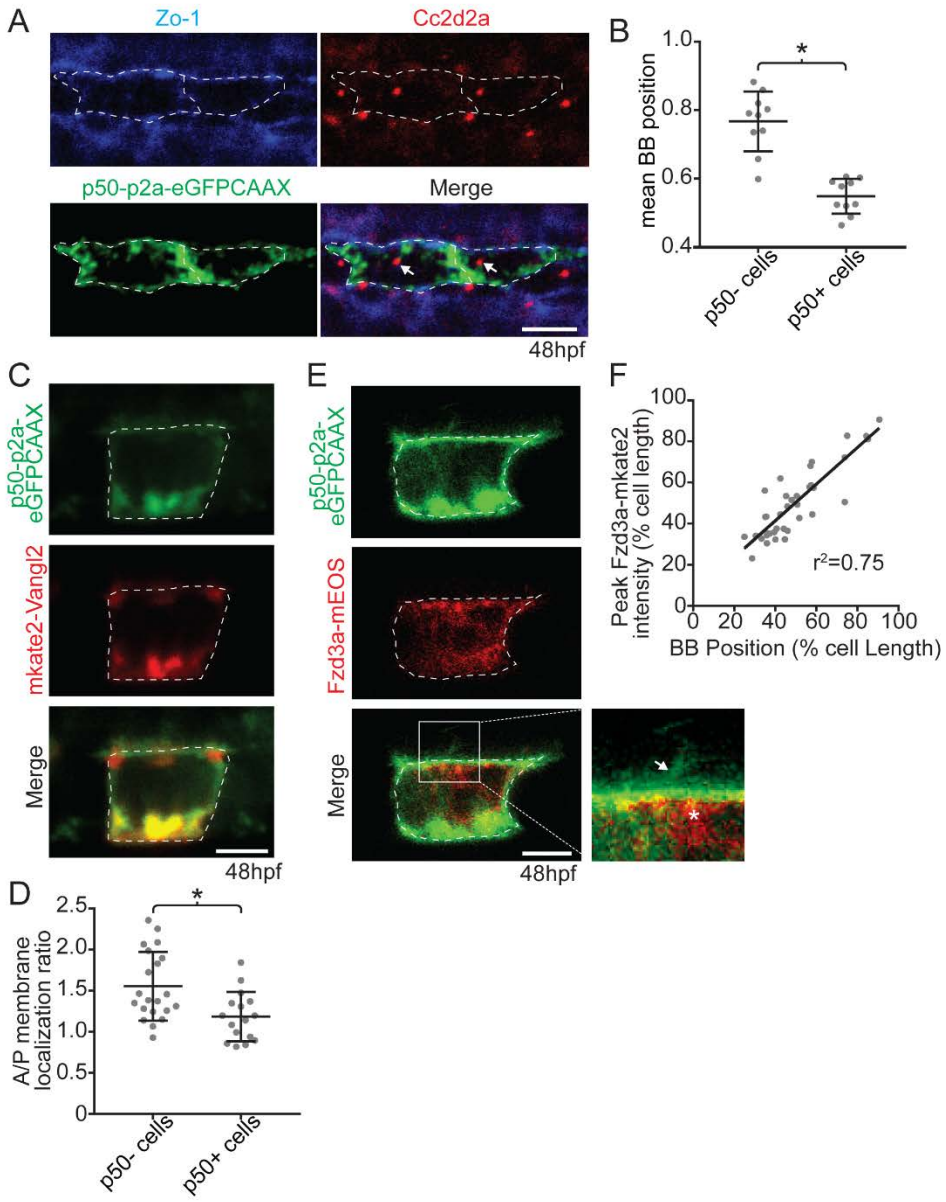

Supplemental Figure 3. Disrupting directed MT-based trafficking in the floorplate disrupts cellular polarity.

(A-F) Fixed ventral (A) and live lateral (C, E) views and quantitation (B, D, F) of expressing and non-expressing floorplate cells in 48hpf Tg(shh:Gal4VP16); Tg(uas:p50-p2a-eGFPCAAX) (A-B), Tg(uas:p50-p2a-eGFPCAAX); Tg(shh:Gal4VP16); Tg(uas:mkate2-Vangl2) (C-D), or Tg(shh:Gal4VP16); Tg(uas:p50-p2a-eGFPCAAX); Tg(uas:Fzd3a-mEOS) (E-F) embryos. (A) Arrows highlight BB position which is mislocalized to cell centers in cells expressing p50-p2a-eGFPCAAX. (B) Quantitation of the BB polarity index in p50-p2a-eGFPCAAX expressing and non-expressing floorplate cells. N=230 cells, 20 embryos; *p<0.0001; significance was determined with a Mann-Whitney test. (C) Live lateral views of dual transgene expressing floorplate cell. (D) Quantitation of average anterior vs. posterior membrane mkate2-

Vangl2 localization ratios (same method as Fig 2D). N=38 cells, 20 embryos; *p=0.0225; significance was determined with a Mann-Whitney test. (E) Live lateral views of a dual transgene expressing floorplate cell. Inset is a magnified view of the region around the primary cilium (arrow) where Fzd3a-mEOS (asterisk) aggregates. (F) Quantitation of primary cilia position vs. position of peak Fzd3a-mEOS localization in dual transgene expressing floorplate cells (see Fig 2F for method). Note that peak Fzd3a-GFP correlates closely with BB position even when the BB is not polarized to posterior membranes. R2=0.75; N=37 cells, 7 embryos. Anterior to left in all images. Approximate cell boundaries indicated by white dotted lines. Scale bars: 5µm.

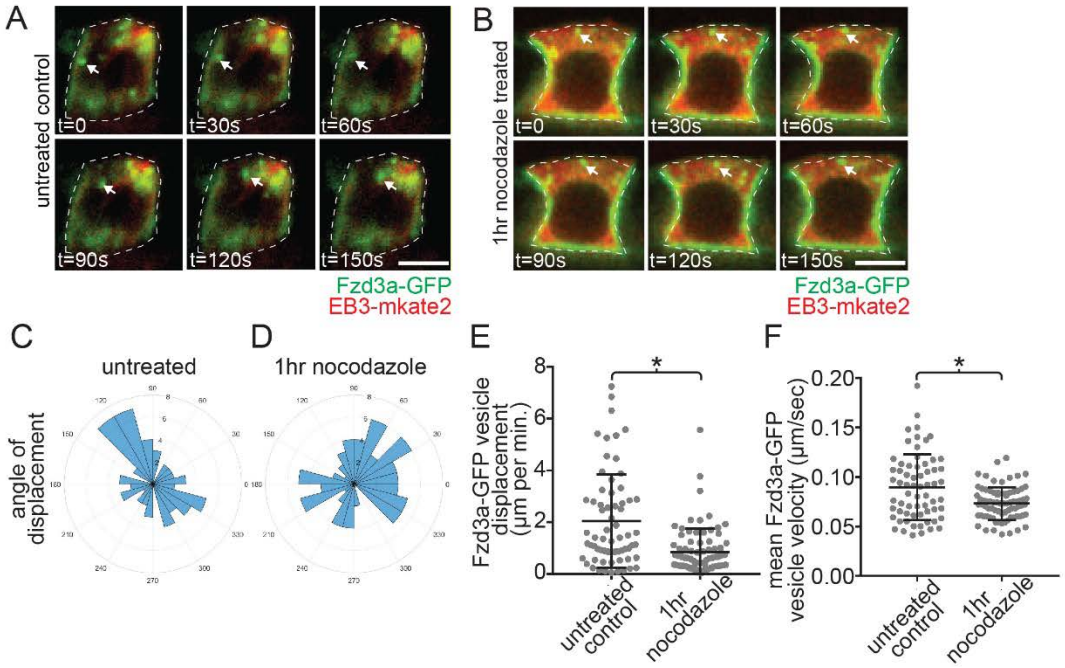

Supplemental Figure 4. Nocodazole disrupts vesicular Fzd3a-GFP dynamics.
(A-B) Single timepoints from time lapse movies of an untreated (A) or 1hr nocodazole treated (B) floorplate cell in lateral view in a 30hpf *Tg(shh:Gal4VP16); Tg(uas:Fzd3a-GFP); Tg(uas:EB3-mkate2)* embryo. Arrows track the position of single Fzd3a-GFP (green) vesicles across timepoints. Fzd3a-GFP vesicles travel along MT tracks marked by EB3-mkate2 (red) in control embryos (A), whereas Fzd3a-GFP vesicle movements are reduced embryos treated with nocodazole for 1hr (B). (C-F) quantitation of Fzd3a veside movement in control and 1hr nocodazole treated *Tg(shh:Gal4VP16); Tg(uas:Fzd3a-GFP); Tg(uas:EB3-mkate2)* embryos. N=145 vesicles, 43 cells, 7 embryos. (C-D) Rose plots of final relative displacement angles of individual Fzd3a-GFP containing vesicles between first and last measured positions in untreated control embryos (C) or embryos that were treated with nocodazole for 1hr (D). (E) Quantitation of overall Fzd3a-GFP vesicle displacement distances between first and last timepoint measured divided but total tracking time. *p=0.0001; significance was determined with a Mann-Whitney test. (F) Quantitation of average velocities of individual Fzd3a-GFP vesicle between first and last timepoint measured. *p=0.0043; significance was determined with a Mann-Whitney test. Anterior is to left in all images. Approximate cell boundaries are indicated by white dotted lines based Fzd3a membrane localization. Scale bars: 5µm.

DNA Element	Primer Sequence
Shh_F	GGT ACC GGC CTG CAT GGC
Shh_R	ACT AGT CTT CAC GGC TCA TCA
gata2_F	TGC AAT AGG CCA AAT CGA CAT TCA
gata2_R	CAA GTG TCC GCG CTT AGA AAA TGC
Gal4VP16_F	ATG AAG CTA CTG TCT TCT ATC GAA
Gal4VP16_R	CTA CAT ATC CAG AGC GCC GTA GGG
Vangl2_F	ATG GAT AAC GAG TCG CAG TAC TCA
Vangl2_R	TCA CAC CGA GGT TTC CGA CTG GAG
Fzd3a_F	ATG GTT CTG CTT TGG GCT CTG
Fzd3a_R	TGC TTT GGT CGC GTC CTC CTC
GFP_F	ATG AGT AAA GGA GAA GAA CTT TTC
GFP_R	GGC TTG TTT GTA TAG TTC ATC CAT GCC
mKate2_F	ATG GTG AGC GAG CTG ATT AAG
mKate2_R	TCT GTG CCC CAG TTT GCT AGG
p50_F	ATG GCC GAC CCG AAG TAC
p50_p2a_R	AGG TCC AGG GTT CTC CTC CAC GTC TCC AGC CTG CTT CAG CAG GCT GAA GTT AGT AGC TCC GCT TCC GGC CTT GTT GAG TTT CTT CAT CCT
Eb3_F	ATG GCC GTC AAT GTG TA
Eb3_R	AGC TAC TCG TCC TGG TC
mAppleCAAX_F	ATG GTG AGC AAG GGC GAG
mApple_R	CTT GTA CAG CTC GTC CATG
mAppleCAAX_R	TCA GGA GAG CAC ACA CTT GCA

Supplemental Table 1. Gene Specific Primer Sequences

Supplemental Movie Legends

Supplemental Movie 1. Floorplate motile primary cilia are labeled by mAppleCAAX. Live lateral view of two mAppleCAAX expressing cells at 36hpf. mAppleCAAX labels membranes, including those that line motile primary cilia (arrows). Anterior to left, dorsal up. 5 second intervals. Scale bar: 5µm

Supplemental Movie 2. Fzd3a-GFP localizes at the base of floorplate primary cilia. Live lateral view of two Fzd3a-GFP and mAppleCAAX expressing cells at 36hpf. mAppleCAAX labels membranes, including motile primary cilia (arrows). Cytosolic Fzd3a-GFP localizes near the bases of the primary cilia. Anterior to left, dorsal up. 5 second intervals. Scale bar: 5µm

Supplemental Movie 3. Fzd3a-GFP moves in dynamic puncta. Live lateral view of six Fzd3a-GFP expressing cells at 60hpf. Colored arrows highlight individual puncta. Anterior to left, dorsal up. 5 second intervals. Scale bar: 5µm

Supplemental Movie 4: Rab5c localizes to Fzd3a-GFP-containing vesicles. Live lateral view of a Fzd3a-GFP (green channel) and mApple-Rab5c (red channel) expressing cell at 72hpf. Colored arrows in the merged channel highlight individual puncta where Fzd3a-GFP and Rab5c colocalize. Anterior to left, dorsal up. 5 second intervals. Scale bar: 5µm

Supplemental Movie 5: Rab7 localizes to Fzd3a-GFP-containing vesicles. Live lateral view of a Fzd3a-GFP (green channel) and mApple-Rab7 (red channel) expressing cell at 72hpf. Colored arrows in the merged channel highlight individual puncta where Fzd3a-GFP and Rab7 colocalize Anterior to left, dorsal up. 5 second intervals. Scale bar: 5µm

Supplemental Movie 6. EB3-mkate2 labels dynamic microtubule plus ends in the floorplate at 30hpf. Live lateral view of two EB3-mkate2 expressing cells at 30hpf. EB3-mkate2 "comets" label dynamic microtubule plus ends. Microtubule plus ends emanate from apical posterior cell corners near the presumptive BB. Anterior to left, dorsal up. 5 second intervals. Scale bar: 5µm

Supplemental Movie 7. EB3-mkate2 comets line cytosolic and membrane-associated microtubules at 48hpf. Live lateral view of four EB3-mkate2 expressing cells at 48hpf. Anterior to left, dorsal up. 5 second intervals. Scale bar: 5µm

Supplemental Movie 8. EB3-mkate2 lines stable microtubule polymers at 60hpf. Live lateral view of five EB3-mkate2 expressing cells at 60hpf. Anterior to left, dorsal up. 5 second intervals. Scale bar: 5µm

Supplemental Movie 9. Fzd3a-GFP traffics along stable microtubules. Live lateral view of two Fzd3a-GFP and EB3-mkate2 expressing cells at 60hpf. Colored arrows highlight individual Fzd3a-GFP-containing vesicles across timepoints. Anterior to left, dorsal up. 5 second intervals. Scale bar: 5µm

Supplemental Movie 10. Sample Fzd3a-GFP tracking time lapse. Live lateral view of two Fzd3a-GFP and EB3-mkate2 expressing cells at 60hpf. Fzd3a-GFP vesicle dynamics were recorded by tracking individual Fzd3a-GFP puncta over time using the MTrackJ plugin in ImageJ. Anterior to left, dorsal up. 5 second intervals. Scale bar: 5µm

Supplemental Movie 11 - Rare example of dynamic GFP-Vangl2 vesicles. Live lateral view of a single GFP-Vangl2 expressing floorplate cell at 48hpf. Arrow indicates position of dynamic GFP-Vangl2 containing vesicles. Anterior to left, dorsal up 5 second intervals. Scale bar: 5µm

Supplemental Movie 12. Loss of microtubules disrupts Fzd3a-GFP vesicular trafficking. Live lateral view of multiple Fzd3a-GFP and EB3-mkate2 expressing floorplate cells at 30hpf, after one hour of cold nocodazole treatment. Nocodazole disrupts microtubules (note diffuse mkate2 signal) and disrupts the directional movement of Fzd3a-GFP vesicles (colored arrows). Anterior to left, dorsal up. 5 second intervals. Scale bar: 5µm

Supplemental Movie 13. Fzd3a-GFP trafficking is restored post-nocodazole treatment after overnight recovery. Live lateral view of multiple Fzd3a-GFP and EB3-mkate2 expressing cells at 48hpf. Embryos were treated for one hour with cold nocodazole and allowed to recover overnight. Colored arrows highlight individual Fzd3a-GFP-containing vesicles across timepoints. Anterior to left, dorsal up. 5 second intervals. Scale bar: 5µm

Bibliography

Adler, P.N., Krasnow, R.E., and Liu, J. (1997). Tissue polarity points from cells that have higher Frizzled levels towards cells that have lower Frizzled levels. Curr. Biol. *7*, 940–949.

Adler, P.N., Zhu, C., and Stone, D. (2004). Inturned Localizes to the Proximal Side of Wing Cells under the Instruction of Upstream Planar Polarity Proteins. Curr. Biol. *14*, 2046–2051.

Aigouy, B., Farhadifar, R., Staple, D.B., Sagner, A., Röper, J.-C., Jülicher, F., and Eaton, S. (2010). Cell Flow Reorients the Axis of Planar Polarity in the Wing Epithelium of Drosophila. Cell *142*, 773–786.

Anastas, J.N., Biechele, T.L., Robitaille, M., Muster, J., Allison, K.H., Angers, S., and Moon, R.T. (2012). A protein complex of SCRIB, NOS1AP and VANGL1 regulates cell polarity and migration, and is associated with breast cancer progression. Oncogene *31*, 3696–3708.

Antic, D., Stubbs, J.L., Suyama, K., Kintner, C., Scott, M.P., and Axelrod, J.D. (2010). Planar Cell Polarity Enables Posterior Localization of Nodal Cilia and Left-Right Axis Determination during Mouse and Xenopus Embryogenesis. PLOS ONE *5*, e8999.

Avasthi, P., and Marshall, W.F. (2012). Stages of Ciliogenesis and Regulation of Ciliary Length. Differ. Res. Biol. Divers. *83*, S30–S42.

Aw, W.Y., Heck, B.W., Joyce, B., and Devenport, D. (2016). Transient Tissue-Scale Deformation Coordinates Alignment of Planar Cell Polarity Junctions in the Mammalian Skin. Curr. Biol. *26*, 2090–2100.

Axelrod, J.D. (2001). Unipolar membrane association of Dishevelled mediates Frizzled planar cell polarity signaling. Genes Dev. *15*, 1182–1187.

Axelrod, J.D., Miller, J.R., Shulman, J.M., Moon, R.T., and Perrimon, N. (1998). Differential recruitment of Dishevelled provides signaling specificity in the planar cell polarity and Wingless signaling pathways. Genes Dev. *12*, 2610–2622.

Azimzadeh, J., and Marshall, W.F. (2010). Building the Centriole. Curr. Biol. CB *20*, R816–R825.

Baas, P.W., Rao, A.N., Matamoros, A.J., and Leo, L. (2016). Stability properties of neuronal microtubules. Cytoskeleton *73*, 442–460.

Babayeva, S., Zilber, Y., and Torban, E. (2011). Planar cell polarity pathway regulates actin rearrangement, cell shape, motility, and nephrin distribution in podocytes. Am. J. Physiol. - Ren. Physiol. *300*, F549–F560.

Bachmann-Gagescu, R., Phelps, I.G., Stearns, G., Link, B.A., Brockerhoff, S.E., Moens, C.B., and Doherty, D. (2011). The ciliopathy gene cc2d2a controls zebrafish photoreceptor outer segment development through a role in Rab8-dependent vesicle trafficking. Hum. Mol. Genet. *20*, 4041–4055.

Badano, J.L., Teslovich, T.M., and Katsanis, N. (2005). The centrosome in human genetic disease. Nat. Rev. Genet. *6*, 194–205.

Baena-López, L.A., Baonza, A., and García-Bellido, A. (2005). The Orientation of Cell Divisions Determines the Shape of Drosophila Organs. Curr. Biol. *15*, 1640–1644.

Basto, R., Lau, J., Vinogradova, T., Gardiol, A., Woods, C.G., Khodjakov, A., and Raff, J.W. (2006). Flies without Centrioles. Cell *125*, 1375–1386.

Bastock, R., Strutt, H., and Strutt, D. (2003). Strabismus is asymmetrically localised and binds to Prickle and Dishevelled during Drosophila planar polarity patterning. Development *130*, 3007–3014.

Beisson, J., and Wright, M. (2003). Basal body/centriole assembly and continuity. Curr. Opin. Cell Biol. *15*, 96–104.

Bettencourt-Dias, M., and Glover, D.M. (2007). Centrosome biogenesis and function: centrosomics brings new understanding. Nat. Rev. Mol. Cell Biol. *8*, 451–463.

Bingham, S., Higashijima, S., Okamoto, H., and Chandrasekhar, A. (2002). The Zebrafish trilobite Gene Is Essential for Tangential Migration of Branchiomotor Neurons. Dev. Biol. *242*, 149–160.

Blacque, O.E., and Leroux, M.R. (2006). Bardet-Biedl syndrome: an emerging pathomechanism of intracellular transport. Cell. Mol. Life Sci. CMLS *63*, 2145–2161.

Blitzer, A.L., Panagis, L., Gusella, G.L., Danias, J., Mlodzik, M., and Iomini, C. (2011). Primary cilia dynamics instruct tissue patterning and repair of corneal endothelium. Proc. Natl. Acad. Sci. U. S. A. *108*, 2819–2824.

Boisvieux-Ulrich, E., Laine, M.C., and Sandoz, D. (1985). The orientation of ciliary basal bodies in quail oviduct is related to the ciliary beating cycle commencement. Biol. Cell *55*, 147–150.

Boisvieux-Ulrich, E., Lainé, M.-C., and Sandoz, D. (1990). Cytochalasin D inhibits basal body migration and ciliary elongation in quail oviduct epithelium. Cell Tissue Res. *259*, 443–454.

Bokoch, G.M. (2003). Biology of the p21-activated kinases. Annu. Rev. Biochem. *72*, 743–781.

Bornens, M. (2012). The Centrosome in Cells and Organisms. Science *335*, 422–426.

Borovina, A., Superina, S., Voskas, D., and Ciruna, B. (2010). Vangl2 directs the posterior tilting and asymmetric localization of motile primary cilia. Nat. Cell Biol. *12*, 407–412.

Boutin, C., Labedan, P., Dimidschstein, J., Richard, F., Cremer, H., André, P., Yang, Y., Montcouquiol, M., Goffinet, A.M., and Tissir, F. (2014). A dual role for planar cell polarity genes in ciliated cells. Proc. Natl. Acad. Sci. *111*, E3129–E3138.

Brodu, V., Baffet, A.D., Le Droguen, P.-M., Casanova, J., and Guichet, A. (2010). A Developmentally Regulated Two-Step Process Generates a Noncentrosomal Microtubule Network in Drosophila Tracheal Cells. Dev. Cell *18*, 790–801.

Brooks, E.R., and Wallingford, J.B. (2014). Multiciliated cells: a review. Curr. Biol. CB *24*, R973–R982.

Brzoska, H.L., d'Esposito, A.M., Kolatsi-Joannou, M., Patel, V., Igarashi, P., Lei, Y., Finnell, R.H., Lythgoe, M.F., Woolf, A.S., Papakrivopoulou, E., et al. (2016). Planar cell polarity genes Celsr1 and Vangl2 are necessary for kidney growth, differentiation and rostrocaudal patterning. Kidney Int. *90*, 1274–1284.

Buendia (1990). Cytoskeletal control of centrioles movement during the establishment of polarity in Madin-Darby canine kidney cells. J. Cell Biol. *110*, 1123–1135.

Bulinski, J.C., and Gundersen, G.G. (1991). Stabilization and post-translational modification of microtubules during cellular morphogenesis. BioEssays *13*, 285–293.

Burkhardt, J.K., Echeverri, C.J., Nilsson, T., and Vallee, R.B. (1997). Overexpression of the Dynamitin (p50) Subunit of the Dynactin Complex Disrupts Dynein-dependent Maintenance of Membrane Organelle Distribution. J. Cell Biol. *139*, 469–484.

Butler, M.T., and Wallingford, J.B. (2015). Control of vertebrate core planar cell polarity protein localization and dynamics by Prickle 2. Development *142*, 3429–3439.

Butler, M.T., and Wallingford, J.B. (2017). Planar cell polarity in development and disease. Nat. Rev. Mol. Cell Biol. *18*, 375–388.

Calisto, J.D., Araya, C., Marchant, L., Riaz, C.F., and Mayor, R. (2005). Essential role of non-canonical Wnt signalling in neural crest migration. Development *132*, 2587–2597.

Carmona-Fontaine, C., Matthews, H.K., Kuriyama, S., Moreno, M., Dunn, G.A., Parsons, M., Stern, C.D., and Mayor, R. (2008). Contact inhibition of locomotion in vivo controls neural crest directional migration. Nature *456*, 957–961.

Carreira-Barbosa, F., Concha, M.L., Takeuchi, M., Ueno, N., Wilson, S.W., and Tada, M. (2003). Prickle 1 regulates cell movements during gastrulation and neuronal migration in zebrafish. Development *130*, 4037–4046.

Carvajal-Gonzalez, J.M., Balmer, S., Mendoza, M., Dussert, A., Collu, G., Roman, A.-C., Weber, U., Ciruna, B., and Mlodzik, M. (2015). The clathrin adaptor AP-1 complex and Arf1 regulate planar cell polarity *in vivo*. Nat. Commun. *6*, ncomms7751.

Carvajal-Gonzalez, J.M., Roman, A.-C., and Mlodzik, M. (2016a). Positioning of centrioles is a conserved readout of Frizzled planar cell polarity signalling. Nat. Commun. *7*, 11135.

Carvajal-Gonzalez, J.M., Mulero-Navarro, S., and Mlodzik, M. (2016b). Centriole positioning in epithelial cells and its intimate relationship with planar cell polarity. BioEssays *38*, 1234–1245.

Carvalho-Santos, Z., Azimzadeh, J., Pereira-Leal, J.B., and Bettencourt-Dias, M. (2011). Tracing the origins of centrioles, cilia, and flagella. J Cell Biol *194*, 165–175.

Chandrasekhar, A. (2004). Turning Heads: Development of Vertebrate Branchiomotor Neurons. Dev. Dyn. Off. Publ. Am. Assoc. Anat. *229*, 143–161.

Charron, F., Stein, E., Jeong, J., McMahon, A.P., and Tessier-Lavigne, M. (2003). The Morphogen Sonic Hedgehog Is an Axonal Chemoattractant that Collaborates with Netrin-1 in Midline Axon Guidance. Cell *113*, 11–23.

Chen, W.-S., Antic, D., Matis, M., Logan, C.Y., Povelones, M., Anderson, G.A., Nusse, R., and Axelrod, J.D. (2008). Asymmetric Homotypic Interactions of the Atypical Cadherin Flamingo Mediate Intercellular Polarity Signaling. Cell *133*, 1093–1105.

Chien, Y.-H., Keller, R., Kintner, C., and Shook, D.R. (2015). Mechanical Strain Determines the Axis of Planar Polarity in Ciliated Epithelia. Curr. Biol. *25*, 2774–2784.

Cho, B., Pierre-Louis, G., Sagner, A., Eaton, S., and Axelrod, J.D. (2015). Clustering and Negative Feedback by Endocytosis in Planar Cell Polarity Signaling Is Modulated by Ubiquitinylation of Prickle. PLOS Genet. *11*, e1005259.

Chu, C.-W., and Sokol, S.Y. (2016). Wnt proteins can direct planar cell polarity in vertebrate ectoderm. eLife *5*, e16463.

Ciruna, B., Jenny, A., Lee, D., Mlodzik, M., and Schier, A.F. (2006). Planar cell polarity signalling couples cell division and morphogenesis during neurulation. Nature *439*, 220–224.

Classen, A.-K., Anderson, K.I., Marois, E., and Eaton, S. (2005). Hexagonal Packing of Drosophila Wing Epithelial Cells by the Planar Cell Polarity Pathway. Dev. Cell *9*, 805–817.

Clevers, H., and Nusse, R. (2012). Wnt/β-Catenin Signaling and Disease. Cell *149*, 1192–1205.

Collier, S., and Gubb, D. (1997). Drosophila tissue polarity requires the cell-autonomous activity of the fuzzy gene, which encodes a novel transmembrane protein. Development *124*, 4029–4037.

Collier, S., Lee, H., Burgess, R., and Adler, P. (2005). The WD40 Repeat Protein Fritz Links Cytoskeletal Planar Polarity to Frizzled Subcellular Localization in the Drosophila Epidermis. Genetics *169*, 2035–2045.

Courbard, J.-R., Djiane, A., Wu, J., and Mlodzik, M. (2009). The apical/basal-polarity determinant Scribble cooperates with the PCP core factor Stbm/Vang and functions as one of its effectors. Dev. Biol. *333*, 67–77.

Curtin, J.A., Quint, E., Tsipouri, V., Arkell, R.M., Cattanach, B., Copp, A.J., Henderson, D.J., Spurr, N., Stanier, P., Fisher, E.M., et al. (2003). Mutation of Celsr1 Disrupts Planar Polarity of Inner Ear Hair Cells and Causes Severe Neural Tube Defects in the Mouse. Curr. Biol. *13*, 1129–1133.

Das, G., Jenny, A., Klein, T.J., Eaton, S., and Mlodzik, M. (2004). Diego interacts with Prickle and Strabismus/Van Gogh to localize planar cell polarity complexes. Development *131*, 4467–4476.

Davey, C.F., and Moens, C.B. (2017). Planar cell polarity in moving cells: think globally, act locally. Development *144*, 187–200.

Davey, C.F., Mathewson, A.W., and Moens, C.B. (2016). PCP Signaling between Migrating Neurons and their Planar-Polarized Neuroepithelial Environment Controls Filopodial Dynamics and Directional Migration. PLOS Genet. *12*, e1005934.

Dawe, H.R., Farr, H., and Gull, K. (2007). Centriole/basal body morphogenesis and migration during ciliogenesis in animal cells. J. Cell Sci. *120*, 7–15.

Devenport, D., and Fuchs, E. (2008). Planar polarization in embryonic epidermis orchestrates global asymmetric morphogenesis of hair follicles. Nat. Cell Biol. *10*, 1257–1268.

Devenport, D., Oristian, D., Heller, E., and Fuchs, E. (2011). Mitotic Internalization of Planar Cell Polarity Proteins Preserves Tissue Polarity. Nat. Cell Biol. *13*, 893–902.

Eaton, S., Auvinen, P., Luo, L., Jan, Y.N., and Simons, K. (1995). CDC42 and Rac1 control different actin-dependent processes in the Drosophila wing disc epithelium. J. Cell Biol. *131*, 151–164.

Eaton, S., Wepf, R., and Simons, K. (1996). Roles for Rac1 and Cdc42 in planar polarization and hair outgrowth in the wing of Drosophila. J. Cell Biol. *135*, 1277–1289.

Ertzer, R., Müller, F., Hadzhiev, Y., Rathnam, S., Fischer, N., Rastegar, S., and Strähle, U. (2007). Cooperation of sonic hedgehog enhancers in midline expression. Dev. Biol. *301*, 578–589.

Essner, J.J., Vogan, K.J., Wagner, M.K., Tabin, C.J., Yost, H.J., and Brueckner, M. (2002). Left–right development: Conserved function for embryonic nodal cilia. Nature *418*, 37–38.

Etheridge, S.L., Ray, S., Li, S., Hamblet, N.S., Lijam, N., Tsang, M., Greer, J., Kardos, N., Wang, J., Sussman, D.J., et al. (2008). Murine Dishevelled 3 Functions in Redundant Pathways with Dishevelled 1 and 2 in Normal Cardiac Outflow Tract, Cochlea, and Neural Tube Development. PLOS Genet. *4*, e1000259.

Euteneur, U., and Schliwa, M. (1992). Mechanism of centrosome positioning during the wound response in BSC-1 cells. J. Cell Biol. *116*, 1157–1166.

Ezan, J., Lasvaux, L., Gezer, A., Novakovic, A., May-Simera, H., Belotti, E., Lhoumeau, A.-C., Birnbaumer, L., Beer-Hammer, S., Borg, J.-P., et al. (2013). Primary cilium migration depends on G-protein signalling control of subapical cytoskeleton. Nat. Cell Biol. *15*, 1107–1115.

Feng, Y., and Irvine, K.D. (2009). Processing and phosphorylation of the Fat receptor. Proc. Natl. Acad. Sci. *106*, 11989–11994.

Gao, B., Song, H., Bishop, K., Elliot, G., Garrett, L., English, M.A., Andre, P., Robinson, J., Sood, R., Minami, Y., et al. (2011). Wnt Signaling Gradients Establish Planar Cell Polarity by Inducing Vangl2 Phosphorylation through Ror2. Dev. Cell *20*, 163–176.

Gerdes, J.M., Liu, Y., Zaghloul, N.A., Leitch, C.C., Lawson, S.S., Kato, M., Beachy, P.A., Beales, P.L., DeMartino, G.N., Fisher, S., et al. (2007). Disruption of the basal body compromises proteasomal function and perturbs intracellular Wnt response. Nat. Genet. *39*, 1350–1360.

Gogendeau, D., and Basto, R. (2010). Centrioles in flies: The exception to the rule? Semin. Cell Dev. Biol. *21*, 163–173.

Goll, M.G., Anderson, R., Stainier, D.Y.R., Spradling, A.C., and Halpern, M.E. (2009). Transcriptional Silencing and Reactivation in Transgenic Zebrafish. Genetics *182*, 747–755.

Goodrich, L.V., and Strutt, D. (2011). Principles of planar polarity in animal development. Development *138*, 1877–1892.

Grant, P.K., and Moens, C.B. (2010). The neuroepithelial basement membrane serves as a boundary and a substrate for neuron migration in the zebrafish hindbrain. Neural Develop. *5*, 9.

Gray, R.S., Abitua, P.B., Wlodarczyk, B.J., Szabo-Rogers, H.L., Blanchard, O., Lee, I., Weiss, G.S., Liu, K.J., Marcotte, E.M., Wallingford, J.B., et al. (2009). The planar cell polarity effector Fuz is essential for targeted membrane trafficking, ciliogenesis and mouse embryonic development. Nat. Cell Biol. *11*, 1225–1232.

Gubb, D., and García-Bellido, A. (1982). A genetic analysis of the determination of cuticular polarity during development in *Drosophila melanogaster*. Development *68*, 37–57.

Gubb, D., Green, C., Huen, D., Coulson, D., Johnson, G., Tree, D., Collier, S., and Roote, J. (1999). The balance between isoforms of the Prickle LIM domain protein is critical for planar polarity in Drosophila imaginal discs. Genes Dev. *13*, 2315–2327.

Guirao, B., Meunier, A., Mortaud, S., Aguilar, A., Corsi, J.-M., Strehl, L., Hirota, Y., Desoeuvre, A., Boutin, C., Han, Y.-G., et al. (2010). Coupling between hydrodynamic forces and planar cell polarity orients mammalian motile cilia. Nat. Cell Biol. *12*, 341–350.

Hale, R., and Strutt, D. (2015). Conservation of Planar Polarity Pathway Function Across the Animal Kingdom. Annu. Rev. Genet. *49*, 529–551.

Hannus, M., Feiguin, F., Heisenberg, C.-P., and Eaton, S. (2002). Planar cell polarization requires Widerborst, a B′ regulatory subunit of protein phosphatase 2A. Development *129*, 3493–3503.

Harumoto, T., Ito, M., Shimada, Y., Kobayashi, T.J., Ueda, H.R., Lu, B., and Uemura, T. (2010). Atypical Cadherins Dachsous and Fat Control Dynamics of Noncentrosomal Microtubules in Planar Cell Polarity. Dev. Cell *19*, 389–401.

Hashimoto, M., Shinohara, K., Wang, J., Ikeuchi, S., Yoshiba, S., Meno, C., Nonaka, S., Takada, S., Hatta, K., Wynshaw-Boris, A., et al. (2010). Planar polarization of node cells determines the rotational axis of node cilia. Nat. Cell Biol. *12*, 170–176.

Heisenberg, C.-P., Tada, M., Rauch, G.-J., Saúde, L., Concha, M.L., Geisler, R., Stemple, D.L., Smith, J.C., and Wilson, S.W. (2000). Silberblick/Wnt11 mediates convergent extension movements during zebrafish gastrulation. Nature *405*, 76–81.

Jenny, A., Darken, R.S., Wilson, P.A., and Mlodzik, M. (2003). Prickle and Strabismus form a functional complex to generate a correct axis during planar cell polarity signaling. EMBO J. *22*, 4409–4420.

Jenny, A., Reynolds-Kenneally, J., Das, G., Burnett, M., and Mlodzik, M. (2005). Diego and Prickle regulate Frizzled planar cell polarity signalling by competing for Dishevelled binding. Nat. Cell Biol. *7*, 691–697.

Jessen, J.R., Topczewski, J., Bingham, S., Sepich, D.S., Marlow, F., Chandrasekhar, A., and Solnica-Krezel, L. (2002). Zebrafish trilobite identifies new roles for Strabismus in gastrulation and neuronal movements. Nat. Cell Biol. *4*, 610–615.

Jones, C., Roper, V.C., Foucher, I., Qian, D., Banizs, B., Petit, C., Yoder, B.K., and Chen, P. (2008). Ciliary proteins link basal body polarization to planar cell polarity regulation. Nat. Genet. *40*, 69–77.

Kawakami, K., Shima, A., and Kawakami, N. (2000). Identification of a functional transposase of the Tol2 element, an Ac-like element from the Japanese medaka fish, and its transposition in the zebrafish germ lineage. Proc. Natl. Acad. Sci. *97*, 11403–11408.

Kibar, Z., Torban, E., McDearmid, J.R., Reynolds, A., Berghout, J., Mathieu, M., Kirillova, I., De Marco, P., Merello, E., Hayes, J.M., et al. (2007). Mutations in VANGL1 Associated with Neural-Tube Defects. N. Engl. J. Med. *356*, 1432–1437.

Kim, J.H., Lee, S.-R., Li, L.-H., Park, H.-J., Park, J.-H., Lee, K.Y., Kim, M.-K., Shin, B.A., and Choi, S.-Y. (2011). High Cleavage Efficiency of a 2A Peptide Derived from Porcine Teschovirus-1 in Human Cell Lines, Zebrafish and Mice. PLOS ONE *6*, e18556.

Kim, S.K., Shindo, A., Park, T.J., Oh, E.C., Ghosh, S., Gray, R.S., Lewis, R.A., Johnson, C.A., Attie-Bittach, T., Katsanis, N., et al. (2010). Planar Cell Polarity Acts Through Septins to Control Collective Cell Movement and Ciliogenesis. Science *329*, 1337–1340.

Kimmel, C.B., Ballard, W.W., Kimmel, S.R., Ullmann, B., and Schilling, T.F. (1995). Stages of embryonic development of the zebrafish. Dev. Dyn. *203*, 253–310.

Kimura, Y., Hisano, Y., Kawahara, A., and Higashijima, S. (2014). Efficient generation of knock-in transgenic zebrafish carrying reporter/driver genes by CRISPR/Cas9-mediated genome engineering. Sci. Rep. *4*.

Kourakis, M.J., Reeves, W., Newman-Smith, E., Maury, B., Abdul-Wajid, S., and Smith, W.C. (2014). A one-dimensional model of PCP signaling: Polarized cell behavior in the notochord of the ascidian Ciona. Dev. Biol. *395*, 120–130.

Lawrence, P.A., Casal, J., and Struhl, G. (2002). Towards a model of the organisation of planar polarity and pattern in the Drosophila abdomen. Development *129*, 2749–2760.

Lawrence, P.A., Casal, J., and Struhl, G. (2004). Cell interactions and planar polarity in the abdominal epidermis of *Drosophila*. Development *131*, 4651–4664.

Lechler, T., and Fuchs, E. (2007). Desmoplakin: an unexpected regulator of microtubule organization in the epidermis. J. Cell Biol. *176*, 147–154.

Lee, H., and Adler, P.N. (2002). The function of the frizzled pathway in the Drosophila wing is dependent on inturned and fuzzy. Genetics *160*, 1535–1547.

Lu, Q., Yan, J., and Adler, P.N. (2010). The Drosophila Planar Polarity Proteins Inturned and Multiple Wing Hairs Interact Physically and Function Together. Genetics *185*, 549–558.

Lu, Q., Schafer, D.A., and Adler, P.N. (2015). The Drosophila planar polarity gene multiple wing hairs directly regulates the actin cytoskeleton. Dev. Camb. Engl. *142*, 2478–2486.

Luga, V., Zhang, L., Viloria-Petit, A.M., Ogunjimi, A.A., Inanlou, M.R., Chiu, E., Buchanan, M., Hosein, A.N., Basik, M., and Wrana, J.L. (2012). Exosomes Mediate Stromal Mobilization of Autocrine Wnt-PCP Signaling in Breast Cancer Cell Migration. Cell *151*, 1542–1556.

Ma, D., Yang, C., McNeill, H., Simon, M.A., and Axelrod, J.D. (2003). Fidelity in planar cell polarity signalling. Nature *421*, 543–547.

MacMillan, C.D., Leong, H.S., Dales, D.W., Robertson, A.E., Lewis, J.D., Chambers, A.F., and Tuck, A.B. (2014). Stage of Breast Cancer Progression Influences Cellular Response to Activation of the WNT/Planar Cell Polarity Pathway. Sci. Rep. *4*, 6315.

Mahaffey, J.P., Grego-Bessa, J., Liem, K.F., and Anderson, K.V. (2013). Cofilin and Vangl2 cooperate in the initiation of planar cell polarity in the mouse embryo. Development *140*, 1262–1271.

Mao, Y., Tournier, A.L., Bates, P.A., Gale, J.E., Tapon, N., and Thompson, B.J. (2011). Planar polarization of the atypical myosin Dachs orients cell divisions in Drosophila. Genes Dev. *25*, 131–136.

Mapp, O.M., Wanner, S.J., Rohrschneider, M.R., and Prince, V.E. (2010). Prickle1b mediates interpretation of migratory cues during zebrafish facial branchiomotor neuron migration. Dev. Dyn. *239*, 1596–1608.

Mapp, O.M., Walsh, G.S., Moens, C.B., Tada, M., and Prince, V.E. (2011). Zebrafish Prickle1b mediates facial branchiomotor neuron migration via a farnesylation-dependent nuclear activity. Development *138*, 2121–2132.

Matakatsu, H., and Blair, S.S. (2004). Interactions between Fat and Dachsous and the regulation of planar cell polarity in the *Drosophila wing*. Development *131*, 3785–3794.

Matis, M., Russler-Germain, D.A., Hu, Q., Tomlin, C.J., and Axelrod, J.D. (2014). Microtubules provide directional information for core PCP function. eLife *3*, e02893.

May-Simera, H.L., Kai, M., Hernandez, V., Osborn, D.P.S., Tada, M., and Beales, P.L. (2010). Bbs8, together with the planar cell polarity protein Vangl2, is required to establish left–right asymmetry in zebrafish. Dev. Biol. *345*, 215–225.

May-Simera, H.L., Petralia, R.S., Montcouquiol, M., Wang, Y.-X., Szarama, K.B., Liu, Y., Lin, W., Deans, M.R., Pazour, G.J., and Kelley, M.W. (2015). Ciliary proteins Bbs8 and Ift20 promote planar cell polarity in the cochlea. Development *142*, 555–566.

McFarland, R.J., Brown, S.P., Vital, E., Werner, J.M., and Brewster, R.M. (2017). Use of Immunolabeling to Analyze Stable, Dynamic, and Nascent Microtubules in the Zebrafish Embryo. JoVE J. Vis. Exp. e55792–e55792.

Meijering, E., Dzyubachyk, O., and Smal, I. (2012). Methods for Cell and Particle Tracking (Elsevier).

Mirzadeh, Z., Han, Y.-G., Soriano-Navarro, M., García-Verdugo, J.M., and Alvarez-Buylla, A. (2010). Cilia Organize Ependymal Planar Polarity. J. Neurosci. *30*, 2600–2610.

Mitchell, B., Jacobs, R., Li, J., Chien, S., and Kintner, C. (2007). A positive feedback mechanism governs the polarity and motion of motile cilia. Nature *447*, 97–101.

Mitchell, B., Stubbs, J.L., Huisman, F., Taborek, P., Yu, C., and Kintner, C. (2009). The PCP Pathway Instructs the Planar Orientation of Ciliated Cells in the Xenopus Larval Skin. Curr. Biol. *19*, 924–929.

Montcouquiol, M., Rachel, R.A., Lanford, P.J., Copeland, N.G., Jenkins, N.A., and Kelley, M.W. (2003). Identification of Vangl2 and Scrb1 as planar polarity genes in mammals. Nature *423*, 173–177.

Montcouquiol, M., Sans, N., Huss, D., Kach, J., Dickman, J.D., Forge, A., Rachel, R.A., Copeland, N.G., Jenkins, N.A., Bogani, D., et al. (2006). Asymmetric Localization of Vangl2 and Fz3 Indicate Novel Mechanisms for Planar Cell Polarity in Mammals. J. Neurosci. *26*, 5265–5275.

Moritz, M., and Agard, D.A. (2001). γ-Tubulin complexes and microtubule nucleation. Curr. Opin. Struct. Biol. *11*, 174–181.

Mottola, G., Classen, A.-K., González-Gaitán, M., Eaton, S., and Zerial, M. (2010). A novel function for the Rab5 effector Rabenosyn-5 in planar cell polarity. Development *137*, 2353–2364.

Murdoch, J.N., Henderson, D.J., Doudney, K., Gaston-Massuet, C., Phillips, H.M., Paternotte, C., Arkell, R., Stanier, P., and Copp, A.J. (2003). Disruption of scribble (Scrb1) causes severe neural tube defects in the circletail mouse. Hum. Mol. Genet. *12*, 87–98.

Muroyama, A., and Lechler, T. (2017). Microtubule organization, dynamics and functions in differentiated cells. Development *144*, 3012–3021.

Narimatsu, M., Bose, R., Pye, M., Zhang, L., Miller, B., Ching, P., Sakuma, R., Luga, V., Roncari, L., Attisano, L., et al. (2009). Regulation of Planar Cell Polarity by Smurf Ubiquitin Ligases. Cell *137*, 295–307.

Newman-Smith, E., Kourakis, M.J., Reeves, W., Veeman, M., and Smith, W.C. (2015). Reciprocal and dynamic polarization of planar cell polarity core components and myosin. eLife *4*, e05361.

Nigg, E.A., and Raff, J.W. (2009). Centrioles, Centrosomes, and Cilia in Health and Disease. Cell *139*, 663–678.

Nonaka, S., Yoshiba, S., Watanabe, D., Ikeuchi, S., Goto, T., Marshall, W.F., and Hamada, H. (2005). De Novo Formation of Left–Right Asymmetry by Posterior Tilt of Nodal Cilia. PLoS Biol. *3*.

Ohata, S., and Álvarez-Buylla, A. (2016). Planar organization of multiciliated ependymal (E1) cells in the brain ventricular epithelium. Trends Neurosci. *39*, 543–551.

Ohata, S., Nakatani, J., Herranz-Pérez, V., Cheng, J., Belinson, H., Inubushi, T., Snider, W.D., García-Verdugo, J.M., Wynshaw-Boris, A., and Álvarez-Buylla, A. (2014). Loss of Dishevelleds disrupts planar polarity in ependymal motile cilia and results in hydrocephalus. Neuron *83*, 558–571.

Okada, Y., Takeda, S., Tanaka, Y., Belmonte, J.-C.I., and Hirokawa, N. (2005). Mechanism of Nodal Flow: A Conserved Symmetry Breaking Event in Left-Right Axis Determination. Cell *121*, 633–644.

Olofsson, J., Sharp, K.A., Matis, M., Cho, B., and Axelrod, J.D. (2014). Prickle/spiny-legs isoforms control the polarity of the apical microtubule network in planar cell polarity. Development *141*, 2866–2874.

Ossipova, O., Kim, K., Lake, B.B., Itoh, K., Ioannou, A., and Sokol, S.Y. (2014). Role of Rab11 in planar cell polarity and apical constriction during vertebrate neural tube closure. Nat. Commun. *5*, 3734.

Ossipova, O., Kim, K., and Sokol, S.Y. (2015). Planar polarization of Vangl2 in the vertebrate neural plate is controlled by Wnt and Myosin II signaling. Biol. Open *4*, 722–730.

Park, T.J., Haigo, S.L., and Wallingford, J.B. (2006). Ciliogenesis defects in embryos lacking inturned or fuzzy function are associated with failure of planar cell polarity and Hedgehog signaling. Nat. Genet. *38*, 303–311.

Park, T.J., Mitchell, B.J., Abitua, P.B., Kintner, C., and Wallingford, J.B. (2008). Dishevelled controls apical docking and planar polarization of basal bodies in ciliated epithelial cells. Nat. Genet. *40*, 871–879.

Park, W.J., Liu, J., Sharp, E.J., and Adler, P.N. (1996). The Drosophila tissue polarity gene inturned acts cell autonomously and encodes a novel protein. Development *122*, 961–969.

Patten, I., and Placzek*, M. (2000). The role of Sonic hedgehog in neural tube patterning. Cell. Mol. Life Sci. CMLS *57*, 1695–1708.

Placzek, M., and Briscoe, J. (2005). The floor plate: multiple cells, multiple signals. Nat. Rev. Neurosci. *6*, 230–240.

Qian, D., Jones, C., Rzadzinska, A., Mark, S., Zhang, X., Steel, K.P., Dai, X., and Chen, P. (2007). Wnt5a functions in planar cell polarity regulation in mice. Dev. Biol. *306*, 121–133.

Qu, Y., Glasco, D.M., Zhou, L., Sawant, A., Ravni, A., Fritzsch, B., Damrau, C., Murdoch, J.N., Evans, S., Pfaff, S.L., et al. (2010). Atypical Cadherins Celsr1-3 Differentially Regulate Migration of Facial Branchiomotor Neurons in Mice. J. Neurosci. *30*, 9392–9401.

Reiter, J.F., Blacque, O.E., and Leroux, M.R. (2012). The base of the cilium: roles for transition fibres and the transition zone in ciliary formation, maintenance and compartmentalization. EMBO Rep. *13*, 608–618.

Rodriguez-Boulan, E., and Macara, I.G. (2014). Organization and execution of the epithelial polarity programme. Nat. Rev. Mol. Cell Biol. *15*, 225–242.

Rodríguez-Fraticelli, A.E., Auzan, M., Alonso, M.A., Bornens, M., and Martín-Belmonte, F. (2012). Cell confinement controls centrosome positioning and lumen initiation during epithelial morphogenesis. J. Cell Biol. *198*, 1011–1023.

Rogers, G.C., Rusan, N.M., Peifer, M., and Rogers, S.L. (2008). A Multicomponent Assembly Pathway Contributes to the Formation of Acentrosomal Microtubule Arrays in Interphase Drosophila Cells. Mol. Biol. Cell *19*, 3163–3178.

Rohrschneider, M.R., Elsen, G.E., and Prince, V.E. (2007). Zebrafish Hoxb1a regulates multiple downstream genes including prickle1b. Dev. Biol. *309*, 358–372.

Ross, A.J., May-Simera, H., Eichers, E.R., Kai, M., Hill, J., Jagger, D.J., Leitch, C.C., Chapple, J.P., Munro, P.M., Fisher, S., et al. (2005). Disruption of Bardet-Biedl syndrome ciliary proteins perturbs planar cell polarity in vertebrates. Nat. Genet. *37*, 1135–1140.

Roszko, I., Sawada, A., and Solnica-Krezel, L. (2009). Regulation of convergence and extension movements during vertebrate gastrulation by the Wnt/PCP pathway. Semin. Cell Dev. Biol. *20*, 986–997.

Sanchez, A.D., and Feldman, J.L. (2016). Microtubule-organizing centers: from the centrosome to non-centrosomal sites. Curr. Opin. Cell Biol.

Sawyer, J.M., Harrell, J.R., Shemer, G., Sullivan-Brown, J., Roh-Johnson, M., and Goldstein, B. (2010). Apical Constriction: A Cell Shape Change that Can Drive Morphogenesis. Dev. Biol. *341*, 5–19.

Schneider, C.A., Rasband, W.S., and Eliceiri, K.W. (2012). NIH Image to ImageJ: 25 years of image analysis. Nat. Methods *9*, 671–675.

Sepich, D.S., and Solnica-Krezel, L. (2016). Intracellular Golgi Complex organization reveals tissue specific polarity during zebrafish embryogenesis. Dev. Dyn. *245*, 678–691.

Sepich, D.S., Usmani, M., Pawlicki, S., and Solnica-Krezel, L. (2011). Wnt/PCP signaling controls intracellular position of MTOCs during gastrulation convergence and extension movements. Development *138*, 543–552.

Shafer, B., Onishi, K., Lo, C., Colakoglu, G., and Zou, Y. (2011). Vangl2 Promotes Wnt/Planar Cell Polarity-like Signaling by Antagonizing Dvl1-Mediated Feedback Inhibition in Growth Cone Guidance. Dev. Cell *20*, 177–191.

Shi, D., Komatsu, K., Hirao, M., Toyooka, Y., Koyama, H., Tissir, F., Goffinet, A.M., Uemura, T., and Fujimori, T. (2014). Celsr1 is required for the generation of polarity at multiple levels of the mouse oviduct. Development *141*, 4558–4568.

Shi, D., Usami, F., Komatsu, K., Oka, S., Abe, T., Uemura, T., and Fujimori, T. (2016). Dynamics of planar cell polarity protein Vangl2 in the mouse oviduct epithelium. Mech. Dev. *141*, 78–89.

Shimada, Y., Yonemura, S., Ohkura, H., Strutt, D., and Uemura, T. (2006). Polarized Transport of Frizzled along the Planar Microtubule Arrays in Drosophila Wing Epithelium. Dev. Cell *10*, 209–222.

Shrestha, R., Little, K.A., Tamayo, J.V., Li, W., Perlman, D.H., and Devenport, D. (2015). Mitotic Control of Planar Cell Polarity by Polo-like Kinase 1. Dev. Cell *33*, 522–534.

Simon, M.A. (2004). Planar cell polarity in the *Drosophila* eye is directed by graded Four-jointed and Dachsous expression. Development *131*, 6175–6184.

Simons, M., Gault, W.J., Gotthardt, D., Rohatgi, R., Klein, T.J., Shao, Y., Lee, H.-J., Wu, A.-L., Fang, Y., Satlin, L.M., et al. (2009). Electrochemical cues regulate assembly of the Frizzled/Dishevelled complex at the plasma membrane during planar epithelial polarization. Nat. Cell Biol. *11*, 286–294.

Sipe, C.W., and Lu, X. (2011). Kif3a regulates planar polarization of auditory hair cells through both ciliary and non-ciliary mechanisms. Development *138*, 3441–3449.

Sokol, S.Y. (2015). Spatial and temporal aspects of Wnt signaling and planar cell polarity during vertebrate embryonic development. Semin. Cell Dev. Biol. *42*, 78–85.

Song, H., Hu, J., Chen, W., Elliott, G., Andre, P., Gao, B., and Yang, Y. (2010). Planar cell polarity breaks bilateral symmetry by controlling ciliary positioning. Nature *466*, 378–382.

Sopko, R., Silva, E., Clayton, L., Gardano, L., Barrios-Rodiles, M., Wrana, J., Varelas, X., Arbouzova, N.I., Shaw, S., Saburi, S., et al. (2009). Phosphorylation of the tumour suppressor Fat is regulated via interaction with its ligand Dachsous, and the kinase, Discs Overgrown. Curr. Biol. CB *19*, 1112–1117.

Stepanova, T., Slemmer, J., Hoogenraad, C.C., Lansbergen, G., Dortland, B., Zeeuw, C.I.D., Grosveld, F., Cappellen, G. van, Akhmanova, A., and Galjart, N. (2003). Visualization of Microtubule Growth in Cultured Neurons via the Use of EB3-GFP (End-Binding Protein 3-Green Fluorescent Protein). J. Neurosci. *23*, 2655–2664.

Struhl, G., Casal, J., and Lawrence, P.A. (2012). Dissecting the molecular bridges that mediate the function of Frizzled in planar cell polarity. Development *139*, 3665–3674.

Strutt, D.I. (2001). Asymmetric Localization of Frizzled and the Establishment of Cell Polarity in the Drosophila Wing. Mol. Cell *7*, 367–375.

Strutt, D., and Strutt, H. (2007). Differential activities of the core planar polarity proteins during Drosophila wing patterning. Dev. Biol. *302*, 181–194.

Strutt, D., and Warrington, S.J. (2008). Planar polarity genes in the Drosophila wing regulate the localisation of the FH3-domain protein Multiple Wing Hairs to control the site of hair production. Development *135*, 3103–3111.

Strutt, H., and Strutt, D. (2002). Nonautonomous Planar Polarity Patterning in Drosophila. Dev. Cell *3*, 851–863.

Strutt, H., and Strutt, D. (2008). Differential Stability of Flamingo Protein Complexes Underlies the Establishment of Planar Polarity. Curr. Biol. *18*, 1555–1564.

Strutt, D., Johnson, R., Cooper, K., and Bray, S. (2002). Asymmetric Localization of Frizzled and the Determination of Notch-Dependent Cell Fate in the Drosophila Eye. Curr. Biol. *12*, 813–824.

Strutt, D.I., Weber, U., and Mlodzik, M. (1997). The role of RhoA in tissue polarity and Frizzled signalling. Nature *387*, 292–295.

Strutt, H., Mundy, J., Hofstra, K., and Strutt, D. (2004). Cleavage and secretion is not required for Four-jointed function in *Drosophila* patterning. Development *131*, 881–890.

Strutt, H., Warrington, S.J., and Strutt, D. (2011). Dynamics of Core Planar Polarity Protein Turnover and Stable Assembly into Discrete Membrane Subdomains. Dev. Cell *20*, 511–525.

Strutt, H., Searle, E., Thomas-MacArthur, V., Brookfield, R., and Strutt, D. (2013). A Cul-3-BTB ubiquitylation pathway regulates junctional levels and asymmetry of core planar polarity proteins. Development *140*, 1693–1702.

Sugiyama, Y., Stump, R.J.W., Nguyen, A., Wen, L., Chen, Y., Wang, Y., Murdoch, J.N., Lovicu, F.J., and McAvoy, J.W. (2010). Secreted frizzled-related protein disrupts PCP in eye lens fiber cells that have polarised primary cilia. Dev. Biol. *338*, 193.

Tada, M., and Smith, J.C. (2000). Xwnt11 is a target of Xenopus Brachyury: regulation of gastrulation movements via Dishevelled, but not through the canonical Wnt pathway. Development *127*, 2227–2238.

Tanaka, N., Meng, W., Nagae, S., and Takeichi, M. (2012). Nezha/CAMSAP3 and CAMSAP2 cooperate in epithelial-specific organization of noncentrosomal microtubules. Proc. Natl. Acad. Sci. U. S. A. *109*, 20029–20034.

Taylor, J., Abramova, N., Charlton, J., and Adler, P.N. (1998). Van Gogh: A New Drosophila Tissue Polarity Gene. Genetics *150*, 199–210.

Tissir, F., Qu, Y., Montcouquiol, M., Zhou, L., Komatsu, K., Shi, D., Fujimori, T., Labeau, J., Tyteca, D., Courtoy, P., et al. (2010). Lack of cadherins Celsr2 and Celsr3 impairs ependymal ciliogenesis, leading to fatal hydrocephalus. Nat. Neurosci. *13*, 700–707.

Tree, D.R.P., Shulman, J.M., Rousset, R., Scott, M.P., Gubb, D., and Axelrod, J.D. (2002). Prickle Mediates Feedback Amplification to Generate Asymmetric Planar Cell Polarity Signaling. Cell *109*, 371–381.

Tsujikawa, M., Omori, Y., Biyanwila, J., and Malicki, J. (2007). Mechanism of positioning the cell nucleus in vertebrate photoreceptors. Proc. Natl. Acad. Sci. U. S. A. *104*, 14819–14824.

Turner, C.M., and Adler, P.N. (1998). Distinct roles for the actin and microtubule cytoskeletons in the morphogenesis of epidermal hairs during wing development in Drosophila. Mech. Dev. *70*, 181–192.

Usui, T., Shima, Y., Shimada, Y., Hirano, S., Burgess, R.W., Schwarz, T.L., Takeichi, M., and Uemura, T. (1999). Flamingo, a Seven-Pass Transmembrane Cadherin, Regulates Planar Cell Polarity under the Control of Frizzled. Cell *98*, 585–595.

Vinson, C.R., and Adler, P.N. (1987). Directional non-cell autonomy and the transmission of polarity information by the frizzled gene of Drosophila. Nature *329*, 549–551.

Vivancos, V., Chen, P., Spassky, N., Qian, D., Dabdoub, A., Kelley, M., Studer, M., and Guthrie, S. (2009). Wnt activity guides facial branchiomotor neuron migration, and involves the PCP pathway and JNK and ROCK kinases. Neural Develop. *4*, 7.

Vladar, E.K., Bayly, R.D., Sangoram, A.M., Scott, M.P., and Axelrod, J.D. (2012). Microtubules Enable the Planar Cell Polarity of Airway Cilia. Curr. Biol. *22*, 2203–2212.

Wada, H., Iwasaki, M., Sato, T., Masai, I., Nishiwaki, Y., Tanaka, H., Sato, A., Nojima, Y., and Okamoto, H. (2005). Dual roles of zygotic and maternal Scribble1 in neural migration and convergent extension movements in zebrafish embryos. Development *132*, 2273–2285.

Wada, H., Tanaka, H., Nakayama, S., Iwasaki, M., and Okamoto, H. (2006). Frizzled3a and Celsr2 function in the neuroepithelium to regulate migration of facial motor neurons in the developing zebrafish hindbrain. Development *133*, 4749–4759.

Wallingford, J.B. (2012). Planar Cell Polarity and the Developmental Control of Cell Behavior in Vertebrate Embryos. Annu. Rev. Cell Dev. Biol. *28*, 627–653.

Wallingford, J.B., and Harland, R.M. (2001). Xenopus Dishevelled signaling regulates both neural and mesodermal convergent extension: parallel forces elongating the body axis. Development *128*, 2581–2592.

Wallingford, J.B., Rowning, B.A., Vogeli, K.M., Rothbächer, U., Fraser, S.E., and Harland, R.M. (2000). Dishevelled controls cell polarity during Xenopus gastrulation. Nature *405*, 81–85.

Wallingford, J.B., Niswander, L.A., Shaw, G.M., and Finnell, R.H. (2013). The Continuing Challenge of Understanding, Preventing, and Treating Neural Tube Defects. Science *339*, 1222002.

Walsh, G.S., Grant, P.K., Morgan, J.A., and Moens, C.B. (2011). Planar polarity pathway and Nance-Horan syndrome-like 1b have essential cell-autonomous functions in neuronal migration. Development *138*, 3033–3042.

Wang, Y., Guo, N., and Nathans, J. (2006). The Role of Frizzled3 and Frizzled6 in Neural Tube Closure and in the Planar Polarity of Inner-Ear Sensory Hair Cells. J. Neurosci. *26*, 2147–2156.

Wanner, S.J., and Prince, V.E. (2013). Axon tracts guide zebrafish facial branchiomotor neuron migration through the hindbrain. Development *140*, 906–915.

Werner, M.E., and Mitchell, B.J. (2012). Planar Cell Polarity: Microtubules Make the Connection with Cilia. Curr. Biol. *22*, R1001–R1004.

Werner, M.E., Hwang, P., Huisman, F., Taborek, P., Yu, C.C., and Mitchell, B.J. (2011). Actin and microtubules drive differential aspects of planar cell polarity in multiciliated cells. J Cell Biol *195*, 19–26.

Werner, M.E., Mitchell, J.W., Putzbach, W., Bacon, E., Kim, S.K., and Mitchell, B.J. (2014). Radial intercalation is regulated by the Par complex and the microtubule-stabilizing protein CLAMP/Spef1. J. Cell Biol. *206*, 367–376.

Westerfield, M. (2000). The zebrafish book. A guide for the laboratory use of zebrafish (Danio rerio) (Univ. of Oregon Press, Eugene.).

Westermann, S., and Weber, K. (2003). Post-translational modifications regulate microtubule function. Nat. Rev. Mol. Cell Biol. *4*, 938–948.

Wong, H.-C., Bourdelas, A., Krauss, A., Lee, H.-J., Shao, Y., Wu, D., Mlodzik, M., Shi, D.-L., and Zheng, J. (2003). Direct Binding of the PDZ Domain of Dishevelled to a Conserved Internal Sequence in the C-Terminal Region of Frizzled. Mol. Cell *12*, 1251–1260.

Wu, J., and Mlodzik, M. (2008). The Frizzled Extracellular Domain Is a Ligand for Van Gogh/Stbm during Nonautonomous Planar Cell Polarity Signaling. Dev. Cell *15*, 462–469.

Wu, J., Roman, A.-C., Carvajal-Gonzalez, J.M., and Mlodzik, M. (2013). Wg and Wnt4 provide long-range directional input to planar cell polarity orientation in Drosophila. Nat. Cell Biol. *15*, 1045–1055.

Yadav, S., Puri, S., and Linstedt, A.D. (2009). A Primary Role for Golgi Positioning in Directed Secretion, Cell Polarity, and Wound Healing. Mol. Biol. Cell *20*, 1728–1736.

Yan, J., Huen, D., Morely, T., Johnson, G., Gubb, D., Roote, J., and Adler, P.N. (2008). The multiple-wing-hairs Gene Encodes a Novel GBD–FH3 Domain-Containing Protein That Functions Both Prior to and After Wing Hair Initiation. Genetics *180*, 219–228.

Yang, C., Axelrod, J.D., and Simon, M.A. (2002). Regulation of Frizzled by Fat-like Cadherins during Planar Polarity Signaling in the Drosophila Compound Eye. Cell *108*, 675–688.

Yang, T., Bassuk, A.G., Stricker, S., and Fritzsch, B. (2014). Prickle1 is necessary for the caudal migration of murine facial branchiomotor neurons. Cell Tissue Res. *357*, 549–561.

Ybot-Gonzalez, P., Savery, D., Gerrelli, D., Signore, M., Mitchell, C.E., Faux, C.H., Greene, N.D.E., and Copp, A.J. (2007). Convergent extension, planar-cell-polarity signalling and initiation of mouse neural tube closure. Development *134*, 789–799.

Yu, A., Rual, J.-F., Tamai, K., Harada, Y., Vidal, M., He, X., and Kirchhausen, T. (2007). Association of Dishevelled with the Clathrin AP-2 Adaptor Is Required for Frizzled Endocytosis and Planar Cell Polarity Signaling. Dev. Cell *12*, 129–141.

Yu, W., Centonze, V.E., Ahmad, F.J., and Baas, P.W. (1993). Microtubule nucleation and release from the neuronal centrosome. J. Cell Biol. *122*, 349–359.

Yun, U.J., Kim, S.Y., Liu, J., Adler, P.N., Bae, E., Kim, J., and Park, W.J. (1999). The inturned protein of Drosophila melanogaster is a cytoplasmic protein located at the cell periphery in wing cells. Dev. Genet. *25*, 297–305.

Zeidler, M.P., Perrimon, N., and Strutt, D.I. (1999). The four-jointed gene is required in the Drosophila eye for ommatidial polarity specification. Curr. Biol. *9*, 1363–1372.

Zeng, H., Hoover, A.N., and Liu, A. (2010). PCP effector gene Inturned is an important regulator of cilia formation and embryonic development in mammals. Dev. Biol. *2*, 418–428.

Zhu, J., Burakov, A., Rodionov, V., and Mogilner, A. (2010). Finding the Cell Center by a Balance of Dynein and Myosin Pulling and Microtubule Pushing: A Computational Study. Mol. Biol. Cell *21*, 4418–4427.

Chapter 3: PCP Signaling between Migrating Neurons and their Planar-Polarized Neuroepithelial Environment Controls Filopodial Dynamics and Directional Migration

Note: this manuscript was published in PLOS Genetics in March of 2016 and can be found at:http://journals.plos.org/plosgenetics/article?id=10.1371/journal.pgen.1005934#sec024

PLOS | GENETICS

RESEARCH ARTICLE

PCP Signaling between Migrating Neurons and their Planar-Polarized Neuroepithelial Environment Controls Filopodial Dynamics and Directional Migration

Crystal F. Davey[☯], **Andrew W. Mathewson**[☯], **Cecilia B. Moens***

Division of Basic Science, Fred Hutchinson Cancer Research Center, and University of Washington Molecular and Cellular Biology Graduate Program, Seattle, Washington, United States of America

☯ These authors contributed equally to this work.
* cmoens@fredhutch.org

OPEN ACCESS

Citation: Davey CF, Mathewson AW, Moens CB (2016) PCP Signaling between Migrating Neurons and their Planar-Polarized Neuroepithelial Environment Controls Filopodial Dynamics and Directional Migration. PLoS Genet 12(3): e1005934. doi:10.1371/journal.pgen.1005934

Editor: Xiaowei Lu, University of Virginia Health System, UNITED STATES

Received: June 9, 2015

Accepted: February 24, 2016

Published: March 18, 2016

Data Availability Statement: All relevant data are within the paper and its Supporting Information files.

Funding: This work was funded by the National Institutes of Health R01 NS082567 http://www.nih.gov/ to CBM; and National Institutes of Health Training Grant T32HD007183 to CFD and AWM. The funders had no role in study design, data collection and analysis, decision to publish, or preparation of the manuscript.

Competing Interests: The authors have declared that no competing interests exist.

Abstract

The planar cell polarity (PCP) pathway is a cell-contact mediated mechanism for transmitting polarity information between neighboring cells. PCP "core components" (Vangl, Fz, Pk, Dsh, and Celsr) are essential for a number of cell migratory events including the posterior migration of facial branchiomotor neurons (FBMNs) in the plane of the hindbrain neuroepithelium in zebrafish and mice. While the mechanism by which PCP signaling polarizes static epithelial cells is well understood, how PCP signaling controls highly dynamic processes like neuronal migration remains an important outstanding question given that PCP components have been implicated in a range of directed cell movements, particularly during vertebrate development. Here, by systematically disrupting PCP signaling in a rhombomere-restricted manner we show that PCP signaling is required both within FBMNs and the hindbrain rhombomere 4 environment at the time when they initiate their migration. Correspondingly, we demonstrate planar polarized localization of PCP core components Vangl2 and Fzd3a in the hindbrain neuroepithelium, and transient localization of Vangl2 at the tips of retracting FBMN filopodia. Using high-resolution timelapse imaging of FBMNs in genetic chimeras we uncover opposing cell-autonomous and non-cell-autonomous functions for Fzd3a and Vangl2 in regulating FBMN protrusive activity. Within FBMNs, Fzd3a is required to stabilize filopodia while Vangl2 has an antagonistic, destabilizing role. However, in the migratory environment Fzd3a acts to destabilize FBMN filopodia while Vangl2 has a stabilizing role. Together, our findings suggest a model in which PCP signaling between the planar polarized neuroepithelial environment and FBMNs directs migration by the selective stabilization of FBMN filopodia.

Author Summary

Planar cell polarity (PCP) is a common feature of many animal tissues. This type of polarity is most obvious in cells that are organized into epithelial sheets, where PCP signaling components act to orient cells in the plane of the tissue. Although, PCP is best understood for its function in polarizing stable epithelia, PCP is also required for the dynamic process of cell migration in animal development and disease. The goal of this study was to determine how PCP functions to control cell migration. We used the migration of facial branchiomotor neurons in the zebrafish hindbrain, which requires almost the entire suite of PCP core components, to address this question. We present evidence that PCP signaling within migrating neurons, and between migrating neurons and cells of their migratory environment promote migration by regulating filopodial dynamics. Our results suggest that broadly conserved interactions between PCP components control the cytoskeleton in motile cells and non-motile epithelia alike.

Introduction

The Planar Cell Polarity (PCP) signaling pathway is best understood as a cell contact dependent mechanism for generating and maintaining polarity in the plane of an epithelium [1, 2]. Its function was first described in the static epithelial cells of the fly where the molecular asymmetry of "core" PCP proteins results in the morphological asymmetry of a single actin-rich hair at the distal side of each wing cell [3–5]. Subsequently, planar polarity established by the core pathway has been shown to be a characteristic of many epithelial tissues in vertebrates and invertebrates alike [6–10]. The core PCP pathway is comprised of two protein complexes that localize to distinct cell membranes. In the fly wing, the transmembrane protein Frizzled (Fz) is confined to distal apical cell junctions along with the cytosolic proteins Disheveled (Dsh) and Diego (Dgo), while the transmembrane protein Van Gogh (Vang) (Strabismus(Stbm)) and the cytosolic protein Prickle (Pk) are proximally localized. This molecular asymmetry of PCP promotes actin polymerization at the distal side of the cell, downstream of Fz and Dsh [11–13]. While the factors that initially polarize PCP components are context dependent [14], the asymmetric localization of PCP proteins is maintained within polarized cells via intracellular destabilizing interactions between the Vang complex and the Fz complex [15, 16]. This polarization of PCP proteins is coordinated between cells by the formation of intercellular stabilizing interactions between Vang and Fz complexes across cell junctions [17–21]. In spite of the antagonistic roles of Vang and Fz complexes, loss of function of any core PCP component results in a loss of polarity.

While PCP is well known for its role in stable epithelia [22–24], core PCP components have also been implicated in dynamic cellular processes such as cell migration. How PCP controls directed cell movements is best, though incompletely, understood in coherently migrating cells such as those undergoing convergent extension [25–37]. However, independently migrating cells also require PCP [38–44]. Here, as our model we use the stereotyped and conserved migration of cranial motor neurons in the vertebrate hindbrain [45–47]. This enabled us to study *in vivo* how PCP can regulate the migration of non-coherent cells and to determine how PCP signaling between different cell types, the migrating neurons and the cells through which they migrate, can modulate migratory cell behaviors.

The PCP pathway drives the stereotyped tangential migration of facial branchiomotor neurons (FBMNs) in the vertebrate hindbrain. FBMNs are a subset of cranial branchiomotor neurons that originate ventrally in rhombomere (r)4 and undergo a posterior migration to r6

where they form the facial motor nucleus, whose axons exit the hindbrain in r4 and innervate muscles derived from the second branchial arch [45, 47]. Forward genetic screens in the zebrafish have identified multiple core PCP components (Vangl2, Pk1b, Fzd3a, Celsr2 and Scribble) as being required for FBMN migration [31, 48–51]; this PCP requirement has also been shown for mouse FBMN migration [52–54]. Unlike the cell migrations mentioned above, screens have failed to identify a role for Wnts or other chemotactic cues. Although it is clear that many components of the PCP pathway are required for tangential FBMN migration, how these components regulate this highly dynamic process is unknown.

As a first step in answering this question we defined the cell types participating in PCP signaling during FBMN migration, as previous studies using a range of approaches have yielded conflicting results [31, 48, 49, 51, 55]. Using the Gal4/UAS system to systematically disrupt PCP in a cell-type and rhombomere-specific manner, we demonstrate the dual requirement for PCP within FBMNs and the planar-polarized r4 neuroepithelial environment in which they arise, and identify reciprocal PCP-dependent interactions between FBMNs and the planar-polarized floorplate as being sufficient, though not required, to promote migration. Since cell migration results from the contact-dependent stabilization of cellular protrusions and PCP signaling is known to regulate actin dynamics, we examined the protrusive activity of single FBMNs using high-resolution single-cell time-lapse microscopy in chimeric embryos and demonstrate opposing functions for the PCP core components Fzd3a and Vangl2 in regulating FBMN filopodial protrusive activity *in vivo*. Within FBMNs we show that Fzd3a is required to stabilize filopodia while Vangl2 has an antagonistic, destabilizing role. However, in the migratory environment we show that Fzd3a is required to destabilize filopodia while Vangl2 has a stabilizing role. In spite of having antagonistic roles at the cellular level, Vangl2 and Fzd3a mutants have the same FBMN migration phenotype. These findings are thus reminiscent of the intracellular antagonistic versus intercellular stabilizing roles that core PCP proteins perform in stably polarized epithelia. Consistent with a role for Vangl2 in regulating filopodial dynamics, we show that Vangl2 localizes transiently to the tips of retracting FBMN filopodia; consistent with a role for Vangl2 and Fzd3a in the microenvironment, we show planar polarized localization of these proteins in the adjacent floorplate. Together, our findings support a model in which canonical interactions between PCP components within FBMNs and between the FBMNs and their planar polarized neuroepithelial environment promotes migration via the selective stabilization of FBMN filopodia.

Results

PCP signaling within FBMNs is required for their migration

Initial chimeric analyses suggested that the PCP components Vangl2, Fzd3a, Celsr2 and Scrib primarily act non-cell-autonomously to regulate FBMN migration [31, 48, 49]. An additional cell-*autonomous* role for Vangl2 and Scrib in FBMN migration has been demonstrated [51], but refuted by others [55]. To determine whether PCP signaling is required cell-autonomously within FBMNs for their migration, we expressed a dominant negative (DN) form of the PCP core component Dvl specifically in branchiomotor neurons using the *islet-1* (*isl1*) CREST enhancer (Fig 1A, 1B and 1C) [56]. Dvl is the branching point between multiple Wnt signaling pathways, and the overexpression of its individual domains exert pathway-specific DN properties [57]. Work in multiple vertebrate systems has demonstrated that Xdd1 and Dvl-DEP, two truncated forms of Dvl, act as PCP-specific DNs [25–27].

In previous studies mRNA injection of these DNs failed to disrupt zebrafish FBMN migration [31, 54]. We reasoned that this could be due to decreased DN mRNA levels or activity by the time of FBMN migration. To stably express DN forms of Dvl in FBMNs we raised stable *Tg*

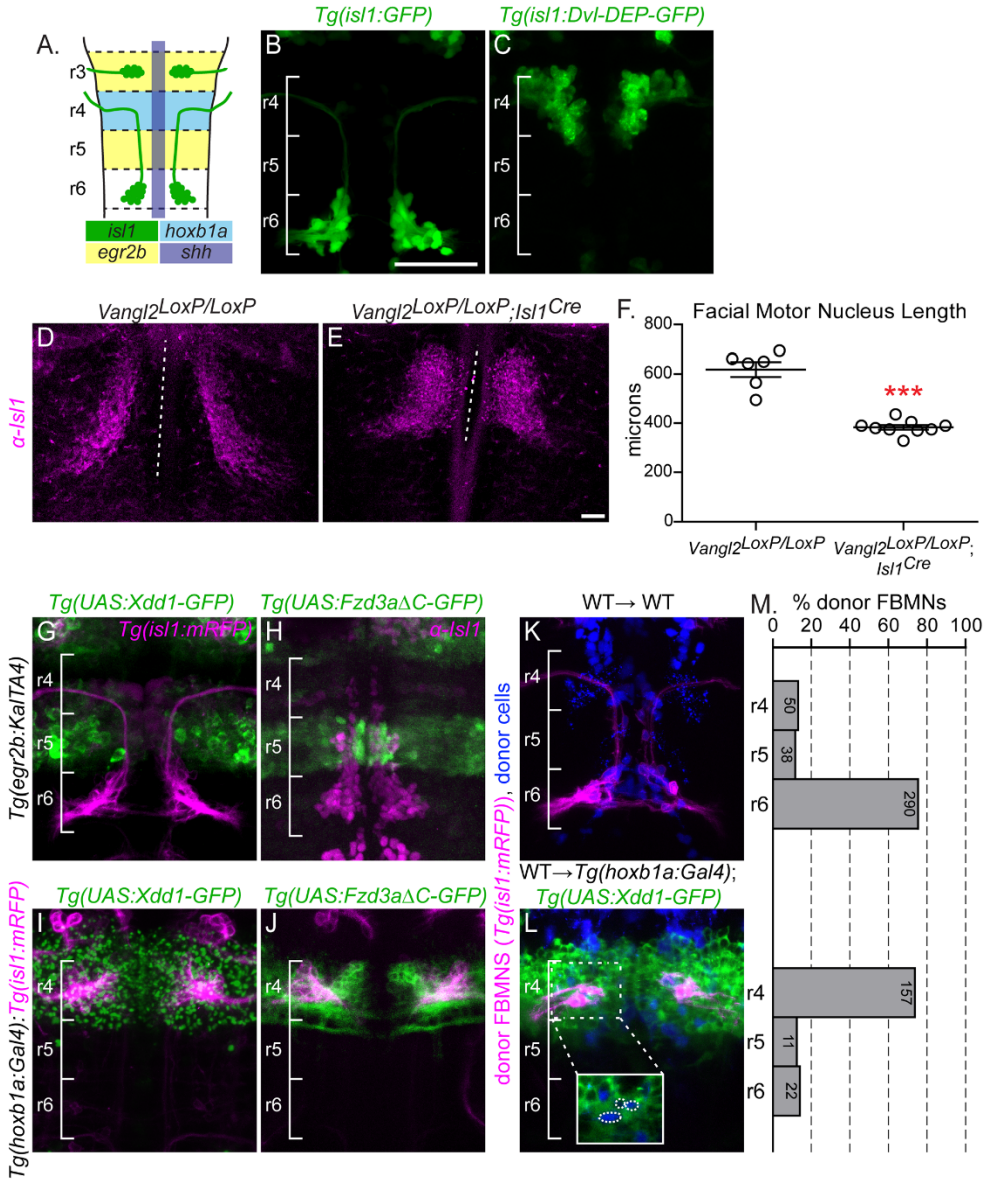

Fig 1. PCP signaling is required within FBMNs and in their r4 environment. (A) Schematic showing a dorsal view of a 48 hours post fertilization (hpf) zebrafish hindbrain with anterior to the top. Facial Branchiomotor neurons (FBMNs) (green) migrate posteriorly from rhombomere (r) 4 to r6, leaving a trailing axon that exits from r4. The enhancer element *islet-1* (*isl1*) CREST drives expression in branchiomotor neurons (green); the *hoxb1a* element drives expression in r4 (light blue); *egr2b* drives expression in r3 and r5 (yellow) and *shh* drives expression in the floorplate (purple). (B,C, G-L) Live or (H) fixed confocal images showing dorsal views of the hindbrain of 48 hpf zebrafish embryos with anterior to the top. Brackets mark rhombomere (r) position. Scale

Bar: 50μm (B) *Tg(isl1:GFP)* expression in a wild type embryo at 48 hpf. (C) *Tg(isl1:Dvl-DEP-GFP)* embryo with unmigrated Dvl-DEP-GFP-expressing FBMNs in r4. (D,E) Dorsal view of E12.5 mouse hindbrains with FBMNs (magenta) labeled with anti-Isl1 antibody. Dotted lines indicate the length of facial motor nucleus. Scale Bar: 100μm (D) Migrating FBMNs in $Vangl2^{LoxP/LoxP}$ control embryos. N = 6 embryos. (E) Blocked FBMNs in $Vangl2^{LoxP/LoxP}$;$Isl1^{Cre}$ embryos. N = 9 embryos. (F) Quantitation of FBMN migration stream length in $Vangl2^{LoxP/LoxP}$ control embryos and $Vangl2^{LoxP/LoxP}$;$Isl1^{Cre}$ embryos. ***p = 0.0003. Significance was determined using an unpaired, two-tail t-test. (G-L) FBMNs (magenta) are either expressing *Tg(isl1:mRFP)*(G,I-L) or are stained with anti-Isl1 (H). (G,H) *Tg(egr2b:KalTA4)*-driven expression of *Tg(UAS:Xdd1-GFP)* (G) and *Tg(UAS:Fzd3aΔC-GFP)* (H), throughout r3 and r5 does not block FBMN migration. (I,J) *Tg(hoxb1a:Gal4)*-driven expression of *Tg(UAS:Xdd1-GFP)* (I) and *Tg(UAS:Fzd3aΔC-GFP)* (J), throughout r4 blocks FBMN migration out of r4. (K,L) Chimeric embryos with transplant conditions indicated as donor→ host. Cascade blue-dextran marks all donor-derived cells (blue) and *Tg(isl-1:mRFP)* marks all donor-derived FBMNs (magenta). (K) Wild type donor-derived FBMNs migrate normally in a non-transgenic control host. N = 37 embryos, 378 FBMNs. (L) Wild type donor-derived FBMNs fail to migrate out of r4 that is expressing *Tg(UAS:Xdd1-GFP)*. N = 26 embryos, 190 FBMNs. Inset: same image without the magenta channel showing that donor-derived FBMNs (blue, circled) are not themselves expressing Xdd1-GFP (green). (M) Histograms indicate the percent of donor-derived FBMNs at 48 hpf that failed to migrate (r4), migrated partially (r5) or migrated fully (r6). Each histogram corresponds to the chimeric condition in the image to its left and numbers indicate the number of FBMNs represented in each bar.

doi:10.1371/journal.pgen.1005934.g001

(isl1:Dvl-DEP-GFP) zebrafish in which FBMNs express Dvl-DEP-GFP. In wild type embryos, FBMNs fully migrate to r6 by 48 hours post fertilization (Fig 1B). However Dvl-DEP-GFP expressing FBMNs largely fail to migrate, with 31/35 of *Tg(isl1:Dvl-DEP-GFP)* embryos displaying FBMN migration defects where most FBMNs (>75%) remain in in r4 (Fig 1C). This demonstrates that PCP signaling within FBMNs is required for their migration.

To further confirm this, and to test specifically whether the core transmembrane PCP component Fzd3a, like Vangl2 [51], is required within FBMNs for migration, we used chimeric analysis to assess the ability of $fzd3a^{rw689}$ mutant FBMNs to migrate in a normal planar polarized neuroepithelium. In these experiments we prevented host FBMN migration using a *pk1b* morpholino since it is well known that migrating FBMNs can carry other FBMNs with them independent of PCP signaling, complicating the interpretation of chimeras [51, 58]. *pk1b* morphants precisely phenocopy *pk1b* mutants in which FBMNs fail to migrate even though the surrounding neuroepithelium can support wild type FBMN migration [50, 51, 59]. While 70.9% of wild type FBMNs migrate out of r4 in a *pk1b* morphant environment, only 19% of *fzd3a* mutant FBMNs do so (S1 Fig). This suggests that Fzd3a is required within FBMNs for migration.

The requirement for the core PCP components Vangl2, Fzd3 and Celsr1-3 is conserved in mouse FBMN migration [52, 54, 60]. In order to confirm a FBMN-autonomous requirement for PCP signaling we employed tissue-specific knockout of *Vangl2* in mouse FBMNs using a floxed *Vangl2* allele and *Isl1*-driven Cre recombinase [61, 62]. In the mouse embryo, FBMN migration occurs between E10.5 and E14.5 with neurons reaching r6 by E12.5 [45]. In E12.5 homozygous floxed animals ($Vangl2^{LoxP/LoxP}$) lacking $Isl1^{Cre}$ FBMNs migrate to r6 and the mean length of the migration stream is 618μm (Fig 1D and 1F; N = 6). In contrast FBMNs in $Vangl2^{LoxP/LoxP}$; $Isl1^{Cre}$ animals are significantly blocked in r4 with FBMNs occupying an average of 383μm along the hindbrain (Fig 1E and 1F; N = 9; p = 0.0003).

Taken together, the disruption of migration due to FBMN-restricted DN expression, our chimeric analysis of $fzd3a^{-/-}$ and previous chimeric analysis of $vangl2^{-/-}$ FBMNs [51] and the failure of FBMN migration after FBMN-specific disruption of *Vangl2* in the mouse confirms a FBMN-autonomous requirement for PCP signaling in migration.

FBMN migration requires PCP signaling non-autonomously in r4

While these data support a cell-autonomous requirement for PCP signaling in FBMN migration, PCP signaling in FBMNs is not *sufficient* for their migration. Indeed, a non-autonomous requirement for PCP signaling in FBMN migration has been well established in chimeras in which wild type FBMNs are unable to migrate in *vangl2*, *fzd3a*, *celsr2* or *scrib* mutant hosts [31, 48, 49, 51]. Since PCP is a cell-contact mediated signaling pathway in which the same transmembrane protein components are required in both contacting cells [2], an attractive

hypothesis is that FBMNs receive PCP cues from cells in their environment that promote or direct their migration. Thus we sought to determine where PCP signaling is required in the FBMN migratory path for migration.

To block PCP signaling in distinct compartments of the hindbrain, we used the Gal4/UAS system to drive rhombomere-restricted expression of *Tg(UAS:Xdd1-GFP)* as well as a C-terminally truncated Fzd3a *Tg(UAS:Fzd3aΔC-GFP)* that lacks its cytoplasmic region, which has been shown to function as a potent PCP DN tool in zebrafish [49]. We used *Tg(egr2b:KalTA4)* to drive expression throughout r3 and r5 starting at 12 hpf [63] and *Tg(hoxb1a:Gal4)* [64] to drive expression throughout r4 starting at 10 hpf (Fig 1A). Expression of Xdd1-GFP or Fzd3aΔC-GFP along the migration path in the r5 neuroepithelium does not affect migration (Fig 1G and 1H). In contrast, r4-restricted expression of Xdd1-GFP or FzdΔC-GFP completely blocks FBMN migration (Fig 1I and 1J). This suggests that PCP signaling is required at the onset, but not throughout the course of FBMN migration. However we note that r5 expression of Xdd1-GFP or Fzd3aΔC-GFP using *egr2b:KalTA4* comes on slightly later than r4 expression using *hoxb1a:Gal4* (12 hpf compared to 10 hpf), so the caveat remains that PCP signaling is not fully disrupted in r5 at the time of migration with the available tools.

It was not surprising that FBMNs fail to migrate in *Tg(hoxb1a:Gal4); Tg(UAS:DN-GFP)* embryos given that FBMNs arise in r4, and thus express *hoxb1a* throughout their early development, and we had already shown a cell-autonomous requirement for PCP signaling within FBMNs. To assess whether PCP signaling plays a role in the r4 neuroepithelium outside of FBMNs, we transplanted wild type *Tg(isl1:mRFP)* donor FBMNs into the presumptive ventral hindbrain of *Tg(hoxb1a:Gal4); Tg(UAS:Xdd1-GFP)* embryos and assessed the positions of donor-derived FBMNs at 48 hpf. In control hosts, 87% (328/378) of wild type donor-derived FBMNs migrated out of r4. In contrast, in hosts expressing Xdd1-GFP in r4, only 17% (33/190) of donor-derived wild type FBMNs migrate out of r4 (Fig 1K, 1L and 1M). Thus, expression of Xdd1-GFP throughout r4 significantly hinders wild type FBMNs from initiating migration ($p<0.0001$, $\chi^2 = 207.8$) (Fig 1M). This demonstrates that there is a non-autonomous requirement for PCP signaling for FBMN migration in r4.

Environmental PCP signaling is required for the migration of post-mitotic FBMNs

Having established that PCP signaling is required both within FBMNs and their r4 neuroepithelial environment for migration to occur; we asked *when* this signaling is required. PCP signaling polarizes neuroepithelial progenitors before FBMNs differentiate [7, 65, 66]. It is possible that this early neuroepithelial polarity is maintained in FBMNs to orient their initial migration. Alternatively, PCP signaling active at the time of migration initiation may promote migration. We reasoned that in the former case a planar polarized environment would not be required for migration after FBMNs had differentiated while in the latter case PCP function in the r4 environment would continue to be essential for migration.

To determine when PCP signaling is required for FBMN migration, we transplanted a small number (1–5) of pre-migratory but post-mitotic FBMNs directly from r4 of a *Tg(isl1:GFP)* donor into r4 of a stage-matched wild type or *vangl2*^{m209} mutant *Tg(isl1:mRFP)* host (Fig 2A). During this extraction procedure, transplanted cells round up and become separated in the transplant pipette and are unlikely to retain polarity information. Nevertheless, 28% (48/174) of surviving post-mitotic FBMNs transplanted into a wild type host r4 migrated to r6 (Fig 2B and 2D). To rule out the possibility that the transplanted FBMNs are simply being carried by migrating host FBMNs, we transplanted post-mitotic FBMNs into a *pk1b* mutant host, which has normal neuroepithelial PCP but no host FBMN migration; in this environment 11%, (17/

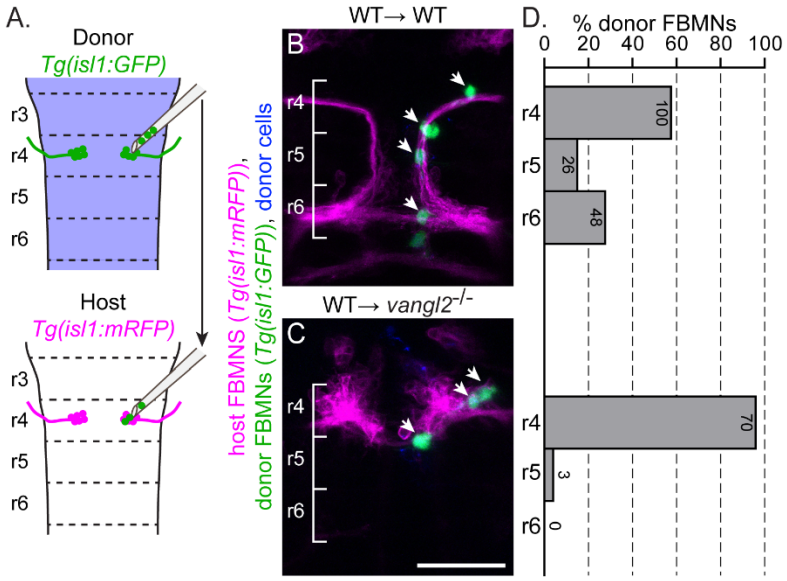

Fig 2. Post-mitotic FBMNs require PCP signaling for migration. (A) Schematic of the late stage FBMN transplantation procedure in which a small number (1–5) of post-mitotic, pre-migratory FBMNs are moved from r4 of a *Tg(isl1:GFP)* donor into r4 of a stage-matched, 16 hpf *Tg(isl1:mRFP)* host. (B, C) Live confocal images showing dorsal views of chimeras at 48 hpf with anterior to the top. Transplant conditions are indicated as donor→host. Cascade blue-dextran marks all donor-derived cells (blue), *Tg(isl1:mRFP)* marks host FBMNs (magenta) and *Tg(isl1:GFP)* marks donor-derived FBMNs (green). White arrows indicate donor-derived FBMNs at 48 hpf. (D) Quantitation of the percent of donor-derived FBMNs at 48 hpf that failed to migrate (r4), partially migrated (r5) or fully migrated (r6). Each histogram refers to the transplant condition in the image to its left and numbers indicate the number of FBMNs represented in each bar. WT→WT, N = 42 embryos, 174 FBMNs; WT→ *vangl2*$^{-/-}$, N = 16 embryos, 73 FBMNs. ***p<0.0001 compared to WT→WT control. Brackets indicate rhombomere location. Scale bar: 50μm.

doi:10.1371/journal.pgen.1005934.g002

152) of transplanted FBMNs migrated (S2 Fig). This suggests that host neurons do contribute to migration [51, 58], but that post-mitotic transplanted FBMNs can migrate without contribution from migrating host neurons. Importantly, 0% (0/73) of FBMNs migrated to r6 after being transplanted into a *vangl2* mutant host (Fig 2C and 2D). Together, these results suggest that post-mitotic FBMNs engage PCP signaling as they initiate their migration out of r4.

Floorplate PCP is not required for FBMN migration

FBMNs migrate in the ventral neural tube adjacent to the floorplate (Fig 1A, [49, 67]) making the floorplate a potential source of PCP signaling for FBMN migration. A recent report found that floorplate expression of Vangl2 is both necessary and sufficient for FBMN migration [55]. Here, to investigate whether PCP signaling in the floorplate is required for FBMN migration, we generated a *Tg(shh:Gal4)* line (see Methods) to drive Xdd1-GFP or Fzd3aΔC-GFP expression in the notochord and floorplate (S3A, S3B and S3C Fig). In order to determine if dominant negative expression does indeed disrupt floorplate planar polarity, we quantified the anterior-posterior position of the basal body in single floorplate cells as the ratio of its distance from the anterior membrane to the full anterior-posterior cell length (S3G Fig). Basal bodies in wild type floorplate cells are planar polarized to the posterior membrane (average positon = 78% of cell length, S3D and S3H Fig, [6]). Conversely, basal body planar polarization is significantly

disrupted in floorplate cells expressing Xdd1-GFP or Fzd3aΔC-GFP (average position = 63% and 59% of cell length respectively; S3E, S3F and S3H Fig). By comparison, floorplate cells in *vangl2* mutants display a complete loss of basal body planar polarity (average position = 47% of cell length, [51]) (S3H Fig). With the caveat that this effect on floorplate planar polarity was scored after FBMN migration was complete (48 hpf) rather than at the onset of migration (18–24 hpf), DN expression in the floorplate in the floorplate had no effect on FBMN migration (Fig 3A and 3B). To confirm this, we specifically knocked Vangl2 out in the mouse floorplate using the floxed *Vangl2* allele described above [61] and *Shh*-driven Cre recombinase [68]. We found that Cre-mediated deletion of Vangl2 in the mouse floorplate does not disrupt FBMN migration (S4 Fig). These results suggest that PCP signaling in the floorplate is not required for FBMN migration, and point to the possibility that loss of PCP in the floorplate can be compensated for by other planar polarized cells in the r4 neuroepithelial environment.

Floorplate PCP could nevertheless be sufficient to rescue FBMN migration as has been suggested [55]. We tested the sufficiency of Vangl2 in the floorplate for FBMN migration in two ways. We expressed a GFP-Vangl2 fusion protein specifically in the floorplate of *vangl2* mutants and wild type siblings using stable *Tg(shh:Gal4)* driver and *Tg(UAS:GFP-Vangl2)* transgenic lines (*vangl2*$^{m209/m209}$; *Tg(shh:Gal4); Tg(UAS:GFP-Vangl2)*). Although GFP-Vangl2 was expressed broadly in the floorplate in these otherwise mutant embryos starting at 14 hpf, and exhibits planar-polarized localization (S3A Fig and see below), it neither disrupted FBMN migration in a wild type embryo nor rescued migration in a *vangl2* mutant embryo (Fig 3C and 3D). Since a caveat of this experiment is that Vangl2 over-expression can itself disrupt planar polarity, we used targeted transplantation of wild type cells into the floorplate of *vangl2* mutants to test whether floorplate Vangl2 is sufficient to rescue FBMN migration. We never observed rescue of host FBMN migration in *vangl2* mutant *Tg(isl1:mRFP)* hosts with wild type donor-derived cells in the hindbrain floorplate (Fig 3E). This includes 9 cases with 10 or more wild type floorplate cells in rhombomere 4. This is contrary to the findings of Sittarmane et al. (2013) [55] who found that a single wild type floorplate cell in r4 of a *vangl2* mutant could rescue FBMN migration. Together, our findings suggest that Vangl2 function in the floorplate is not sufficient for FBMN migration.

In these transplant experiments we noted that FBMNs as well as floorplate cells differentiate from donor-derived cells. This is not unexpected, given the close proximity of floorplate and branchiomotor neuron progenitors in the early embryo [70]. Interestingly, we observed that unlike the mutant host FBMNs, wild type donor-derived FBMNs sometimes migrate (Fig 3F), and their ability to do so correlates with the number of wild type cells in the hindbrain floor plate ($R^2 = 0.244$; $p = 0.005$). We conclude that Vangl2 function in the floorplate is not sufficient for FBMN migration, but that Vangl2 function in the floor plate can support the migration of *vangl2*$^+$ FBMNs in an otherwise *vangl2* mutant neuroepithelium. Taken together, we conclude that the floorplate can serve as a source of PCP signals for FBMN migration, but other cells in the r4 environment, which are also planar polarized (see below) can compensate for the loss of normal floorplate PCP signaling.

Vangl2 localization in the migratory environment

Thus far, we have shown that PCP signaling in FBMNs and their immediate neuroepithelial/floorplate r4 environment can drive migration. The localization of core PCP components is known to be crucial for many PCP mediated processes [2, 22]. Therefore, to better understand how PCP signaling might be used in neuronal migration we asked where PCP proteins localize within FBMNs and in their neuroepithelial microenvironment. Using a polyclonal antibody against zebrafish Vangl2, we observed localization of Vangl2 to cell membranes throughout the

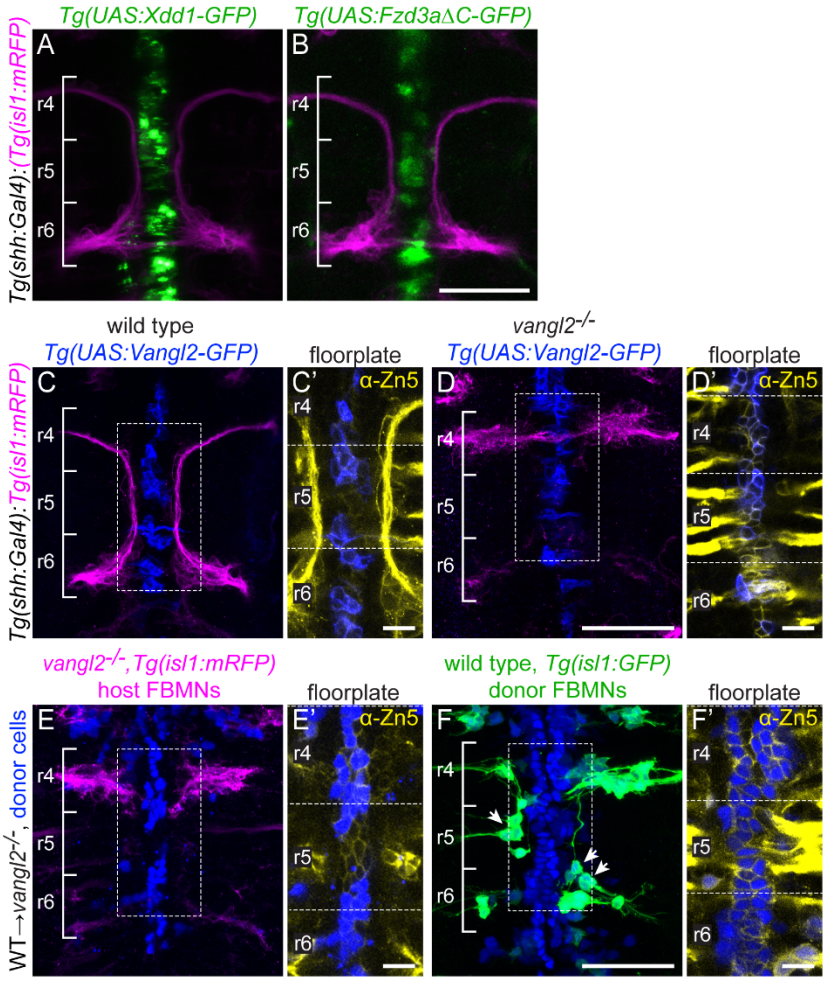

Fig 3. Floorplate PCP is neither required nor sufficient for FBMN migration but can support the migration of WT FBMNs. Confocal images showing dorsal views of 48 hpf hindbrains with anterior to the top. (A,B) *Tg(shh:Gal4)*-driven expression of *Tg(UAS:Xdd1-GFP)* (A) and *Tg(UAS:Fzd3aΔC-GFP)* (B) does not disrupt FBMN (magenta) migration. N = 13 Xdd1-GFP expressing embryos and 26 Fzd3aΔC-GFP expressing embryos. (C,D) *Tg(shh:Gal4)*-driven floorplate expression of GFP-Vangl2 (blue) in the floorplate of a wild type sibling does not disrupt FBMN migration (magenta) (C) and does not rescue migration in a *vangl2* mutant (D). N = 24 *vangl2* mutants with GFP-Vangl2 expression in the r4 floorplate, 14 with 5 or more expressing floorplate cells in r4. (C',D') Boxed regions from panels C and D respectively, showing a single z-plane where GFP-Vangl2 (blue) is expressed broadly in floorplate cells whose membranes are marked with the Zn5 antibody (yellow) [69]. (E,F) Genetic chimeras. Cascade blue-dextran marks all donor-derived cells (blue), *Tg(isl1:mRFP)* marks host FBMNs (magenta in E) and *Tg(isl1:GFP)* marks wild type donor-derived FBMNs (green in F). (E) The presence of wild type floorplate cells (blue) in a *vangl2* mutant host embryo does not rescue the migration of host FBMNs. N = 16 embryos with extensive contribution of WT cells to the floorplate. (F) The presence of wild type floorplate cells (blue) in a *vangl2* mutant can, however, support the migration of co-transplanted wild type donor derived FBMNs (green, arrows). N = 8 embryos with migrated donor-derived FBMNs/22 embryos with donor-derived FBMNs; N = 76 migrated FBMNs/383 total donor-derived FBMNs. (E',F') Single Z-planes of the boxed regions from panels E and F respectively, show that donor-derived cells (blue) are in the Zn-5-positive floorplate (yellow). Scale bars: 50 μm, 5μm in the insets.

doi:10.1371/journal.pgen.1005934.g003

hindbrain neuroepithelium (S5 Fig). In the r4 floorplate, we noted a 1.6-fold enrichment of Vangl2 protein at anterior/posterior membranes of floorplate cells compared to their lateral membranes (Fig 4A and 4B). Co-staining with ZO1 shows that this staining is sub-apical, at the level of the tight junctions (Fig 4A'). In order to distinguish anterior from posterior membrane localization we mosaically expressed GFP-Vangl2 in the floorplate so we could visualize Vangl2 localization in isolated floorplate cells. This revealed that Vangl2 is specifically enriched at the anterior subapical membrane (Fig 4C and 4E). The normalized mean fluorescent intensity ratio of GFP-Vangl2 at the anterior membrane versus the posterior membrane in expressing floorplate cells is 2.2 (std. deviation 0.9; N = 29 cells in 8 embryos). Conversely, Fzd3a-GFP is enriched at the posterior membrane (Fig 4D). These findings for PCP protein localization in the floorplate are consistent both with the requirement for PCP core components in the posterior localization of the floor plate primary cilium [6], and with a conserved deployment of PCP core components in vertebrate and invertebrate epithelia.

While the regular organization of floorplate cells makes it easy to visualize their planar polarization, our findings suggest that the primary source of environmental PCP signaling in FBMN migration comes from neuroepithelial progenitor cells outside of the floorplate. Previous studies demonstrated a planar polarization of GFP-Pk and GFP-Vangl2 in neuroepithelial progenitor cells during zebrafish neurulation [7, 65], and of endogenous Vangl2 in the Xenopus neural plate [66]. We asked whether neuroepithelial progenitor cells display planar polarization of Vangl2 in r4 at the time of FBMN migration. Using the *Tg(hoxb1a:Gal4)* line we mosaically expressed GFP-Vangl2 and observed a subtle but significant asymmetry of GFP-Vangl2 to the anterior sub-apical side of r4 neural progenitors. While GFP-Vangl2 polarization is subtle and not detectable in all expressing neuroepithelial progenitors, in blinded experiments we were able to correctly guess the A-P orientation of embryos based exclusively on GFP-Vangl2 localization in r4 progenitors in 18/23 mosaically expressing embryos ($p = 0.004$ that 18/23 correct guesses were due to chance alone). The normalized mean fluorescent intensity ratio of GFP-Vangl2 at the anterior membrane versus the posterior membrane in cells where asymmetry is detectable is 1.82 (std. deviation 0.47, N = 17 embryos, 23 cells.) (Fig 4F). Thus both the r4 neuroepithelium and floorplate exhibit planar polarized Vangl2 localization at the time of FBMN migration.

Vangl2 is enriched at the tips of retracting FBMN filopodia

We next sought to determine where Vangl2 localizes in migrating FBMNs. Endogenous Vangl2 in FBMN membranes and the membranes of surrounding cells could not be resolved using the anti-Vangl2 antibody and, unlike static floorplate cells and neuroepithelial progenitors, FBMNS are highly dynamic, extending primarily filopodia-like protrusions as they migrate [51, 71]. Reasoning that Vangl2 localization would be similarly dynamic, we mosaically expressed GFP-Vangl2 in FBMNs and visualized localization using spinning disc time-lapse imaging. We found that GFP-Vangl2 localizes throughout the membrane as well as in putative cytoplasmic vesicles, as is predicted for a transmembrane protein (Fig 5A). However, in addition to its membrane localization, we observe transient enrichment of GFP-Vangl2 at the tips of a subset filopodia immediately preceding filopodia retraction (Fig 5A'–5C and S1 Movie). Before enrichment the mean fluorescent intensity ratio of GFP at the filopodia tip versus the filopodia base is approximately 1 (0.99 ± 0.01), as is the case for mRFP (background membrane marker) (0.92 ± 0.02). During the enrichment event, this ratio for GFP-Vangl2 increased to 1.31 ± 0.05 while the ratio for mRFP remained close to 1 (0.97 ± 0.02) (Fig 5B). Since the ratio for mRFP remained close to 1, this suggests that the enrichment of GFP-Vangl2 correlates with increased Vangl2 protein levels at filopodia tips and not simply condensation of the membrane

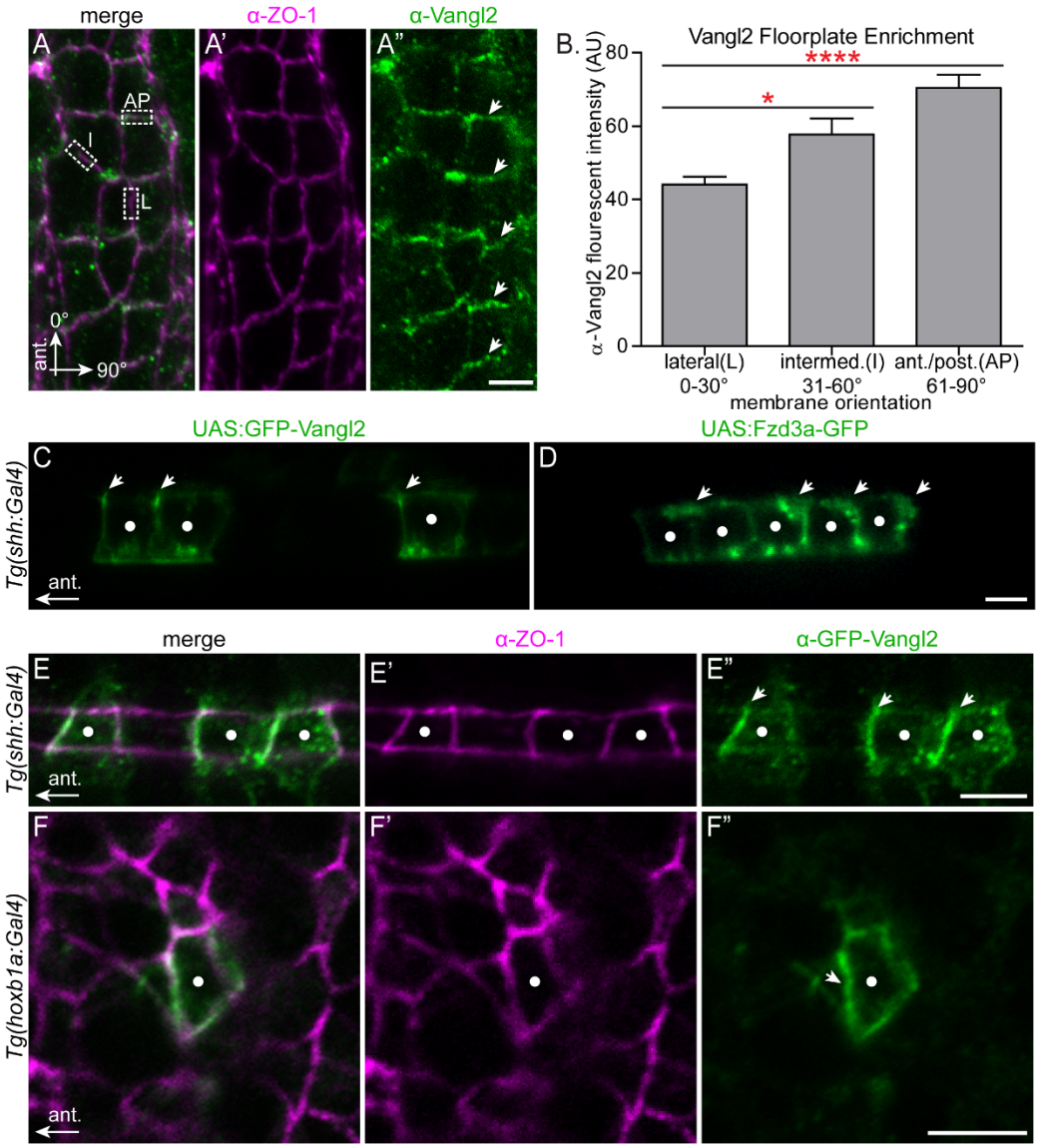

Fig 4. Polarization of PCP protein localization in the migratory environment. (A-A") Dorsal view with anterior to the top of a 24 hpf wild type floorplate at the level of r4 co-immunostained with anti-Vangl2 (green) and anti-ZO-1 (magenta), a marker of apical tight junctions. The boxed regions in A are examples of anterior-posterior membranes (AP) (61–90° from AP axis), intermediate membranes (I) (31–60° from AP axis) and lateral membranes (L) (0–30° from AP axis). Arrows in A" indicate enrichment of anti-Vangl2 labeling at AP membranes. (B) Quantitation of fluorescent intensity of anti-Vangl2 labeling for AP, I and L membranes. N = 5 embryos, 192 membranes (57 L, 47 I, 88, AP). Graph represents data as mean ± SEM. *p = 0.018, ****p<0.0001; Significance was determined using a paired two-tail t-test with Welch's correction. (C-D) Live lateral views of 48 hpf wild type floorplate cells at the level of the spinal cord with mosaic expression of GFP-Vangl2 (C) and Fzd3a-GFP (D). Anterior is to the left and dorsal/apical is up; white dots indicate the center of each expressing

floorplate cell, arrows indicate anterior subapical membrane enrichment of GFP-Vangl2 (C) and posterior subapical enrichment of Fzd3a-GFP (D). (E-E") Dorsal view of the apical surface of floorplate cells in a 48 hpf embryo expressing GFP-Vangl2 (green) and stained for ZO-1 (magenta) Anterior is to the left; white dots indicate the center of the expressing cell. Arrows in E" indicate anterior enrichment of GFP-Vangl2. (F-F") *En face* view of the apical endfeet of neuroepitheilial cells in r4 of a 24 hpf embryo expressing GFP-Vangl2 (green) and stained for ZO-1 (magenta). Anterior is to the left; white dot indicates the center of the expressing cell. Arrow in F" indicates anterior enrichment of GFP-Vangl2. N = 17 embryos, 23 cells. Scale bars: 5 μm.

doi:10.1371/journal.pgen.1005934.g004

due to retraction. Furthermore, as described below, addition of exogenous GFP-Vangl2 in FBMNs results in a reduced filopodial lifetime which is opposite to the effect of loss of Vangl2 in FBMNs. This suggests that exogenous GFP-Vangl2 is functioning in FBMNs and that this observed localization of Vangl2 at the tips of filopodia is correlated with retraction. This enrichment of GFP-Vangl2 in filopodia never lasted for more than one time-point (images were taken at 30–45 second intervals) and was only detected in a subset of filopodia (N = 11/84 filopodia on 8 neurons in 7 embryos); it is likely that due to the transient nature of enrichment events and the constraints of our imaging rate we failed to observe many enrichment events. Importantly, however, the enrichment events we captured invariably preceded filopodial

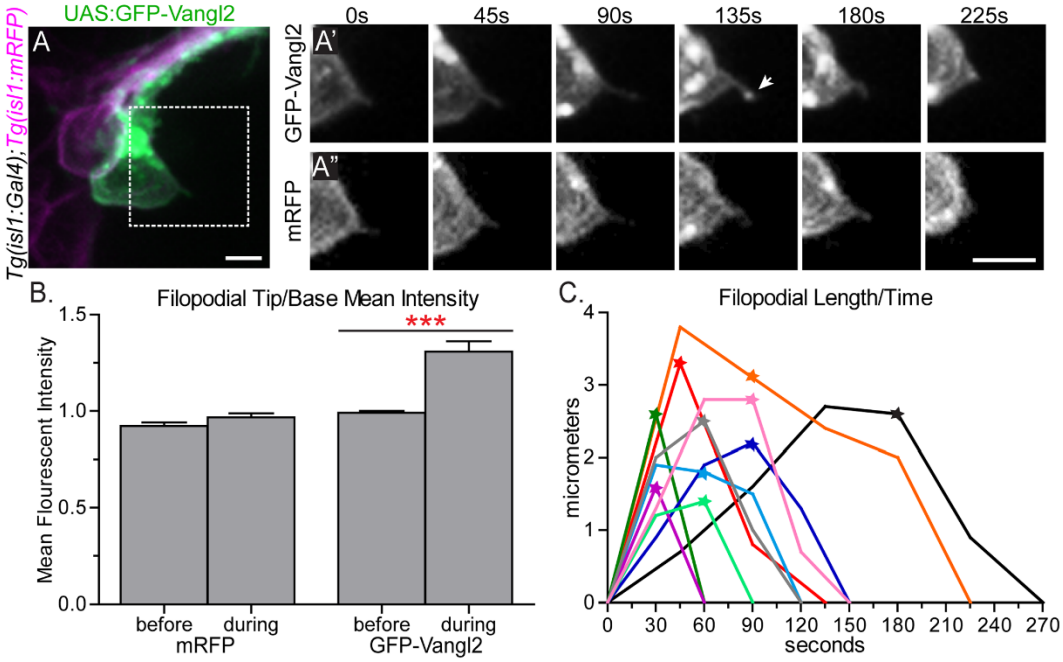

Fig 5. GFP-Vangl2 is enriched to the tip of retracting FBMN filopodia. (A) Live confocal image of a single GFP-Vangl2 expressing FBMN (green) in a *Tg (isl1:mRFP)* (magenta) 24 hpf embryo. Scale bar: 10 μm. (A',A") Magnified views of the boxed region in A of the individual channels, GFP-Vangl2 and *Tg(isl1:mRFP)* respectively, at the time points indicated. The arrow in E' indicates enrichment of GFP-Vangl2 at the filopodial tip. Scale bar: 10 μm. (B) Quantitation of filopodia tip/base mean fluorescent intensity ratio for mRFP and GFP-Vangl2 at the time-point before and during GFP-Vangl2 enrichment. Before enrichment the mean fluorescent intensity ratio of GFP and mRFP at the filopodia tip versus the filopodia base is approximately 1 (N = 9 filopodia). During the enrichment event this ratio for GFP-Vangl2 is 1.31 while the ratio remains close to 1 for mRFP (N = 12 filopodia). (C) Plot showing the change in filopodial length over time for 10 filopodia. The stars indicate the time-point that GFP-Vangl2 is enriched at each filopodium tip. The black trace corresponds to the filopodium in A',A". Graph represents data as mean ± SEM. ***p<0.001; Significance was determined using an unpaired, two-tail t-test with Welch's correction.

doi:10.1371/journal.pgen.1005934.g005

retraction; filopodia never extended further after an enrichment event (Fig 5C). Consequently, we infer that Vangl2 may function in FBMN filopodia to signal retraction events.

Vangl2 and Fzd3a function cell-autonomously to regulate FBMN filopodial activity in an antagonistic manner

Our findings that PCP signaling is required within FBMNs for migration, and that Vangl2 localizes transiently to the tips of retracting filopodia, suggested the possibility that PCP signaling influences filopodial dynamics in migrating neurons *in vivo*. In order to determine the cellular basis of FBMN migration defects in PCP mutants, we imaged the protrusive dynamics of single mutant FBMNs at high resolution *in vivo*. Previous studies have described membrane protrusions in fixed or live embryos expressing cytoplasmic GFP or membrane-RFP in bulk FBMNs at low time resolution, however the overlap between FBMNs allows only a subset of protrusions to be visualized and their dynamics could only be inferred from distant time points [31, 55, 58, 71]. To visualize the protrusive activity of single FBMNs at high time resolution, we utilized cell transplantation to generate embryos in which one or a few FBMNs express membrane-localized teal fluorescent protein (*Tg(isl1:mTFP)*), and imaged protrusion dynamics of single FBMNs at 30-second intervals, the shortest interval at which we could acquire comprehensive z-stacks on our instruments. We focused on the function of Vangl2 and Fzd3a, the mutually antagonistic transmembrane core components, whose localized activity is both the hallmark and the driver of classical epithelial planar polarity [2].

Time-lapse imaging of FBMN membranes and f-actin dynamics revealed that filopodia are the prevalent protrusion type in FBMNs (Fig 6A–6E and S2 Movie). To determine whether PCP affects the polarized orientation of filopodia on migrating cells, we quantified the positions of filopodia on single isl1:mTFP-expressing FBMNs by measuring the angle from the anterior-posterior axis of a vector from the center of the cell to the base of each filopodium (S6A Fig). When wild type FBMNs are in r4, protrusive activity is largely radial 46.4% (13/28) of filopodia are located in the anterior half of the neuron, while 53.6% (15/28) of filopodia were on the posterior side (S6A and S6B Fig). Once neurons are migrating through r5 and r6, membrane protrusive activity becomes highly enriched posteriorly, in the direction of migration with 84.6% (44/52) of filopodia on the posterior side of the cell (S6C and S6D Fig). However, filopodia on *vangl2* mutant FBMNs fail to polarize. Time-lapse images were collected at a developmental time-point at which wild type neurons would have already migrated out of r4. Similar to wild type neurons in r4, filopodia in *vangl2* mutant FBMNs are fairly evenly distributed along the anterior-posterior axis with 47.5% (29/61) of filopodia located anteriorly and 52.5% (32/61) located posteriorly (S6E and S6F Fig). These findings suggest that PCP signaling through Vangl2 is required to properly localize cytoskeletal dynamics in FBMNs.

To characterize protrusive membrane dynamics we quantified filopodial lifetime (number of seconds each filopodium is present during a 15 minute time-lapse period) and filopodial maximum length (the greatest length during the lifetime of filopodia lasting 90 seconds or longer) of *Tg(isl1:mTFP)* FBMNs. Wild type FBMNs generate filopodia with an average lifetime of 224.5 ± 18.66 (SEM) seconds and an average maximum length of 3.6 ± 0.3 μm (Fig 6A, 6F and 6G and S3 Movie). This filopodial lifetime is comparable to that observed in other vertebrate cells both *in vivo* and in culture [72–75]. When compared to wild type, FBMNs in *vangl2* mutant embryos have much more stable filopodia with a longer average lifetime of 537.3 ± 81.78 seconds (Fig 6F, S4 Movie; $p = 0.0059$). Filopodia of these *vangl2* mutant FBMNs also reach a greater average maximum length of 6.4 ± 1.1 μm (Fig 6G; $p = 0.0406$). We saw a similar trend when we used microinjection rather than transplantation to mosaically express

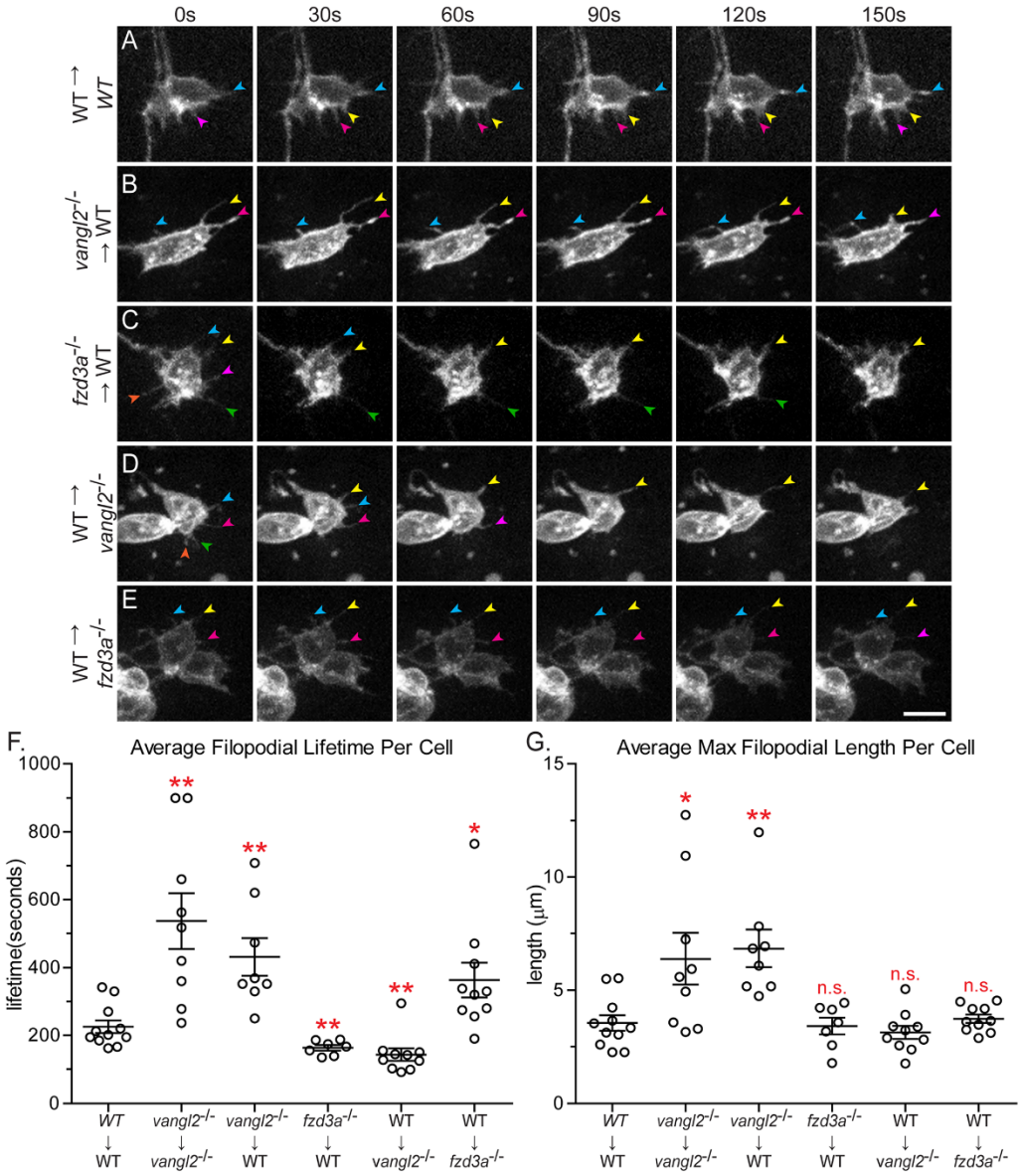

Fig 6. Vangl2 and Fzd3a have opposing cell-autonomous and non-cell-autonomous roles in modulating filopodial dynamics. (A-E) Time-lapse spinning-disc confocal series of donor-derived FBMNs in chimeric embryos at 24–30 hours post-fertilization (hpf). Transplant conditions are indicated on the left as donor→host. Colored arrows indicate individual filopodia at different time-points. Anterior is to the top and medial is to the right. Scale bar: 5 μm. (F) Quantitation of filopodial lifetime for donor-derived FBMNs. Each data point is an average of all the filopodial lifetimes for one FBMN. (G) Quantitation of the maximum filopodial length for donor-derived FBMNs. Each data point is the average maximum length for all the filopodia of one FBMN. WT→WT: N = 6

embryos, 11 neurons (3 in r4, 4 in r5, 4 in r6), 70 filopodia; *vangl2*$^{-/-}$→*vangl2*$^{-/-}$: N = 6 embryos, 9 neurons, 43 filopodia; *vangl2*$^{-/-}$→WT: N = 6 embryos, 8 neurons, 44 filopodia; *fzd3a*$^{-/-}$→WT: N = 7 embryos, 7 neurons, 73 filopodia; WT→ *vangl2*$^{-/-}$: N = 8 embryos, 10 neurons, 152 filopodia; WT→ *fzd3a*$^{-/-}$: N = 6 embryos, 10 neurons, 65 filopodia. Graphs represent data as mean ± SEM. *p<0.05, **p<0.01 compared to WT→WT control; n.s., not significant. Significance was determined using an unpaired, two-tail t-test with Welch's correction.

doi:10.1371/journal.pgen.1005934.g006

mTFP in FBMNs in wild type and *vangl2* mutant embryos. These results suggest that Vangl2 is required to destabilize FBMN membrane protrusions. Previous studies have demonstrated that FBMNs in *vangl2* mutants move more slowly than wild type FBMNs and in random directions, which is consistent with Vangl2 being required to destabilize protrusions [31].

Since Vangl2 is required within FBMNs *and* their r4 microenvironment for migration, we sought to determine where Vangl2 functions to regulate filopodia dynamics. To determine the cell-autonomous function of Vangl2, we transplanted *vangl2* mutant FBMNs into a wild type host. Donor embryos carried the *Tg(isl1:mTFP)* transgene to visualize FBMNs and contained rhodamine dextran to track other donor-derived cells so we could ensure that donor-derived FBMNs were in fact in a genetically chimeric environment (S7 Fig). We found that *vangl2* mutant FBMNs in a wild type environment have longer, more stable filopodia with a mean lifetime of 432.0 ± 55.65 seconds and a maximum length of 6.8 ± 0.8 μm, similar to *vangl2* mutant FBMNs in a *vangl2* mutant host (Fig 6B, 6F and 6G and S5 Movie; p = 0.005 and p = 0.0078 respectively). To further test if Vangl2 functions cell-autonomously to control FBMN protrusive dynamics, we mosaically expressed GFP-Vangl2 in wild type FBMNs. FBMNs expressing GFP-Vangl2 in wild type embryos have less stable filopodia compared to wild type FBMNs, with an average lifetime of 123.4 ± 14.27 seconds (S1 Movie; N = 6 embryos, 7 neurons, 42 filopodia, p = 0.0013). Together, these loss- and gain-of-function findings suggest that Vangl2 functions within FBMNs to destabilize filopodia, since filopodia are affected in *vangl2* mutant and GFP-Vangl2-expressing FBMNs regardless of the genotype of cells in their microenvironment.

Fzd3a, like Vangl2, is required cell-autonomously and cell non-autonomously for FBMN migration (S1 Fig, [49]). To determine whether Fzd3a has a cell-autonomous role in FBMN protrusive activity, we transplanted *fzd3a* mutant FBMNs into a wild type host. We found that filopodia of *fzd3a* mutant FBMNs are significantly less stable than filopodia of wild type neurons, with a mean lifetime of 163.3 ± 8.006 seconds (Fig 6C and 6F and S6 movie; p = 0.0092). However, mean maximum filopodia length (3.4 ± 0.4 μm) was not significantly different than that of wild type FBMNs (Fig 6G). This suggests that Fzd3a normally functions within FBMNs to stabilize filopodia protrusions, consistent with a conserved role for Fzd in actin polymerization [11–13]. Taken together, our results suggest that Vangl2 and Fzd3a function antagonistically within FBMNs to regulate filopodial stability.

Given that we observed this cell-autonomous function for Vangl2 and Fzd3a in regulating FBMN membrane protrusions, we asked whether these proteins regulate FBMN protrusive dynamics independently of cells in the migratory environment. To address this question, we analyzed the protrusive dynamics of isolated FBMNs in primary culture. We found that cultured FBMNs display altered filopodial dynamics compared to FBMNs *in vivo*. Cultured wild type FBMNs have a mean lifetime of 537.5 ± 32.28 seconds (during a 600 second time-lapse) and an average maximum length of 6.0 ± 0.5 μm (S9 Fig). Furthermore, there is no difference in filopodial dynamics between cultured wild type and cultured *vangl2* mutant FBMNs (S9 Fig). This suggested to us that the cell-autonomous functions we observe for Vangl2 and Fzd3a *in vivo* depend on interactions with cells in the migratory environment.

Vangl2 and Fzd3a have opposing cell *non*-autonomous functions in regulating FBMN filopodial activity

Since Fzd3a and Vangl2 are also required non-autonomously for FBMN migration and since FBMN protrusive dynamics depend on cells in the migratory environment, we asked whether cells in the FBMN environment influence FBMN protrusive activity in a PCP-dependent manner. In order to assess the role of Vangl2 in the environment, we imaged protrusion dynamics of wild type FBMNs in a *vangl2* mutant environment. Interestingly we found that wild type FBMNs have less stable filopodia in a *vangl2* mutant environment compared to a wild type environment, with a mean lifetime of 143.3 ± 18.28 seconds (Fig 6D and 6F and S7 Movie; $p = 0.0056$). The decrease in the average filopodia lifetime of wild type FBMNs in a *vangl2* mutant environment is largely due to these neurons having a larger proportion of filopodia present for only one (30 seconds) or two (60 seconds) time-points (S8 Fig). The mean average length however was not different between wild-type FBMNs in a wild type environment and wild type FBMNs in a *vangl2* mutant environment (Fig 6G) (3.1 ± 0.2 μm). Removing Fzd3a from the migratory environment had the opposite effect on FBMN filopodia. Wild type neurons in a *fzd3a* mutant environment generate dramatically more stable filopodia compared to those in a wild type environment, with a mean lifetime of 363.8 ± 51.12 seconds (Fig 6E and 6F and S8 Movie; $p = 0.0273$). Together our results suggest that the core PCP components Vangl2 and Fzd3a antagonize each other's activity to control filopodial dynamics during neuronal migration *in vivo* and they do so by functioning both within FBMNs and in cells in their migratory environment.

Discussion

Based on our findings, we propose a model for the role of PCP signaling in FBMN migration in which canonical interactions between the transmembrane PCP core components Vangl2 and Fzd3a regulate filopodial dynamics, thereby signaling and/or regulating adhesion for directional migration (Fig 7). We note that this model for filopodial dynamics is based on genetics and that our work does not elucidate the molecular nature of these interactions, which remain controversial even in the context of epithelial polarity [17, 76]. This model is consistent with 1) a dual cell-autonomous and cell-non-autonomous requirement for PCP core components, specifically for the transmembrane components Vangl2 and Fzd3a, in FBMNs and their rhombomere 4 environment for migration; (this work, [31, 49, 51]); 2) the cytoskeletal and conserved molecular planar polarization of the r4 neuroepithelial environment including the floorplate (this work, [6]); 3) the ability of the planar polarized floorplate to promote the migration of wild type but not mutant FBMNs; 4) the localization of Vangl2 to retracting FBMN filopodial tips; 5) the antagonistic cell-autonomous roles of Fzd3a and Vangl2 in FBMN filopodial stability and 6) the opposite roles of Fzd3a and Vangl2 in the FBMN environment on FBMN filopodial stability.

Mutual antagonism of Vangl2 and Fzd3a

Our *in vivo* observations of filopodial dynamics in genetic chimeras demonstrate an antagonistic intracellular relationship between Vangl2 and Fzd3a in migrating FBMNs that regulates the stability of filopodium-like protrusions. While occurring in the context of a highly dynamic structure, this antagonistic relationship of Vangl2 and Fzd3a is reminiscent of the situation in stably polarized epithelia, where mutual intracellular antagonism between Fzd and Vangl complexes sets up polarized actin dynamics within the cell, with Fzd activating actin polymerization distally and Vangl suppressing it proximally [11–13, 77, 78]. This conserved interaction

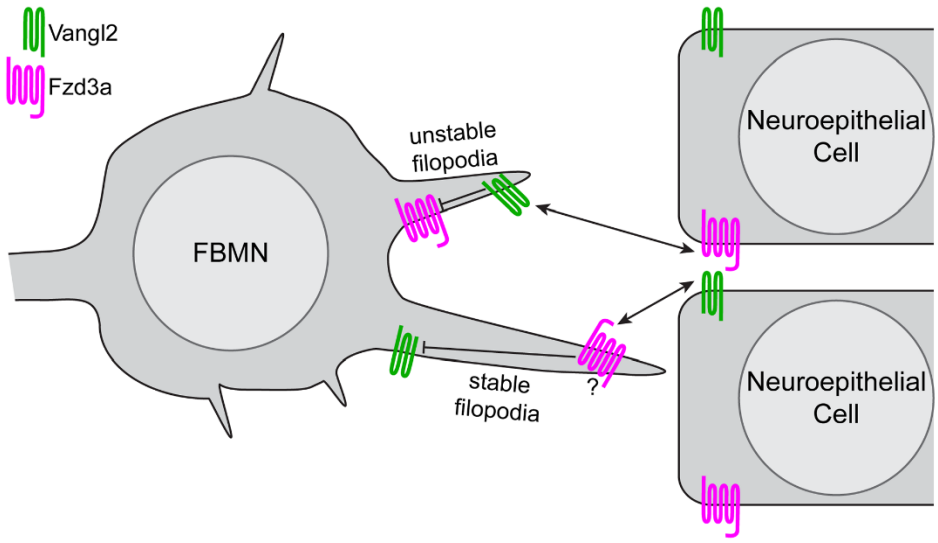

Fig 7. Model of PCP regulation of directed neuron migration. Based on the filopodial dynamics and migratory behaviors of FBMNs we observed in genetic chimeras, and the localization of Vangl2 and Fzd3a we observed in FBMNs and the cells of their migratory environment, we suggest a model in which antagonistic interactions between Vangl2 and Fzd3a mediate the observed effects on FBMN filopodial dynamics and through them, directional neuron migration. Within FBMNs, Vangl2 (green) localizes to filopodial tips and destabilizes them while Fzd3a (magenta) has the opposite, stabilizing effect. In the planar-polarized cells of the migratory environment Vangl2 serves to stabilize filopodia while Fzd3a destabilizes them. In light of the known intracellular and intercellular interactions between Vangl and Fzd that underlie epithelial planar polarization, we hypothesize that interactions between Fzd3a and Vangl2 complexes destabilize one another intracellularly while they promote one another's effects on the actin cytoskeleton when they interact across cell membranes. Whether these interactions provide *directional* cues for migration remains to be discovered.

doi:10.1371/journal.pgen.1005934.g007

between Fzd promoting and Vangl suppressing actin growth may be common to other migratory cells. In metastatic breast cancer cells induced by stromal Wnt11-containing exosomes, Fzd6 and Vangl1 exhibit mutually exclusive localizations, with Fzd6 on the leading edge of cell protrusions and Vangl1 on non-protrusive cell surfaces, and knock-down of either protein decreases cell motility [44]. Similarly in migrating leukemia cells, Dvl-3 (part of the Fzd complex) localizes to the leading edge while Vangl2 localizes to the trailing edge [79]. During mesodermal and neuroectodermal convergence, mediolaterally oriented cell surfaces exhibit increased actomyosin contractility [33, 80] that correlates with the asymmetric localization of PCP components Dvl and Pk (part of the Vangl complex) [7, 81], suggestive of a conserved intracellular antagonism of these complexes mediating actin dynamics. In contrast, in commissural growth cones, Vangl2 *promotes* Fzd3-dependent outgrowth induced by diffusible Wnt5a by antagonizing a non-canonical inhibitory interaction between Dvl1 and Fzd3 identified in that context [41]. These examples show that core PCP components localize to discrete domains of moving cells and we have shown *in vivo* for the first time that this results in opposing effects on filopodial stability.

The role of filopodia in FBMN cell migration

Filopodia are commonly associated with the promotion of directed cell migration, although in some instances, axons and cells can achieve proper targeting and guidance without filopodia [82–84]. Due to their dynamics and long thin architecture, filopodia are capable of probing a

wide area around cells, and they can contain receptors for diverse diffusible and membrane-bound signals and extracellular matrix molecules [85]. Thus, it is thought that the primary function of filopodia is as "antennae" that cells use to sense their microenvironment to orient directed cell migration [86]. Indeed it has been demonstrated that elimination of filopodia in axon growth cones does not impair axon outgrowth, but instead impairs growth cone turning in response to environmental cues [87–89]. This sensing role for filopodia has also been demonstrated in cell migration [84, 90]. In addition to a sensing role, filopodia are thought to contribute directly to cell motility, as cells lacking filopodia tend to migrate more slowly due to the absence of filopodial adhesion molecules which could induce traction and also through force generated by actin streaming in filopodia [82, 90–93]. In the context of FBMN migration, filopodia extend in all directions from neurons when they initiate their migration, and we see no bias in the orientation of the filopodia that are affected in PCP mutants. We hypothesize that filopodia act as sensors of asymmetrically localized cell-surface PCP components on the neuroepithelial cells through which they are migrating and that this sensing fine tunes filopodium dynamics such that these filopodia can promote migration by acting as force generators or appropriately sensing other, as-yet unidentified environmental cues. In other migrating cells, several effectors have been identified as possible links between PCP signaling and cytoskeletal regulation [33, 94, 95]. While our work does not elucidate how those signals are transduced to the filopodial actin cytoskeleton in FBMNs, our previous work identified the WAVE-homology domain containing actin regulator Nhsl1 as localizing to FBMN filopodia and being required cell-autonomously for FBMN migration [51, 96]; we hypothesize that PCP signals may be transduced to the actin cytoskeleton in FBMNs via Nhsl1.

Fzd3a and Vangl2 function in the migratory environment

A more surprising finding than opposing cell autonomous roles for Fzd3a and Vangl2 in FBMN filopodial dynamics and migration is that the same PCP components function in the FBMN environment to influence filopodial dynamics but in the opposite way: Fzd3a in the environment destabilizes filopodia while Vangl2 in the environment stabilizes them. These non-autonomous functions for Fzd3a and Vangl2 in filopodial dynamics correlate with their non-autonomous roles in FBMN migration [31, 49]. Again, this is reminiscent of classical planar-polarity, where localized Fzd activity depends on the presence of Vangl in adjacent cells in the epithelium and vice versa; this is the mechanism by which PCP is coordinated across an epithelium [17–21]. We hypothesize that the cell-autonomous activities of Fzd3a and Vangl2 are activated in different filopodia when they contact Vangl2 and Fzd3a domains of neuroepithelial cells in the r4 environment (Fig 7), with consequences on the actin dynamics regulating filopodial stability, leading to changes in signaling and/or adhesion. We have shown here that Vangl2 and Fzd3a exhibit planar polarized localization in the r4 neuroepithelium and floorplate at the time of FBMN migration. In PCP mutants, this polarized information is absent and/or cannot be correctly interpreted by filopodia resulting in a failure of directional cell migration. We note that the cell-autonomous filopodial phenotypes appear to be dominant, since in constitutive mutants filopodia have the cell-autonomous phenotype (long and stable in *vangl2* mutants; unstable in *fzd3a* mutants). Together our findings suggest that conserved intracellular and intercellular interactions between PCP core components can have divergent effects on actin dynamics and consequently on cell behaviors.

While the similar effects on filopodial dynamics when Vangl2 is depleted from FBMNs and when Fzd3a is depleted from their environment suggest that the two proteins are working together, environmental PCP may also influence filopodia dynamics of FBMNs through an indirect mechanism. For instance, core PCP proteins have been implicated in the trafficking

and regulation of membrane levels of cadherins in fly and in vertebrate epithelial cells [97–99]. Therefore, Vangl2 and Fzd3a in the migratory environment may modulate FBMN filopodia dynamics by regulating N-cadherin levels at the surface of neuroepithelial cells. Another potential mechanism by which PCP in the migratory environment may regulate FBMN filopodial dynamics is through regulation of membrane type-1 matrix metalloproteinase (MMP14), which are known to degrade extracellular matrix proteins. During zebrafish gastrulation, an increase in Mmp14 activity was observed in *vangl2* mutant embryos [100]. Thus, the decreased FBMN filopodial stability observed when Vangl2 is absent in the migratory environment could be due to decreased extracellular matrix.

Which cells in the environment of FBMNs are the source of PCP cues for filopodial dynamics and migration? We have shown that disruption of PCP signaling in the r4 environment prevents FBMN migration, demonstrating that PCP signaling is required to initiate directional migration. It was recently reported that Vangl2 expression even in a single cell in the r4 floorplate is sufficient to rescue FBMN migration in a *vangl2* mutant [55]. In contrast, our results show that floorplate Vangl2 is neither required nor sufficient for FBMN migration. Neither the widespread presence of GFP-Vangl2 expressing cells or of wild type donor-derived cells in the floorplate of *vangl2* mutants rescued the migration of *vang2* mutant FBMNs. The rescue of FBMN migration observed by Sittaramane et al. (2013) may have been due to undetected early expression of Vangl2 outside of the floorplate driven by the Gal4 genetrap line used in their experiments [101, 102].

We did, however, note that the presence of wild type cells in the floorplate could partially rescue the migration of wild type FBMNs in an otherwise *vangl2* mutant embryo. This suggests that bidirectional PCP signaling between the planar-polarized floorplate and the FBMNs can promote migration. However this rescue was incomplete, indicating that other planar polarized cells in the r4 environment normally contribute to the pro-migratory environment. Consistent with this hypothesis, we found that disrupting the planar polarization of the floorplate alone in both fish and mouse embryos was insufficient to prevent FBMN migration (Fig 3 and S4 Fig). We conclude that the planar polarization of the entire r4 environment surrounding the FBMNs is required to effectively initiate migration. We were unable to confirm this by rescuing FBMN migration in a *vangl2* mutant with r4-restricted expression of GFP-Vangl2, likely because the over-expression of PCP components disrupts planar polarity as efficiently as their loss [28, 31, 103, 104].

Our study provides new insights into the role of the planar cell polarity pathway in neuronal migration by identifying when and where PCP signaling is required and how it affects the dynamic cell behaviors of migrating neurons *in vivo*. Our data suggests that a planar polarized hindbrain rhombomere 4 neuroepithelium serves to promote FBMN migration through the selective stabilization and destabilization of FBMN filopodia using conserved intra- and intercellular interactions between the PCP components Vangl2 and Fzd3a. Whether neuroepithelial planar polarity directs posterior migration or simply enables it, and through what effectors PCP signaling regulates filopodial dynamics *in vivo* are important questions to be answered in future work.

Methods

Ethics statement

Experiments using animals were performed under the Fred Hutchinson Cancer Research Center Institutional Animal Care and Use Committee protocols #1392 (zebrafish, approved on 3/31/2015) and #50857 (mice, approved 4/1/2015). The Fred Hutchinson Cancer Research Center Institutional Animal Care and Use Committee (IACUC) follow the guidelines of the Office

of Laboratory Animal Welfare and set its policies according to The Guide for the Care and Use of Laboratory Animals. Fred Hutchinson Cancer Research Center maintains full accreditation from the Association for Assessment and Accreditation of Laboratory Animal Care (AAALAC) and has letters of assurance on file with OLAW. The IACUC routinely evaluates the Fred Hutchinson animal facilities and programs to assure compliance with federal, state, local, and institution laws, regulations, and policies. The OLAW Assurance number is A3226-01.

Zebrafish lines and maintenance

Zebrafish (*Danio rerio*) were raised at the Fred Hutchinson Cancer Research Center, and animal care and experiments were approved by the Institutional Animal Care and Use Committee. All animals were maintained according to standard procedures [105] and staged as previously described [106]. All mutant lines used were previously described and are registered at The Zebrafish International Resource Center (ZIRC): *fzd3a*^{rw689} (*olt*^{rw689}) [49], *prickle1b*^{fh122} [50], and *vangl2*^{m209} (*tri*^{m209}) [31]. Previously described transgenic lines used were as follows: *Tg(isl1:GFP)rw0* [56], *Tg(isl1CREST-hsp70l:mRFP)fh1* [67], *TgBAC(hoxb1a:RFP)fh3* [67], *Tg(egr2b:KalTA4)* [63] and *Tg(hoxb1a(β-globin):Gal4VP16)um60* [64].

Cloning and transgenic line generation

The following transgenic lines were generated for this study: *Tg(shh:Gal4VP16)fh445*, *Tg(isl1:Gal4VP16)fh452*, *Tg(isl1-hsp70:mTFP)fh350*, *Tg(isl-hsp70:dvl-DEP-GFP)fh444*, *Tg(10XUAS:xdd1-GFP)fh446*, *Tg(10XUAS:fzdΔC-GFP)fh447* and *Tg(10XUAS:GFP-vangl2)fh453*. The Gal4VP16 sequence was obtained from the Nonet Lab (http://pcg.wustl.edu/nonetlab/ResourcesF/Zebrafish.html) and the 10XUAS plasmid was obtained from the Tol2 kit (http://tol2kit.genetics.utah.edu/index.php/List_of_entry_and_destination_vectors) [107]. The mTFP construct was obtained from Alleleustrious, Inc (Cat# ABP-FP-TFA1000).

To generate *Tg(shh:Gal4VP16)fh445*, the ar-B enhancer element of zebrafish *sonic hedgehog (shh)* [108, 109] was amplified from a plasmid (gift from Uwe Strähle). For the Gal4 lines, the *shh* and *isl1* enhancers were inserted upstream of the *gata2* minimal promoter element [110]. The Xdd1 and full-length *Xenopus* Dvl are described in Sokol et al. (1996) [25]. Transgenic elements were cloned using the Gateway (Life Technologies) system using the primer sequences listed in S1 Table. Final DNA constructs were assembled in the pDESTpBHR4R3 plasmid (gift from the Brockerhoff Lab) or the CG5 Tol2 expression vector [107]. Transgenic embryos were generated by Tol2 transposase RNA co-injection with each plasmid at the single cell stage [111].

Mouse lines and husbandry

All mice were maintained at Fred Hutchinson Cancer Research Center under Institutional Animal Care and Use Committee approved guidelines. For general colony maintenance, all mouse lines were crossed into the C57BL/6J background (The Jackson Laboratory strain 00064). The *Vangl2*^{Lexp} and *Vangl2*$^{\Delta TM}$ lines were a gift from the Deans laboratory [61], the *Isl1Cre* (*Isl*$^{tm1(cre)Sev}$) line was a gift from the Evans laboratory [62] and the Shh:gfp-cre (*Shh*$^{tm1(EGFP/cre)Cjt}$) line was purchased from The Jackson Laboratory (strain 005622).

Cell transplantation

Chimeric embryos were generated by transplantation at the blastula or gastrula stage as previously described [51, 112]. To track transplanted cells, donor embryos carrying the *Tg(isl1:GFP)rw0*, *Tg(isl1:mRFP)fh1* or *Tg(isl1:mTFP)fh350* transgene were injected with 1% cascade blue-

dextran or rhodamine-dextran (for live imaging) and 1% biotin-dextran (for imaging after fixation) (10,000 mw, Life Technologies). Host embryos were then processed and imaged for all donor-derived cells, donor-derived FBMNs or floorplate cells, and host FBMNs. Host and donor embryo genotypes were identified either by observing body axis elongation defects (for *vangl2* mutant hosts), by examining FBMN location at 48 hpf or by genotyping (for *fzd3a* mutant hosts).

For transplantation of post-mitotic FBMNs, cascade blue-dextran labeled donor embryos and unlabeled host embryos were mounted in agar on coverslips at the 15-somite stage. The head of each animal was exposed by careful removal of agar with insect pins, and a hole was cut in the skin overlying the forebrain to enable entry of a thin (10 μm diameter) transplant pipette. Pre-migratory FBMNs (visualized by *isl1*:*GFP* or *isl1*:*mRFP* expression) were removed from r4 of a donor embryo and transplanted into r4 of a host embryo using a Zeiss AxioSkop fixed-stage microscope fitted with a 40X long working-distance water-immersion ("dipping") lens. During this process some non-*isl1*:*GFP/mRFP*-expressing neuroepithelial progenitor cells were inevitably co-transplanted but these usually died shortly after transplantation; any surviving donor-derived cells that were not FBMNs were detected by the presence of the cascade blue dye. Due to the disruptive approach, which removes nascent axons and other processes, even wild type FBMNs transplanted into a wild type environment do not migrate as well as FBMNs transplanted at earlier stages.

Whole-mount immunohistochemistry

Anesthetized zebrafish embryos were fixed in 2% trichloroacetic (TCA) acid for 3 hours or 4% paraformaldehyde (PFA)/ 4% sucrose in PBS for 1 hour at room temperature. Dissected mouse hindbrains were fixed in 4% paraformaldehyde (PFA)/ 4% sucrose in PBS overnight at 4°C and permeablized in PBS + 1% TritonX100. Fixed tissue was washed in PBS + 0.5% TritonX100 followed by standard blocking and antibody incubations. Following staining, brain tissue was dissected, cleared step-wise in a 25%, 50%, 75% glycerol series and mounted for confocal imaging. The following antibodies were used: rabbit anti-zebrafish Vangl2 (1:250, Anaspec Cat# AS-55659), mouse anti-islet1 39.4D5 (1:10 for zebrafish tissue and 1:100 for mouse tissue, Developmental Studies Hybridoma Bank); chicken anti-GFP (1:500, Abcam Cat# ab13970); rabbit anti-ZO-1 (1:1000, Zymed Cat# 61–7300); mouse anti-Cc2d2a (1:100, [113]); rabbit anti-RFP (1:1000, Abcam Cat# ab62341). For analysis of chimeric embryos after fixation, host embryos were additionally stained with a fluorescently conjugated streptavidin (Life Technologies Cat# S32351) to enhance the detection of Biotin-Dextran-containing donor-derived cells.

Primary cell culture

Primary cultures of FBMNs were prepared from 24 hour post fertilization *Tg(isl1:mTFP); Tg(hoxb1a:RFP)* embryos. The hindbrains of embryos were micro-dissected and dissociated as previously reported [114]. Cells were plated on a chambered coverglass (Sigma Z734756) coated with 5μg/mL poly-D-lysine (Sigma L8021) and 5μg/mL laminin (Sigma L2020) at a density of 4–5 hindbrains per 1.7 cm^2. FBMNs were distinguished from other *Tg(isl1:mTFP)*-expressing hindbrain motor neurons by virtue of *Tg(hoxb1a:RFP)* expression, which is restricted to hindbrain r4 and r4-derived neurons. Live imaging of explanted neurons was performed 5 hours after plating.

Imaging and data analysis

Imaging was performed using a Zeiss 700 confocal microscope or a Zeiss spinning disc microscope with a QuantEM EMCCD camera for live time-lapse imaging. For timelapse imaging, Z-

stack images at 1μm steps were captured every 30 seconds for 15 minutes for *in vivo* time-lapse images and every 5 seconds for 10 minutes for cultured neurons. Filopodia were defined as long thin protrusions, less than 0.2 μm in diameter and more than 0.75 μm in length, measured from the cell body margin to the protrusion tip. *In vivo* filopodia lengths, lifetimes and fluorescent intensities of mRFP and GFP-Vangl2 were quantified using Zeiss Zen 2012 software. For cultured neurons, filopodium quantification was performed semi-automatically using Imaris FilamentTracer software (http://www.bitplane.com/imaris/filamenttracer). Mean anti-Vangl2 fluorescent intensity for all cell membranes were measured in user-drawn regions of interest using Zeiss Zen 2011 software or ImageJ's "Plot Profile" tool. Anterior/posterior GFP-Vangl2 fluorescent intensity ratios for each cell were normalized by dividing this value by the anterior/posterior ZO-1 fluorescent intensity ratio. Graphs were generated and statistics were computed using GraphPad Prism software. All statistical analyses were performed using a 95% confidence interval. In most cases significance was determined using an unpaired, two-tail t-test with Welch's correction. For the anti-Vangl2 staining quantification significance was determined using a paired two-tail t-test with Welch's correction. Differences in FBMN distributions were analyzed using a Chi-square test where the distribution of FBMNs in control animals served as the expected frequencies or null hypothesis to determine if the observed frequencies were significantly different. Circular plots were generated using Oriana 4 software. Figure images were created using Adobe Photoshop and Adobe Illustrator.

Supporting Information

S1 Fig. Fzd3a has a cell-autonomous function in FBMN migration. (A-B) Live confocal images of 48 hpf chimeric embryos with anterior to the top. Transplant conditions are indicated as donor→host. Pk1bMO host embryos were used because they have normal neuroepithelial planar polarity but unmigrated FBMNs; this prevents donor-derived FBMNs from being carried to r6 by migrating host neurons in a PCP-independent manner. Cascade blue-dextran marks all donor-derived cells (blue), *Tg(isl1:mRFP)* marks host FBMNs (magenta) and *Tg(isl1:GFP)* marks donor-derived FBMNs (green). Histograms on the right indicate the percent of donor-derived FBMNs at 48 hpf that failed to migrate (rhombomere (r)4), partially migrated (r5) or fully migrated (r6) and numbers indicate the number of FBMNs represented in each bar. N indicates the number of chimeric embryos and n indicates the number of FBMNs scored in each condition. Brackets indicate rhombomere positon. Scale bar: 50 μm. (TIF)

S2 Fig. Post-mitotic FBMNs require PCP signaling for migration. (A) Live confocal image showing the dorsal view of a *pk1b* mutant embryo hindbrain at 48 hpf after transplantation of post-mitotic FBMNs from a wild type donor. Cascade blue-dextran marks all donor-derived cells (blue), *Tg(isl1:GFP)* marks host FBMNs (green) and *Tg(isl1:mRFP)* marks donor-derived FBMNs (magenta). (B) Histogram indicates the percent of donor-derived FBMNs at 48 hpf that failed to migrate, (rhombomere (r)4), partially migrated (r5) or fully migrated (r6) and numbers indicate the number of FBMNs represented in each bar. White arrows indicate migrated donor derived FBMNs. While post-mitotic FBMNs in general migrate poorly after being transplanted, they do sometimes migrate in WT and *pk1b* mutant hosts but never in *vangl2* mutant hosts (see Fig 2). Brackets indicate rhombomere positon. Scale bar: 50μm. (TIF)

S3 Fig. PCP-DN expression in the floorplate disrupts planar polarity. (A-C) *Tg(shh:Gal4)* driven expression of *Tg(UAS:Kaede)* in the notochord and floorplate of a 14 hpf (A) 24 hpf embryo (B) and a 48 hpf embryo (C). Anterior is to the left. Images are live lateral views in A-C

and live dorsal views at the hindbrain level, A',B'. (D-F) Confocal images showing floorplate planar polarity of the anterior spinal cord in 48 hpf zebrafish embryos. Anterior is to the top. Anti-ZO-1 marks subapical tight junctions (white), anti-Cc2d2a marks the basal bodies of the primary cilia (magenta, arrows), and anti-GFP indicates dominant negative protein expression (green). Scale bar: 10μm. Whereas basal bodies are localized toward the posterior membrane in wild type embryos (D), this polarity is disrupted in floorplate cells expressing Xdd1-GFP (E) or Fzd3aΔC-GFP (F) (arrows in E' and F'). (G) Schematic of the method used to quantify floorplate planar polarity. Total cell length (x) is measured as the distance between the anterior and posterior membranes (white) at the level of the basal body (magenta). Basal body position (y) is measured as the distance between the anterior membrane and the basal body. Cellular planar polarity is quantified as the ratio of x/y. (H) Quantitation of average basal body position in the floor plate of 48 hpf embryos. Each data point represents the mean basal body position for all cells quantitated in a single embryo. WT: N = 34 embryos, 411 cells; Xdd1-GFP: N = 14 embryos, 207 expressing cells; FzdΔC-GFP: N = 29 embryos, 484 expressing cells; *vangl2*$^{-/-}$: N = 10 embryos, 96 cells. Quantitation of floorplate polarity in *vangl2*$^{-/-}$ embryos is included for comparison. Graph represents data as mean ± SD. $^{**}p<0.0001$ compared to wild-type control.
(TIF)

S4 Fig. Vangl2 is not required in the mouse floorplate for FBMN migration. (A-B) Dorsal view of E13.5 mouse hindbrains with FBMNs (magenta) labeled with anti-Isl1 staining. Dotted lines indicate length of facial motor nucleus. To improve the chances that a Cre-expressing cell will have a biallelic deletion of Vangl2, in these experiments we used the *Vangl2*$^{\Delta TM}$ null allele, which we discovered belatedly to cause a mild FBMN migration defect in compound heterozygotes with the floxed *Vangl2*^{LoxP} allele. Nevertheless, deleting the floxed allele with *Shh*^{Cre} did not enhance the partial migration defect in *Vangl2*$^{LoxP/\Delta TM}$ controls. For the experiments using *Isl1Cre* shown in Fig 1 we did not use the *Vangl2*$^{\Delta TM}$ allele. (A) FBMNs in a *Vangl2*$^{LoxP/\Delta TM}$ control embryo. N = 6 embryos. (B) FBMNs in *Vangl2*$^{LoxP/\Delta TM}$;*Shh*^{Cre} embryo. Addition of *Shh*^{Cre} does not further disrupt FBMN migration. N = 4 embryos. (C) Quantitation of FBMN migration stream length in *Vangl2*$^{LoxP/\Delta TM}$ control embryos and *Vangl2*$^{LoxP/\Delta TM}$;*Shh*^{Cre} embryos. Scale bar: 100μm
(TIF)

S5 Fig. Specificity of the anti-Vangl2 antibody. (A-B) Dorsal view of wild type (A) and *vangl2* mutant (B) 24 hpf neural tubes immunostained with anti-Vangl2-NT (green). The neuroepithelial membrane staining visible in wild type is absent in the mutant. (C) Western blot analysis of whole embryo lysates with anti-Vangl2 antibody. Anti-alpha-tubulin was used as a loading control. Zebrafish Vangl2 is expected to run at approximately 60kDa. For the anti-Vangl2 blot there is a band that is present in the wild type and absent in the *vangl2* mutant, see asterisk.
(TIF)

S6 Fig. Migrating FBMNs display polarized protrusions that fail to polarize in *vangl2* mutants. (A,C,E) Representative frames of mTFP expressing FBMNs from time-lapse images taken at 24 hpf to 32 hpf. (B,D,F) Each raw data point for protrusion angle is plotted on the circular graph below. Each division is 10 degrees. A, anterior. P, posterior. M, medial. L, lateral. Filopodia are radial in wild type FBMNs prior to exiting r4 (A,B, N = 3 embryos, 5 neurons, 28 filopodia) and become polarized to the posterior side of the cell during migration (C,D, N = 8 embryos, 10 neurons (6 in r5 and 4 in r6), 52 filopodia). FBMN protrusions fail to polarize in *vangl2* mutants (E,F, N = 5 embryos, 7 neurons, 61 protrusions). Scale bar: 16μm.
(TIF)

S7 Fig. Donor-derived FBMNs used to quantitate filopodial dynamics were in a genetically chimeric environment. (A-E) Live confocal images of donor-derived FBMNs (green) and all other nearby donor-derived cells (magenta). Transplant conditions are indicated on as donor→host as in Fig 5. Rhodamine dextran marks all donor-derived cells (magenta), *Tg(isl1:mTFP)* marks donor-derived FBMNs (green). Anterior is to the top and medial is to the right. Scale bar: 5 μm.
(TIF)

S8 Fig. Raw filopodial quantitation data. (A) Quantitation of filopodial lifetime for donor-derived FBMNs. Each data point represents one filopodium. The maximum filopodial lifetime (900 seconds) corresponds to the full length of the time-lapse. (B) Quantitation of maximum filopodial length for filopodia lasting longer than 90 seconds on donor-derived FBMNs. Each data point represents one filopodium.
(TIF)

S9 Fig. The effect of PCP on protrusion dynamics is dependent on the migratory environment. (A) Method used to isolate and identify FBMNs in primary culture. Embryos used were *Tg(isl1:mTFP);Tg(hoxb1a:RFP)* allowing for the differentiation between FBMNs and other branchiomotor neurons labeled by *Tg(isl1:mTFP)*. (B,C) Cultured *Tg(isl1:mTFP); Tg(hoxb1a:RFP)* FBMNs from a wild type (B) and a *vangl2* mutant embryo (C). (B',C') Time-lapse spinning-disc confocal series of boxed region from B and C. (D) Quantitation of filopodial lifetime for cultured FBMNs. Each timelapse was 600 seconds total. $p = 0.9044$, n.s. (E) Quantitation of the maximum filopodial length for cultured FBMNs. $p = 0.0856$, n.s. Wild type: N = 8 neurons, 64 filopodia. *vangl2*$^{-/-}$: N = 8 neurons, 61 filodpodia. Graphs represent data as mean ± SEM. Each data point is the average lifetime (D) or maximum length (E) for all the filopodia of one FBMN. Significance was determined using an unpaired, two-tail t-test with Welch's correction.
(TIF)

S1 Movie. Time-lapse of a GFP-Vangl2; *Tg(isl1:mRFP)* expressing FBMN. Note GFP-Vangl2 enrichment events preceding filopodia retraction. Movie is 4 frames per second (fps) with a 45 second time interval.
(AVI)

S2 Movie. Time-lapse of LifeAct-GFP expressing FBMN. Movie is 4fps with a 13 second time interval.
(AVI)

S3 Movie. Time-lapse of a *Tg(isl1:mTFP)* wild type FBMN in a wild type host. This and all subsequent movies are 4fps with 30 second time intervals.
(AVI)

S4 Movie. Time-lapse of *Tg(isl1:mTFP) vangl2* mutant FBMNs in a *vangl2* mutant host.
(AVI)

S5 Movie. Time-lapse of a *Tg(isl1:mTFP) vangl2* mutant FBMN in a wild type host.
(AVI)

S6 Movie. Time-lapse of a *Tg(isl1:mTFP) fzd3a* mutant FBMN in a wild type host.
(AVI)

S7 Movie. Time-lapse of a *Tg(isl1:mTFP)* wild type FBMN in a *vangl2* mutant host.
(AVI)

S8 Movie. Time-lapse of a *Tg(isl1:mTFP)* wild type FBMNs in a *fzd3a* mutant host.
(AVI)

S1 Table. Primers used in the creation of transgenic constructs.
(PDF)

Acknowledgments

We would like to thank Dan Berman, for the image of localized Fzd3a-GFP and quantitation of GFP-Vangl in the floorplate; Greg Walsh, who contributed to the conception and design of these experiments; Michael Deans, Sylvia Evans, Charles Sagerström, Uwe Strähle, Randy Moon, Sue Brockerhoff and Martin Distel for constructs and transgenic lines; Julio Vasquez and David McDonald at the FHCRC imaging core for assistance with filopodia quantification; members of the Moens lab for ideas, support and critical review of the manuscript and Rachel Garcia for expert fish care.

Author Contributions

Conceived and designed the experiments: CFD AWM CBM. Performed the experiments: CFD AWM CBM. Analyzed the data: CFD AWM CBM. Contributed reagents/materials/analysis tools: CFD AWM CBM. Wrote the paper: CFD AWM CBM.

References

1. Gray R.S., Roszko I., and Solnica-Krezel L., Planar cell polarity: coordinating morphogenetic cell behaviors with embryonic polarity. Dev Cell, 2011. 21(1): p. 120–33. doi: 10.1016/j.devcel.2011.06.011 PMID: 21763613
2. Goodrich L.V. and Strutt D., Principles of planar polarity in animal development. Development, 2011. 138(10): p. 1877–92. doi: 10.1242/dev.054080 PMID: 21521735
3. Gubb D. and Garcia-Bellido A., A genetic analysis of the determination of cuticular polarity during development in Drosophila melanogaster. J Embryol Exp Morphol, 1982. 68: p. 37–57. PMID: 6809878
4. Wong L.L. and Adler P.N., Tissue polarity genes of Drosophila regulate the subcellular location for prehair initiation in pupal wing cells. J Cell Biol, 1993. 123(1): p. 209–21. PMID: 8408199
5. Adler P.N., The genetic control of tissue polarity in Drosophila. Bioessays, 1992. 14(11): p. 735–41. PMID: 1365886
6. Borovina A., et al., Vangl2 directs the posterior tilting and asymmetric localization of motile primary cilia. Nat Cell Biol, 2010. 12(4): p. 407–12. doi: 10.1038/ncb2042 PMID: 20305649
7. Ciruna B., et al., Planar cell polarity signalling couples cell division and morphogenesis during neurulation. Nature, 2006. 439(7073): p. 220–4. PMID: 16407953
8. Wang Y., Guo N., and Nathans J., The role of Frizzled3 and Frizzled6 in neural tube closure and in the planar polarity of inner-ear sensory hair cells. J Neurosci, 2006. 26(8): p. 2147–56. PMID: 16495441
9. Wang J., et al., Regulation of polarized extension and planar cell polarity in the cochlea by the vertebrate PCP pathway. Nat Genet, 2005. 37(9): p. 980–5. PMID: 16116426
10. Montcouquiol M., et al., Identification of Vangl2 and Scrb1 as planar polarity genes in mammals. Nature, 2003. 423(6936): p. 173–7. PMID: 12724779
11. Strutt D.I., Weber U., and Mlodzik M., The role of RhoA in tissue polarity and Frizzled signalling. Nature, 1997. 387(6630): p. 292–5. PMID: 9153394
12. Winter C.G., et al., Drosophila Rho-associated kinase (Drok) links Frizzled-mediated planar cell polarity signaling to the actin cytoskeleton. Cell, 2001. 105(1): p. 81–91. PMID: 11301004
13. Fanto M., et al., Nuclear signaling by Rac and Rho GTPases is required in the establishment of epithelial planar polarity in the Drosophila eye. Curr Biol, 2000. 10(16): p. 979–88. PMID: 10985385
14. Carvajal-Gonzalez J.M. and Mlodzik M., Mechanisms of planar cell polarity establishment in Drosophila. F1000Prime Rep, 2014. 6: p. 98. doi: 10.12703/P6-98 PMID: 25580252
15. Jenny A., et al., Diego and Prickle regulate Frizzled planar cell polarity signalling by competing for Dishevelled binding. Nat Cell Biol, 2005. 7(7): p. 691–7. PMID: 15937478

16. Tree D.R., Ma D., and Axelrod J.D., A three-tiered mechanism for regulation of planar cell polarity. Semin Cell Dev Biol, 2002. 13(3): p. 217–24. PMID: 12137730

17. Wu J. and Mlodzik M., The frizzled extracellular domain is a ligand for Van Gogh/Stbm during nonautonomous planar cell polarity signaling. Dev Cell, 2008. 15(3): p. 462–9. doi: 10.1016/j.devcel.2008.08.004 PMID: 18804440

18. Strutt D. and Strutt H., Differential activities of the core planar polarity proteins during Drosophila wing patterning. Dev Biol, 2007. 302(1): p. 181–94. PMID: 17045581

19. Chin M.L. and Mlodzik M., The Drosophila selectin furrowed mediates intercellular planar cell polarity interactions via frizzled stabilization. Dev Cell, 2013. 26(5): p. 455–68. doi: 10.1016/j.devcel.2013.07.006 PMID: 23973164

20. Taylor J., et al., Van Gogh: a new Drosophila tissue polarity gene. Genetics, 1998. 150(1): p. 199–210. PMID: 9725839

21. Vinson C.R. and Adler P.N., Directional non-cell autonomy and the transmission of polarity information by the frizzled gene of Drosophila. Nature, 1987. 329(6139): p. 549–51. PMID: 3116434

22. Wallingford J.B., Planar cell polarity and the developmental control of cell behavior in vertebrate embryos. Annu Rev Cell Dev Biol, 2012. 28: p. 627–53. doi: 10.1146/annurev-cellbio-092910-154208 PMID: 22905955

23. Tissir F. and Goffinet A.M., Shaping the nervous system: role of the core planar cell polarity genes. Nat Rev Neurosci, 2013. 14(8): p. 525–35. doi: 10.1038/nrn3525 PMID: 23839596

24. Tada M. and Kai M., Planar cell polarity in coordinated and directed movements. Curr Top Dev Biol, 2012. 101: p. 77–110. doi: 10.1016/B978-0-12-394592-1.00004-1 PMID: 23140626

25. Sokol S.Y., Analysis of Dishevelled signalling pathways during Xenopus development. Curr Biol, 1996. 6(11): p. 1456–67. PMID: 8939601

26. Tada M. and Smith J.C., Xwnt11 is a target of Xenopus Brachyury: regulation of gastrulation movements via Dishevelled, but not through the canonical Wnt pathway. Development, 2000. 127(10): p. 2227–38. PMID: 10769246

27. Wallingford J.B., et al., Dishevelled controls cell polarity during Xenopus gastrulation. Nature, 2000. 405(6782): p. 81–5. PMID: 10811222

28. Darken R.S., et al., The planar polarity gene strabismus regulates convergent extension movements in Xenopus. EMBO J, 2002. 21(5): p. 976–85. PMID: 11867525

29. Goto T. and Keller R., The planar cell polarity gene strabismus regulates convergence and extension and neural fold closure in Xenopus. Dev Biol, 2002. 247(1): p. 165–81. PMID: 12074560

30. Djiane A., et al., Role of frizzled 7 in the regulation of convergent extension movements during gastrulation in Xenopus laevis. Development, 2000. 127(14): p. 3091–100. PMID: 10862746

31. Jessen J.R., et al., Zebrafish trilobite identifies new roles for Strabismus in gastrulation and neuronal movements. Nat Cell Biol, 2002. 4(8): p. 610–5. PMID: 12105418

32. Wallingford J.B. and Harland R.M., Xenopus Dishevelled signaling regulates both neural and mesodermal convergent extension: parallel forces elongating the body axis. Development, 2001. 128(13): p. 2581–92. PMID: 11493574

33. Shindo A. and Wallingford J.B., PCP and septins compartmentalize cortical actomyosin to direct collective cell movement. Science, 2014. 343(6171): p. 649–52. doi: 10.1126/science.1243126 PMID: 24503851

34. Wallingford J.B. and Harland R.M., Neural tube closure requires Dishevelled-dependent convergent extension of the midline. Development, 2002. 129(24): p. 5815–25. PMID: 12421719

35. Wang J., et al., Dishevelled genes mediate a conserved mammalian PCP pathway to regulate convergent extension during neurulation. Development, 2006. 133(9): p. 1767–78. PMID: 16571627

36. Ybot-Gonzalez P., et al., Convergent extension, planar-cell-polarity signalling and initiation of mouse neural tube closure. Development, 2007. 134(4): p. 789–99. PMID: 17229766

37. Williams M., et al., Distinct apical and basolateral mechanisms drive planar cell polarity-dependent convergent extension of the mouse neural plate. Dev Cell, 2014. 29(1): p. 34–46. doi: 10.1016/j.devcel.2014.02.007 PMID: 24703875

38. Lyuksyutova A.I., et al., Anterior-posterior guidance of commissural axons by Wnt-frizzled signaling. Science, 2003. 302(5652): p. 1984–8. PMID: 14671310

39. Tissir F., et al., Protocadherin Celsr3 is crucial in axonal tract development. Nat Neurosci, 2005. 8(4): p. 451–7. PMID: 15778712

40. Wang Y., et al., Frizzled-3 is required for the development of major fiber tracts in the rostral CNS. J Neurosci, 2002. 22(19): p. 8563–73. PMID: 12351730

41. Shafer B., et al., Vangl2 promotes Wnt/planar cell polarity-like signaling by antagonizing Dvl1-mediated feedback inhibition in growth cone guidance. Dev Cell, 2011. 20(2): p. 177–91. doi: 10.1016/j.devcel.2011.01.002 PMID: 21316586

42. Fenstermaker A.G., et al., Wnt/planar cell polarity signaling controls the anterior-posterior organization of monoaminergic axons in the brainstem. J Neurosci, 2010. 30(47): p. 16053–64. doi: 10.1523/JNEUROSCI.4508-10.2010 PMID: 21106844

43. Cantrell V.A. and Jessen J.R., The planar cell polarity protein Van Gogh-Like 2 regulates tumor cell migration and matrix metalloproteinase-dependent invasion. Cancer Lett, 2010. 287(1): p. 54–61. doi: 10.1016/j.canlet.2009.05.041 PMID: 19577357

44. Luga V., et al., Exosomes mediate stromal mobilization of autocrine Wnt-PCP signaling in breast cancer cell migration. Cell, 2012. 151(7): p. 1542–56. doi: 10.1016/j.cell.2012.11.024 PMID: 23260141

45. Chandrasekhar A., Turning heads: development of vertebrate branchiomotor neurons. Dev Dyn, 2004. 229(1): p. 143–61. PMID: 14699587

46. Wanner S.J., et al., Facial motor neuron migration advances. Curr Opin Neurobiol, 2013. 23(6): p. 943–50. doi: 10.1016/j.conb.2013.09.001 PMID: 24090878

47. Guthrie S., Patterning and axon guidance of cranial motor neurons. Nat Rev Neurosci, 2007. 8(11): p. 859–71. PMID: 17948031

48. Wada H., et al., Dual roles of zygotic and maternal Scribble1 in neural migration and convergent extension movements in zebrafish embryos. Development, 2005. 132(10): p. 2273–85. PMID: 15829519

49. Wada H., et al., Frizzled3a and Celsr2 function in the neuroepithelium to regulate migration of facial motor neurons in the developing zebrafish hindbrain. Development, 2006. 133(23): p. 4749–59. PMID: 17079269

50. Mapp O.M., et al., Zebrafish Prickle1b mediates facial branchiomotor neuron migration via a farnesylation-dependent nuclear activity. Development, 2011. 138(10): p. 2121–32. doi: 10.1242/dev.060442 PMID: 21521740

51. Walsh G.S., et al., Planar polarity pathway and Nance-Horan syndrome-like 1b have essential cell-autonomous functions in neuronal migration. Development, 2011. 138(14): p. 3033–42. doi: 10.1242/dev.063842 PMID: 21693519

52. Vivancos V., et al., Wnt activity guides facial branchiomotor neuron migration, and involves the PCP pathway and JNK and ROCK kinases. Neural Dev, 2009. 4: p. 7. doi: 10.1186/1749-8104-4-7 PMID: 19210786

53. Qu Y., et al., Atypical cadherins Celsr1-3 differentially regulate migration of facial branchiomotor neurons in mice. J Neurosci, 2010. 30(28): p. 9392–401. doi: 10.1523/JNEUROSCI.0124-10.2010 PMID: 20631168

54. Glasco D.M., et al., The mouse Wnt/PCP protein Vangl2 is necessary for migration of facial branchiomotor neurons, and functions independently of Dishevelled. Dev Biol, 2012. 369(2): p. 211–22. doi: 10.1016/j.ydbio.2012.06.021 PMID: 22771245

55. Sittaramane V., et al., The PCP protein Vangl2 regulates migration of hindbrain motor neurons by acting in floor plate cells, and independently of cilia function. Dev Biol, 2013. 382(2): p. 400–12. doi: 10.1016/j.ydbio.2013.08.017 PMID: 23988578

56. Higashijima S., Hotta Y., and Okamoto H., Visualization of cranial motor neurons in live transgenic zebrafish expressing green fluorescent protein under the control of the islet-1 promoter/enhancer. J Neurosci, 2000. 20(1): p. 206–18. PMID: 10627598

57. Boutros M., et al., Dishevelled activates JNK and discriminates between JNK pathways in planar polarity and wingless signaling. Cell, 1998. 94(1): p. 109–18. PMID: 9674432

58. Wanner S.J. and Prince V.E., Axon tracts guide zebrafish facial branchiomotor neuron migration through the hindbrain. Development, 2013. 140(4): p. 906–15. doi: 10.1242/dev.087148 PMID: 23325758

59. Rohrschneider M.R., Elsen G.E., and Prince V.E., Zebrafish Hoxb1a regulates multiple downstream genes including prickle1b. Dev Biol, 2007. 309(2): p. 358–72. PMID: 17651720

60. Qu Y., et al., Genetic evidence that Celsr3 and Celsr2, together with Fzd3, regulate forebrain wiring in a Vangl-independent manner. Proc Natl Acad Sci U S A, 2014. 111(29): p. E2996–3004. doi: 10.1073/pnas.1402105111 PMID: 25002511

61. Copley C.O., et al., Postnatal refinement of auditory hair cell planar polarity deficits occurs in the absence of Vangl2. J Neurosci, 2013. 33(35): p. 14001–16. doi: 10.1523/JNEUROSCI.1307-13.2013 PMID: 23986237

62. Yang L., et al., Isl1Cre reveals a common Bmp pathway in heart and limb development. Development, 2006. 133(8): p. 1575–85. PMID: 16556916

63. Distel M., Wullimann M.F., and Koster R.W., Optimized Gal4 genetics for permanent gene expression mapping in zebrafish. Proc Natl Acad Sci U S A, 2009. 106(32): p. 13365–70. doi: 10.1073/pnas.0903060106 PMID: 19628697

64. Choe S.K., et al., A Gal4/UAS system for conditional transgene expression in rhombomere 4 of the zebrafish hindbrain. Dev Dyn, 2012. 241(6): p. 1125–32. doi: 10.1002/dvdy.23794 PMID: 22499412

65. Roszko I., et al., A dynamic intracellular distribution of Vangl2 accompanies cell polarization during zebrafish gastrulation. Development, 2015. 142(14): p. 2508–20. doi: 10.1242/dev.119032 PMID: 26062934

66. Ossipova O., Kim K., and Sokol S.Y., Planar polarization of Vangl2 in the vertebrate neural plate is controlled by Wnt and Myosin II signaling. Biol Open, 2015. 4(6): p. 722–30. doi: 10.1242/bio.201511676 PMID: 25910938

67. Grant P.K. and Moens C.B., The neuroepithelial basement membrane serves as a boundary and a substrate for neuron migration in the zebrafish hindbrain. Neural Dev, 2010. 5: p. 9. doi: 10.1186/1749-8104-5-9 PMID: 20350296

68. Harfe B.D., et al., Evidence for an expansion-based temporal Shh gradient in specifying vertebrate digit identities. Cell, 2004. 118(4): p. 517–28. PMID: 15315763

69. Trevarrow B., Marks D.L., and Kimmel C.B., Organization of hindbrain segments in the zebrafish embryo. Neuron, 1990. 4(5): p. 669–79. PMID: 2344406

70. Xiong F., et al., Specified neural progenitors sort to form sharp domains after noisy Shh signaling. Cell, 2013. 153(3): p. 550–61. doi: 10.1016/j.cell.2013.03.023 PMID: 23622240

71. Mapp O.M., et al., Prickle1b mediates interpretation of migratory cues during zebrafish facial branchiomotor neuron migration. Dev Dyn, 2010. 239(6): p. 1596–608. doi: 10.1002/dvdy.22283 PMID: 20503357

72. Portera-Cailliau C., Pan D.T., and Yuste R., Activity-regulated dynamic behavior of early dendritic protrusions: evidence for different types of dendritic filopodia. J Neurosci, 2003. 23(18): p. 7129–42. PMID: 12904473

73. Lim K.B., et al., The Cdc42 effector IRSp53 generates filopodia by coupling membrane protrusion with actin dynamics. J Biol Chem, 2008. 283(29): p. 20454–72. doi: 10.1074/jbc.M710185200 PMID: 18448434

74. Ahmed S., Goh W.I., and Bu W., I-BAR domains, IRSp53 and filopodium formation. Semin Cell Dev Biol, 2010. 21(4): p. 350–6. doi: 10.1016/j.semcdb.2009.11.008 PMID: 19913105

75. Villefranc J.A., et al., A truncation allele in vascular endothelial growth factor c reveals distinct modes of signaling during lymphatic and vascular development. Development, 2013. 140(7): p. 1497–506. doi: 10.1242/dev.084152 PMID: 23462469

76. Chen W.S., et al., Asymmetric homotypic interactions of the atypical cadherin flamingo mediate intercellular polarity signaling. Cell, 2008. 133(6): p. 1093–105. doi: 10.1016/j.cell.2008.04.048 PMID: 18555784

77. Strutt D. and Warrington S.J., Planar polarity genes in the Drosophila wing regulate the localisation of the FH3-domain protein Multiple Wing Hairs to control the site of hair production. Development, 2008. 135(18): p. 3103–11. doi: 10.1242/dev.025205 PMID: 18701542

78. Yan J., et al., The multiple-wing-hairs gene encodes a novel GBD-FH3 domain-containing protein that functions both prior to and after wing hair initiation. Genetics, 2008. 180(1): p. 219–28. doi: 10.1534/genetics.108.091314 PMID: 18723886

79. Kaucka M., et al., Asymmetry of VANGL2 in migrating lymphocytes as a tool to monitor activity of the mammalian WNT/planar cell polarity pathway. Cell Commun Signal, 2015. 13: p. 2. doi: 10.1186/s12964-014-0079-1 PMID: 25627785

80. Nishimura T., Honda H., and Takeichi M., Planar cell polarity links axes of spatial dynamics in neural-tube closure. Cell, 2012. 149(5): p. 1084–97. doi: 10.1016/j.cell.2012.04.021 PMID: 22632972

81. Yin C., et al., Cooperation of polarized cell intercalations drives convergence and extension of presomitic mesoderm during zebrafish gastrulation. J Cell Biol, 2008. 180(1): p. 221–32. doi: 10.1083/jcb.200704150 PMID: 18195109

82. Phng L.K., Stanchi F., and Gerhardt H., Filopodia are dispensable for endothelial tip cell guidance. Development, 2013. 140(19): p. 4031–40. doi: 10.1242/dev.097352 PMID: 24046319

83. Dwivedy A., et al., Ena/VASP function in retinal axons is required for terminal arborization but not pathway navigation. Development, 2007. 134(11): p. 2137–46. PMID: 17507414

84. Boer E.F., et al., Fascin1-dependent Filopodia are required for directional migration of a subset of neural crest cells. PLoS Genet, 2015. 11(1): p. e1004946. doi: 10.1371/journal.pgen.1004946 PMID: 25607881

85. Mattila P.K. and Lappalainen P., Filopodia: molecular architecture and cellular functions. Nat Rev Mol Cell Biol, 2008. 9(6): p. 446–54. doi: 10.1038/nrm2406 PMID: 18464790

86. Heckman C.A. and Plummer H.K. 3rd, Filopodia as sensors. Cell Signal, 2013. 25(11): p. 2298–311. doi: 10.1016/j.cellsig.2013.07.006 PMID: 23876793

87. Bentley D. and Toroian-Raymond A., Disoriented pathfinding by pioneer neurone growth cones deprived of filopodia by cytochalasin treatment. Nature, 1986. 323(6090): p. 712–5. PMID: 3773996

88. Chien C.B., et al., Navigational errors made by growth cones without filopodia in the embryonic Xenopus brain. Neuron, 1993. 11(2): p. 237–51. PMID: 8352941

89. Zheng J.Q., Wan J.J., and Poo M.M., Essential role of filopodia in chemotropic turning of nerve growth cone induced by a glutamate gradient. J Neurosci, 1996. 16(3): p. 1140–9. PMID: 8558243

90. Meyen D., et al., Dynamic filopodia are required for chemokine-dependent intracellular polarization during guided cell migration in vivo. Elife, 2015. 4.

91. Galbraith C.G., Yamada K.M., and Galbraith J.A., Polymerizing actin fibers position integrins primed to probe for adhesion sites. Science, 2007. 315(5814): p. 992–5. PMID: 17303755

92. Steketee M.B. and Tosney K.W., Three functionally distinct adhesions in filopodia: shaft adhesions control lamellar extension. J Neurosci, 2002. 22(18): p. 8071–83. PMID: 12223561

93. Johnson H.E., et al., F-actin bundles direct the initiation and orientation of lamellipodia through adhesion-based signaling. J Cell Biol, 2015. 208(4): p. 443–55. doi: 10.1083/jcb.201406102 PMID: 25666809

94. Habas R., Kato Y., and He X., Wnt/Frizzled activation of Rho regulates vertebrate gastrulation and requires a novel Formin homology protein Daam1. Cell, 2001. 107(7): p. 843–54. PMID: 11779461

95. Ulmer B., et al., Calponin 2 acts as an effector of noncanonical Wnt-mediated cell polarization during neural crest cell migration. Cell Rep, 2013. 3(3): p. 615–21. doi: 10.1016/j.celrep.2013.02.015 PMID: 23499442

96. Brooks S.P., et al., The Nance-Horan syndrome protein encodes a functional WAVE homology domain (WHD) and is important for co-ordinating actin remodelling and maintaining cell morphology. Hum Mol Genet, 2010. 19(12): p. 2421–32. doi: 10.1093/hmg/ddq125 PMID: 20332100

97. Classen A.K., et al., Hexagonal packing of Drosophila wing epithelial cells by the planar cell polarity pathway. Dev Cell, 2005. 9(6): p. 805–17. PMID: 16326392

98. Warrington S.J., Strutt H., and Strutt D., The Frizzled-dependent planar polarity pathway locally promotes E-cadherin turnover via recruitment of RhoGEF2. Development, 2013. 140(5): p. 1045–54. doi: 10.1242/dev.088724 PMID: 23364328

99. Nagaoka T., et al., Vangl2 regulates E-cadherin in epithelial cells. Sci Rep, 2014. 4: p. 6940. doi: 10.1038/srep06940 PMID: 25373475

100. Williams B.B., et al., VANGL2 regulates membrane trafficking of MMP14 to control cell polarity and migration. J Cell Sci, 2012. 125(Pt 9): p. 2141–7. doi: 10.1242/jcs.097964 PMID: 22357946

101. Asakawa K., et al., Genetic dissection of neural circuits by Tol2 transposon-mediated Gal4 gene and enhancer trapping in zebrafish. Proc Natl Acad Sci U S A, 2008. 105(4): p. 1255–60. doi: 10.1073/pnas.0704963105 PMID: 18202183

102. Koide T., et al., Olfactory neural circuitry for attraction to amino acids revealed by transposon-mediated gene trap approach in zebrafish. Proc Natl Acad Sci U S A, 2009. 106(24): p. 9884–9. doi: 10.1073/pnas.0900470106 PMID: 19497864

103. Tree D.R., et al., Prickle mediates feedback amplification to generate asymmetric planar cell polarity signaling. Cell, 2002. 109(3): p. 371–81. PMID: 12015986

104. Heisenberg C.P., et al., Silberblick/Wnt11 mediates convergent extension movements during zebrafish gastrulation. Nature, 2000. 405(6782): p. 76–81. PMID: 10811221

105. Westerfield M., *The Zebrafish Book*. University of Oregon Press, Eugene, OR. 1993.

106. Kimmel C.B., et al., Stages of embryonic development of the zebrafish. Dev Dyn, 1995. 203(3): p. 253–310. PMID: 8589427

107. Kwan K.M., et al., The Tol2kit: a multisite gateway-based construction kit for Tol2 transposon transgenesis constructs. Dev Dyn, 2007. 236(11): p. 3088–99. PMID: 17937395

108. Ertzer R., et al., Cooperation of sonic hedgehog enhancers in midline expression. Dev Biol, 2007. 301(2): p. 578–89. PMID: 17157288

109. Muller F., et al., Intronic enhancers control expression of zebrafish sonic hedgehog in floor plate and notochord. Development, 1999. 126(10): p. 2103–16. PMID: 10207136

110. Meng A., et al., Promoter analysis in living zebrafish embryos identifies a cis-acting motif required for neuronal expression of GATA-2. Proc Natl Acad Sci U S A, 1997. 94(12): p. 6267–72. PMID: 9177206

111. Kawakami K., Shima A., and Kawakami N., Identification of a functional transposase of the Tol2 element, an Ac-like element from the Japanese medaka fish, and its transposition in the zebrafish germ lineage. Proc Natl Acad Sci U S A, 2000. 97(21): p. 11403–8. PMID: 11027340

112. Carmany-Rampey A. and Moens C.B., Modern mosaic analysis in the zebrafish. Methods, 2006. 39 (3): p. 228–38. PMID: 16829130

113. Bachmann-Gagescu R., et al., The ciliopathy gene cc2d2a controls zebrafish photoreceptor outer segment development through a role in Rab8-dependent vesicle trafficking. Hum Mol Genet, 2011. 20(20): p. 4041–55. doi: 10.1093/hmg/ddr332 PMID: 21816947

114. Andersen S.S., Preparation of dissociated zebrafish spinal neuron cultures. Methods Cell Sci, 2001. 23(4): p. 205–9. PMID: 12486331

Supplemental Figures

Note: additional supplemental files can be found at:
http://journals.plos.org/plosgenetics/article?id=10.1371/journal.pgen.1005934#sec024

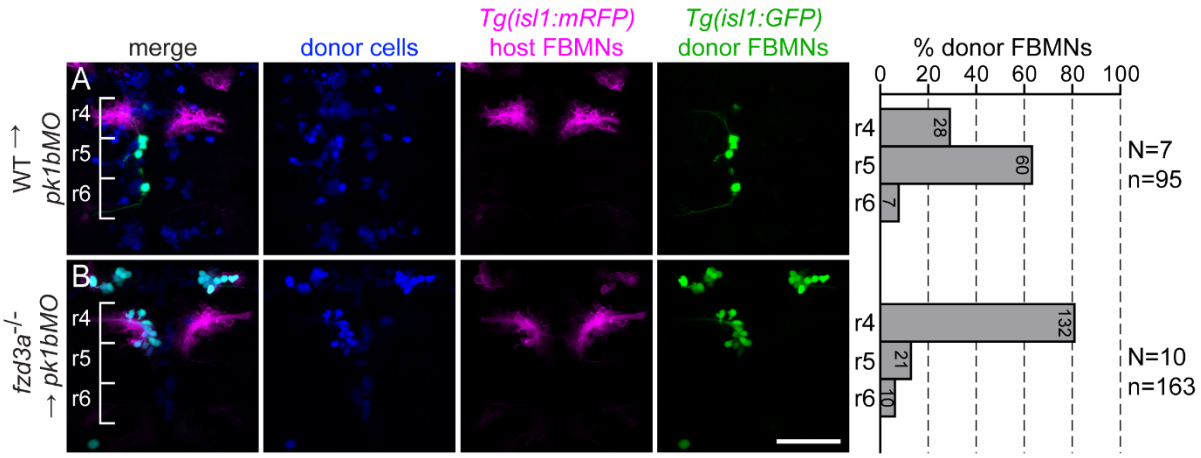

Figure S 1. Fzd3a has a cell-autonomous function in FBMN migration.

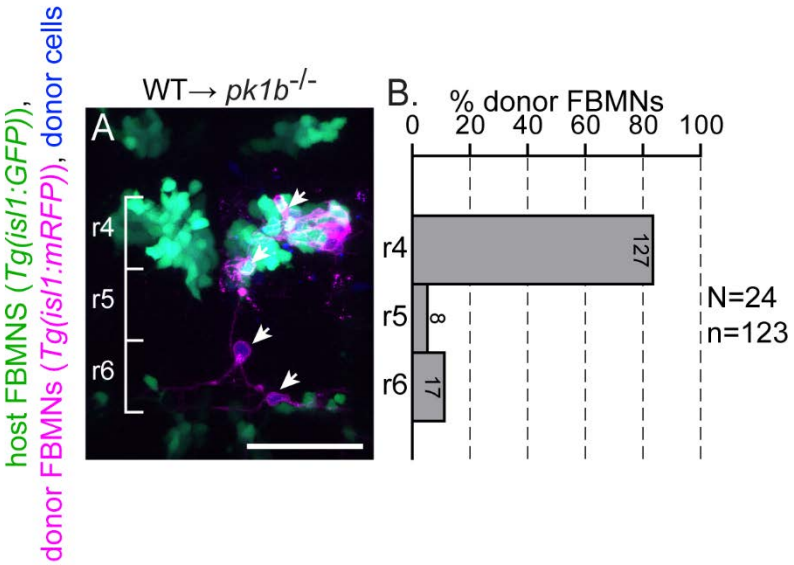

Figure S 2. Post-mitotic FBMNs require PCP signaling for migration.

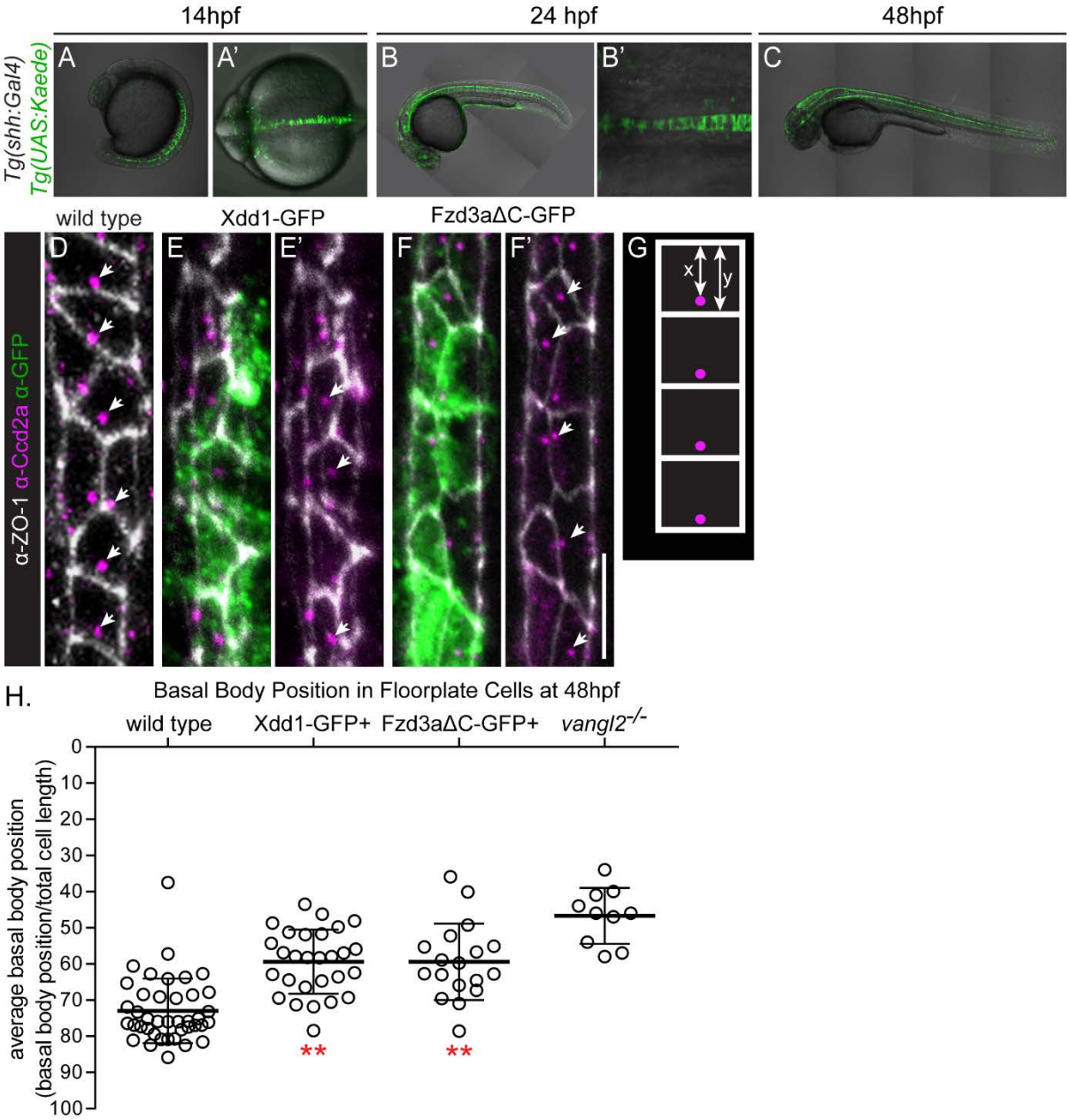

Figure S 3. PCP-DN expression in the floorplate disrupts planar polarity.

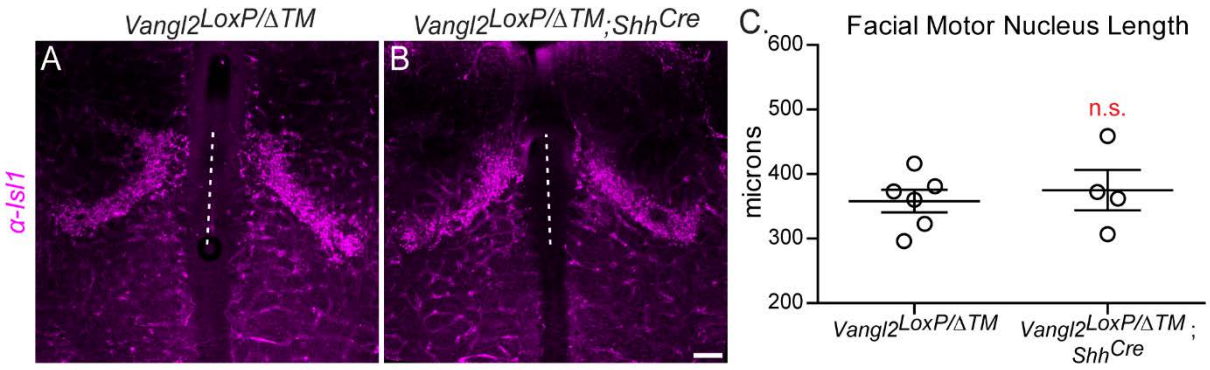

Figure S 4. Vangl2 is not required in the mouse floorplate for FBMN migration.

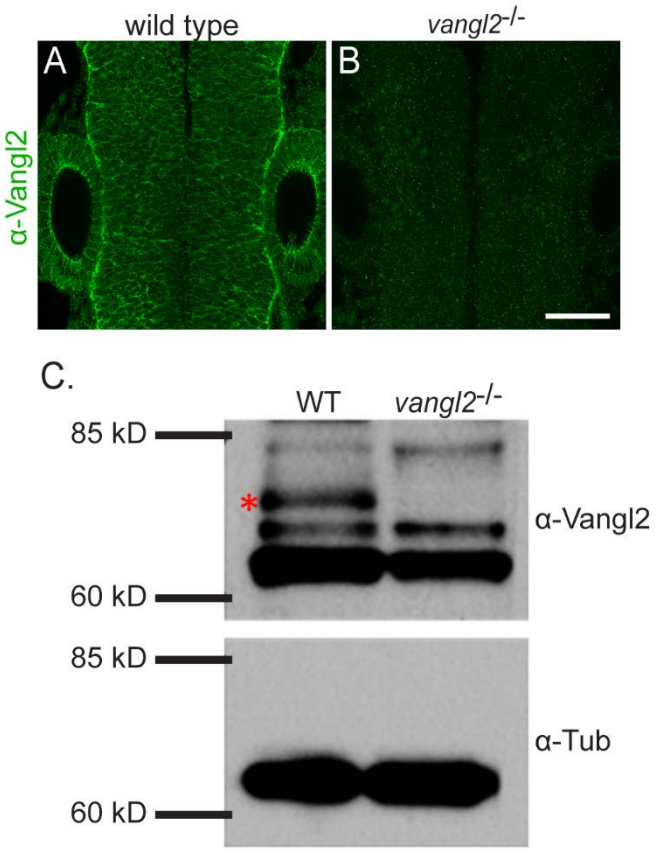

Figure S 5. Specificity of the anti-Vangl2 antibody.

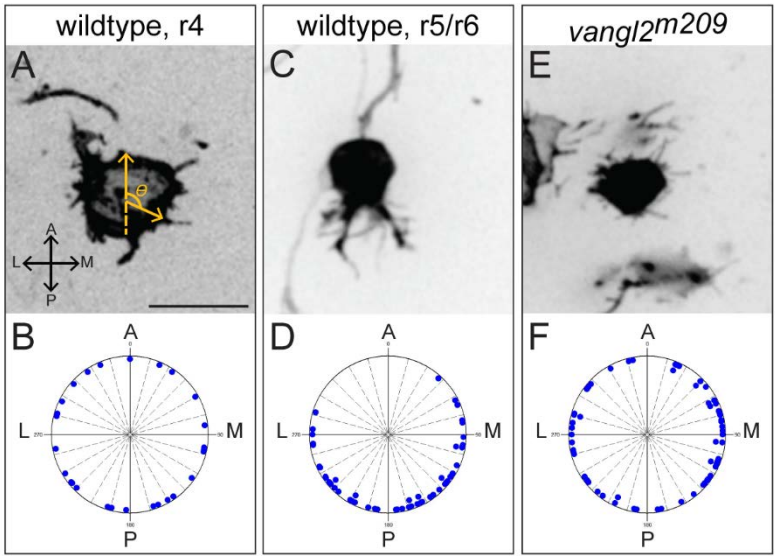

Figure S 6. Migrating FBMNs display polarized protrusions that fail to polarize in Vangl2 mutants.

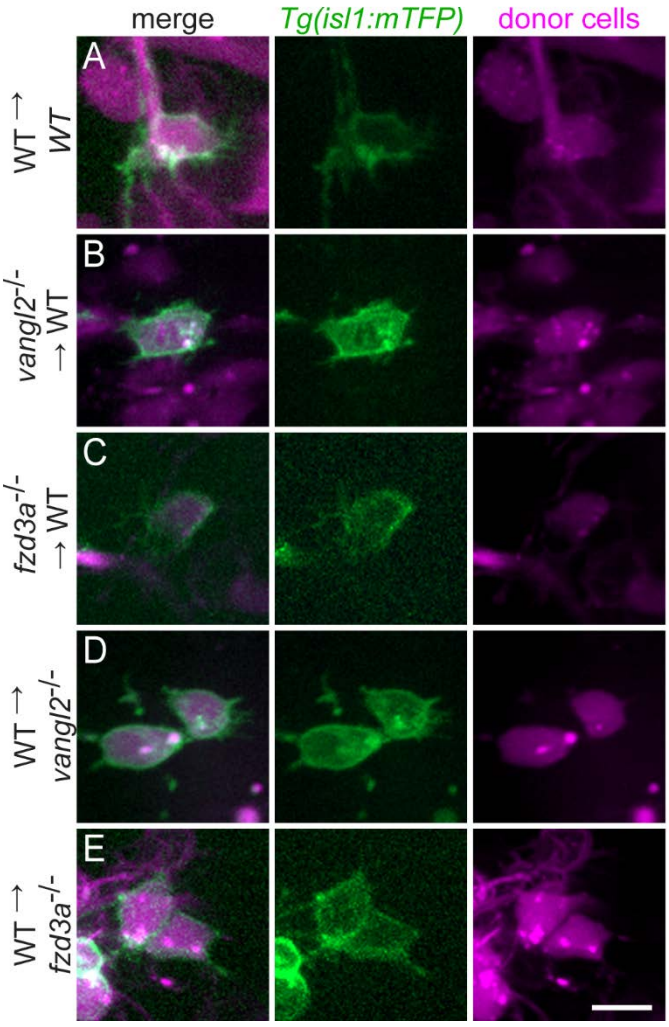

Figure S 7. Donor-derived FBMNs used to quantitate filopodial dynamics are in a genetically chimeric environment.

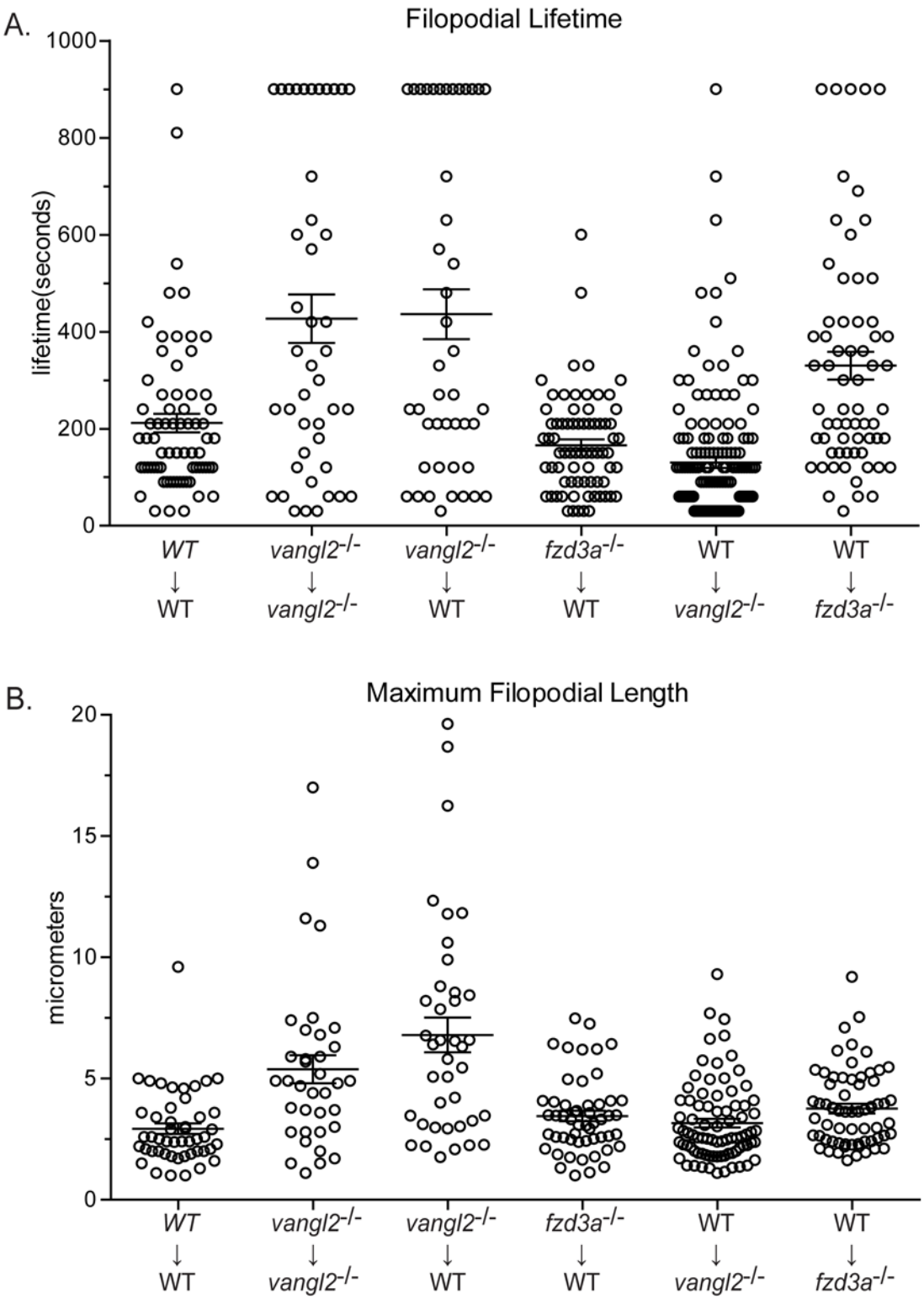

Figure S 8. Raw filopodial quantitation data.

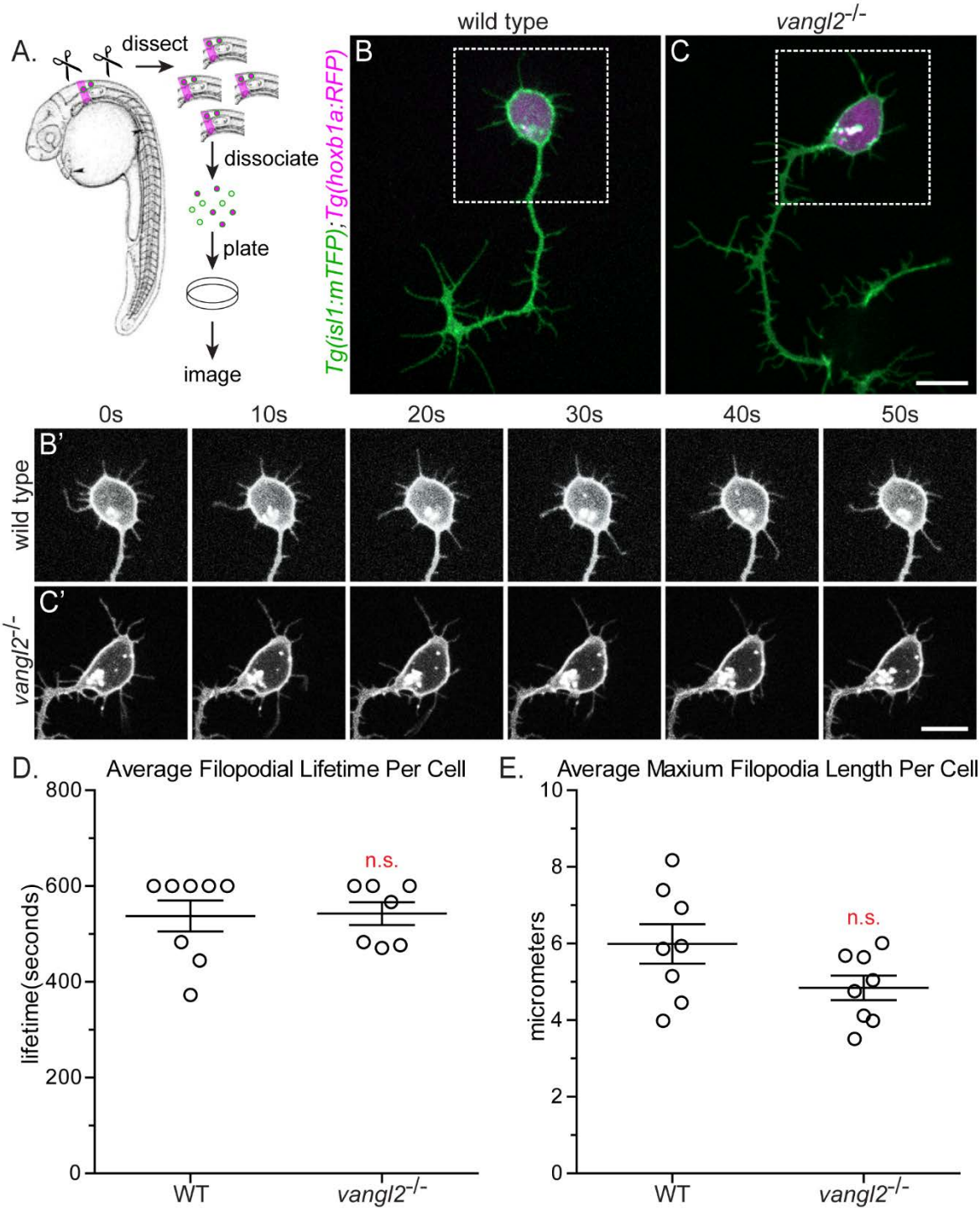

Figure S 9. The effect of PCP on protrusion dynamics is dependent on the migratory environment.

Chapter 4: Conclusions and Future Directions

The Basal Body and PCP

The links between PCP signaling and BB positioning are complex and not fully understood at a mechanistic level. Though it is well-established that PCP signaling is required for the actin-based translational positioning of the BB in many systems (Borovina et al., 2010; Carvajal-Gonzalez et al., 2016a; Hashimoto et al., 2010; Vladar et al., 2012), whether the asymmetric position of the BB can reciprocally influence the establishment and maintenance of PCP protein asymmetry has not been investigated. As we determined in Chapter 2 that nocodazole-induced loss of BB asymmetry occurred simultaneously with a decrease of asymmetric GFP-Vangl2 at the membrane, we were curious if BB position could influence PCP protein distribution. Intriguingly, we discovered that restoration of MTs after their disruption does not rescue BB posterior positioning, but largely restores GFP-Vangl2 asymmetry at the membrane as well as vesicular Fzd3a-GFP dynamics **(Fig 5)**. This decoupling of asymmetrically localized BBs from the polarized localization of GFP-Vangl2 is strong evidence that BB position does not significantly affect PCP protein asymmetry. This is surprising, as the BB likely retains at least partial MTOC function and we directly observed Fzd3a-GFP localizing near the BB and trafficking along MTs. The position of the MTOC must affect the orientation of MTs that nucleate there, which could affect the careful balance of directional trafficking of PCP protein-containing vesicles to specific membranes. Indeed, unpolarized BBs do correlate with differences in overall displacement angles and distances of Fzd3a-GFP vesicles, yet appear to

have no effect on vesicle velocities **(Fig 5)**. We hypothesize that these changes are due to distinct BB positioning between these two conditions as the more centrally-localized BBs of nocodazole-treated embryos can extend MTs in both A/P directions (as well as A/B), whereas a posteriorly polarized BB is limited to more anterior facing MTs **(Fig 5)**. Alternatively, non-centrosomal MTs may be sufficient to enable directional trafficking and asymmetric localization of PCP proteins, as many differentiated cell types reassign primary MTOC function to non-centrosomal sites (Muroyama and Lechler, 2017). As the functional consequences MTOC reassignment and a changing MT organization are poorly characterized in any context, how floorplate cells regulate the maintenance of asymmetric MT-based directional trafficking of PCP protein-containing vesicles remains to be determined.

Vangl2 Asymmetry

Although the BB is stably positioned to floorplate cell posteriors by 30hpf (Fig 1a), the asymmetric localization of GFP-Vangl2 to anterior membranes continues to increase until at least 48hpf (Fig 2d versus 3i). This is not surprising, as asymmetric distributions of core PCP proteins are known to self-amplify over time in other contexts (see (Goodrich and Strutt, 2011) for review), and this does not conflict with our model that cellular PCP is actively maintained after 30hpf. As PCP proteins are known to internalize during mitosis (Devenport et al., 2011), and we noticed that floorplate cells continue to divide between 30hpf and 48hpf, it is possible that some of our 30hpf measurements of GFP-Vangl2 localization occurred in cells prior to their final division and differentiation. It would be interesting to assess asymmetric localization of

Vangl2 after 48hpf to see if it continues to become more enriched to anterior membranes throughout development. Furthermore, though we confirmed that Vangl2 is necessary for establishment of BB asymmetry within the floorplate (Borovina et al., 2010), whether Vangl2 asymmetry is actively required for maintenance of BB asymmetry has not been investigated. This could be assessed by developing an inducible technique to disrupt PCP protein asymmetry within the floorplate after BB asymmetry has been established, perhaps through inducible PCP-specific dominant-negatives (DNs) or inducible CRISPR-based gene excision. Additionally, though the anterior localization of GFP-Vangl2 is consistent with Vangl2 localizing opposite to cilia in other contexts (Antic et al., 2010), it is unclear how well our transgenic tools reflect all aspects of endogenous PCP protein behavior. This is a concern because the over- or under-expression of individual PCP components is known to disrupt the balance and behavior of other core PCP proteins in other contexts (Jessen et al., 2002). We could confirm our results through the endogenous knock-in (Kimura et al., 2014) of fluorescently fused core PCP genes so that PCP gene expression levels could be regulated by endogenous promoters and enhancers. A major challenge of this technique is that expression would not be limited to the floorplate, and as the floorplate is centrally-located this additional expression would likely obscure its visualization. Additionally, endogenous promoters may not express highly enough to visualize PCP protein dynamics and localization with our current tools.

Other groups have used fluorescence recovery after photobleaching (FRAP) analysis to examine Vangl2 stability at the membrane and have determined that Vangl2 is most stable where it is locally enriched (Shi et al., 2016; Strutt et al., 2011). Each of these studies found that

roughly half of fluorescently-fused Vangl2 signal in less-enriched membrane regions recovered from photobleaching in a matter of minutes, whereas areas that were locally enriched with Vangl2 recovered more slowly. In mouse oviduct cells, only twenty percent of the prebleached signal of membrane regions containing highly concentrated fluorescently-fused Vangl2 protein recovered from photobleaching over a period of an hour, suggesting that Vangl2 is very stably localized at these locations (Shi et al., 2016). Our analysis examined the changes in asymmetric accumulations of mEOS-Vangl2 at anterior and posterior membranes three hours after photoconversion. Though it is difficult to directly compare these FRAP analyses to our own photoconversion experiments, the maintenance of enrichment of mEOS-Vangl2 at the anterior membrane may reflect stable fraction of Vangl2 similar to those identified in these previous studies. However, it remains to be formally determined if this protein is truly static on the membrane or if it is being actively recycled to and from the plasma membrane to maintain its asymmetry.

Though we highlight the accumulation of cytosolic Fzd3a-GFP at the BB, we also observed multiple instances where fluorescently-fused Vangl2 aggregated at low levels near the BB under control conditions (Fig 3h, 4c). Importantly, nocodazole-induced MT-loss caused dramatic enrichment of this population near the BB (Fig 4c). Based on these observations, we propose that Vangl2, like Fzd3a, uses a MT-based mode of transportation that becomes disrupted in the absence of MTs. However, we have not yet determined if the GFP-Vangl2 that aggregates near the BB upon MT-loss is newly synthesized protein that cannot be distributed to membranes, or if it represents protein that has been endocytosed from the membrane and is

undergoing recycling processes. One way to address this would be to combine photoconversion of mEOS-Vangl2 with nocodazole-induced MT loss. In brief, we could photoconvert cells expressing mEOS-Vangl2 and then immediately treat embryos with nocodazole to eliminate MTs. As in Fig 3h, we could assess $mEOS^{red}$-Vangl2 and $mEOS^{green}$-Vangl2 localization at the membrane and near the BB. If $mEOS^{red}$-Vangl2 remains polarized at the membrane after nocodazole treatment, it would suggest that maintenance of Vangl2 asymmetry does not require the MT-based trafficking of vesicles during endocytic flux. Alternatively, if $mEOS^{red}$-Vangl2 becomes less enriched at anterior membranes and $mEOS^{green}$-Vangl2 localizes near the BB, it would suggest that MTs are used to traffic newly-synthesized Vangl2 from the BB to cell membranes to maintain Vangl2 asymmetry.

When does the BB stop being the primary MTOC?

The process of MTOC reassignment is poorly understood in any context and it is unclear how the changes in MT organization associated with this reassignment affects ongoing PCP processes (Muroyama and Lechler, 2017). As mentioned above, we detected multiple cell divisions within the floorplate between 30hpf and 48hpf during our experiments. This timing is consistent with how MT organization changes within the floorplate during this developmental window. Specifically, MTs radiate out from the presumptive BB at 30hpf and 48hpf (Supp Fig 2c), which suggests the BB is the primary MTOC during these times, but MTs extend between multiple positions along the apical and basal membranes by 72hpf, which is more typical of differentiated cell types that have at least partially reassigned MTOC function to other cellular

locales (Muroyama and Lechler, 2017; Sanchez and Feldman, 2016). Additionally, the positioning of BBs in the floorplate is actively maintained and requires MTs at 30hpf, as nocodazole treatment rapidly disrupts BB asymmetry (Fig 4a), much like within mouse ependymal cells that rely on posteriorly-localized crescents of tyrosinated tubulin to tether BBs to posterior membranes (Vladar et al., 2012). The removal of nocodazole and reestablishment of MTs is insufficient to repolarize BBs within the floorplate (Fig 5a-b), yet we observed that unpolarized BBs reestablish radial MTs after recovering from MT loss at 48hpf (Fig 5f), which we speculate may anchor the BB in its new position within the cell. Though this could suggest that BBs need to become asymmetrically localized during a specific developmental time window, the radial projection of MT from the BB suggest that it retains at least some MTOC function at 48hpf. In the future, it would be useful to express a BB marker like a fluorescently-labeled centrin in the context of mkate2-EB3 labelled MTs to track how MTs change their association with the BB over time, which may help us identify when the BB ceases to be the primary MTOC. Additionally, as MTOC reassignment is coincident with γ-tubulin delocalization at the centrosome in other contexts (Brodu et al., 2010), we could carry out a γ-tubulin immunostaining time course to better determine the timing of this transition in the floorplate.

Developmental outcomes of PCP maintenance

Most research on PCP signaling has focused on the establishment of polarity, as developmental defects associated with PCP are largely due to a failure in setting up and coordinating cellular asymmetry. Consequently, the requirement for PCP signaling in the

maintenance of cell polarity and the functional consequences of its loss after establishment remain largely unexplored. We believe that examining the ongoing requirements for PCP signaling may elucidate new aspects of how cells use this pathway during development. My work presented in Chapter 2 sought to characterize the dynamic requirement for MTs in the maintenance of planar polarity, whereas my work presented in Chapter 3 illustrates a potential developmental outcome of PCP maintenance in the developing hindbrain. As discussed above, FBMNs migrate through the plane of the neuroepithelium adjacent to the floorplate while maintaining contact with neuroepithelial progenitors as well as with other migrating neurons (Grant and Moens, 2010). Though It is well established that many core PCP and PCP-related signaling components are required for the tangential migration of FBMNs, how PCP signaling is used and whether PCP protein asymmetry needs to be maintained throughout migration remain not well understood. As PCP signaling is known to regulate actin dynamics in many contexts, and filopodia are actin-based structures, ongoing regulation of local PCP protein distribution within FBMNs is likely required to coordinate FBMN filopodial orientation and motility. Indeed, though we were unable to discern a classical polarization pattern of these PCP proteins within migrating FBMNs, FBMNs consistently bias filopodial orientation in the direction of their migration and we discovered that Vangl2 transiently localizes to filopodial tips where it works to destabilize cellular protrusions. We further demonstrated that Fzd3a within FBMNs works to stabilize filopodia, indicating that the cell-autonomous coordination of both these PCP proteins is likely to be necessary for the regulation of these dynamic structures. We also found that Vangl2 and Fzd3a in the FBMN environment have inverse roles on FBMN filopodial

stability, with Fzd3a destabilizing filopodia and Vangl2 stabilizing filopodia. As discussed in Chapter 3, we propose that these reciprocal relationships between PCP proteins within FBMNs and their environment work to precisely control the stability of filopodia, which perform signaling and/or adhesion functions during cellular migration. As FBMNs continue to display oriented filopodial protrusions throughout the course of their migration, active regulation and maintenance of local PCP protein asymmetry within migrating FBMNs and their migratory environment is an inherent requirement for this model of migration. Importantly, FBMNs initiate migration in r4 of the hindbrain at 18hpf, when the floorplate (Fig 1e) and surrounding neuroepithelium (Ciruna et al., 2006) are planar polarized, and move posteriorly into r6 until 48hpf, when planar polarity is stably maintained within the floorplate (Fig 1e). Though we determined that floorplate polarization is not required for FBMN migration, we also demonstrated that a WT floorplate in an PCP mutant background is sufficient to restore migration to WT FBMNs. This suggests that the presence of a limited number of planar polarized cells in the FBMN environment in some cases is sufficient to enable FBMN migration. This would also explain how FBMNs are able to migrate through PCP-disrupted r5 neuroepithelium, as FBMNs remain in contact with normally polarized cells adjacent to r5. These observations together with our model suggest that the PCP-dependent migration of FBMNs requires an active maintenance and regulation of PCP protein asymmetric localization both within FBMNs and their migratory environment. In the future, it would be fascinating to develop tools to temporally control PCP protein polarization within FBMNs and their migratory

environment to further probe how the maintenance of PCP signaling influences cellular motility and migration.

Chapter 5: Bibliography

Adler, P.N., Krasnow, R.E., and Liu, J. (1997). Tissue polarity points from cells that have higher Frizzled levels towards cells that have lower Frizzled levels. Curr. Biol. *7*, 940–949.

Adler, P.N., Zhu, C., and Stone, D. (2004). Inturned Localizes to the Proximal Side of Wing Cells under the Instruction of Upstream Planar Polarity Proteins. Curr. Biol. *14*, 2046–2051.

Aigouy, B., Farhadifar, R., Staple, D.B., Sagner, A., Röper, J.-C., Jülicher, F., and Eaton, S. (2010). Cell Flow Reorients the Axis of Planar Polarity in the Wing Epithelium of Drosophila. Cell *142*, 773–786.

Anastas, J.N., Biechele, T.L., Robitaille, M., Muster, J., Allison, K.H., Angers, S., and Moon, R.T. (2012). A protein complex of SCRIB, NOS1AP and VANGL1 regulates cell polarity and migration, and is associated with breast cancer progression. Oncogene *31*, 3696–3708.

Antic, D., Stubbs, J.L., Suyama, K., Kintner, C., Scott, M.P., and Axelrod, J.D. (2010). Planar Cell Polarity Enables Posterior Localization of Nodal Cilia and Left-Right Axis Determination during Mouse and Xenopus Embryogenesis. PLOS ONE *5*, e8999.

Avasthi, P., and Marshall, W.F. (2012). Stages of Ciliogenesis and Regulation of Ciliary Length. Differ. Res. Biol. Divers. *83*, S30–S42.

Aw, W.Y., Heck, B.W., Joyce, B., and Devenport, D. (2016). Transient Tissue-Scale Deformation Coordinates Alignment of Planar Cell Polarity Junctions in the Mammalian Skin. Curr. Biol. *26*, 2090–2100.

Axelrod, J.D. (2001). Unipolar membrane association of Dishevelled mediates Frizzled planar cell polarity signaling. Genes Dev. *15*, 1182–1187.

Axelrod, J.D., Miller, J.R., Shulman, J.M., Moon, R.T., and Perrimon, N. (1998). Differential recruitment of Dishevelled provides signaling specificity in the planar cell polarity and Wingless signaling pathways. Genes Dev. *12*, 2610–2622.

Azimzadeh, J., and Marshall, W.F. (2010). Building the Centriole. Curr. Biol. CB *20*, R816–R825.

Baas, P.W., Rao, A.N., Matamoros, A.J., and Leo, L. (2016). Stability properties of neuronal microtubules. Cytoskeleton *73*, 442–460.

Babayeva, S., Zilber, Y., and Torban, E. (2011). Planar cell polarity pathway regulates actin rearrangement, cell shape, motility, and nephrin distribution in podocytes. Am. J. Physiol. - Ren. Physiol. *300*, F549–F560.

Bachmann-Gagescu, R., Phelps, I.G., Stearns, G., Link, B.A., Brockerhoff, S.E., Moens, C.B., and Doherty, D. (2011). The ciliopathy gene cc2d2a controls zebrafish photoreceptor outer segment development through a role in Rab8-dependent vesicle trafficking. Hum. Mol. Genet. *20*, 4041–4055.

Badano, J.L., Teslovich, T.M., and Katsanis, N. (2005). The centrosome in human genetic disease. Nat. Rev. Genet. *6*, 194–205.

Baena-López, L.A., Baonza, A., and García-Bellido, A. (2005). The Orientation of Cell Divisions Determines the Shape of Drosophila Organs. Curr. Biol. *15*, 1640–1644.

Basto, R., Lau, J., Vinogradova, T., Gardiol, A., Woods, C.G., Khodjakov, A., and Raff, J.W. (2006). Flies without Centrioles. Cell *125*, 1375–1386.

Bastock, R., Strutt, H., and Strutt, D. (2003). Strabismus is asymmetrically localised and binds to Prickle and Dishevelled during Drosophila planar polarity patterning. Development *130*, 3007–3014.

Beisson, J., and Wright, M. (2003). Basal body/centriole assembly and continuity. Curr. Opin. Cell Biol. *15*, 96–104.

Bettencourt-Dias, M., and Glover, D.M. (2007). Centrosome biogenesis and function: centrosomics brings new understanding. Nat. Rev. Mol. Cell Biol. *8*, 451–463.

Bingham, S., Higashijima, S., Okamoto, H., and Chandrasekhar, A. (2002). The Zebrafish trilobite Gene Is Essential for Tangential Migration of Branchiomotor Neurons. Dev. Biol. *242*, 149–160.

Blacque, O.E., and Leroux, M.R. (2006). Bardet-Biedl syndrome: an emerging pathomechanism of intracellular transport. Cell. Mol. Life Sci. CMLS *63*, 2145–2161.

Blitzer, A.L., Panagis, L., Gusella, G.L., Danias, J., Mlodzik, M., and Iomini, C. (2011). Primary cilia dynamics instruct tissue patterning and repair of corneal endothelium. Proc. Natl. Acad. Sci. U. S. A. *108*, 2819–2824.

Boisvieux-Ulrich, E., Laine, M.C., and Sandoz, D. (1985). The orientation of ciliary basal bodies in quail oviduct is related to the ciliary beating cycle commencement. Biol. Cell *55*, 147–150.

Boisvieux-Ulrich, E., Lainé, M.-C., and Sandoz, D. (1990). Cytochalasin D inhibits basal body migration and ciliary elongation in quail oviduct epithelium. Cell Tissue Res. *259*, 443–454.

Bokoch, G.M. (2003). Biology of the p21-activated kinases. Annu. Rev. Biochem. *72*, 743–781.

Bornens, M. (2012). The Centrosome in Cells and Organisms. Science *335*, 422–426.

Borovina, A., Superina, S., Voskas, D., and Ciruna, B. (2010). Vangl2 directs the posterior tilting and asymmetric localization of motile primary cilia. Nat. Cell Biol. *12*, 407–412.

Boutin, C., Labedan, P., Dimidschstein, J., Richard, F., Cremer, H., André, P., Yang, Y., Montcouquiol, M., Goffinet, A.M., and Tissir, F. (2014). A dual role for planar cell polarity genes in ciliated cells. Proc. Natl. Acad. Sci. *111*, E3129–E3138.

Brodu, V., Baffet, A.D., Le Droguen, P.-M., Casanova, J., and Guichet, A. (2010). A Developmentally Regulated Two-Step Process Generates a Noncentrosomal Microtubule Network in Drosophila Tracheal Cells. Dev. Cell *18*, 790–801.

Brooks, E.R., and Wallingford, J.B. (2014). Multiciliated cells: a review. Curr. Biol. CB *24*, R973–R982.

Brzoska, H.L., d'Esposito, A.M., Kolatsi-Joannou, M., Patel, V., Igarashi, P., Lei, Y., Finnell, R.H., Lythgoe, M.F., Woolf, A.S., Papakrivopoulou, E., et al. (2016). Planar cell polarity genes Celsr1 and Vangl2 are necessary for kidney growth, differentiation and rostrocaudal patterning. Kidney Int. *90*, 1274–1284.

Buendia (1990). Cytoskeletal control of centrioles movement during the establishment of polarity in Madin-Darby canine kidney cells. J. Cell Biol. *110*, 1123–1135.

Bulinski, J.C., and Gundersen, G.G. (1991). Stabilization and post-translational modification of microtubules during cellular morphogenesis. BioEssays *13*, 285–293.

Burkhardt, J.K., Echeverri, C.J., Nilsson, T., and Vallee, R.B. (1997). Overexpression of the Dynamitin (p50) Subunit of the Dynactin Complex Disrupts Dynein-dependent Maintenance of Membrane Organelle Distribution. J. Cell Biol. *139*, 469–484.

Butler, M.T., and Wallingford, J.B. (2015). Control of vertebrate core planar cell polarity protein localization and dynamics by Prickle 2. Development *142*, 3429–3439.

Butler, M.T., and Wallingford, J.B. (2017). Planar cell polarity in development and disease. Nat. Rev. Mol. Cell Biol. *18*, 375–388.

Calisto, J.D., Araya, C., Marchant, L., Riaz, C.F., and Mayor, R. (2005). Essential role of non-canonical Wnt signalling in neural crest migration. Development *132*, 2587–2597.

Carmona-Fontaine, C., Matthews, H.K., Kuriyama, S., Moreno, M., Dunn, G.A., Parsons, M., Stern, C.D., and Mayor, R. (2008). Contact inhibition of locomotion in vivo controls neural crest directional migration. Nature *456*, 957–961.

Carreira-Barbosa, F., Concha, M.L., Takeuchi, M., Ueno, N., Wilson, S.W., and Tada, M. (2003). Prickle 1 regulates cell movements during gastrulation and neuronal migration in zebrafish. Development *130*, 4037–4046.

Carvajal-Gonzalez, J.M., Balmer, S., Mendoza, M., Dussert, A., Collu, G., Roman, A.-C., Weber, U., Ciruna, B., and Mlodzik, M. (2015). The clathrin adaptor AP-1 complex and Arf1 regulate planar cell polarity *in vivo*. Nat. Commun. *6*, ncomms7751.

Carvajal-Gonzalez, J.M., Roman, A.-C., and Mlodzik, M. (2016a). Positioning of centrioles is a conserved readout of Frizzled planar cell polarity signalling. Nat. Commun. *7*, 11135.

Carvajal-Gonzalez, J.M., Mulero-Navarro, S., and Mlodzik, M. (2016b). Centriole positioning in epithelial cells and its intimate relationship with planar cell polarity. BioEssays *38*, 1234–1245.

Carvalho-Santos, Z., Azimzadeh, J., Pereira-Leal, J.B., and Bettencourt-Dias, M. (2011). Tracing the origins of centrioles, cilia, and flagella. J Cell Biol *194*, 165–175.

Chandrasekhar, A. (2004). Turning Heads: Development of Vertebrate Branchiomotor Neurons. Dev. Dyn. Off. Publ. Am. Assoc. Anat. *229*, 143–161.

Charron, F., Stein, E., Jeong, J., McMahon, A.P., and Tessier-Lavigne, M. (2003). The Morphogen Sonic Hedgehog Is an Axonal Chemoattractant that Collaborates with Netrin-1 in Midline Axon Guidance. Cell *113*, 11–23.

Chen, W.-S., Antic, D., Matis, M., Logan, C.Y., Povelones, M., Anderson, G.A., Nusse, R., and Axelrod, J.D. (2008). Asymmetric Homotypic Interactions of the Atypical Cadherin Flamingo Mediate Intercellular Polarity Signaling. Cell *133*, 1093–1105.

Chien, Y.-H., Keller, R., Kintner, C., and Shook, D.R. (2015). Mechanical Strain Determines the Axis of Planar Polarity in Ciliated Epithelia. Curr. Biol. *25*, 2774–2784.

Cho, B., Pierre-Louis, G., Sagner, A., Eaton, S., and Axelrod, J.D. (2015). Clustering and Negative Feedback by Endocytosis in Planar Cell Polarity Signaling Is Modulated by Ubiquitinylation of Prickle. PLOS Genet. *11*, e1005259.

Chu, C.-W., and Sokol, S.Y. (2016). Wnt proteins can direct planar cell polarity in vertebrate ectoderm. eLife *5*, e16463.

Ciruna, B., Jenny, A., Lee, D., Mlodzik, M., and Schier, A.F. (2006). Planar cell polarity signalling couples cell division and morphogenesis during neurulation. Nature *439*, 220–224.

Classen, A.-K., Anderson, K.I., Marois, E., and Eaton, S. (2005). Hexagonal Packing of Drosophila Wing Epithelial Cells by the Planar Cell Polarity Pathway. Dev. Cell *9*, 805–817.

Clevers, H., and Nusse, R. (2012). Wnt/β-Catenin Signaling and Disease. Cell *149*, 1192–1205.

Collier, S., and Gubb, D. (1997). Drosophila tissue polarity requires the cell-autonomous activity of the fuzzy gene, which encodes a novel transmembrane protein. Development *124*, 4029–4037.

Collier, S., Lee, H., Burgess, R., and Adler, P. (2005). The WD40 Repeat Protein Fritz Links Cytoskeletal Planar Polarity to Frizzled Subcellular Localization in the Drosophila Epidermis. Genetics *169*, 2035–2045.

Courbard, J.-R., Djiane, A., Wu, J., and Mlodzik, M. (2009). The apical/basal-polarity determinant Scribble cooperates with the PCP core factor Stbm/Vang and functions as one of its effectors. Dev. Biol. *333*, 67–77.

Curtin, J.A., Quint, E., Tsipouri, V., Arkell, R.M., Cattanach, B., Copp, A.J., Henderson, D.J., Spurr, N., Stanier, P., Fisher, E.M., et al. (2003). Mutation of Celsr1 Disrupts Planar Polarity of Inner Ear Hair Cells and Causes Severe Neural Tube Defects in the Mouse. Curr. Biol. *13*, 1129–1133.

Das, G., Jenny, A., Klein, T.J., Eaton, S., and Mlodzik, M. (2004). Diego interacts with Prickle and Strabismus/Van Gogh to localize planar cell polarity complexes. Development *131*, 4467–4476.

Davey, C.F., and Moens, C.B. (2017). Planar cell polarity in moving cells: think globally, act locally. Development *144*, 187–200.

Davey, C.F., Mathewson, A.W., and Moens, C.B. (2016). PCP Signaling between Migrating Neurons and their Planar-Polarized Neuroepithelial Environment Controls Filopodial Dynamics and Directional Migration. PLOS Genet. *12*, e1005934.

Dawe, H.R., Farr, H., and Gull, K. (2007). Centriole/basal body morphogenesis and migration during ciliogenesis in animal cells. J. Cell Sci. *120*, 7–15.

Devenport, D., and Fuchs, E. (2008). Planar polarization in embryonic epidermis orchestrates global asymmetric morphogenesis of hair follicles. Nat. Cell Biol. *10*, 1257–1268.

Devenport, D., Oristian, D., Heller, E., and Fuchs, E. (2011). Mitotic Internalization of Planar Cell Polarity Proteins Preserves Tissue Polarity. Nat. Cell Biol. *13*, 893–902.

Eaton, S., Auvinen, P., Luo, L., Jan, Y.N., and Simons, K. (1995). CDC42 and Rac1 control different actin-dependent processes in the Drosophila wing disc epithelium. J. Cell Biol. *131*, 151–164.

Eaton, S., Wepf, R., and Simons, K. (1996). Roles for Rac1 and Cdc42 in planar polarization and hair outgrowth in the wing of Drosophila. J. Cell Biol. *135*, 1277–1289.

Ertzer, R., Müller, F., Hadzhiev, Y., Rathnam, S., Fischer, N., Rastegar, S., and Strähle, U. (2007). Cooperation of sonic hedgehog enhancers in midline expression. Dev. Biol. *301*, 578–589.

Essner, J.J., Vogan, K.J., Wagner, M.K., Tabin, C.J., Yost, H.J., and Brueckner, M. (2002). Left–right development: Conserved function for embryonic nodal cilia. Nature *418*, 37–38.

Etheridge, S.L., Ray, S., Li, S., Hamblet, N.S., Lijam, N., Tsang, M., Greer, J., Kardos, N., Wang, J., Sussman, D.J., et al. (2008). Murine Dishevelled 3 Functions in Redundant Pathways with Dishevelled 1 and 2 in Normal Cardiac Outflow Tract, Cochlea, and Neural Tube Development. PLOS Genet. *4*, e1000259.

Euteneur, U., and Schliwa, M. (1992). Mechanism of centrosome positioning during the wound response in BSC-1 cells. J. Cell Biol. *116*, 1157–1166.

Ezan, J., Lasvaux, L., Gezer, A., Novakovic, A., May-Simera, H., Belotti, E., Lhoumeau, A.-C., Birnbaumer, L., Beer-Hammer, S., Borg, J.-P., et al. (2013). Primary cilium migration depends on G-protein signalling control of subapical cytoskeleton. Nat. Cell Biol. *15*, 1107–1115.

Feng, Y., and Irvine, K.D. (2009). Processing and phosphorylation of the Fat receptor. Proc. Natl. Acad. Sci. *106*, 11989–11994.

Gao, B., Song, H., Bishop, K., Elliot, G., Garrett, L., English, M.A., Andre, P., Robinson, J., Sood, R., Minami, Y., et al. (2011). Wnt Signaling Gradients Establish Planar Cell Polarity by Inducing Vangl2 Phosphorylation through Ror2. Dev. Cell *20*, 163–176.

Gerdes, J.M., Liu, Y., Zaghloul, N.A., Leitch, C.C., Lawson, S.S., Kato, M., Beachy, P.A., Beales, P.L., DeMartino, G.N., Fisher, S., et al. (2007). Disruption of the basal body compromises proteasomal function and perturbs intracellular Wnt response. Nat. Genet. *39*, 1350–1360.

Gogendeau, D., and Basto, R. (2010). Centrioles in flies: The exception to the rule? Semin. Cell Dev. Biol. *21*, 163–173.

Goll, M.G., Anderson, R., Stainier, D.Y.R., Spradling, A.C., and Halpern, M.E. (2009). Transcriptional Silencing and Reactivation in Transgenic Zebrafish. Genetics *182*, 747–755.

Goodrich, L.V., and Strutt, D. (2011). Principles of planar polarity in animal development. Development *138*, 1877–1892.

Grant, P.K., and Moens, C.B. (2010). The neuroepithelial basement membrane serves as a boundary and a substrate for neuron migration in the zebrafish hindbrain. Neural Develop. *5*, 9.

Gray, R.S., Abitua, P.B., Wlodarczyk, B.J., Szabo-Rogers, H.L., Blanchard, O., Lee, I., Weiss, G.S., Liu, K.J., Marcotte, E.M., Wallingford, J.B., et al. (2009). The planar cell polarity effector Fuz is essential for targeted membrane trafficking, ciliogenesis and mouse embryonic development. Nat. Cell Biol. *11*, 1225–1232.

Gubb, D., and García-Bellido, A. (1982). A genetic analysis of the determination of cuticular polarity during development in *Drosophila melanogaster*. Development *68*, 37–57.

Gubb, D., Green, C., Huen, D., Coulson, D., Johnson, G., Tree, D., Collier, S., and Roote, J. (1999). The balance between isoforms of the Prickle LIM domain protein is critical for planar polarity in Drosophila imaginal discs. Genes Dev. *13*, 2315–2327.

Guirao, B., Meunier, A., Mortaud, S., Aguilar, A., Corsi, J.-M., Strehl, L., Hirota, Y., Desoeuvre, A., Boutin, C., Han, Y.-G., et al. (2010). Coupling between hydrodynamic forces and planar cell polarity orients mammalian motile cilia. Nat. Cell Biol. *12*, 341–350.

Hale, R., and Strutt, D. (2015). Conservation of Planar Polarity Pathway Function Across the Animal Kingdom. Annu. Rev. Genet. *49*, 529–551.

Hannus, M., Feiguin, F., Heisenberg, C.-P., and Eaton, S. (2002). Planar cell polarization requires Widerborst, a B′ regulatory subunit of protein phosphatase 2A. Development *129*, 3493–3503.

Harumoto, T., Ito, M., Shimada, Y., Kobayashi, T.J., Ueda, H.R., Lu, B., and Uemura, T. (2010). Atypical Cadherins Dachsous and Fat Control Dynamics of Noncentrosomal Microtubules in Planar Cell Polarity. Dev. Cell *19*, 389–401.

Hashimoto, M., Shinohara, K., Wang, J., Ikeuchi, S., Yoshiba, S., Meno, C., Nonaka, S., Takada, S., Hatta, K., Wynshaw-Boris, A., et al. (2010). Planar polarization of node cells determines the rotational axis of node cilia. Nat. Cell Biol. *12*, 170–176.

Heisenberg, C.-P., Tada, M., Rauch, G.-J., Saúde, L., Concha, M.L., Geisler, R., Stemple, D.L., Smith, J.C., and Wilson, S.W. (2000). Silberblick/Wnt11 mediates convergent extension movements during zebrafish gastrulation. Nature *405*, 76–81.

Jenny, A., Darken, R.S., Wilson, P.A., and Mlodzik, M. (2003). Prickle and Strabismus form a functional complex to generate a correct axis during planar cell polarity signaling. EMBO J. *22*, 4409–4420.

Jenny, A., Reynolds-Kenneally, J., Das, G., Burnett, M., and Mlodzik, M. (2005). Diego and Prickle regulate Frizzled planar cell polarity signalling by competing for Dishevelled binding. Nat. Cell Biol. *7*, 691–697.

Jessen, J.R., Topczewski, J., Bingham, S., Sepich, D.S., Marlow, F., Chandrasekhar, A., and Solnica-Krezel, L. (2002). Zebrafish trilobite identifies new roles for Strabismus in gastrulation and neuronal movements. Nat. Cell Biol. *4*, 610–615.

Jones, C., Roper, V.C., Foucher, I., Qian, D., Banizs, B., Petit, C., Yoder, B.K., and Chen, P. (2008). Ciliary proteins link basal body polarization to planar cell polarity regulation. Nat. Genet. *40*, 69–77.

Kawakami, K., Shima, A., and Kawakami, N. (2000). Identification of a functional transposase of the Tol2 element, an Ac-like element from the Japanese medaka fish, and its transposition in the zebrafish germ lineage. Proc. Natl. Acad. Sci. *97*, 11403–11408.

Kibar, Z., Torban, E., McDearmid, J.R., Reynolds, A., Berghout, J., Mathieu, M., Kirillova, I., De Marco, P., Merello, E., Hayes, J.M., et al. (2007). Mutations in VANGL1 Associated with Neural-Tube Defects. N. Engl. J. Med. *356*, 1432–1437.

Kim, J.H., Lee, S.-R., Li, L.-H., Park, H.-J., Park, J.-H., Lee, K.Y., Kim, M.-K., Shin, B.A., and Choi, S.-Y. (2011). High Cleavage Efficiency of a 2A Peptide Derived from Porcine Teschovirus-1 in Human Cell Lines, Zebrafish and Mice. PLOS ONE *6*, e18556.

Kim, S.K., Shindo, A., Park, T.J., Oh, E.C., Ghosh, S., Gray, R.S., Lewis, R.A., Johnson, C.A., Attie-Bittach, T., Katsanis, N., et al. (2010). Planar Cell Polarity Acts Through Septins to Control Collective Cell Movement and Ciliogenesis. Science *329*, 1337–1340.

Kimmel, C.B., Ballard, W.W., Kimmel, S.R., Ullmann, B., and Schilling, T.F. (1995). Stages of embryonic development of the zebrafish. Dev. Dyn. *203*, 253–310.

Kimura, Y., Hisano, Y., Kawahara, A., and Higashijima, S. (2014). Efficient generation of knock-in transgenic zebrafish carrying reporter/driver genes by CRISPR/Cas9-mediated genome engineering. Sci. Rep. *4*.

Kourakis, M.J., Reeves, W., Newman-Smith, E., Maury, B., Abdul-Wajid, S., and Smith, W.C. (2014). A one-dimensional model of PCP signaling: Polarized cell behavior in the notochord of the ascidian Ciona. Dev. Biol. *395*, 120–130.

Lawrence, P.A., Casal, J., and Struhl, G. (2002). Towards a model of the organisation of planar polarity and pattern in the Drosophila abdomen. Development *129*, 2749–2760.

Lawrence, P.A., Casal, J., and Struhl, G. (2004). Cell interactions and planar polarity in the abdominal epidermis of *Drosophila*. Development *131*, 4651–4664.

Lechler, T., and Fuchs, E. (2007). Desmoplakin: an unexpected regulator of microtubule organization in the epidermis. J. Cell Biol. *176*, 147–154.

Lee, H., and Adler, P.N. (2002). The function of the frizzled pathway in the Drosophila wing is dependent on inturned and fuzzy. Genetics *160*, 1535–1547.

Lu, Q., Yan, J., and Adler, P.N. (2010). The Drosophila Planar Polarity Proteins Inturned and Multiple Wing Hairs Interact Physically and Function Together. Genetics *185*, 549–558.

Lu, Q., Schafer, D.A., and Adler, P.N. (2015). The Drosophila planar polarity gene multiple wing hairs directly regulates the actin cytoskeleton. Dev. Camb. Engl. *142*, 2478–2486.

Luga, V., Zhang, L., Viloria-Petit, A.M., Ogunjimi, A.A., Inanlou, M.R., Chiu, E., Buchanan, M., Hosein, A.N., Basik, M., and Wrana, J.L. (2012). Exosomes Mediate Stromal Mobilization of Autocrine Wnt-PCP Signaling in Breast Cancer Cell Migration. Cell *151*, 1542–1556.

Ma, D., Yang, C., McNeill, H., Simon, M.A., and Axelrod, J.D. (2003). Fidelity in planar cell polarity signalling. Nature *421*, 543–547.

MacMillan, C.D., Leong, H.S., Dales, D.W., Robertson, A.E., Lewis, J.D., Chambers, A.F., and Tuck, A.B. (2014). Stage of Breast Cancer Progression Influences Cellular Response to Activation of the WNT/Planar Cell Polarity Pathway. Sci. Rep. *4*, 6315.

Mahaffey, J.P., Grego-Bessa, J., Liem, K.F., and Anderson, K.V. (2013). Cofilin and Vangl2 cooperate in the initiation of planar cell polarity in the mouse embryo. Development *140*, 1262–1271.

Mao, Y., Tournier, A.L., Bates, P.A., Gale, J.E., Tapon, N., and Thompson, B.J. (2011). Planar polarization of the atypical myosin Dachs orients cell divisions in Drosophila. Genes Dev. *25*, 131–136.

Mapp, O.M., Wanner, S.J., Rohrschneider, M.R., and Prince, V.E. (2010). Prickle1b mediates interpretation of migratory cues during zebrafish facial branchiomotor neuron migration. Dev. Dyn. *239*, 1596–1608.

Mapp, O.M., Walsh, G.S., Moens, C.B., Tada, M., and Prince, V.E. (2011). Zebrafish Prickle1b mediates facial branchiomotor neuron migration via a farnesylation-dependent nuclear activity. Development *138*, 2121–2132.

Matakatsu, H., and Blair, S.S. (2004). Interactions between Fat and Dachsous and the regulation of planar cell polarity in the *Drosophila wing*. Development *131*, 3785–3794.

Matis, M., Russler-Germain, D.A., Hu, Q., Tomlin, C.J., and Axelrod, J.D. (2014). Microtubules provide directional information for core PCP function. eLife *3*, e02893.

May-Simera, H.L., Kai, M., Hernandez, V., Osborn, D.P.S., Tada, M., and Beales, P.L. (2010). Bbs8, together with the planar cell polarity protein Vangl2, is required to establish left–right asymmetry in zebrafish. Dev. Biol. *345*, 215–225.

May-Simera, H.L., Petralia, R.S., Montcouquiol, M., Wang, Y.-X., Szarama, K.B., Liu, Y., Lin, W., Deans, M.R., Pazour, G.J., and Kelley, M.W. (2015). Ciliary proteins Bbs8 and Ift20 promote planar cell polarity in the cochlea. Development *142*, 555–566.

McFarland, R.J., Brown, S.P., Vital, E., Werner, J.M., and Brewster, R.M. (2017). Use of Immunolabeling to Analyze Stable, Dynamic, and Nascent Microtubules in the Zebrafish Embryo. JoVE J. Vis. Exp. e55792–e55792.

Meijering, E., Dzyubachyk, O., and Smal, I. (2012). Methods for Cell and Particle Tracking (Elsevier).

Mirzadeh, Z., Han, Y.-G., Soriano-Navarro, M., García-Verdugo, J.M., and Alvarez-Buylla, A. (2010). Cilia Organize Ependymal Planar Polarity. J. Neurosci. *30*, 2600–2610.

Mitchell, B., Jacobs, R., Li, J., Chien, S., and Kintner, C. (2007). A positive feedback mechanism governs the polarity and motion of motile cilia. Nature *447*, 97–101.

Mitchell, B., Stubbs, J.L., Huisman, F., Taborek, P., Yu, C., and Kintner, C. (2009). The PCP Pathway Instructs the Planar Orientation of Ciliated Cells in the Xenopus Larval Skin. Curr. Biol. *19*, 924–929.

Montcouquiol, M., Rachel, R.A., Lanford, P.J., Copeland, N.G., Jenkins, N.A., and Kelley, M.W. (2003). Identification of Vangl2 and Scrb1 as planar polarity genes in mammals. Nature *423*, 173–177.

Montcouquiol, M., Sans, N., Huss, D., Kach, J., Dickman, J.D., Forge, A., Rachel, R.A., Copeland, N.G., Jenkins, N.A., Bogani, D., et al. (2006). Asymmetric Localization of Vangl2 and Fz3 Indicate Novel Mechanisms for Planar Cell Polarity in Mammals. J. Neurosci. *26*, 5265–5275.

Moritz, M., and Agard, D.A. (2001). γ-Tubulin complexes and microtubule nucleation. Curr. Opin. Struct. Biol. *11*, 174–181.

Mottola, G., Classen, A.-K., González-Gaitán, M., Eaton, S., and Zerial, M. (2010). A novel function for the Rab5 effector Rabenosyn-5 in planar cell polarity. Development *137*, 2353–2364.

Murdoch, J.N., Henderson, D.J., Doudney, K., Gaston-Massuet, C., Phillips, H.M., Paternotte, C., Arkell, R., Stanier, P., and Copp, A.J. (2003). Disruption of scribble (Scrb1) causes severe neural tube defects in the circletail mouse. Hum. Mol. Genet. *12*, 87–98.

Muroyama, A., and Lechler, T. (2017). Microtubule organization, dynamics and functions in differentiated cells. Development *144*, 3012–3021.

Narimatsu, M., Bose, R., Pye, M., Zhang, L., Miller, B., Ching, P., Sakuma, R., Luga, V., Roncari, L., Attisano, L., et al. (2009). Regulation of Planar Cell Polarity by Smurf Ubiquitin Ligases. Cell *137*, 295–307.

Newman-Smith, E., Kourakis, M.J., Reeves, W., Veeman, M., and Smith, W.C. (2015). Reciprocal and dynamic polarization of planar cell polarity core components and myosin. eLife *4*, e05361.

Nigg, E.A., and Raff, J.W. (2009). Centrioles, Centrosomes, and Cilia in Health and Disease. Cell *139*, 663–678.

Nonaka, S., Yoshiba, S., Watanabe, D., Ikeuchi, S., Goto, T., Marshall, W.F., and Hamada, H. (2005). De Novo Formation of Left–Right Asymmetry by Posterior Tilt of Nodal Cilia. PLoS Biol. *3*.

Ohata, S., and Álvarez-Buylla, A. (2016). Planar organization of multiciliated ependymal (E1) cells in the brain ventricular epithelium. Trends Neurosci. *39*, 543–551.

Ohata, S., Nakatani, J., Herranz-Pérez, V., Cheng, J., Belinson, H., Inubushi, T., Snider, W.D., García-Verdugo, J.M., Wynshaw-Boris, A., and Álvarez-Buylla, A. (2014). Loss of Dishevelleds disrupts planar polarity in ependymal motile cilia and results in hydrocephalus. Neuron *83*, 558–571.

Okada, Y., Takeda, S., Tanaka, Y., Belmonte, J.-C.I., and Hirokawa, N. (2005). Mechanism of Nodal Flow: A Conserved Symmetry Breaking Event in Left-Right Axis Determination. Cell *121*, 633–644.

Olofsson, J., Sharp, K.A., Matis, M., Cho, B., and Axelrod, J.D. (2014). Prickle/spiny-legs isoforms control the polarity of the apical microtubule network in planar cell polarity. Development *141*, 2866–2874.

Ossipova, O., Kim, K., Lake, B.B., Itoh, K., Ioannou, A., and Sokol, S.Y. (2014). Role of Rab11 in planar cell polarity and apical constriction during vertebrate neural tube closure. Nat. Commun. *5*, 3734.

Ossipova, O., Kim, K., and Sokol, S.Y. (2015). Planar polarization of Vangl2 in the vertebrate neural plate is controlled by Wnt and Myosin II signaling. Biol. Open *4*, 722–730.

Park, T.J., Haigo, S.L., and Wallingford, J.B. (2006). Ciliogenesis defects in embryos lacking inturned or fuzzy function are associated with failure of planar cell polarity and Hedgehog signaling. Nat. Genet. *38*, 303–311.

Park, T.J., Mitchell, B.J., Abitua, P.B., Kintner, C., and Wallingford, J.B. (2008). Dishevelled controls apical docking and planar polarization of basal bodies in ciliated epithelial cells. Nat. Genet. *40*, 871–879.

Park, W.J., Liu, J., Sharp, E.J., and Adler, P.N. (1996). The Drosophila tissue polarity gene inturned acts cell autonomously and encodes a novel protein. Development *122*, 961–969.

Patten, I., and Placzek*, M. (2000). The role of Sonic hedgehog in neural tube patterning. Cell. Mol. Life Sci. CMLS *57*, 1695–1708.

Placzek, M., and Briscoe, J. (2005). The floor plate: multiple cells, multiple signals. Nat. Rev. Neurosci. *6*, 230–240.

Qian, D., Jones, C., Rzadzinska, A., Mark, S., Zhang, X., Steel, K.P., Dai, X., and Chen, P. (2007). Wnt5a functions in planar cell polarity regulation in mice. Dev. Biol. *306*, 121–133.

Qu, Y., Glasco, D.M., Zhou, L., Sawant, A., Ravni, A., Fritzsch, B., Damrau, C., Murdoch, J.N., Evans, S., Pfaff, S.L., et al. (2010). Atypical Cadherins Celsr1-3 Differentially Regulate Migration of Facial Branchiomotor Neurons in Mice. J. Neurosci. *30*, 9392–9401.

Reiter, J.F., Blacque, O.E., and Leroux, M.R. (2012). The base of the cilium: roles for transition fibres and the transition zone in ciliary formation, maintenance and compartmentalization. EMBO Rep. *13*, 608–618.

Rodriguez-Boulan, E., and Macara, I.G. (2014). Organization and execution of the epithelial polarity programme. Nat. Rev. Mol. Cell Biol. *15*, 225–242.

Rodríguez-Fraticelli, A.E., Auzan, M., Alonso, M.A., Bornens, M., and Martín-Belmonte, F. (2012). Cell confinement controls centrosome positioning and lumen initiation during epithelial morphogenesis. J. Cell Biol. *198*, 1011–1023.

Rogers, G.C., Rusan, N.M., Peifer, M., and Rogers, S.L. (2008). A Multicomponent Assembly Pathway Contributes to the Formation of Acentrosomal Microtubule Arrays in Interphase Drosophila Cells. Mol. Biol. Cell *19*, 3163–3178.

Rohrschneider, M.R., Elsen, G.E., and Prince, V.E. (2007). Zebrafish Hoxb1a regulates multiple downstream genes including prickle1b. Dev. Biol. *309*, 358–372.

Ross, A.J., May-Simera, H., Eichers, E.R., Kai, M., Hill, J., Jagger, D.J., Leitch, C.C., Chapple, J.P., Munro, P.M., Fisher, S., et al. (2005). Disruption of Bardet-Biedl syndrome ciliary proteins perturbs planar cell polarity in vertebrates. Nat. Genet. *37*, 1135–1140.

Roszko, I., Sawada, A., and Solnica-Krezel, L. (2009). Regulation of convergence and extension movements during vertebrate gastrulation by the Wnt/PCP pathway. Semin. Cell Dev. Biol. *20*, 986–997.

Sanchez, A.D., and Feldman, J.L. (2016). Microtubule-organizing centers: from the centrosome to non-centrosomal sites. Curr. Opin. Cell Biol.

Sawyer, J.M., Harrell, J.R., Shemer, G., Sullivan-Brown, J., Roh-Johnson, M., and Goldstein, B. (2010). Apical Constriction: A Cell Shape Change that Can Drive Morphogenesis. Dev. Biol. *341*, 5–19.

Schneider, C.A., Rasband, W.S., and Eliceiri, K.W. (2012). NIH Image to ImageJ: 25 years of image analysis. Nat. Methods *9*, 671–675.

Sepich, D.S., and Solnica-Krezel, L. (2016). Intracellular Golgi Complex organization reveals tissue specific polarity during zebrafish embryogenesis. Dev. Dyn. *245*, 678–691.

Sepich, D.S., Usmani, M., Pawlicki, S., and Solnica-Krezel, L. (2011). Wnt/PCP signaling controls intracellular position of MTOCs during gastrulation convergence and extension movements. Development *138*, 543–552.

Shafer, B., Onishi, K., Lo, C., Colakoglu, G., and Zou, Y. (2011). Vangl2 Promotes Wnt/Planar Cell Polarity-like Signaling by Antagonizing Dvl1-Mediated Feedback Inhibition in Growth Cone Guidance. Dev. Cell *20*, 177–191.

Shi, D., Komatsu, K., Hirao, M., Toyooka, Y., Koyama, H., Tissir, F., Goffinet, A.M., Uemura, T., and Fujimori, T. (2014). Celsr1 is required for the generation of polarity at multiple levels of the mouse oviduct. Development *141*, 4558–4568.

Shi, D., Usami, F., Komatsu, K., Oka, S., Abe, T., Uemura, T., and Fujimori, T. (2016). Dynamics of planar cell polarity protein Vangl2 in the mouse oviduct epithelium. Mech. Dev. *141*, 78–89.

Shimada, Y., Yonemura, S., Ohkura, H., Strutt, D., and Uemura, T. (2006). Polarized Transport of Frizzled along the Planar Microtubule Arrays in Drosophila Wing Epithelium. Dev. Cell *10*, 209–222.

Shrestha, R., Little, K.A., Tamayo, J.V., Li, W., Perlman, D.H., and Devenport, D. (2015). Mitotic Control of Planar Cell Polarity by Polo-like Kinase 1. Dev. Cell *33*, 522–534.

Simon, M.A. (2004). Planar cell polarity in the *Drosophila* eye is directed by graded Four-jointed and Dachsous expression. Development *131*, 6175–6184.

Simons, M., Gault, W.J., Gotthardt, D., Rohatgi, R., Klein, T.J., Shao, Y., Lee, H.-J., Wu, A.-L., Fang, Y., Satlin, L.M., et al. (2009). Electrochemical cues regulate assembly of the Frizzled/Dishevelled complex at the plasma membrane during planar epithelial polarization. Nat. Cell Biol. *11*, 286–294.

Sipe, C.W., and Lu, X. (2011). Kif3a regulates planar polarization of auditory hair cells through both ciliary and non-ciliary mechanisms. Development *138*, 3441–3449.

Sokol, S.Y. (2015). Spatial and temporal aspects of Wnt signaling and planar cell polarity during vertebrate embryonic development. Semin. Cell Dev. Biol. *42*, 78–85.

Song, H., Hu, J., Chen, W., Elliott, G., Andre, P., Gao, B., and Yang, Y. (2010). Planar cell polarity breaks bilateral symmetry by controlling ciliary positioning. Nature *466*, 378–382.

Sopko, R., Silva, E., Clayton, L., Gardano, L., Barrios-Rodiles, M., Wrana, J., Varelas, X., Arbouzova, N.I., Shaw, S., Saburi, S., et al. (2009). Phosphorylation of the tumour suppressor Fat is regulated via interaction with its ligand Dachsous, and the kinase, Discs Overgrown. Curr. Biol. CB *19*, 1112–1117.

Stepanova, T., Slemmer, J., Hoogenraad, C.C., Lansbergen, G., Dortland, B., Zeeuw, C.I.D., Grosveld, F., Cappellen, G. van, Akhmanova, A., and Galjart, N. (2003). Visualization of Microtubule Growth in Cultured Neurons via the Use of EB3-GFP (End-Binding Protein 3-Green Fluorescent Protein). J. Neurosci. *23*, 2655–2664.

Struhl, G., Casal, J., and Lawrence, P.A. (2012). Dissecting the molecular bridges that mediate the function of Frizzled in planar cell polarity. Development *139*, 3665–3674.

Strutt, D.I. (2001). Asymmetric Localization of Frizzled and the Establishment of Cell Polarity in the Drosophila Wing. Mol. Cell *7*, 367–375.

Strutt, D., and Strutt, H. (2007). Differential activities of the core planar polarity proteins during Drosophila wing patterning. Dev. Biol. *302*, 181–194.

Strutt, D., and Warrington, S.J. (2008). Planar polarity genes in the Drosophila wing regulate the localisation of the FH3-domain protein Multiple Wing Hairs to control the site of hair production. Development *135*, 3103–3111.

Strutt, H., and Strutt, D. (2002). Nonautonomous Planar Polarity Patterning in Drosophila. Dev. Cell *3*, 851–863.

Strutt, H., and Strutt, D. (2008). Differential Stability of Flamingo Protein Complexes Underlies the Establishment of Planar Polarity. Curr. Biol. *18*, 1555–1564.

Strutt, D., Johnson, R., Cooper, K., and Bray, S. (2002). Asymmetric Localization of Frizzled and the Determination of Notch-Dependent Cell Fate in the Drosophila Eye. Curr. Biol. *12*, 813–824.

Strutt, D.I., Weber, U., and Mlodzik, M. (1997). The role of RhoA in tissue polarity and Frizzled signalling. Nature *387*, 292–295.

Strutt, H., Mundy, J., Hofstra, K., and Strutt, D. (2004). Cleavage and secretion is not required for Four-jointed function in *Drosophila* patterning. Development *131*, 881–890.

Strutt, H., Warrington, S.J., and Strutt, D. (2011). Dynamics of Core Planar Polarity Protein Turnover and Stable Assembly into Discrete Membrane Subdomains. Dev. Cell *20*, 511–525.

Strutt, H., Searle, E., Thomas-MacArthur, V., Brookfield, R., and Strutt, D. (2013). A Cul-3-BTB ubiquitylation pathway regulates junctional levels and asymmetry of core planar polarity proteins. Development *140*, 1693–1702.

Sugiyama, Y., Stump, R.J.W., Nguyen, A., Wen, L., Chen, Y., Wang, Y., Murdoch, J.N., Lovicu, F.J., and McAvoy, J.W. (2010). Secreted frizzled-related protein disrupts PCP in eye lens fiber cells that have polarised primary cilia. Dev. Biol. *338*, 193.

Tada, M., and Smith, J.C. (2000). Xwnt11 is a target of Xenopus Brachyury: regulation of gastrulation movements via Dishevelled, but not through the canonical Wnt pathway. Development *127*, 2227–2238.

Tanaka, N., Meng, W., Nagae, S., and Takeichi, M. (2012). Nezha/CAMSAP3 and CAMSAP2 cooperate in epithelial-specific organization of noncentrosomal microtubules. Proc. Natl. Acad. Sci. U. S. A. *109*, 20029–20034.

Taylor, J., Abramova, N., Charlton, J., and Adler, P.N. (1998). Van Gogh: A New Drosophila Tissue Polarity Gene. Genetics *150*, 199–210.

Tissir, F., Qu, Y., Montcouquiol, M., Zhou, L., Komatsu, K., Shi, D., Fujimori, T., Labeau, J., Tyteca, D., Courtoy, P., et al. (2010). Lack of cadherins Celsr2 and Celsr3 impairs ependymal ciliogenesis, leading to fatal hydrocephalus. Nat. Neurosci. *13*, 700–707.

Tree, D.R.P., Shulman, J.M., Rousset, R., Scott, M.P., Gubb, D., and Axelrod, J.D. (2002). Prickle Mediates Feedback Amplification to Generate Asymmetric Planar Cell Polarity Signaling. Cell *109*, 371–381.

Tsujikawa, M., Omori, Y., Biyanwila, J., and Malicki, J. (2007). Mechanism of positioning the cell nucleus in vertebrate photoreceptors. Proc. Natl. Acad. Sci. U. S. A. *104*, 14819–14824.

Turner, C.M., and Adler, P.N. (1998). Distinct roles for the actin and microtubule cytoskeletons in the morphogenesis of epidermal hairs during wing development in Drosophila. Mech. Dev. *70*, 181–192.

Usui, T., Shima, Y., Shimada, Y., Hirano, S., Burgess, R.W., Schwarz, T.L., Takeichi, M., and Uemura, T. (1999). Flamingo, a Seven-Pass Transmembrane Cadherin, Regulates Planar Cell Polarity under the Control of Frizzled. Cell *98*, 585–595.

Vinson, C.R., and Adler, P.N. (1987). Directional non-cell autonomy and the transmission of polarity information by the frizzled gene of Drosophila. Nature *329*, 549–551.

Vivancos, V., Chen, P., Spassky, N., Qian, D., Dabdoub, A., Kelley, M., Studer, M., and Guthrie, S. (2009). Wnt activity guides facial branchiomotor neuron migration, and involves the PCP pathway and JNK and ROCK kinases. Neural Develop. *4*, 7.

Vladar, E.K., Bayly, R.D., Sangoram, A.M., Scott, M.P., and Axelrod, J.D. (2012). Microtubules Enable the Planar Cell Polarity of Airway Cilia. Curr. Biol. *22*, 2203–2212.

Wada, H., Iwasaki, M., Sato, T., Masai, I., Nishiwaki, Y., Tanaka, H., Sato, A., Nojima, Y., and Okamoto, H. (2005). Dual roles of zygotic and maternal Scribble1 in neural migration and convergent extension movements in zebrafish embryos. Development *132*, 2273–2285.

Wada, H., Tanaka, H., Nakayama, S., Iwasaki, M., and Okamoto, H. (2006). Frizzled3a and Celsr2 function in the neuroepithelium to regulate migration of facial motor neurons in the developing zebrafish hindbrain. Development *133*, 4749–4759.

Wallingford, J.B. (2012). Planar Cell Polarity and the Developmental Control of Cell Behavior in Vertebrate Embryos. Annu. Rev. Cell Dev. Biol. *28*, 627–653.

Wallingford, J.B., and Harland, R.M. (2001). Xenopus Dishevelled signaling regulates both neural and mesodermal convergent extension: parallel forces elongating the body axis. Development *128*, 2581–2592.

Wallingford, J.B., Rowning, B.A., Vogeli, K.M., Rothbächer, U., Fraser, S.E., and Harland, R.M. (2000). Dishevelled controls cell polarity during Xenopus gastrulation. Nature *405*, 81–85.

Wallingford, J.B., Niswander, L.A., Shaw, G.M., and Finnell, R.H. (2013). The Continuing Challenge of Understanding, Preventing, and Treating Neural Tube Defects. Science *339*, 1222002.

Walsh, G.S., Grant, P.K., Morgan, J.A., and Moens, C.B. (2011). Planar polarity pathway and Nance-Horan syndrome-like 1b have essential cell-autonomous functions in neuronal migration. Development *138*, 3033–3042.

Wang, Y., Guo, N., and Nathans, J. (2006). The Role of Frizzled3 and Frizzled6 in Neural Tube Closure and in the Planar Polarity of Inner-Ear Sensory Hair Cells. J. Neurosci. *26*, 2147–2156.

Wanner, S.J., and Prince, V.E. (2013). Axon tracts guide zebrafish facial branchiomotor neuron migration through the hindbrain. Development *140*, 906–915.

Werner, M.E., and Mitchell, B.J. (2012). Planar Cell Polarity: Microtubules Make the Connection with Cilia. Curr. Biol. *22*, R1001–R1004.

Werner, M.E., Hwang, P., Huisman, F., Taborek, P., Yu, C.C., and Mitchell, B.J. (2011). Actin and microtubules drive differential aspects of planar cell polarity in multiciliated cells. J Cell Biol *195*, 19–26.

Werner, M.E., Mitchell, J.W., Putzbach, W., Bacon, E., Kim, S.K., and Mitchell, B.J. (2014). Radial intercalation is regulated by the Par complex and the microtubule-stabilizing protein CLAMP/Spef1. J. Cell Biol. *206*, 367–376.

Westerfield, M. (2000). The zebrafish book. A guide for the laboratory use of zebrafish (Danio rerio) (Univ. of Oregon Press, Eugene.).

Westermann, S., and Weber, K. (2003). Post-translational modifications regulate microtubule function. Nat. Rev. Mol. Cell Biol. *4*, 938–948.

Wong, H.-C., Bourdelas, A., Krauss, A., Lee, H.-J., Shao, Y., Wu, D., Mlodzik, M., Shi, D.-L., and Zheng, J. (2003). Direct Binding of the PDZ Domain of Dishevelled to a Conserved Internal Sequence in the C-Terminal Region of Frizzled. Mol. Cell *12*, 1251–1260.

Wu, J., and Mlodzik, M. (2008). The Frizzled Extracellular Domain Is a Ligand for Van Gogh/Stbm during Nonautonomous Planar Cell Polarity Signaling. Dev. Cell *15*, 462–469.

Wu, J., Roman, A.-C., Carvajal-Gonzalez, J.M., and Mlodzik, M. (2013). Wg and Wnt4 provide long-range directional input to planar cell polarity orientation in Drosophila. Nat. Cell Biol. *15*, 1045–1055.

Yadav, S., Puri, S., and Linstedt, A.D. (2009). A Primary Role for Golgi Positioning in Directed Secretion, Cell Polarity, and Wound Healing. Mol. Biol. Cell *20*, 1728–1736.

Yan, J., Huen, D., Morely, T., Johnson, G., Gubb, D., Roote, J., and Adler, P.N. (2008). The multiple-wing-hairs Gene Encodes a Novel GBD–FH3 Domain-Containing Protein That Functions Both Prior to and After Wing Hair Initiation. Genetics *180*, 219–228.

Yang, C., Axelrod, J.D., and Simon, M.A. (2002). Regulation of Frizzled by Fat-like Cadherins during Planar Polarity Signaling in the Drosophila Compound Eye. Cell *108*, 675–688.

Yang, T., Bassuk, A.G., Stricker, S., and Fritzsch, B. (2014). Prickle1 is necessary for the caudal migration of murine facial branchiomotor neurons. Cell Tissue Res. *357*, 549–561.

Ybot-Gonzalez, P., Savery, D., Gerrelli, D., Signore, M., Mitchell, C.E., Faux, C.H., Greene, N.D.E., and Copp, A.J. (2007). Convergent extension, planar-cell-polarity signalling and initiation of mouse neural tube closure. Development *134*, 789–799.

Yu, A., Rual, J.-F., Tamai, K., Harada, Y., Vidal, M., He, X., and Kirchhausen, T. (2007). Association of Dishevelled with the Clathrin AP-2 Adaptor Is Required for Frizzled Endocytosis and Planar Cell Polarity Signaling. Dev. Cell *12*, 129–141.

Yu, W., Centonze, V.E., Ahmad, F.J., and Baas, P.W. (1993). Microtubule nucleation and release from the neuronal centrosome. J. Cell Biol. *122*, 349–359.

Yun, U.J., Kim, S.Y., Liu, J., Adler, P.N., Bae, E., Kim, J., and Park, W.J. (1999). The inturned protein of Drosophila melanogaster is a cytoplasmic protein located at the cell periphery in wing cells. Dev. Genet. *25*, 297–305.

Zeidler, M.P., Perrimon, N., and Strutt, D.I. (1999). The four-jointed gene is required in the Drosophila eye for ommatidial polarity specification. Curr. Biol. *9*, 1363–1372.

Zeng, H., Hoover, A.N., and Liu, A. (2010). PCP effector gene Inturned is an important regulator of cilia formation and embryonic development in mammals. Dev. Biol. *2*, 418–428.

Zhu, J., Burakov, A., Rodionov, V., and Mogilner, A. (2010). Finding the Cell Center by a Balance of Dynein and Myosin Pulling and Microtubule Pushing: A Computational Study. Mol. Biol. Cell *21*, 4418–4427.